Post-depositional alterations across varying sediment types from archaeological inhumation burials - a geoarchaeological approach

Volume I of II

Annika Burns

PhD

University of York

Archaeology

September 2015

Abstract

The relationships between inhumation burial and the surrounding sediment in archaeological graves were investigated through micromorphology. Samples were collected from four archaeological sites (Hofstaðir, Al Khiday, Tel Qarassa and Sala Vastmaal) of varying sediment types and an experimental pig burial in a sandy sediment (UK).

Micromorphological analyses from burial sediments at Hofstaðir (Iceland) combined with results from organic geochemical analyses demonstrate complementarity of the two approaches for interpretation of the fate of the buried remains. Micromorphological observations from a single sample block vary between multiple thin sections oriented perpendicular or tangential to the remains, reflecting differences in these sediments at the centimetre to millimetre scale.

Mineral weathering pathways differ between grave sediments and controls and at some sites mineral weathering was significantly accelerated in grave sediments. Results suggest that thin section analysis of post-depositional sediment processes and activities of detrital populations affecting sediment minerals could be used as trace proxy evidence of past inhumation burials. Such mineralogical changes may persist in grave sediments beyond the limits of identification by direct evidence of organic materials and skeletal remains.

Table of Contents

List of Figures

Volume II of II

Image collection of thin section mosaics (digital version only)

List of Tables

Acknowledgements

The research has received funding from the European Research Council under the European Community's Seventh Framework Programme (FP7/2007-2013) / ERC grant agreement n° 230193. Thanks are given to the members of the InterArChive team, including the principal investigator Prof. Don Brothwell and supervisors Prof. Brendan Keely and Dr Raimonda Usai. Micromorphology samples from Tel Qarassa were collected by A. Balbo on behalf of the InterArChive project. Micromorphology samples from the other four sites were collected by members of the InterArChive project.

Author's declaration

I, Annika Burns, declare that this thesis is a presentation of original work and I am the sole author. This work has not previously been presented for an award at this, or any other, University. All sources are acknowledged as References. This work was conducted as part of a larger project examining the archaeological significance of signatures in grave sediments and the work of other members of the team is referred to where it provides context.

Chapter 1. Introduction

1.1 Premise

Archaeological materials are subjected to a suite of post-depositional processes. Once deposited, they become a part of an intricately inter-dependent sedimentological, pedogenic and biological environment. The materials are in a state of constant flux as they undergo degradation *via* pathways that are determined by the controlling factors of their dynamic contextual environment (Chapter 2). In this work, grave fills from archaeological sites of different geographic locations, periods and cultures, as well as from an experimental pig burial, are investigated with reference to information held within the sediments adjacent to the remains of the interred human or animal bodies in relation to burial practices and post-depositional processes. Grave fills were investigated by an analysis of the sediments according to a sampling strategy devised by the InterArChive project (Section 1.1.1).

1.1.1 The InterArChive project

The InterArChive project aims to identify changes made to sediments within archaeological burials, with the objective of retrieving information from deposits adjacent to the remains of the inhumed individual. This may have a significant impact on burial research by expanding the archives to include datasets relating to burials where, for reasons including ethical implications or preservation limitations, the remains of the individual may not be directly accessible for analysis.

A full outline of the objectives and hypotheses of the InterArChive project are available elsewhere (Usai *et al.* 2010b, 2014). The project aims to identify differences, where they exist, in the burial matrix with lateral and vertical distance from the body or along its length by investigation of the sediments through organic geochemistry and micromorphology. Specifically, such differences with distance can include variations in the burial sediment, the extent of preservation of remains near the pelvic or other areas, coffin preservation and signatures of hair and footwear at the head or feet regions, including comparison with other locations around the corpse. Along with intra-grave differences, investigations into inter-grave and inter-site differences are also within the remit of the project, in particular, comparisons between single and mass graves and rural and urban sites. Experimental burials of pigs have been designed to allow for comparisons between experimental and archaeological grave sediments (Usai *et al.* 2014). For micromorphology, the priority sampling sites per burial were pelvis, head, feet, hands and controls.

1.1.2 Thesis aims

Within the broader research topic described in Section 1.1.1, this individual study aimed to assess the limitations in the identification of past organic materials and effects of their degradation within burials and the preservation potential of different sediment types. It is only with a clearer definition of such knowledge that sampling strategies can be tailored on site to maximize the efficient retrieval of information.

The burial environment can create variable micro-environments (Van Veen and Kuikman 1990), which in turn create the conditions required for specific sedimentary and/or pedogenic processes, and favour the preservation of specific types of archaeological materials (Shahack-Gross *et al.* 2004). There is, undoubtedly, some organic material present within the majority of sediments where remains of burials are found (Stein 1992, 198). In most wet, temperate regions of northwest Europe this is often present as root remnants (Limbrey 1975). It is the distinction between depositional and post-depositional organic material, including proxy evidence, and the identification of taphonomic alterations to these materials that requires further discussion (Stein 2001, 37; Holliday 2004, 261). While some categories are self-evident, for example silk fibres are unlikely to be a product of biological activity post-dating time of burial, other circumstances may necessitate a more thorough investigation (Solecki 1977; Sommer 1999). Proxy evidence related to the decay of past organic materials could include post-depositional alterations to the inorganic materials in the burial environment (Chapter 2). More information is needed on whether inorganic materials could remain *in situ* and identifiable longer than the organic materials that have affected them. Concomitant with this is the question of how far organic materials or disruptive biota have moved into the region under examination (Van Nest 2002, 61). Earthworm excrement pellets in combination with chamber- and channel-shaped voids in a linear distribution have been considered as evidence to delineate the past path of bioturbative agents (Stoops 2003, 13 and 123-7; Section 2.2). Microbiological activities must be considered with regard to the stratigraphic relationships between adjacent archaeological sediment contexts (Billen 1982, 16; Section 2.4).

It is possible that significant information could be obtained if the impact of some of the post-depositional processes affecting textiles, wood and other organic materials were visually identified through a collection of images from both archaeological and experimental burials. Associated queries include: are unusual environments (volcanic, desert, heavy clay) more likely to delay or accelerate decomposition, and how do they affect the consolidation of burial matrix or organics? What inferences

can be made to support more generalized recommendations on sampling material that are as unique, dynamic and heterogeneous as a sediment? In order to maximize the effectiveness of sampling, it can be important to establish how/ whether it should be customized in relation to the investigation purpose and analytical approach, which should be established before sampling is carried out (Shennan 1988, 6). Thus, an aim of this thesis was to obtain field data from both archaeological and experimental burials to assess sampling strategies for types of burial sediments in future archaeological excavations.

Understanding individual processes may enable them to be placed within the degradation pathways as an assemblage approaches equilibrium. The characteristics of the burial sedimentary environment could alter an organic assemblage and impinge on the extent and means by which archaeological information may be retrieved.

1.2 Variables

The main variables that are likely to affect organic matter in archaeological include: a) the burial environment, b) the degree and agencies and extent of weathering (of the archaeological record and its associated sediment or sediments), c) time and d) the differences in funerary style and rituals. The burial environment is characterised by the pedological, topographical, geological, mineralogical, biological, and climatological conditions, integrated over time (Jenny 1994). Cultural characteristics, which determine what the archaeological record will contain at the time of burial, can also vary widely both temporally and spatially. Burial characteristics and procedures have often been seen as the result of a compromise between the cultural perceptions of death, the attitudes towards the deceased by those who bury the individual (Parker Pearson 1999, 3), and the resources afforded at the time (Bell and Walker 2005, 4).

Variations in environmental and sedimentological conditions can depend on the interrelated factors of water availability, parent material, Eh (redox potential), pH, porosity, permeability (Hopkins 2008, 57) and associated materials placed into the burial at the time of deposition, all of which may vary over time (Chapter 2). In recognition of this wide range of variables, the InterArChive sampling strategy incorporated three control thin sections, from sediments outside the areas of the burials (C1 control) and within the grave cut, from the upper and lower grave fills (C2 and C3 controls) (Figure 1.1). Such a sampling strategy has been applied to a selection of burials from a range of sediment types and

archaeological periods (Section 1.1.2 and Chapters 4-8) and critically reviewed as an effective approach to investigating burial soils (Section 1.3 and Chapters 9-10).

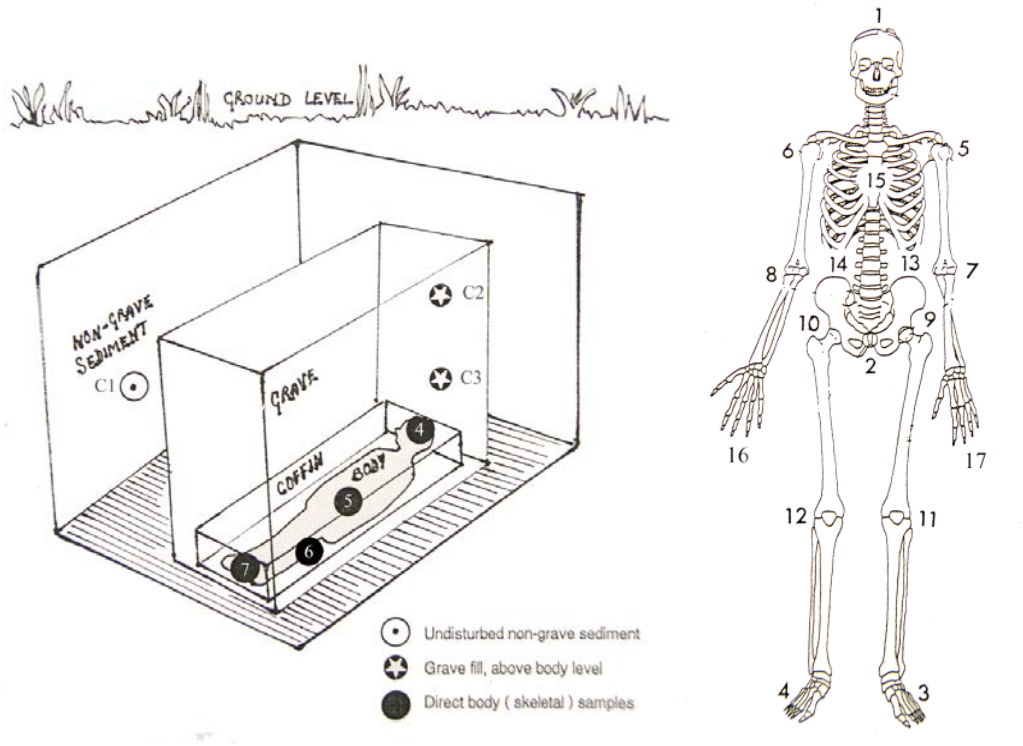

Figure 1.1: InterArChive Project sampling strategy for a) controls: C1 non-grave sediment, C2 upper grave fill and C2 lower grave fill and b) skeletal samples: sediment samples (numbers 1-17 on skeleton above) collected from varying positions around the body and adjacent to the visible remains of the inhumed individual (Usai *et al.* 2014).

1.3 Objectives

1.3.1 Objective 1

To assess the degree to which direct and proxy evidence of organic materials in the burial sediments, especially those that have degraded past the point of visible recognition during excavation, are identifiable through micromorphological analysis.

1.3.1.1 Rationale for objective 1

The material present at the time of excavation is a subset of the archaeology at the time of deposition, which can be further filtered by different methods of retrieval and analysis. Hence, the potential and

limits of the analytical techniques should be repeatedly tested. The anthropogenic disturbance event of burial and subsequent degradation of organic remains could impact on the weathering of minerals in the sediments. For example, if an incomplete skeleton is recovered, can the sediment analysis provide information of which parts of the body were present? Such interpretations could lead to conclusions concerning the completeness of the human remains at the time of burial, versus the incompleteness of the record.

1.3.2 Objective 2

To assess the most appropriate sampling strategy for retrieving the data mentioned in Objective 1 (Section 1.3.1) from each type of burial sediment environment.

1.3.2.1 Rationale for objective 2

The analysis mentioned in Objective 1 can be used to create a methodology and sampling strategies for the efficient collection of data on the organic materials and post-depositional processes within grave fills across varying sediment types. The sampling strategies should detail where, in relation to the skeletal remains, samples should be taken in order to collect products that have moved within the burial environment as a result of post-depositional alterations.

1.3.3 Objective 3

To assess the methodology for the most appropriate manufacture of thin sections in order to retrieve the information for Objective 1 in relation to each type of burial sediment environment.

1.3.3.1 Rationale for objective 3

Samples for micromorphology are blocks of sediment that can be cut along different planes to produce thin sections (Chapter 3). The InterArChive Project's micromorphology samples adjacent to skeletal remains were all cut in two planes, one tangential and the other perpendicular to the skeleton. The thin section plane a sample is cut to should be appropriate to the research questions being asked. Hence, a query to address with Objective 3 is whether the InterArChive's thin section method of tangential and perpendicular sections is the most effective and efficient way to investigate the trace evidence material from a burial?

1.4 Research Outline

The aim to assess the limits of the identification of micro-scale remains and effects of the degradation of the burial (Sections 1.1.2) has been assessed through an investigation of grave soils from archaeological (Chapters 4-7) and experimental (Chapter 8) burials from a range of sediment types (Section 3.2). Post-depositional processes can affect buried remains and the degradation of organic materials can impact geochemical conditions which may be limited to micro-scale environments or the entire grave fill (Chapter 2). Organic materials deposited in a grave during burial along with a body can include textiles, such as clothes or wrappings, and wooden coffins (Section 2.2) and as their decomposition may cause changes in the sediment, such as pH, Eh or moisture content (Chapter 2). Objective 1 of this thesis to identify the direct and proxy evidence of organic materials (Section 1.3.1) was well suited to an investigation by micromorphological analysis of the sediments adjacent to the remains. Proxy evidence of organic materials may include the effects of their degradation on their surrounding sediment, including the inorganic components of the sediment (Sections 2.3 and 2.4). Micromorphology is a technique which allows observations of the micro-contextual spatial associations between sediments and archaeological materials held within them and as such can provide micro-scale evidence of the types of relationships investigated in this aim and Objective 1 (Sections 1.3.1 and 2.1).

The proxy evidence of the degradation of the buried remains through an investigation of the sediments in the grave fill (Objective 1, Section 1.3.1), requires a sampling strategy which should be designed to include the nature of the sediments (Section 1.3.2). The InterArChive sampling strategy (Section 1.1.1) was employed in the burials analysed in this work (Chapters 4-8). The InterArChive micromorphological sampling strategy suggested one site control (C1 control) per site and from each grave an upper grave fill control (C2 control), lower grave fill control (C3 control) and three samples from sediment adjacent to the skeletal remains in the regions of head (S1 sample), pelvis (S2 sample) and feet (S3 sample). The sampling strategy was employed over a range of sediment types (Chapters 4-8) enabling a critique of the suitability of the suggested location of the controls and samples in the InterArChive sampling strategy in relation to intra-layer variability in archaeological sites (Section 9.4.1).

In addition to a micromorphology sampling strategy the InterArChive project also suggested that two thin sections should be produced from each sample. Micromorphology samples can be collected as rectangular blocks of sediment which are then filled with resin and cut to produce a thin section (Sections 2.1 and 3.4.1). Typically, micromorphology samples are cut across a single plane to produce

one thin section per sample (Sections 2.1 and 3.4.1). The InterArChive manufacturing method to produce two thin sections, one tangential and one perpendicular to the skeletal remains (Section 1.1.2), was applied to the investigation of graves from archaeological sites across a range of ages and sediment types (Chapters 4-8). The differences between tangential and perpendicular oriented thin sections have been discussed and assessed in terms of the effectiveness of the InterArChive strategy (Section 9.4.1).

Chapter 2. Literature Review

Investigation of the archaeology through a thorough analysis of the processes that have affected the material remains is essential to understanding their nature and location at the time of burial. It has been many years since the acknowledgement of the faults inherent in the "Pompeii premise" (the suggestion that archaeological assemblages can be understood only as if they are in as excellent a state of preservation as those at Pompeii) and the emphasis that the inhibiting factor in archaeological endeavours is the methodology employed to investigate rather than the archaeology itself (Ascher 1961, 324; Binford 1981, Schiffer 1985). It has been suggested that a detailed and comprehensive knowledge of the current properties and constituents of a deposit and of the processes that have been active since deposition, could enable their description by an algebraic equation (Branch *et al.* 2005, 31). However, using an equation to reconstruct the human past is an approach which may not take into account the factor of human agency, either in the past or during the collection and interpretation by the archaeologist (Shanks and Tilley 1987, Hodder 1987, 7 and Dobres and Robb 2000, 4-7). The term agency was first discussed as the role of the individual when studying the archaeology of communities (Shanks and Tilley 1987 and Hodder 1987). The usefulness of the term was limited by a lack of agreement of its strict definition (Dobres and Robb 2000). Gradually, however, the importance of the role of agency within theoretical archaeology regarding the identification of the micro-scale remains and the reconstruction of single events to understand temporally larger-scale narratives was recognized as an aid in interpretation of field data (Hodder 2000). An appropriate methodological and theoretical framework is necessary when assessing site formation processes. Understanding the preserved remains requires an analysis of what has been degraded, allowing distinction between what is not visible due to poor preservation and what is not visible through lack of deposition (Weiner 2010, 46), an advance from simply stating that archaeological practice is limited by theoretical expectations and retrieval limits (Clarke 1973).

Taphonomic processes can operate at all times in burial environments, albeit at varying rates and trajectories (Behrensmeyer *et al.* 2000). Even the best preserved archaeological deposits, such as the exceptionally well preserved wood remains from Novgorod, have been altered in some form since their deposition in antiquity (Hamilton-Dyer 2002). Archaeological studies which have used the term taphonomy in a strict sense of the transformation ofmaterials from the biosphere to the lithosphere have been criticised as too limited to enable inclusion of the full suite of archaeological evidence of biological and non-biological origin in relation to anthropogenic and pedogenic post-depositional processes processes (Schiffer 1987, Lyman 2010), and the taphonomy of archaeological deposits has been discussed in recent archaeological investigations (O'Connor 2005). Forensic taphonomy concerns

the processes affecting a burial assemblage (Haglund and Sorg 2001). Post-depositional alterations to the archaeological record are determined by processes associated with the burial environment, as a whole, moving towards an equilibrium (Wilson and Pollard 2002). Hence, it has been suggested that archaeologists should not only seek to understand the role of thermodynamics but also reaction rates (Raiswell 2001, 595). The degree of weathering and post-depositional alteration is characterised largely by the burial environment and the length of time the material remains within the archaeological context before rejoining the systemic context (Schiffer 1972, 3).

The mechanisms responsible for the degradation of organic components can be as diverse as the burial environments within which these processes occur. In some cases, recognition of alterations to the archaeological record through understanding such mechanisms has been achieved by analysis of a combination of trace evidence, the micro-contextual spatial relationships of materials in thin sections and bulk chemical analyses to help resolve geoarchaeological questions (Davidson *et al.* 1992). The paper by Davidson *et al.* (1992) was exemplary in discussing micromorphological results directly to archaeological queries and macro-scale field data, however, its scope was limited to sites from Scotland. A more exhaustive discussion of the potential of micromorphology as part of a multidisciplinary approach which can be effective in investigating archaeological sites is given in Courty (1992), and has been supported by following studies (Macphail and Cruise 2001, Goldberg and Berna 2010).

2.1 Micromorphology

The tool of micromorphology is well suited to discern soil and sediment characteristics and has been relied on heavily for this purpose for decades (Kubiena 1938, Cornwall 1958, Dalrymple 1958, Brewer 1964, Bullock *et al.* 1985). Cornwall (1958) contributed to the holistic approach of studying soils and sediments, through micromorphology being employed as a tool to investigate both the archaeological evidence and its surrounding sedimentary environment, as part of an active multifaceted system, and to interpret both together in archaeological studies. Micromorphology enables discerning displacement and movement of materials and organisms through its ability to show micro-contextual relationships (Goldberg and Berna 2010). The technique has been implemented successfully in studies concerning site formation processes and assessing stratigraphic integrity (Macphail and McAvoy 2008). Micromorphology was employed in interpreting the use of space of internal areas in urban contexts through the analysis of a series of samples from archaeological floor sediments from a

Near Eastern tell which had an intricate and complex stratigraphy (Matthews *et al.* 1997). Micromorphology, when used alone, can be limited in relation to its ability to aid in an identification of the origin of features in soils and sediments and the interpretation of post-depositional processes, however this limitation is surpassed when additional complementary techniques are used (Goldberg 1980). Combined with other geoarchaeological techniques (Macphail and Cruise 2001), micromorphology has been effective in testing whether the sampling strategies and analytical methodologies are best suited to the sediment, in order to isolate processes and agents in the degradation of materials (Courty 1992, Matthews 2010). The identification of features in thin section can be aided by a combination of micromorphology and microprobe analyses, which enables both observations on the spatial relationships between materials in thin sections and the elemental analysis of specific features. The identification of the origin of features with elevated phosphorus levels and interpretations of the cause of their post-depositional alterations through micromorphology and SEM-EDX has been implemented on samples from anthrosols (Schaefer *et al.* 2004) and through micromorphology and microfocus X-ray scattering from archaeological sediments in acidic soil conditions (Adderley *et al.* 2004). Hence, identifications of materials in thin sections were aided by SEM-EDX microprobe analyses of certain features in the burial soils of the following case studies (Chapters 4-8).

Micromorphology samples are processed into thin sections by removing the water in the sediments and impregnating the material with a resin. The two main methods for drying micromorphology samples are acetone vapour exchange (Miedema *et al.* 1974) or evaporation through air-drying or in a low temperature oven (Murphy 1982, Courty *et al.* 1989). The method of removing water from the sediments is critical as this stage of the manufacturing process can lead to the formation of cracks and displacement of materials within the sample (Section 3.4.1). Early studies replaced air and water spaces in sediments with a high molecular weight ethylene glycol compound (Carbowax 6000) which was soluble in water (Mackenzie and Dawson 1961, Langton and Lee 1965). Carbowax has been replaced by low-viscosity, colourless epoxy and polyester resins as these offer a permanent embedding medium which can infill small pores spaces and cure at low (<40 C) temperatures (Innes and Pluth 1970, Courty *et al.* 1989). Epoxy and polyester resins have the advantage over crystic resins Murphy 1986) in that they are non-carcinogenic. The developments in the methods of drying and impregnation of micromorphology samples have resulted in minimising the amount of disturbance to the sediments once they reach the laboratory, however the research into minimising the disturbance incurred during transport from the site to the laboratory could benefit from further studies.

Methods of impregnating the soils and sediments with a low-viscosity epoxy embedding medium which is miscible with water could reduce processing time and stabilise aggregates during transport (Prone 1976). Alternatively, micromorphology samples could be processed and thin sections produced on-site (Weiner 2010). However, as yet, on-site production of thin sections of archaeological deposits has been limited to sediments from arid sites which require shorter drying times than sediments from archaeological sites in organic-rich soil types, such as peats, which can contain large quantities of water.

Micromorphology research could also benefit from further studies into the methods of the production of thin sections regarding the appropriate location and plane of the analysed thin section from within a sample block. Micromorphology samples are labelled with an orientation of the ground surface during collection and this orientation is transferred onto the final thin section (Courty *et al.* 1989), however, the notation of a secondary orientation regarding a specific reference feature other than the direction of the ground surface is rarely added. Hence, the InterArChive sampling strategy to produce thin sections at tangential and perpendicular orientations to the skeletal remains from micromorphology samples of grave sediments has been assessed (Section 1.3.3) in the case studies in the following chapters (Chapters 4-8).

Micromorphology can be a useful tool when it is used with an awareness of its limitations and the nature of its relationship to the larger sediment or soil unit(s) and the details of how it represents these materials. Limitations of the technique when identifying past agricultural soils were identified in Carter and Davidson (1998). However, some such limitations were further disputed and seen as contradictory (Macphail 1998). Debates that followed (Macphail 1998 and Carter and Davidson 2000) expanded the development of micromorphology for archaeological investigations through discussing misconceptions and further justifying the role of micromorphology in archaeology. Research regarding the identification and interpretation of pedofeatures and microfabrics has benefited more recently from exemplary work, and has been a valid tool for the understanding of past processes affecting soils and sediments (Stoops *et al.* 2010). However, the applications of micromorphology to the deposits surrounding human remains are rare (Section 2.4), an exception including the InterArChive project's application of micromorphology in association with geochemical analysis of burial sediments (Usai *et al.* 2010b).

2.2 Inhumation burials

Burial archaeology has developed from merely collecting bones and grave goods to assessing the archaeological features within their sedimentary context (Ilan 1995, 118). Studies in the Victorian era of only those artefacts which survived (Easton 1998) has developed into a more holistic approach through processual, post-processual and contextual archaeologies (Hodder and Hutson 2003), investigating the burial environment over time when reconstructing past events. Inhumation burial practices can vary widely in the number of individuals in a grave, or in the types of coffin or wrappings, levels of defleshing or disarticulation prior to burial and grave goods deposited with the remains (Chapman *et al.* 1981; Parker Pearson 2003).

Cleaned bones can undergo different taphonomic pathways than bones within an entire cadaver because of the effects on the burial environment of added organic material from skin, hair, and flesh (Carter 2005 in Carter and Tibbett 2006). The presence of moisture, fatty acids, and oxygen can create hospitable habitats for micro-organisms (*e.g.* bacterial and detrital fungi), significantly impacting the processes of decay (Denys 2002; Fraser *et al.* 2011). Biota, such as intestinal microflora, may be present in the body at the time of interment and can aid in the degradation process (Hopkins *et al.* 2000, Bergmann *et al.* 2014). Biota can also be present on the body, such as flies or maggots on straw bedding or in clothing that the remains are wrapped in for burial, and can aid in the degradation of the body through advancing the rate of the early stages of decay, such as putrefaction (Anderson and Cervenka 2001, Tibbett and Carter 2008). Additional variants may include plant or animal remains already present in the sediment at the time of burial or incorporated after burial, such as earthworms and their excremental granules (Darwin 1881; Canti 2001 and 2007). Microbial populations in soils and sediments may alter over time as a result of changes in the sediment environment through the effects on pH (Nicol *et al.* 2008), oxygen and water availability (Trevors 1984) or other palaeoecological and micro-environmental changes, such as organic carbon content (Aller 1994), associated with degradation of the buried materials. Sporophores (fruiting bodies of fungi) growing at the soil surface due to increased ammonia levels, have been suggested as markers aiding in the identification of recent below ground graves in varied geographical locations (Tibbett and Carter 2003).

Despite the wealth of recent literature on soil microbial, especially bacterial, communities, their impact on archaeological sediments is arguably less clearly defined compared to the studies on the role of macro-scale biota such as earthworms. For example, for earthworms the volume of calcium carbonate granules produced and dissolved has been assessed over time frames from 3 to 18 weeks (Lambkin *et al.* 2011a,b and Versteegh *et al.* 2014). The calcium carbonate granules produced has been assessed in 11 sediments with differing pH values over three weeks (Lambkin *et al.* 2011a) and 3 sediments with

differing temperatures and CO_2 conditions over three weeks (Versteegh *et al.* 2014), and granule dissolution in three soils over 126 days (Lambkin *et al.* 2011b) have been studied for the species *Lumbricus terristris*, which was a suitable choice of species as it is native to the UK soils used in the samples for these three studies. Comparatively, the lab-based studies of the effects of changes in temperature on respiration rates of bacteria and fungi populations in soils have been on experiments of shorter timescales and could differ with longer tests (Pietikäinen *et al.* 2005). Research into the effects of differences in pH levels on bacterial and fungal populations across a single strip of soil as at Hoosfield, Rothampstead Research accurately isolated pH as the single variable in their studies (Rousk *et al.* 2009), however were limited as they were based on very small samples (1 g soil) of a large area (180 m) and while the results of Rousk *et al.* (2009) suggested evidence of general relationships they did not take into account micro-scale environments within the sediments. The relationship between sediment biota, weathering and pedogenesis are critical to a thorough understanding of burial sediments and their post-depositional processes as they may affect inorganic deposits as well as altering the environmental conditions within the sediment (Section 2.3). Thus in the case studies in the following chapters (Chapters 4-8), post-depositional processes in burial sediments have been investigated through an analysis of the micro-contextual spatial relationships and the weathering in the burial sediments from several sampling locations to assess for differences in micro-environments within each grave.

2.3 Geoarchaeology in burial archaeology and biota in grave sediments

Geoarchaeology has been defined as the application of geoscience techniques to archaeological questions (Rapp and Hill 2006, 1). Such a definition has been criticised as a narrow view compared to one of geoarchaeology as a discipline concerned with the study of the effects of anthropogenic effects on a landscape (French 2003, 3). However, the two definitions are not mutually exclusive and both describe ways of contributing to the understanding of soils and sediments in archaeological research.

Geoarchaeological investigation of inhumations may involve the materials surrounding and active in the decomposition of buried remains as well as proxy evidence for the presence of the remains themselves. Bioarchaeological investigations of bulk samples processed by floatation and sieving are capable of producing interpretations on the biota present and previously active within sediments (Celant *et al.* 2015). Information obtained on biota may include, but is not limited to, evidence and proxy evidence for populations of earthworms, beetles, ants, wasps (Eschenbrenner 1994), and

mollusca (Evans 1969). Presence of plants may be evidenced by remains of roots, seeds, wood fragments, or charcoal. Such remains could be useful in interpretations of depositional materials resulting from past cultural burial practices or post-depositional processes that altered the archaeological record, as genera found could have required specific habitat requirements. Parasites found in association with human remains may be able to suggest interpretations on levels of hygiene and afflictions affecting the individual before death (Jones 1985, Bathurst 2005). Parasite ova can be discriminated between true and false parasite depending on the species and as markers of either faecal deposits or background levels in urban strata (Reinhold 1992). Identification of plant macrofossils and parasites in thin section can aid in distinguishing between modern and archaeological remains as micromorphology enables observation of the microstratigraphy and post-depositional alterations affecting sediments through an analysis of the spatial and causal relationships between items and relative time sequences. Hence through looking at the micromorphology of the biota and establishing the spatial, causal and relative occurrence of biota remains in relation to other features within the slides, information can be obtained on the depositional history of the biota.

Once deposited the fill of a grave is referred to as a sediment rather than a soil due to the distinction between these two terms (Goldberg and Macphail 2006, 27). After its deposition, the sediments may be affected by weathering and pedogenic processes. Materials may be transported across sediments and soils as a result of post-depositional processes (Bocek 1986; Balek 2002). A succession of processes resulting in gradual movements, vertically and laterally, through sediments or a single process resulting in an episodic movement may transpose proxy evidence large distances from the location of deposition, if allogenic, or formation, if authigenic (Schiffer 1987). Examples of this include displacement of solid material through catena slope processes such as sediment creep or slump (Wainwright 1994) or in suspension or solution through surface runoff, leaching, or eluviation, all of which are commonly active at archaeological sites (Rapp and Hill 2006, 98-102 and 265-269). Such movements may continue until either the energy transference (movement downslope) is completed or until a physical barrier, such as a coffin, neighbouring skeleton, dense root network or the more tightly packed infill of an animal burrow, impedes further movement down the slope profile. At this point any such objects may serve as a temporary stabiliser and proponent for macro-aggregates (Tisdall and Oades 2006). The transportation of ions in solution, on the other hand, can be traced *via* the presence and locations of precipitates, nodules or coatings, (Stoops 2003, 106-9) or their influence on weathering of inorganic components that they encounter (Kögel-Knabner *et al*. 2008; Favre *et al.* 2002; von Lützow and Kögel-Knabner 2009).

Observations of grave shadows and burial stains have been linked to sedimentological analyses of concentrations of organic and inorganic compounds, including the example of Sutton Hoo's sand men (Carver 1992). Geophysics has contributed to rapid site survey through magnetic susceptibility assessment to aid in the above ground identification of graves (Chianese *et al*. 2004). Phosphate levels have been known since the 1950s to be elevated in graves (Piggot 1954, Petřík *et al.* 2012) and manganese deposits have received similar attention as body signatures in grave sediments (Bethell and Carver 1987). Studies at Bishop's Waltham highlighted the importance of combined analyses of phosphorus and manganese concentrations in these grave stains rather than phosphorus measurements alone (Biek 1957). This was further built upon by studies on graves at the multi-period site of Mucking in Essex, where dark coloured deposits within grave sediments which followed the general outline of the body, termed silhouettes, were observed (Werner and Hughes 1971). Analyses of the manganese concentrations in both bone and silhouettes in a selection of child and adult graves from Mucking were interpreted as suggesting that the manganese concentrations were higher in the silhouette than in the bone (Keeley 1977). Although the concentrations listed by Keeley (1977) for a child's grave support their conclusion (2960 compared to 112 ppm), the values listed in the article for the adult's grave for the sample of the silhouette in the leg region (296 ppm) are lower than those from the leg bone (2976 ppm), suggesting that the proportion in silhouettes compared to bone is prone to some variation.

Analyses of the sediments in Anglo-Saxon graves at Owmby and Lakenheath were interpreted to suggest that in grave sediments magnetotactic bacteria combined with magnetic components in the soil to form secondary ferrimagnetic minerals (Linford 2004). However, the work (Linford 2004) did not explain the level of contribution of the magnetic components in the soil or detail the stages of the process of its deposition. It was later suggested that fires can have an important role in aiding this mineralogical process by contributing the necessary heat (between 180 and 300 °C) for processes leading to magnetite or maghemite production in soils to occur (Linford 2005). This was developed in relation to floodplain sediments from the Iron to Bronze Ages at Yarnton by assessing magnetic minerals formed in the sediments by bacteria in oxygen limited conditions, and their presence was used to infer hydrological changes (Linford *et al.* 2005). However, as yet, sites with well linked optical to microscopic identification of magnetite in grave sediments, such as Linford (2004), are rare and a wider dataset across a wide range of soil types and burial timescales would be crucial to strengthen interpretations of inferences related to the presence of magnetite on skeletal remains. Research into the processes by which such iron oxide deposits are modified or transported within burial sediments, as well as into other possible proxy markers for inhumations *via* mineralogical products, bacterial or

fungal driven decay of organic remains have yet to be developed. Although some recent lab-based studies show the relationships between minerals and detrital bacteria (Bennett *et al.* 2001) and fungi (Huang *et al.* 2008; Gadd 2007), as well as biomineralization related to sulphate-reducing bacteria (Neal *et al.* 2001), such research has yet to be applied to archaeological burials.

2.4 Microarchaeology, post-depositional processes and detrital organisms

Micro-scale remains such as phytoliths (Shillito 2011), diatoms (Bathurst *et al.* 2010) and pollen (Tipping *et al.* 1994) have been investigated from archaeological sediments. Such investigations, however, whether carried out as single studies or multi-disciplinary research into burials, are generally performed from sub-samples of loose bulk sediments (Piperno 1988, Battarbee 1988 and Pearsall 2015, 214-218). On the other hand, micromorphological analysis permits an examination of the *in situ* micro-contextual relationships of sediment constituents and inferences on post-depositional processes (Matthews 2010, Goldberg and Berna 2010, Stahlschmidt *et al.* 2015). The technique, however, has rarely been applied to archaeological graves, exceptions including a multidisciplinary (micromorphological, mineralogical and chemical) analysis of sediments of a prehistoric Amerindian interment which established it as a ritual burial and not an accidental drowning and deposition (Huckleberry *et al.* 2003), the Gokstad ship burial mound where evidence interpreted as a body stain and faecal materials from the gut suggested that an inhumation in an adjacent trench had more intensively degraded, compared to the skeletal remains excavated in the Gokstad burial (Macphail *et al.* 2013), and the recent works by *InterArChive* (Usai *et al.* 2014 and Pickering *et al.* 2014). The study of the Gokstad ship burial (Macphail *et al.* 2013) was exemplary in its use of the combination of the archaeological results with those from experimental earthworks and a thorough appreciation of the roles of detrital organisms and their products of decay within burial soils. Once buried, carbon-based materials can be acted on by detrital organisms, including both anaerobic and aerobic bacteria, which in turn create new organic matter inputs to the sediment system (Carter and Tibbett 2008, 37). Thus, the products and processes of decay must be studied as interconnected, complex and dynamic components in a sedimentary environment.

Interactions between the biotic degradation of organic and mineral materials within a sediment may leave recognisable traces (Huang 2008, 4; Tapanila 2008; Mikuláš 2008). Investigations of the relationships between bacteria and iron oxides and hydroxides through biomineralization have shown that the anaerobic non-light dependent *Acidovorax* can increase production of goethite over

lepidocrocite and decrease crystallinity of iron oxidation products in elevated levels of carbonate and phosphate, respectively (Larese-Casanova *et al.* 2010). Although lab-based studies such as those of Larese-Casanova *et al.* (2010) concern mineral amounts too small to be detected with light microscopy, if developed further their findings could be useful in future burial archaeology research.

Bacteria and fungi have also been shown to affect bone diagenesis (Machiafava *et al.* 1974, Baud and Lacotte 1984, Jans *et al.* 2004). Early studies suggested that the more porous skeletal tissue was more sensitive to effects caused by changes in groundwater and acidity levels than the cortex (Von Endt and Ortner 1984, 252; Cussler and Featherstone 1981 in Lyman 1984, 422). Although porosity and site hydrology have continued to be considered significant factors in bone diagenesis/preservation (Nielsen-Marsh and Hedges 2000), the porosity of bone has also been considered as a response to its environment regarding geochemistry and water fluctuations as complex factors in bone degradation (Hedges 2002). The studies by Nielsen-Marsh and Hedges (2000) discussed the characteristics of archaeological bones from different sites in Europe from a selection of environment types. The variety of sites allowed for inter-site comparisons and large scale considerations of bone preservation/ decay in relation to bone porosity, hydrological fluctuations, protein loss and microbial attack, with detailed descriptions of site sedimentological conditions (Nielsen-Marsh and Hedges 2000) and suggests that such processes could have been present in the sites discussed in the following chapters (Chapters 4-8).

Detailed studies of the characteristics of microbial attack on bone by fungi and bacteria showed an increase in bone micro-porosity in sediments, with the bacteria as the agents of the greatest change in micro-porosity, as inferred from the results of mercury intrusion porosimetry (HgIP), which showed the greatest increase in porosity in the 0.6-1.2 µm range (Jans *et al.* 2004). The merits of the HgIP technique for measuring bone porosity along with an argument supporting bone porosity assessments in determining type and extent of diagenesis are discussed in Smith *et al.* (2007) and Nielsen-Marsh *et al.* (2007). However, although capable of measuring sub-micron sized pores and producing quantifiable results this technique requires the bone fragments to be removed from their sedimentary matrix prior to analysis, thus inhibiting investigation of the spatial associations and a full consideration of the spatial relationship between bone and sediment. Micro-contextual associations between areas of diagenetically altered and relatively preserved bone were evident in 100 µm thick thin sections analysed by SEM, LA-ICP-MS and LA-MS-ICP-MS from samples from six femurs from a cemetery at the edge of Lake Baikal (Scharlotta *et al.* 2013). Hence, the burial sediments sampled for micromorphology in the following case studies (Chapters 4-8) could show evidence of spatial relationships at the micro-scale in terms of areas of bone preservation and levels of diagenetic alteration.

A current limit of geoarchaeological research into graves is that the preservation of micro-remains and the trace geochemical signatures within the fine fraction of the sediments (silt and clay sized, <64 μm) are often dependent upon sedimentary conditions which can vary over short distances and as such could affect intra-layer variability between the sediments within a coffin, within a grave cut above the coffin and those surrounding the grave cut. Micro-scale plant remains such as pollen and phytoliths are sensitive to changes in pH and physical disturbance related to bioturbation (Pearsall 2015 and Piperno and Pearsall 1993, respectively). Bone can be affected by calcite solubilisation and reprecipitation (Berna *et al.* 2004) affecting collagen preservation (Collins *et al.* 2002). Trace signatures of human remains, such as low molecular weight organic *n*-alkanes, fatty acids and sterols, can by washed downwards through soil profiles in freely draining soils beyond the limits of detection (Green 2013, 162 and 212). Sediment conditions such as drainage, pH, Eh, fungi, bacteria, water, oxygen and bioturbation can vary across a single site and within a single grave and differentially affect coffin wood and bone preservation. Thus the burial sediments investigated in the following case studies (Chapters 4-8) were sampled both laterally and vertically across a single grave and the results of micromorphological observations were compared both within and between graves across a site and followed by a discussion of inter-site interpretations (Chapter 9).

2.5 Experimental burials

Further study of the mechanisms of decay through the collection of data from experimental burials where the inputs to the system are recorded and the conditions are monitored could lead to new insights into the details of preservation potential of certain sedimentary environments and intra- and inter-grave variability. Experimental research projects have made advances in the understanding of burial environments and the preservation potentials of objects as evidence of activities (Bell *et al.* 1996; Macphail *et al.* 2003; Macphail and Crowther 2011) and the effects of pedogenic processes over time (Schiffer 1987; Canti 2001). The InterArChive Project (Section 1.1.1) utilised pigs as substitute for human cadavers in their experimental burials to investigate the evidence in the grave fill sediment of past processes of decay during the first three years of burial (Usai *et al.* 2014). Processes occurring in short term burial sediments may include the mechanisms of decay of the remains and changes to the host sediment related to the cutting of the grave and decomposition of the body (Tibbett and Carter 2009). Experimental graves are often sampled after only a few years of burial, when the decay of the remains and formation of the products of post-depositional processes within the sediments may have

already progressed significantly (Schotsmans *et al.* 2012, Ern *et al.* 2012), as the first few years in the ground are considered the most active in terms of degradation (Wilson *et al.* 2007, Forbes 2008).

Forensic archaeology studies have utilised pigs as substitutes for human cadavers for their similarities in dermal and sub-dermal structure, digestive tract, proportional internal cavity sizes and location of internal organs (Tumbleson and Schook 1996). Studies on the decomposition of cadavers utilising pigs have been ongoing for decades (Payne and King 1968; Turner and Wiltshire 1999; Breuning-Madsen *et al*. 2003, Wilson *et al.* 2010), as have studies concerning the effects on sediments by the addition of pig faecal materials (Rochette and Angers 2000; Chantigny *et al.* 2001; Macphail and Crowther 2011). Such experimental burials of pigs have been utilised to test hypotheses regarding decomposition of human cadavers (Schotsmans *et al.* 2012), as these are more difficult to gain access to for purposes of experimental research (Rodriguez and Bass 1985; Mann *et al*. 1989; Carter *et al*. 2007; Carter and Tibbett 2008, 36).

Phosphatic and redox (reduction-oxidation) features, represented through hydrated or hydroxylated Fe/Al compounds present as nodules or coatings, in experimental pig burials have been interpreted as the result of the leaching and precipitation of decay products in solution through the sediments (Ern *et al.* 2012). During such experimental burials, it was tentatively supposed that evidence for remains of the bodily fluids of decomposing pigs could appear as amorphous phosphatic features within the narrow time frames of 1, 6, 12, 20, 24, and 30 months in materials from only two sediment types and results from the later stages (24 and 30 months) of the experiment are still pending (Ern *et al.* 2012). The results of excavations at the Overton experimental earthwork project showed that even short amounts of time can be sufficient to produce iron pans (Crowther *et al.* 1996). Their formation in burials may be significantly influenced by the presence of coffins and the preservations of organic materials, as evidenced at the Lejre experimental farm (Breuning-Madsen *et al.* 2001). The results of the experimental burials by Ern *et al.* (2012) may prove complementary to longer term experiments of buried materials such as at Overton (Crowther *et al.* 1996) by aiding in the interpretation of both the short (months) and longer (years) term processes occurring in burials.

Experimental burials are limited by the substitution of an animal cadaver, usually pig, for a human and the small length of time in the ground, relative to archaeological timescales. Although there are a small set of studies regarding experimental data from human inhumations, such as from the Virginia body farm (Bass and Jefferson 2011), access to this type of dataset is uncommon. Long term experiments such as that at Wareham and Overton Down earthworks are ongoing, with successive excavations having taken place after 1, 2, 4, 8, 16 and 32 years of burial and the 64th year excavation scheduled for

2024 (Bell *et al.* 1996). These two experimental earthworks have been instrumental in the understanding of the degradation of textiles and sediment displacement following disturbance activities, and although cremated human bone and blood were buried at Wareham, an entire cadaver was not (Hillson 1996). The results from the burial of organic materials at Overton Down and Wareham earthworks suggested that some plant-based textiles (linen) could decay within the first four years (results from Jewell and Dimbleby 1966 as reported in Fowler 1996). The earthwork project's conclusions on the rate of decay of other textiles were complicated by their absence in some of the earlier and presence in later excavations and highlight the role of the excavators in the retrieval of archaeological data (Limbrey 1996). The results from the decay of textiles from the experimental earthworks may differ from those from experimental graves as several variables in the sedimentary environment differ. For example, with coffined burials, differences in oxygen and porosity or water saturation levels may occur in comparison with coffined remains, as these may have a large air space between them and the coffin lid, and coffins could retain soil solutions while the coffin base remains intact. The experimental pig burials in the InterArChive project, one of which was investigated in this thesis (Chapter 8), were buried for 3 years (Section 1.1.1), slightly longer than those in the interment by Ern *et al.* (2012), and thus expanding the experimental dataset.

2.6 Developing research into grave sediments

The reconstruction potential of archaeological research is constantly progressing and the limitations repeatedly receding (Brothwell and Pollard 2001, xvii-xviii). The current limitations in interpreting past burial practices and treatments of the dead can be improved through further collection and dissemination of archaeological and experimental data from graves and by using micromorphological and geochemical techniques in combination with field observations. Micromorphological analyses of grave sediments of an experimental pig burial as well as archaeological burials ranging from Viking to Mesolithic age have been assessed in the following chapters (Chapters 4-8) and their contribution to burial archaeology discussed in Chapter 9. An analysis of the grave sediments from the burials in the following case studies (Chapters 4-8) is appropriate to the study of the micro-contextual spatial relationships between the inorganic and the organic materials during the decay of the buried remains (Sections 2.1 and 2.4). Evidence from such analyses could contribute to the interpretations of burials through an assessment of grave sediments. The potential contribution of the InterArChive sampling strategy and method of thin section manufacture and suggestions for the future development of a

geoarchaeological approach to the investigation of archaeological burials are discussed in each case study chapter (Chapters 4-8) and in Chapter 9 (Sections 9.4 and 9.5).

Chapter 3. Methodology

3.1 Methodological approach

Images observed during thin section analysis are a partial, two dimensional representation of a three dimensional reality (Bullock *et al.* 1985; FitzPatrick 1993; Stoops 2003, 11-13). Hence, the displayed size of features may be affected by the plane of the thin section across the material (Harrell 1984) and wedging effects when observing a sample under transmitted light (Stoops 2003, 17), often leading to over-estimation of a clay component (Murphy and Kemp 1984) and a looser packing of closely packed coarse grains (Johnson 1994). Furthermore, by only grinding the thin section to thirty microns thick the smaller components within an assemblage will often still remain hidden to the observer in light microscopy, especially with colourless isotropic materials in a darker groundmass, such as biosiliceous materials (Section 3.4.1.2). Colourless biotic materials (Figure 3.1) can include phytoliths, diatoms, and parasite ova, all of which may be important archaeological markers in interpreting a deposit (Shillito 2013; Battarbee 1988; and Jones 1985, respectively).

a) 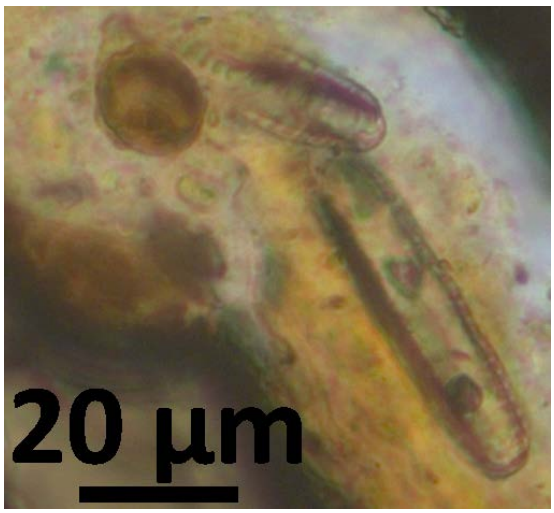

b) 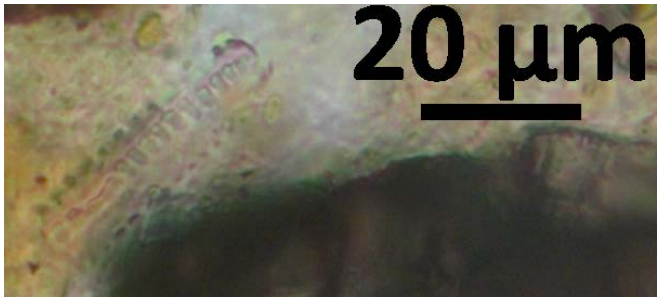

Figure 3.1: Microbes exhibiting colourless (PPL) and isotropic (XPL) characteristics, associated with volcanic glass and a light orange coloured sediment (Site code HST-11, Grave HSM-A-116, Sample 2Z, thin section 842, PPL).

3.2 Dataset

The dataset comprised both archaeological sites (Section 3.2.1) and experimental burials (Section 3.2.2). The samples from the burial sediments were assessed for details of mineral assemblages, organic materials, and micro-scale inter-contextual relationships of assemblages contained within the *gefüge* (for discussion of *gefüge* see FitzPatrick 1993, 35). Controls were taken from all sites, following the predetermined sampling strategy as closely as the individual circumstances would permit. The samples and controls were studied using both micromorphological and geochemical analyses.

3.2.1 Archaeological sites selected

Graves from cemeteries at archaeological sites from Iceland (Hofstaðir), Sudan (Al Khiday), Sweden (Sala Vastmaal) and Syria (Tel Qarassa) were sampled to encompass a range of sediment types and archaeological cultures (Figure 3.2) in order to enable comparison of features from a range of different burial environments. The graves investigated ranged from prehistoric at Tel Qarassa (PPNB) and Al Khiday (Mesolithic) to historic at Hofstaðir and Sala Vastmaal (Sweden). The sediments from the case study sites at Hofstaðir, Al Khiday, and Sala Vastmaal were volcanic, sandy, and clay-rich, respectively. The sediments from these three case studies (Hofstaðir, Al Khiday and Sala Vastmaal) contrasted with the sediments from the burials at Tel Qarassa. Tel Qarassa was a Neolithic tell site, and these types of site characteristically reuse sediments in the area to build the deposits of the site one on top of the other (Shackley 1977, 66), resulting in complex stratigraphic relationships. The analysis of the graves from the Viking cemetery at Hofstaðir (Iceland) offered a comparison to those at Sala Vastmaal (Sweden) through comparable ages (10th and 16th centuries, respectively) and contrasting sediment textures (andosol and vertic cambisol) of the sites. The two prehistoric sites contrasted in their levels of stratigraphic preservation and sediments, with Tel Qarassa presenting the opportunity to sample remains from silty sediments within a building in a tell site compared to the sandy burials at Al Khiday which were exposed to wind erosion. A range of sediment types enabled comparison of micromorphological features in grave sediments from a range of burial environments.

Figure 3.2: Location of archaeological sites selected (adapted from Google maps).

3.2.2 Experimental burials

Pigs were buried by the InterArChive Project (Sections 1.1.1 and 2.5) and the grave fill of one of the pigs has been analysed (Chapter 8). The InterArChive's experimental burials (Section 1.1.1) utilised pigs as substitutes for human cadavers (Usai *et al.* 2014). The InterArChive Project buried ten piglets (stillborn or early post-natal deaths) in five locations around North Yorkshire in 2009, Hovingham (Pigs 1-2), Folkton (Pigs 3-4), Heslington East (Pigs 5-7), West Heslerton (Pigs 8-9), and King's Manor (Pig 10). The pigs were interred for 3 years prior to excavation (Chapter 7). The sites were selected on the basis of a compromise between factors of access and differing sediment types. Variable sediment types were chosen in order to provide a wide range of comparative data for archaeological sites on diverse parent materials and pedogenic processes. An additional variant within the experimental burials was the type of practice associated with the burial depositions (Table 1), including the presence of coffins and grave goods associated with the inhumations. The results from the analysis of the sand sediment from the experimental pig burial at Hovingham (Pig 1) have been discussed in this thesis (Chapter 8).

Table 1: Grave goods and sediment types of the ten piglet burials. Grey cells represent absence of material.

Pig	Location	Sediment type	Coffin	Muslin with foodstuffs	Paint	Hair
1	Hovingham	Sand Limestone				
2						
3	Folkton	Peat bog				
4						
5	Heslington East	Clay				
6						
7						
8	West Heslerton	Sand				
9						
10	King's Manor	Urban				

Since all of the details of the burials were known, traces of materials interred, such as body paint, human hairs, textiles and food items, could be assessed in the samples collected during excavation. Where a trace was found, it was investigated as to how its evidence was preserved in regard to taphonomic pathways and the environment where these processes occurred. The significance of these pathways on the pedological development characteristics of the host sediments was assessed, as was the extent to which this information could be related to the taphonomy and potential to retrieve archaeological evidence from ancient graves.

3.3 Sampling strategy

Samples were collected in relation to the terms of the protocols designed by the InterArChive Project (Usai *et al.* 2014 and Figure 1.1). Parasite and bulk macro samples were collected from the gut region. Multiple samples were collected for chemical and micromorphological analyses, with samples collected around the skeleton (17 for chemistry and 3 for micromorphology) and two controls within each grave (Figure 1.1). Methods of collection (Goldberg and Macphail 2003) and storage conditions (Sheppard and Addison 2007) were standardised for each sample type. All samples were stored at relatively low temperatures (3° C) as a compromise between to limit further fungal and microbial growth (Anderson 1987), while remaining above freezing point to avoid physical disturbance resulting from volume changes and the related destructive formation of ice crystals. Where site and sedimentary conditions allowed, samples for thin sections were collected utilising Kubiena tins. The alternative method used

was block lifting. Both sampling methods were carried out with care to reduce disturbance to a minimum.

The InterArChive project therefore developed a sampling strategy for micromorphology controls and samples to be taken at five locations within each grave and one control per site outside of any grave (Figure 1.1). The quantity of micromorphology samples collected along the skeleton was not increased to the same number as the chemistry samples, due to the size of the Kubiena tins and the inclusive nature of these samples. Unlike chemistry samples, which can be collected by scraping gently across a surface with a leaf trowel, the tins were required to be inserted into a deposit downwards for 3-4 cm. This was not altogether appreciated by the majority of archaeologists directing the excavations at sites, where the protection of bones, particularly phalanges, was in some cases of greater concern. Additionally, for each Kubiena tin collected two thin sections were produced, one tangential and one perpendicular to the body. Time and material resources demanded by each sample differed between chemical organic analysis and micromorphological analysis. These reasons led to a revised strategy for the distribution of micromorphology samples, to be collected at three of four points around the body for each inhumation. The skull, pelvis, and feet areas (location numbers 1, 2, and 3 or 4 respectively), with any additional areas of interest where a tin could be placed adjacent to the body and would physically fit within an often narrow grave cut (these additional samples are listed as Sample A *"x"*). The experimental burials received additional sampling, with a control collected from the site before the pigs were interred (C0 control), in order to enable comparisons between pre- and post-burial sediments to obtain a representative interpretation of the effect of the burial on the sediments.

3.4 Thin section manufacture, observation and analysis

Thin sections which were produced from cutting the micromorphology blocks oriented either tangential or perpendicular to the skeleton, are referred to hereafter as "t" or "p" samples respectively. For example, a thin section tangential to the skull would be written as "1t"; as the number denotes the area of the body (Figure 1.1) and the letter represents the tangential orientation of that section to the body.

3.4.1 Manufacture

Micromorphology samples were collected in the field by inserting Kubiena tins into areas of recently cleaned and undisturbed sediment. The Kubiena tins used were of three sizes but roughly similar rectangular shapes (83 x 50 x 32 mm, 83 x 55 x 42 mm, and 65 x 38 x 28 mm). This sample was then wrapped and stored at 3°C in the laboratory. Samples were dried through acetone vapour exchange, rather than low temperature oven drying (Sections 2.1 and 3.4.1.1), using AR grade acetone and anhydrous granular calcium chloride as a desiccant and impregnated under vacuum conditions with Polylite 32320 resin (Miedema *et al.* 1974). The embedding resin was prepared as a mixture of 375 ml Polylite 32320, 0.5 ml MEKP, and 20 ml AR grade acetone. Acetone was added to the mixture to decrease viscosity and lengthen curing time, allowing the resin to permeate through the smaller pores of the samples. The resin impregnated block was slowly cured over 3 weeks at room temperature in a fume hood and had a final curing in a vacuum oven at 40°C for five days. The finished block was cut with a Buehler Delta Petrocut abrasive cutter, polished using a Buehler Motopol with 800, 1200 and 2500 grit carbide papers and mounted to a glass slide with an epoxy resin (Logitech Epoxy AB at 4:1). The glass used was 11 x 7.6 cm and 1.89 mm thick window glass. The glass slides were hand lapped with 15 µm Al_2O_3(aq.) to create a more effective bonding surface, and produced a slightly textured surface when viewed under plane polarized light (PPL). The mounted samples were then cut again and lapped on a Logitech LP50 using 15 µm Al_2O_3 suspended in ethylene glycol to 30 µm thick (Figure 3.3). Final polishing was performed on a Buehler Motopol using soft cloths saturated with Buehler MetaDi 3 µm and 1 µm monocrystalline oil based suspensions. Polishing created a study surface that was as even in thickness as possible, ensuring that the optical characteristics which alter with the amount of sample that the light had to pass through, such as colour, were similar at high magnifications and aiding in the thresholding properties attributable during image analysis.

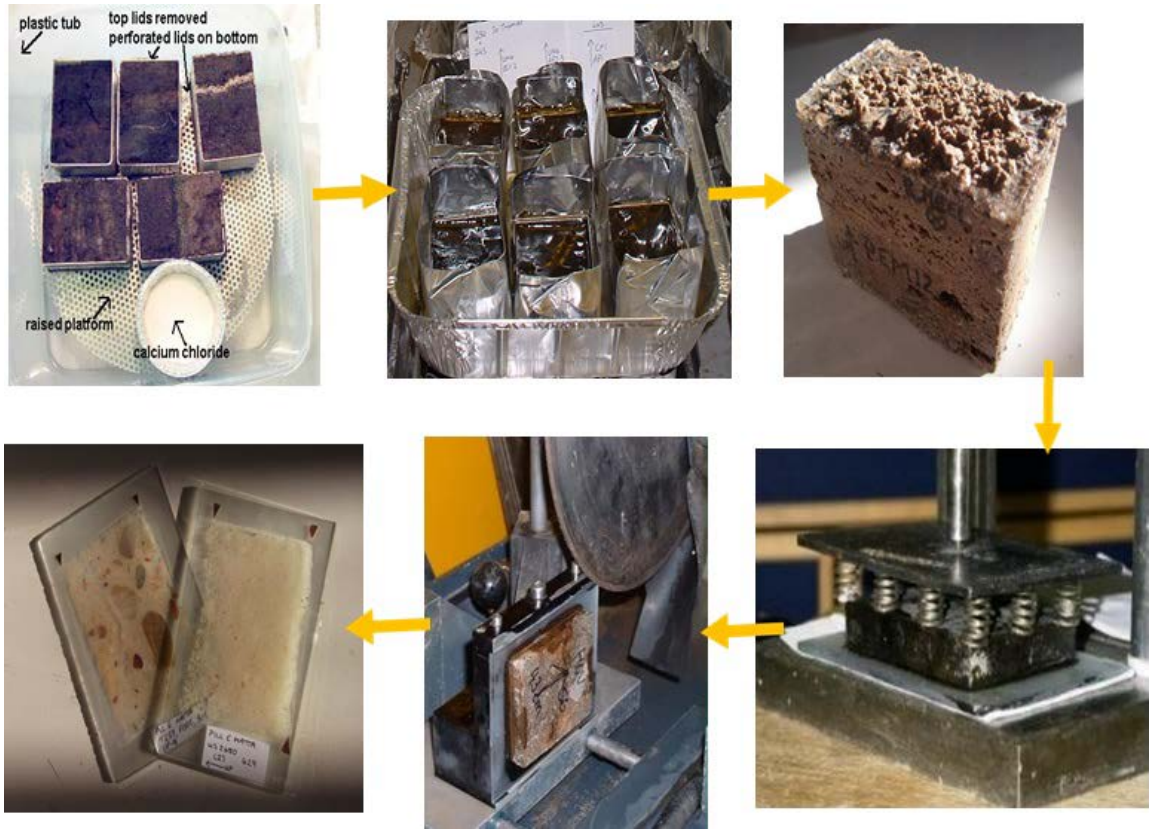

Figure 3.3: Photographs of samples during the stages of thin section manufacture: acetone vapour exchange, resin impregnation, an impregnated uncut block, a cut and mounted block in a compression jig during bonding to a glass slide, the removal of excess material from a slide with an abrasive cutter and a finished thin section (listed from top left to bottom left, photos courtesy of Sabina Ghislandi).

3.4.1.1 Rationale for manufacture method

There are two main methodologies for the removal of water from micromorphology samples currently in use, drying slowly in a low temperature oven between 25-35°C (air drying) and acetone replacement, both of which have their merits (Appendix II). Air drying is well suited to sandy and fragile samples as it reduces handling time before they are impregnated. Acetone replacement however, is well suited to drying samples with high amounts of organic matter and water retention without causing desiccation cracks to appear (Courty *et al.* 1989). Due to the high amounts of organic material possible in samples taken adjacent to a corpse, the importance of the accurate representation of voids within a thin section, and the wide variety of sediments included in the project, which included peaty sediments, acetone vapour was chosen as the standard drying method. In reference to the Icelandic samples (Section 3.2.1), it was noted that air drying was better suited for allowing recognition of the granularity of sediments on volcanic ash deposits than drying through acetone vapour replacement (Shin and Stoops 1988; Colombo *et al.* 2007; Sedov *et al.* 2010, 278). Acetone drying was used on the samples from Hofstaðir despite this factor, in order to keep the methodology consistent for all of the samples in this

research initiative. For the purposes of this research, it was more valuable to have samples processed through a consistent methodology, enabling more reliable and valid interpretations between, as well as across, archaeological sites and against the experimental results, than to highlight the granularity and voids in the sediments from samples of a single site.

3.4.1.2 Visibility of colourless isotropic materials in thin section

Material was generously donated by YAT (Yorkshire Archaeological Trust) from a hearth deposit, which was known to contain phytoliths, wood ash and a dark brown coloured fine material sediment. The deposit was air dried (placed in an low temperature oven at 35°C until less than 1% change in weight was measured to have occurred over a 24 hour period) and embedded in resin (Polylite) (Section 3.4.1). A single thin section was created (Section 3.4) and observed during the grinding process at various stages between 100 and 20 µm sample thickness (Figure 3.4). The images of the fine material in Figure 3.4 changed in colour from a darker brown to a paler yellow-brown colour (PPL) as the sample decreased in thickness. The colourless isotropic biogenic silica materials were more readily identified in transmitted light microscopy when not masked by a dark fine material. It is inferred that materials with these characteristics when embedded in a dark coloured groundmass are more readily identifiable when the thin section is ground thinner than 30 µm, which reduces the amount of sample that the light must pass through, thus diminishing the dark hue of the overlying fine material.

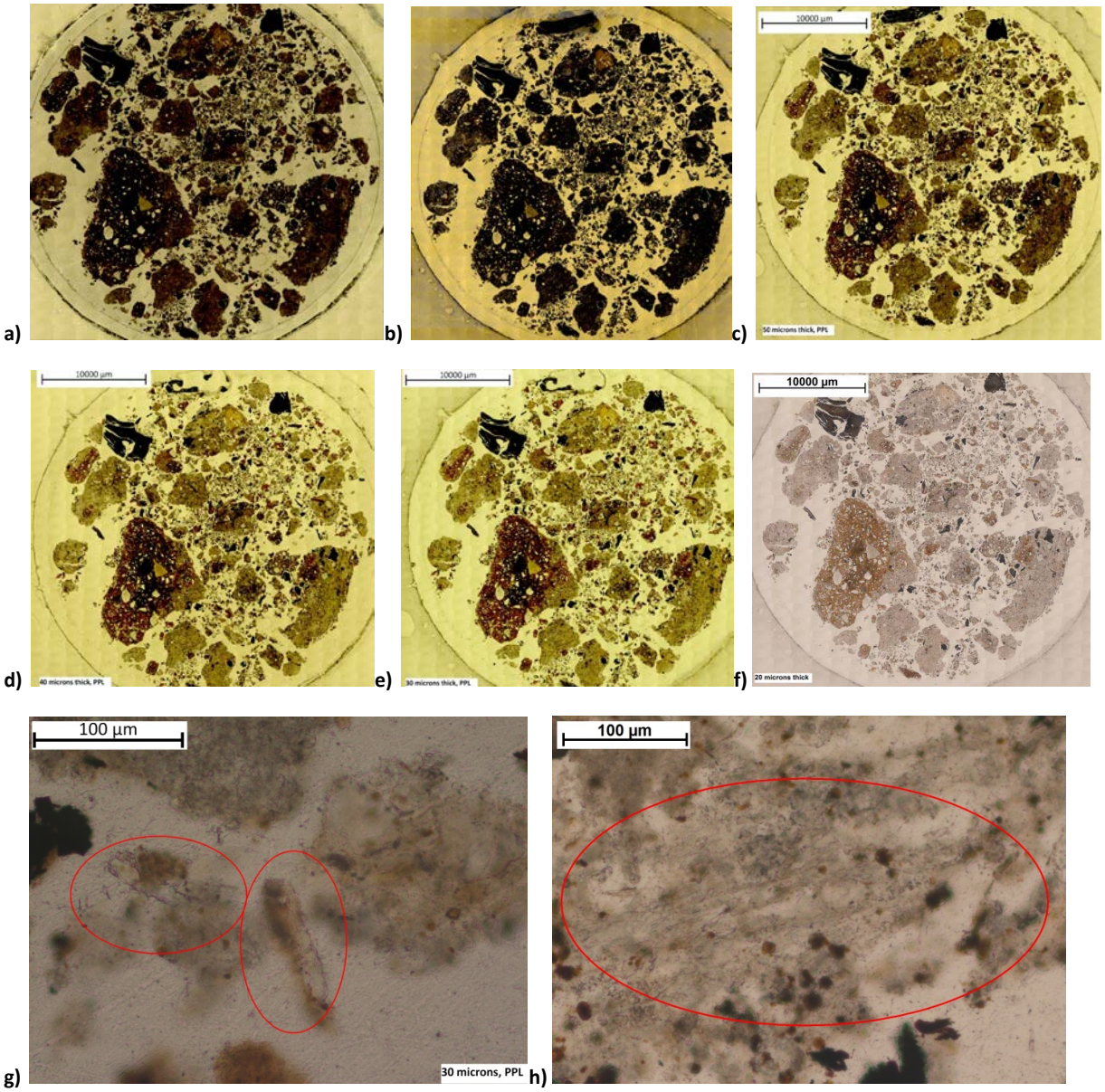

Figure 3.2: Thin section from a hearth deposit photographed at decreasing thickness during the grinding process. a) Mosaic image(PPL) taken at sample thickness of: a) 100 µm , b) 60 µm, c) 50 µm, d) 40 µm, e) 30 µm, and f) 20 µm. g) Photomicrograph of phytoliths observed in the thin section when ground to 30 µm thickness (PPL). h) Photomicrograph of phytoliths observed in the thin section when ground to 20 µm thickness (PPL). Images g) and h) are different phytoliths.

3.4.2 Observations

Thin section observations were made using a petrographic microscope (Zeiss Axio Lab A1) with a 10x magnification in the binoculars and 2.5x, 5x, 10x, 20x, and 40x objectives. A mobile polaroid film was located below the sample and the analyser was held in a fixed position. Discrimination between birefringence values of low order interference colour materials were performed on the Nikon Labophot petrographic microscope, which contained a quartz wedge as well as mobile polariser and analyser. Both the Zeiss Axio Lab A1 and the Nikon petrographic microscopes were equipped with Zeiss

AxioCamERc5s cameras and Axio Vision imaging software. Reflected light images were created through the use of reflected light from a halogen bulb and a dark field cube. Large composite images of entire thin sections were made utilising the Zeiss Axio Vision Mosaix software on the Zeiss Axio Scope A1 microscope with motorized *x/y* stage, 10x binoculars, 2.5x, 5x, 10x, 20x and 40x objectives, and mobile polariser and analyser. The Zeiss Axio Scope A1 was equipped with the higher resolution Zeiss AxioCamMRc camera. SEM-EDX work was performed at the University of Stirling on a Zeiss Evo Ma15 with SE, Backscatter, VPSE and Oxford Instruments 80 mm^2 detectors and was calibrated with a cobalt standard prior to use. SEM-EDX measurements were taken as spot ID points, rather than as evenly spaced points along a transect, to ensure that the impregnating resin was not accidentally scanned during elemental analysis.

Micromorphological observations were made using the terminology of Bullock *et al.* (1985), Stoops (2003), and Courty *et al.* (1989). Related distribution terminology used to describe the relationship between the coarse and fine fraction within the sediments in thin section was used as listed by Courty *et al*. (1989, 73-74) (Appendix II). Where multiple fabrics were visible within a single thin section, the thin section was sub-divided into micro-units 1, 2, *etc.*, in order to preserve the recording of multiple sediment fabrics which could correspond to multiple contexts in line with the theoretical framework of contextual archaeology (Butzer 1982, 12). The terms weathering (transformations in soils or sediments) and alteration (to indicate the visible changes due to the transformation of minerals, or their replacement by other minerals) of minerals refer to different processes (Stoops *et al.* 1979 and Delvigne 1998). The term neoformation refers the new formation of minerals in a soil. The weathering of minerals was described and measured according to the terms and scales of measurement listed in Delvigne (1998, 55-56 and 80-91), of which a brief summary is given below (Table 2 and Table 3), although it is in no way a substitute for a description of the criteria given in the original source (Stoops *et al.* 1979, Stoops 2003, Delvigne 1998). Where textile and organic materials were observed, in light microscopy or SEM, their preservation was measured in accordance with the scales of preservation proposed by Bell *et al.* (1996) for materials excavated through applied experimental archaeology.

Table 2: Summary of scales of measurement to describe the extent of mineral weathering (data taken from Delvigne 1998: 55-56)

Scale number	% Volume of primary mineral	% Volume altered
0	100 to 97.5	0 to 2.5
1	97.5 to 75	2.5 to 25
2	75 to 25	25 to 75
3	25 to 2.5	75 to 97.5
4	2.5 to 0	97.5 to 0

Table 3: Summary of the basic levels of terminology adopted for describing the patterns of mineral weathering (data taken from Delvigne 1998: 80-91)

Descriptive Classes	Sub-classes
Linear	parallel linear
	irregular linear
Pellicular	regular pellicular
	irregular pellicular
Speckled	
Digitate	

Micromorphological observations regarded the identification of materials, their frequency, and the identification of micro-scale spatial relationships in terms of orientation and distribution. Quantifications at the observation stage were made utilizing the abundance charts of Bullock *et al.* (1985, 24-25). The results from the use of estimated abundance charts have been shown to vary between investigators, but they are a useful tool for the aims of micromorphology (Bullock *et al.* 1985, 23).

The results were recorded in micromorphological observation sheets (Figure 3.5). Features were observed under PPL, XPL and some were observed under additional settings such as reflected light (OIL, RLDF) for an assessment of characteristic traits to aid in identification. The observation sheet was based on the work of Courty *et al.* (1989), pedofeatures as described in Stoops (2003), and a detailed description of rocks and minerals. Observation sheets were used to create a more concise table of observations for each case study (Chapters 4-8). Recorded observations included categories pertaining to location and orientation of the section, basic attributes, voids, pedofeatures, rocks and minerals, organics and additional comments (Figure 3.5). The size limit between coarse and fine sized materials was determined by the InterArChive project as 50 μm. The sub-heading "organics" is used in the sense

of carbon based materials and therefore includes some materials of biological origin (shell is a carbon based biologically formed material and phytoliths and diatoms silica-rich biologically formed materials). The coarse to fine related distribution terminology of Stoops (2003) was adopted for the InterArChive project, and has been substituted with the terminology of Courty *et al.* (1989) in order to reflect a broader relevance to geoarchaeology. The terms single population, linked, coated, linked and coated, intergrain aggregate, and embedded, suggested in Courty *et al.* (1989), have been used rather than the terms monic, gefuric, chitonic, enaulic and porphyric used to describe coarse to fine related distribution in Stoops (2003).

The comments area in the table of observations was used to include items of note not otherwise recorded in the observations table including pedality and, where appropriate, on boundaries between micro-units. The term micro-unit is used in the following chapters to differentiate between differences in *gefüge* (*sensu* FitzPatrick 1993, 35) within a single thin section; some recent literature refers to micro-contexts (*e.g.* Matthews *et al.* 1997). Where boundaries between micro-units are horizontal these have been numbered with "1" at the uppermost part of the section, and where the boundaries between micro-units are not horizontal micro-unit "1" in a thin section has been labelled as the largest micro-units based on surface area of the thin section. Where applicable, the numbering of micro-units is provided in mosaic images of the sections (Appendix I), allowing correlation between the images and the descriptions of the observations.

Thin Section Description Recording Sheet

TS: Site code:
Micro-unit: Gr.:
Sample ID: Sk & fills:
Boundary (sharp <30, clear 30-60, diffuse >60µm; smooth, wavy, irreg.):

Groundmass

c/f ratio (50 µm limit):
Related distribution of c/f materials (single population, linked and coated, coated, intergrain aggregate, or embedded (Courty *et al.* 1989*) which correlates with the InterArChive use of Stoops, 2003 terminology of: monic, gefuric, chitonic, enaulic, or porphyric respectively):
Sorting: (unsorted, poorly, well, perfectly):

Micromass

Colour (x5 objective, PPL):
Limpidity (translucent, transparent, cloudy, opaque):
B-fabric (undifferentiated, cristallitic, striated, speckled):

Voids (% abundance, size,)
Vesicles:
Channels:
Chambers:
Vughs:
Cracks:

Coarse materials

Inorganics [type: %, size (µm, max.), colours, form, extent (pellicular, irregular linear, parallel linear, cross-linear, speckled, digitate), degree (0= <2.5% altered, 1=2.5-25%, 2=25-75%, 3=75-97.5%, 4 =<97.5% altered)), distribution and orientation]

Minerals (abundance %, type, colour in PPL & XPL, size, extent and degree of weathering)

Tectosilicates:
Inosilicates:
Nesosilicates:
Phyllosilicates:
Tephra including descriptions of texture (vitric, hypocrystalline or holocrystalline) vesicularity (displayed as vesicles abundance as a % of volume):
Other (e.g. rocks, calcite, ash, diatoms, phytoliths):

Organics type, % abundance, size, colours, form, degree of preservation (excellent, good, fair, or poor), distribution, orientation:

Amorphous:
Plant:
Other (e.g. bone, excrement, textile, fungal remains):

Pedofeatures

Pedofeatures related to voids, grains or agg.: [%, size, related feature, and colours]
Intrusive: Coatings:
Matrix:

Hypo-coatings (related, touching a surface):
Quasi-coatings (not touching):
Infillings:
Impregnative:

Pedofeatures not related to voids, grains or aggregates
Nodules: [% abundance, orientation, distribution, size, colour, laminations (</>30 μm), boundary, fragmentation]
Excremental Pedofeatures (% abundance, colour PPL, size, angularity, size of clasts (*e.g.* CZS):

Peds (type and size)
Other notes and comments on the description of the sample as seen in thin section:

Figure 3.5: Example of a blank micromorphology observations sheet, with text in grey illustrating criteria used in the description and examples of materials possible within the "other" categories. Terminology follows Stoops (2003, 32-128 chapters 4-9) which is in part based on that of Bullock *et al.* (1985). The symbol (*) denotes terminology which does not follow Stoops (*ibid*) but instead is taken from Courty *et al.* (1989, 73-74). Abbreviations used are as follows: plane polarised light (PPL), clay sized (C), silt sized (Z), sand sized (S).

3.4.2.1 Identification of minerals

Mineral grains were identified throughout the samples in the following chapters through observations of their optical characteristics. Within optical microscopy, especially in transmitted light microscopy, it may be that the structural characteristics relating to external morphology are the most well displayed features of minerals along with colours (including pleochroism) and interference colours (as a function of the birefringence value of the material and the thickness of the sample; Figure 3.6). Therefore minerals were first subdivided into order level, (*i.e.* tectosilicates, sorosilicates, cyclosilicates, nesosilicates, inosilicates, phyllosilicates, carbonates, sulphates, *etc.*). Further sub-identifications wherever possible were completed to family level, based on criteria such as cleavage planes and angles, (*e.g.* use of cleavage planes and angles to discern between pyroxenes, single chain silicates, and amphiboles, double chain silicates, from within the larger class of inosilicates).

The combination of the above mentioned characteristics of crystallographic habit, colour, interference colours, cleavage, along with relief, twinning and zoning can in some instances be used to identify some minerals in thin section with a relative degree of confidence (MacKenzie and Adams 1994, 2) to group level (*e.g.* discernment of members of the chlorite group from the muscovites and biotites of the micas, or clinopyroxenes from orthopyroxenes of the pyroxenes). Mineral identifications beyond this (group) level of specificity may require additional analytical techniques capable of illuminating the structural arrangement within a crystal, such as XRD (x-ray diffraction). Results from XRD could give additional structural information compared to SEM-EDS elemental analysis which can not discriminate between polymorphs, minerals which share an identical chemical composition (*e.g.* calcite and aragonite).

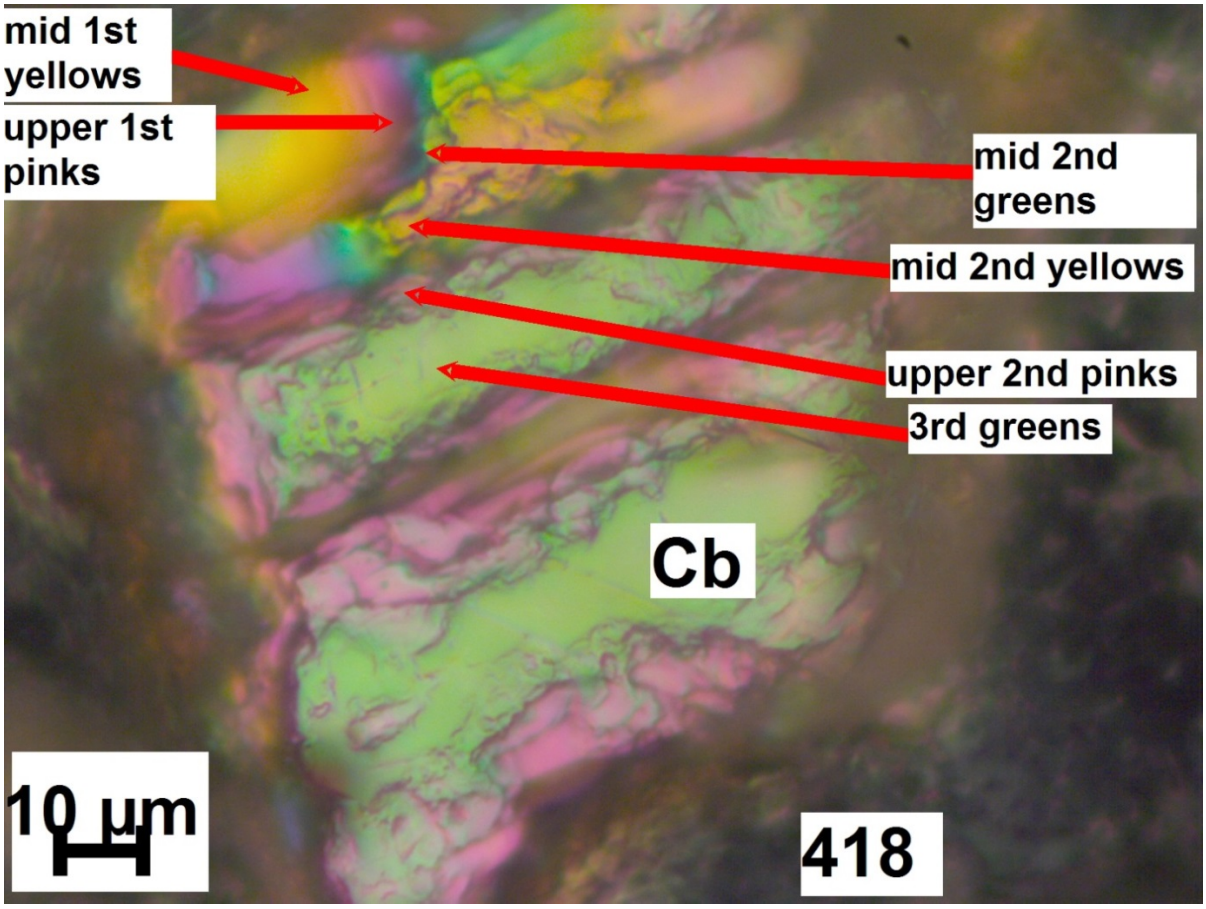

Figure 3.6: Calcite (Cb) grain of rhombohedral habit and fourth order interference colours (TS 418, XPL). Interference colours decrease towards the edges of the crystal (top left corner) (due to the lessening amount of the crystal that the light is traversing through at this angle). The thin section has in this instance been cut parallel to one of the cleavage planes leaving a second cleavage plane perpendicular to the angle of cut (visible as horizontal ridges across the crystal).

3.4.3 Interpretations and analysis

Micromorphological observations were integrated with SEM-EDX and point counting, where applicable. Micromorphology, when used as a stand-alone technique, has been criticised as a methodology which can yield subjective results with discrepancies between different operators, but can be strengthened through the use of additional quantitative and semi-quantitative techniques, which in burial and trace analysis can greatly enhance interpretability of results (Heizer and Cook 1956, 232 and 242; Shennan 1997). Where decisions between observations and interpretations of micromorphological features in relation to processes could be contested, use of specific texts aided in the identification and interpretation of allogenic and authigenic materials (Stoops 2010, 16), decomposition of organics (Babel 1985, 74-87) and the recognition of artefacts of manufacture (Bullock 1985, 15).

3.4.4 Point counting

Most quantitative or semi-quantitative work on thin sections has been on voids and porosity measurements (Jongerius *et al*. 1972; Jongerius 1974; Bouma *et al.* 1979; Marcelino *et al.* 2007; Pagliai 2008; Stoops 2010) or clay coatings and infillings (Grossman 1964). Point counting has been employed successfully for micro-charcoal quantification (Bennett *et al.* 1990) and deposits of illuvial clay (Eswaran 1968; Murphy and Kemp 1984). Quantitative and semi-quantitative analysis in archaeological investigations of burial sediments has produced some valid results capable of supporting interpretations of processes (Heizer and Cook 1956, 232 and 242). Although there have been some criticisms made on the reproducibility of results by different operators (McKeague *et al.* 1978; Murphy 1983; Miedema 2002) and alternative techniques have been tested (Terribile and FitzPatrick 1992, 1995), point counting maintains its effectiveness (Kuhn *et al.* 2010, 238) and was selected for this work.

Point counting was carried out with a Zeiss AxioScope A1 microscope with *x/y* motorised stage, AxioCam MRc camera and the "Point Counting" module from the AxioVision 4.8 software. This combination of equipment allowed for point counting to be carried out on a systematic basis according to distance intervals set by the user to move the slide the desired number of micrometres across on the *x* and *y* axes and for the screen to display an image with a crosshairs over the material to be point counted at each step. The method was only applied to a case study on a site at Hofstaðir (Chapter 4), and full details of the procedure employed in this case study have been listed in Chapter 4 (Sections 4.2.3-4.3.5).

3.5 Geochemical analysis

Sites investigated by the InterArChive Project were sampled for micromorphology and geochemistry. The chemistry samples were collected and analysed by the chemistry team. The samples for geochemical analysis were collected as loose material with a metal trowel and wrapped in a sterilised aluminium sheet in a plastic bag and stored in chilled conditions. The sub-sampling was completed after initial freeze-drying and subsequent homogenization and particle size discrimination of the collected material to produce a sub-sample of only a few grams of <200 μm sized material. This selected sediment material was then analysed for total organic and inorganic carbon (TOC and TIC), basic elemental analysis (CNOH), and gas chromatography (GC). Selected wood samples were analysed by pyrolysis (Py-GC) for information on the source of the woody materials at various levels of decomposition of cellulose, hemi-cellulose and lignin components.

3.6 Bioarchaeological analysis: floatation and parasite analysis

The floatation samples were processed and analysed by Dr Allan Hall, and the parasite samples were processed and analysed by Dr Andrew Jones, as an integral part of the InterArChive Project. The size of the samples for parasite and macro-flora analyses was approximately 150 g. The macro-scale flora analysis by floatation method and the parasite analysis would both have benefited from a sampling set larger than a single 150 g sample, such as 1 kg samples taken at a selection of sampling sites around the body. However, sampling restrictions limited the maximum volume to sediment available. The entirety of the sample collected for macro-scale analysis by floatation was utilised, and a 3 g sub-sample was processed for parasite analysis. Discrimination between ancient and modern macrofossils (Section 2.3) were made where macrofossils were found (Section 4.1.3). No parasite ova were identified by Dr Andrew Jones from any of the case studies discussed in the following chapters (Chapters 4-7).

Chapter 4. Case study: Hofstaðir, Iceland

4.1 Introduction

In the broadest terms, the sediments of Iceland are referred to as andosols (WRB) and mostly comprise basaltic to andesitic volcanic materials (Figure 4.1). The sediments of the island, albeit young, display evidence of erosional and transportation activities (Arnalds 2005). Basaltic volcanic glass, as opposed to more silica rich materials, is more readily weathered by pedogenesis leading to the production of allophane, imogolite and ferrihydrite (Arnalds and Oskarsson 2007, 45). A critical review of the micromorphological study of European volcanic sediments is in Stoops (2007) and Stoops and Gérard (2007).

4.1.2 Archaeology and sediments of Hofstaðir

Hofstaðir is an archaeological site in the district of Myvatnssveit, in north east Iceland (64.23 /-19.64, <50 m OD), dated to the mid-tenth century AD and in use for a duration of 90 years (Lucas 1999 and 2001). It was excavated briefly in 1908 (Bruun and Jonsson 1911), which determined the site to be a Viking settlement containing a large hall considered to be a temple. However, later studies challenged this interpretation of ritual activities and instead proposed the site as a farm with all the everyday, domestic activities that entailed (Roussell 1943). The majority of the detailed information on the site arises from the results of the excavations held between 1991 and 2002 (Lucas 2009). The later excavations were performed by the Institute of Archaeology in Iceland and members of NABO (North Atlantic Biocultural Organisation), funded by several bodies (RANNIS, NSF, NOS-H, NGS, and the Icelandic Ministry of Culture). The interpretation of the site, as a self-sufficient unit engaged with a wide assortment of activities ranging from the rearing of domesticated animals, metal-working (Espelund 2007), and ritual animal sacrifices (Lucas and McGovern 2008), is supported by structures and artefacts, anthropogenic and palaeoecological, recovered in contextual association (Roussell 1943; Lucas 2009, 8; Ogilvie, 2010, 501). Previous excavations at Hofstaðir have yielded a wealth of information on the archaeology (Friðriksson and Vésteinsson 1997; Batey 2011), sediments (Arnalds *et al.* 2001) and micromorphology of the area (Simpson *et al.* 1999; Milek *et al.* 1998; Milek and Simpson 1999). The graves and sediments studied in this research were obtained from the 2011 excavations held by the Institute of Archaeology, Iceland, and InterArChive members from the University of York.

Recent land use of the grass covered andosols at Hofstaðir is limited, with the only structure in continuous use in the area being a farmhouse 100 m away (Ogilvie 2010). The main aggressive factor

to the area is sediment erosion (Arnalds 2005), especially as influenced by grazing practices (Simpson *et al.* 2004). Sediments in Iceland are well documented (Romans *et al.* 1980, Bartoli *et al.* 2003; Arnalds 2004), and the threat of their deterioration is closely monitored (Sigbjarnarson 1969; Arnalds *et al.* 2001). Ongoing works by the Agricultural Research Institute (RALA) and the Sediment Conservation Service (SCSI) are attempting to limit this process.

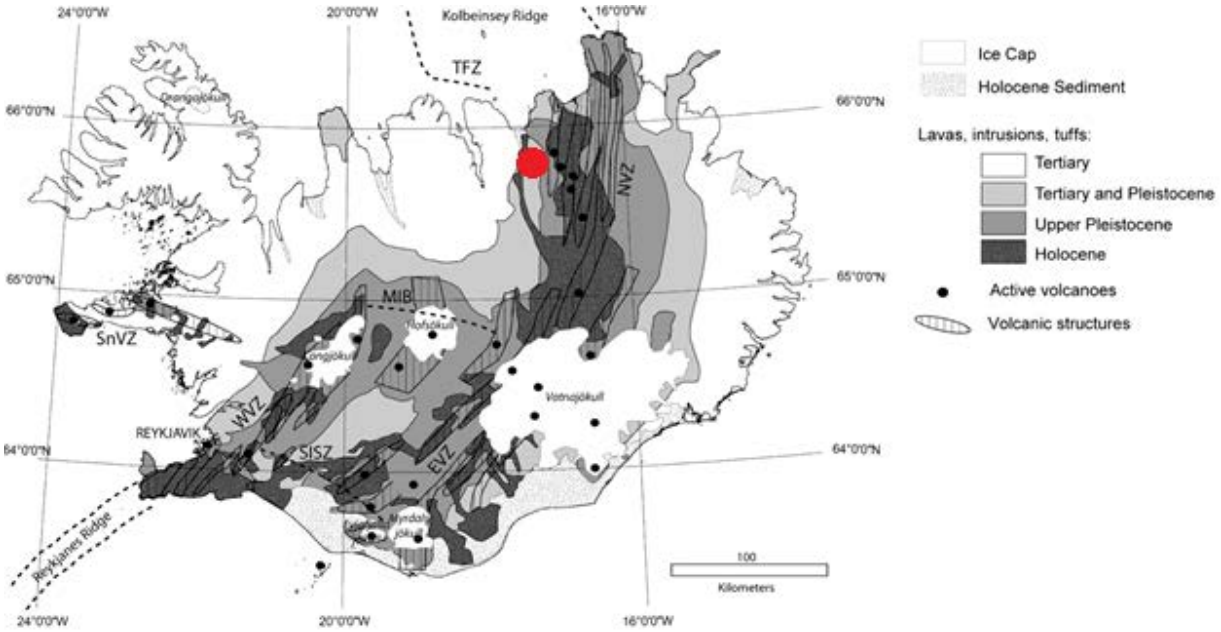

Figure 4.1: Map of sediments and volcanic activity and deposits in Iceland (modified from Le Breton *et al.* 2010). Location of Hofstaðir is shown by the red dot.

The thinly vegetated histic andosols surrounding the site of Hofstaðir in north east Iceland (Arnalds 2010) overlay the mixed Tertiary and Pleistocene deposits, adjacent to the Holocene river alluvium (Figure 4.2). The deposits have mild to undisturbed tephra layers allowing for detailed dating by tephrachronology throughout the settled period of Iceland's history (mid-eighth century AD) (Price and Gestsdottir 2006, 131). Andosols are characterised by a dominant abundance of andic materials, with allophane contents reaching 30%, and frequent (5-15%) ferrihydrite; although, there is a relationship whereby an increase in organic matter correlates with a decrease in ferrihydrite and allophane content (Arnalds 2004). Histosols by contrast are designated by a high (>20%) carbon content (WRB 1998). The parent materials of Iceland are the tephra layers and aeolian sediments, largely from the vitrisols in central Iceland. These unstable desert interior sediments are low in organic matter and high (>30%) in glass content (Arnalds 2004). The interaction between the buried human remains and the rate and method of the progression of weathering on the silicic tephra materials in the graves was assessed for

this work through a detailed micromorphological study. Such analyses may prove useful in answering questions regarding how the degradation of a corpse affects, and is affected by, sediments in a young volcanic sediment. The site was chosen for this study as the burials have been dated to within a narrow timeframe through intact tephra layers, volcanic sediments susceptible to weathering processes to allophane. Hence, the site was appropriate for investigating the weathering processes of the tephra as the inorganic fraction of the sediments can be investigated as well as the post-depositional processes affecting the buried remains.

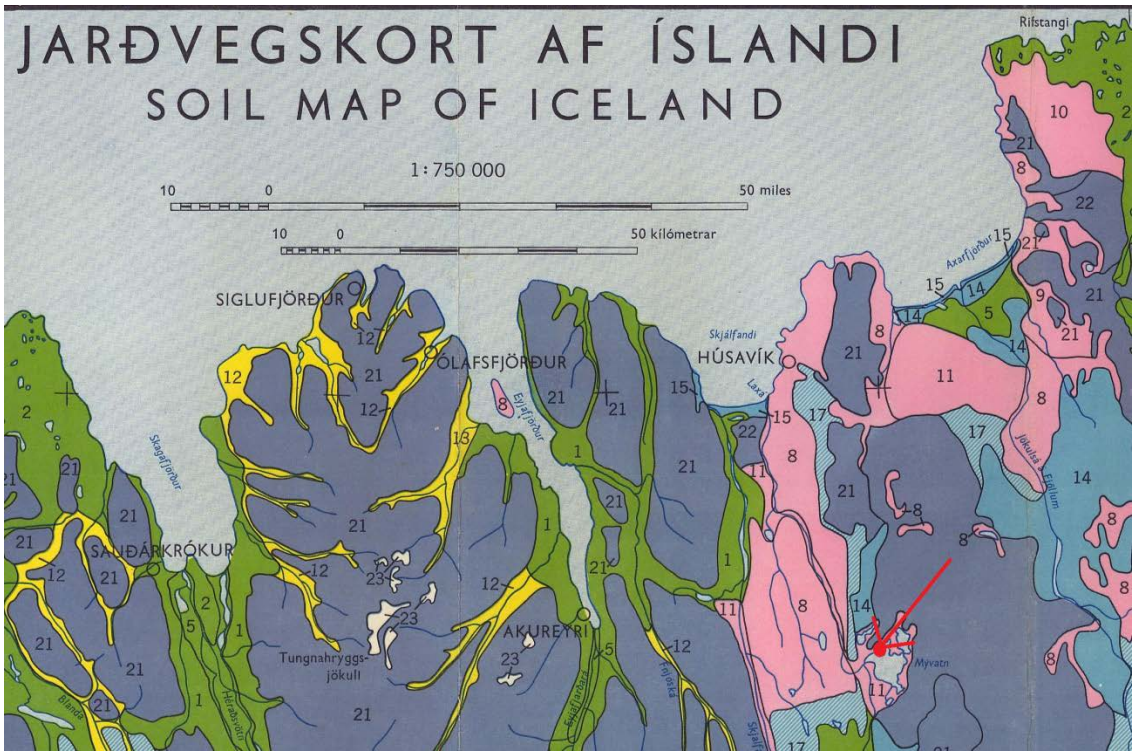

Figure 4.2: Sediment map of north east Iceland at 1:750,000 (adapted from Nygard 1959). Hofstaðir (red arrow and dot) is located on this map as a silty sediment in the pink region no.11, "Silt loam: 15-100 cm thick, on gravelly or stony material. Major associate: peat on gravel and sand. Broad valleys and undulating lowlands" (*ibid*). The surrounding areas (no. 18 and 22, within the dark blue coloured regions on this map) are areas with neither sediment nor vegetation.

4.1.2 Sediment mineral weathering in andosols

The development of a volcanic sediment relies to a significant extent on the weathering of the mineralogical materials deposited during volcanic eruptions. Volcanic silicates are weathered to form allophane and succedent halloysite, both very fine clay-sized materials, and therefore not large enough to be suitable for observations by micromorphology at the scale of light microscopy. Allophanes can be defined as "members of a series of naturally occurring minerals which are hydrous alumina silicates with short-range order and a predominance of Si-O-Al bonds" (van Olphen 1971 in Parfitt 1985, 23).

Halloysites are formed by weathering of allophanes. Also in the group of sub-microscopic tephra weathering products are mineralogical materials known as imogolites. Imogolite is defined as "a tubular mineral about 22 Å in diameter with a wall about 7 Å thick". The term is limited to materials of the formula (OH $3Al_2O_3SiOH$) and a coating of AlOH groups comprising the external surface (Parfitt 1985, 23).

Allophane can form from andesitic glass in as little as 300 years but it may take up to ten times that length to form from a rhyolitic substrate. The weathering product halloysite forms at the opposite rates for andesitic and rhyolitic materials (100,000 years and 7,000 years respectively) (Jongmans *et al.* 1995), the differences having been attributed to weathering patterns affecting the surface of the grains as well as inhibition by iron oxides formed during the allophane stage (Kirkman and McHardy 1980). Although electron microscopy was available and utilised in this work, the sizes of allophane and imogolite (short range order silicates) limited their detailed analysis in this study, which primarily concerns an assessment of sampling strategies for micromorphology and optical microscopy (Objectives 2 and 3 in Chapter 1, Sections 1.3.2 and 1.3.3 respectively).

4.1.3 Biota in the sediments

Sediment biota was analysed by bulk samples (Chapter 2, Section 2.6) of loose sediment from the graves at Hofstaðir by AR Hall. The remains of an elytron (wing) fragment from a beetle, root fragments, lesser clubmoss spores, and fungal sclerotia were identified. The elytron fragment was not able to be identified to a classification narrower than beetle and the root hairs were interpreted by the analyst as most probably modern in origin. By contrast, the spores and sclerotia were interpreted as ancient materials which had been preserved. The lesser clubmoss (*Selaginella selaginoides*; Figure 4.3) is found in wet moorland or peat-like habitats (Stace 2010, 7). This species is particular in the environmental conditions it inhabits, requiring "cool, stable settings and groundwater near the surface during most or all of the growing season" (Heidel and Handley 2006, 3).

Figure 4.3: Lesser clubmoss (*Selaginella-selaginoides*) (Vujik 2015).

Ectomycorrhizal fungi, as found in GR 114, play an important role in plant-sediment nutrient interactions (Smith and Read 1997). These fungi do not reproduce through the production and dispersal of spores but rather through sclerotia (Figure 4.4). Some fungi, such as those in the order *Boletales* which includes parasitic fungi, may reproduce through the production of spores. Spores are isotropic and when they are also colourless and well rounded, care should be taken not to confuse these objects with bubbles of air trapped within the resin during the impregnation process and in the same plane as the thin section (Figure 4.5). Sclerotia have an external rind, which is capable of diminishing and expanding in size in dry and wet conditions, respectively, with no limitation to the number of times this shrink-swell cycle can occur. The preservation of sclerotia in sediments and sediments for many years is a well-known characteristic trait associated with the ability of ectomycorrhizal fungi to persist in even extreme environmental conditions (Hrenko *et al.* 2009).

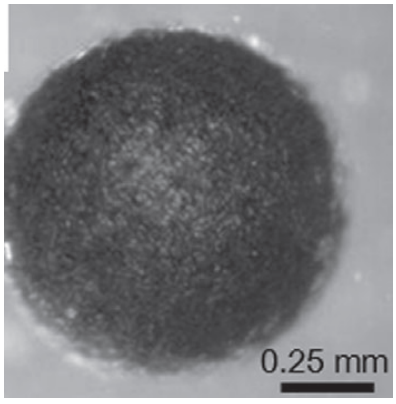

Figure 4.4: The sclerotia of *Cenococcum geophilium*, an example of mycorrhizal fungi (image taken from Obase *et al.* 2014).

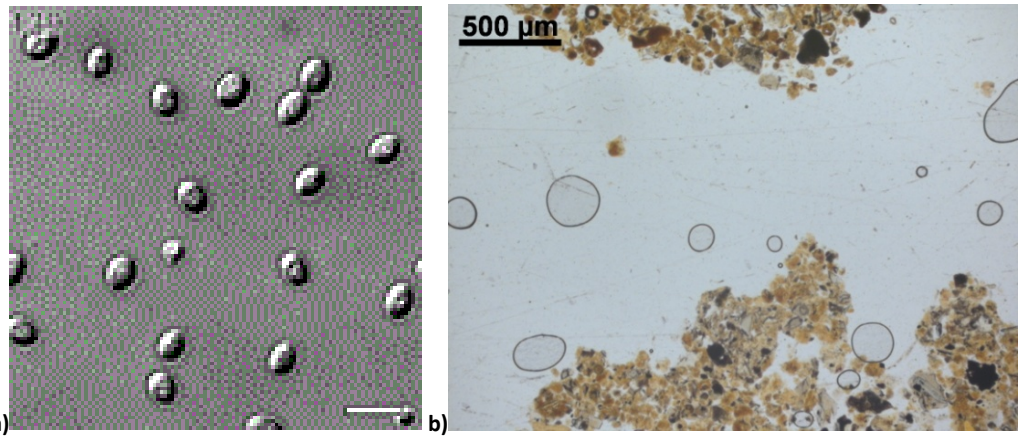

Figure 4.5: Colourless rounded spores and resin bubbles in thin section. a) Rounded colourless disconnected conidia (fungal remains), scale bar is 5 µm (Chaverri *et al.* 2003). b) Bubbles of air trapped in resin during the impregnation process.

Fungal remains have also been used as an indicator of environmental stress, either from drought (Jany *et al.* 2002, 2003) or air-pollution (Kowalski 1987). However, they have also been used as proxy indicators for previous forest cover in an area that is no longer vegetated (Benedict 2011). The presence of sclerotia of this fungus can be inferred as proxy evidence for actively growing root hairs of arboreal populations and not as heterotrophic activity affecting above ground wood growth deposited within the grave, including coffin materials.

4.2 Materials and methods

4.2.1 Excavation and sampling

Seven graves (HSM-A-114 -120) were positioned within the turf walls of a cemetery north east of the earlier excavations at the site, and conform to the strong trend of east-west orientation (Figure 4.6). The samples from these graves were studied in combination with those from the sediment profile created which will act as an extensive C1, congruent with the larger InterArChive sampling strategy. The graves were Christian burials related to the use of the 10th century church on the site and were sealed by the 1300 AD Hekla tephra layer. The burial sediments from the graves at Hofstaðir were assessed for their post-depositional and depositional processes.

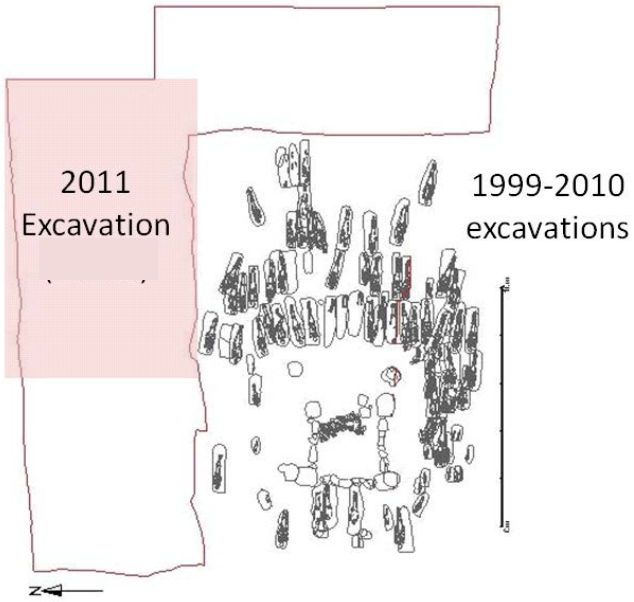

Figure 4.6: Location of 2011 excavations related to earlier excavations (InterArChive database).

The burials in the Hofstaðir graveyard show a trend, with male individuals dominating the south area and females in the northern half of the cemetery. All of the seven graves sampled by InterArChive in 2011 were undisturbed burials from the north-eastern corner of the cemetery, and were mostly complete and articulated skeletons. The exceptions to this were Graves (GR) HSM-A-114 and HSM-A-119, which were reburials (Figure 4.7). Grave numbers from this site are hereafter referred to in this chapter by their grave (GR) number without the "HSM-A" prefix. Results are referenced in the following sections by grave (GR), followed by sample position (S) and thin section number (TS). Five C1 site controls were collected at Hofstaðir (Table 4), representing the range of sedimentary layers, the high level of stratigraphic integrity and the relative thinness of some of the tephra layers deposited at the site. The controls (C2 and C3) and the samples (skull, pelvis or feet adjacent) from the seven graves excavated are summarised in Table 5.

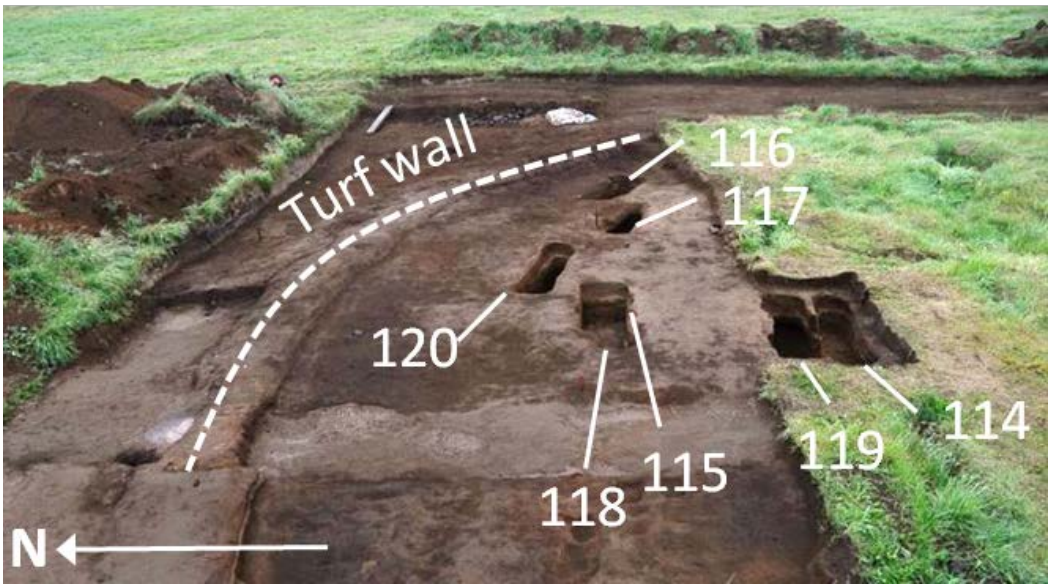

Figure 4.7: Location of graves within cemetery at Hofstaðir (InterArChive database).

Table 4: C1 controls collected as a representation of the sedimentary layers on site.

Control	Thin section number
C1A	715
C1B-C	741
C1D-E	620
C1F-H	623
C1H-J	599

Table 5: Micromorphology C2 and C3 controls (a) and samples (b) from the graves.

a)

Grave	Control	Thin section number
114	C3	727
115	C2	740
	C3	741
116	C2	571, 589
	C3	801
117	C2	621, 714
	C3	581
118	C2	733
	C3	732
119	C2	597
	C3	626, 624
120	C2	625, 679, 622
	C3	800

b)

Grave	Sample	Thin section number
114	1	680, 734, 730
	2	713, 849
	3	729
	16	726
115	1	816, 826
	A6	759
116	1	717, 760
	2Z	788
	3	813
117	1	626, 711, 712, 738
	2	617, 619, 725
	3	724, 850
119	1	731, 758
	2	765, 825
	3	764, 814
120	1	718, 767
	2	716, 829, 824
	4	739, 766
	A1	753, 851

The relative spatial relationships of the thin sections from the control profile (C1; Figure 4.8) and across each grave (C2 and C3 controls and S1, S2, and S3; Figure 4.9) are illustrated in the following figures. The graves in Figure 4.9 are listed according to their relative locations starting with GR 120 as the most northerly of the seven graves sampled, and continuing counter-clockwise through GR 118 and 115, GR 119 and 114, GR 117, and GR 116 (Figure 4.7).

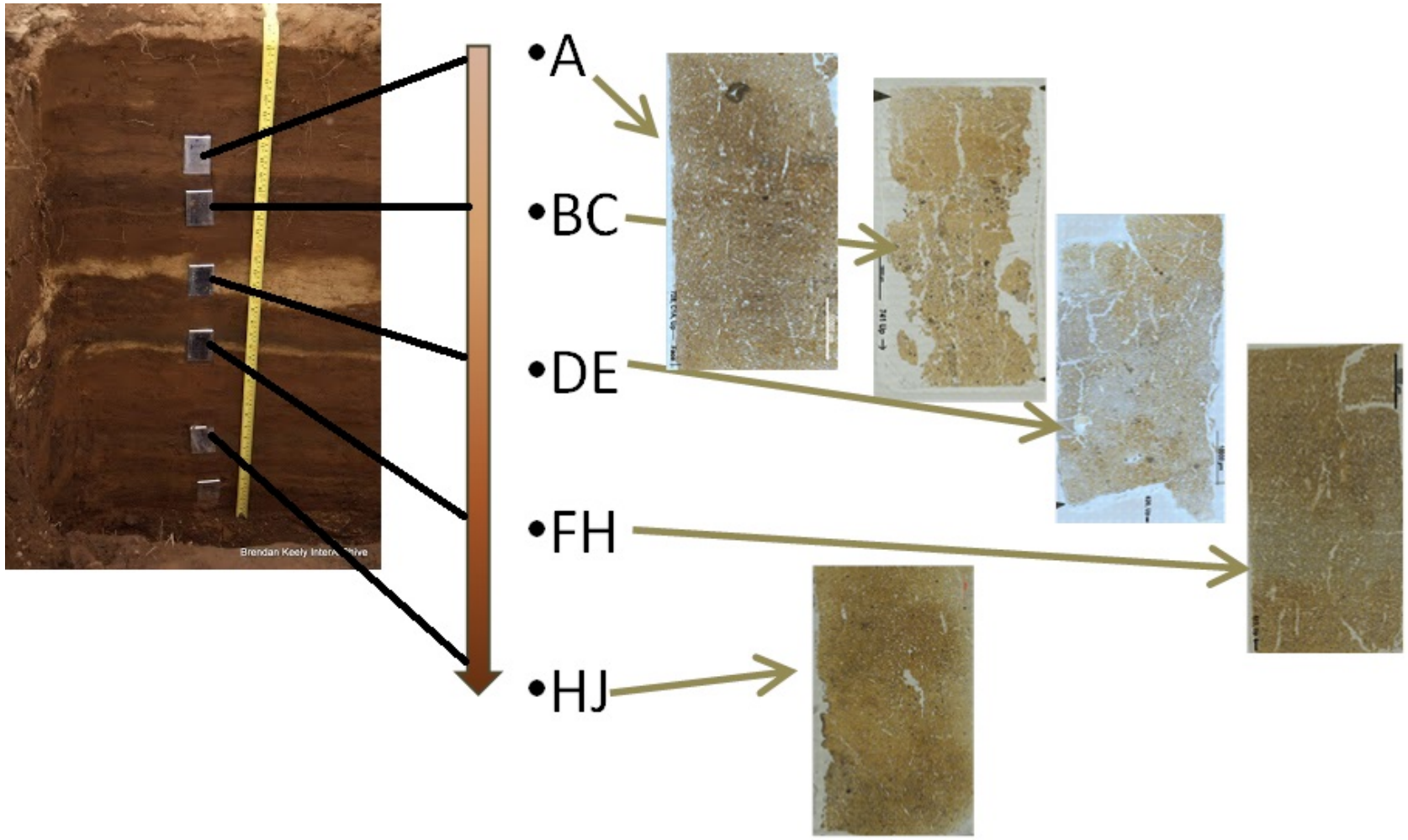

Figure 4.8: C1 control sediment profile photograph and mosaics of thin sections. The letters A-J correspond to the labels of the deposits within this profile as noted in the field by the sampler. All five thin section mosaics above have been oriented so that they have the uppermost part of the thin section at the top.

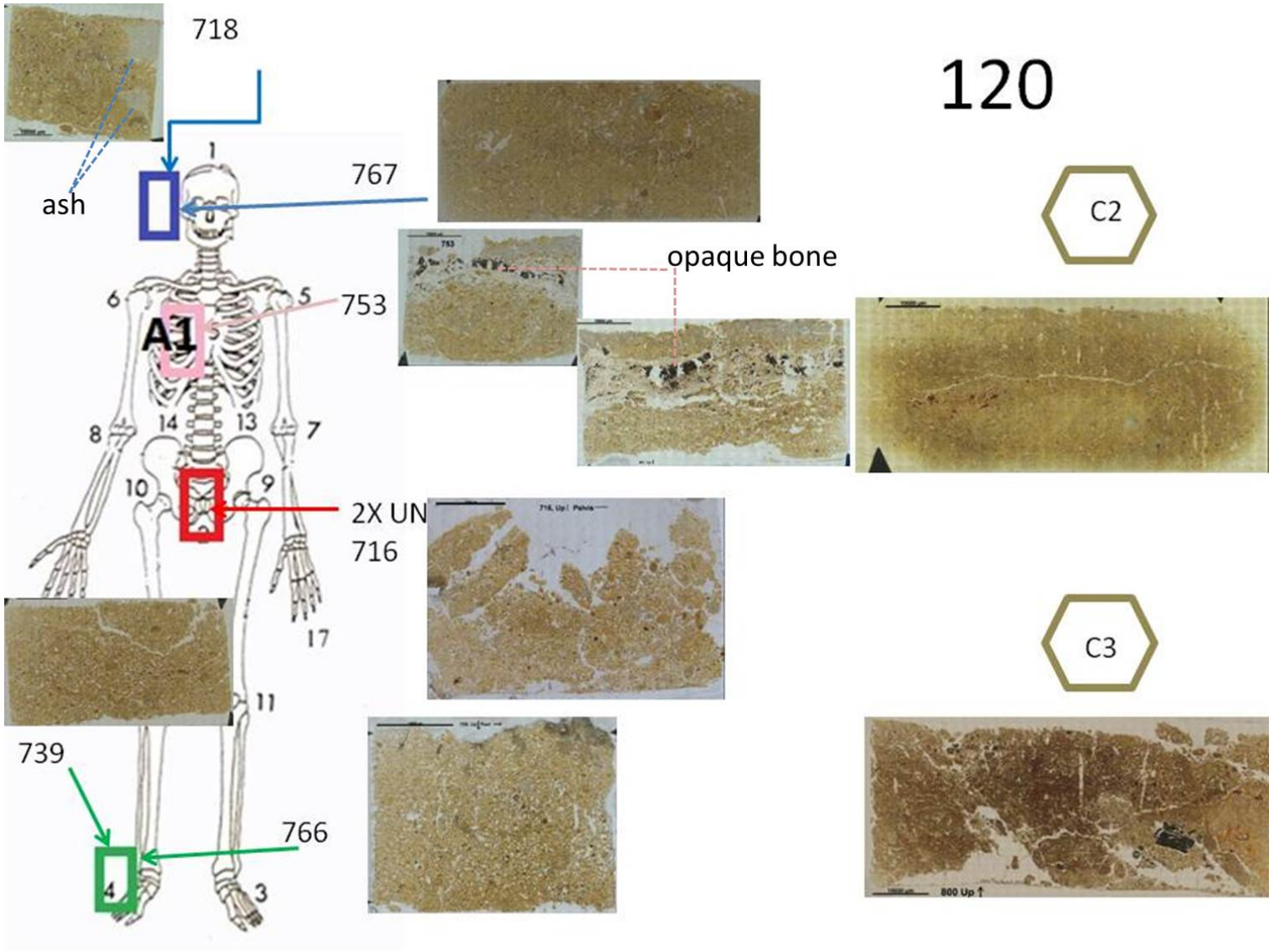
718
ash
767
753
opaque bone
A1
2X UN
716
739
766
120
C2
C3
1
5
6
7
8
9
10
11
13
14
17
3
4

a)

HSM-A-118

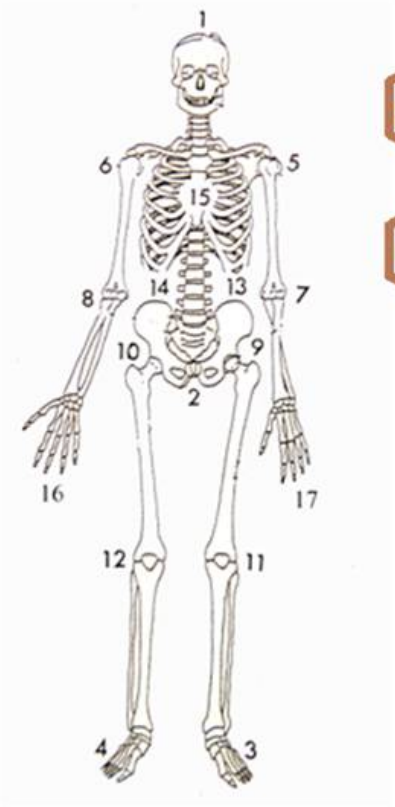

C2

733

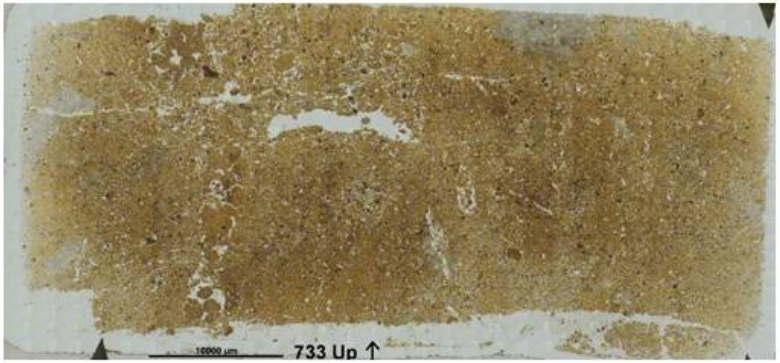

C3

732

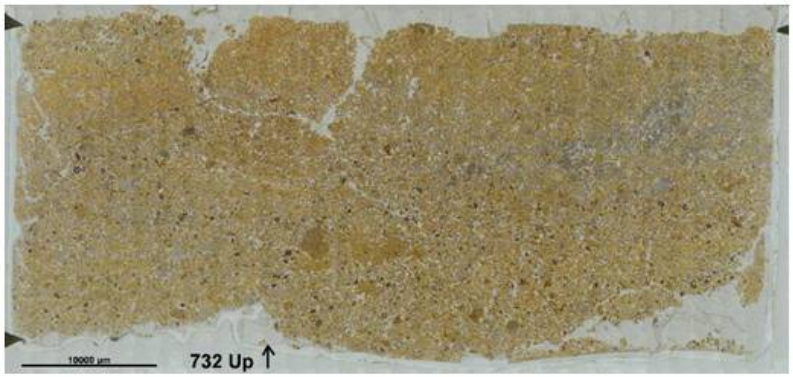

b)

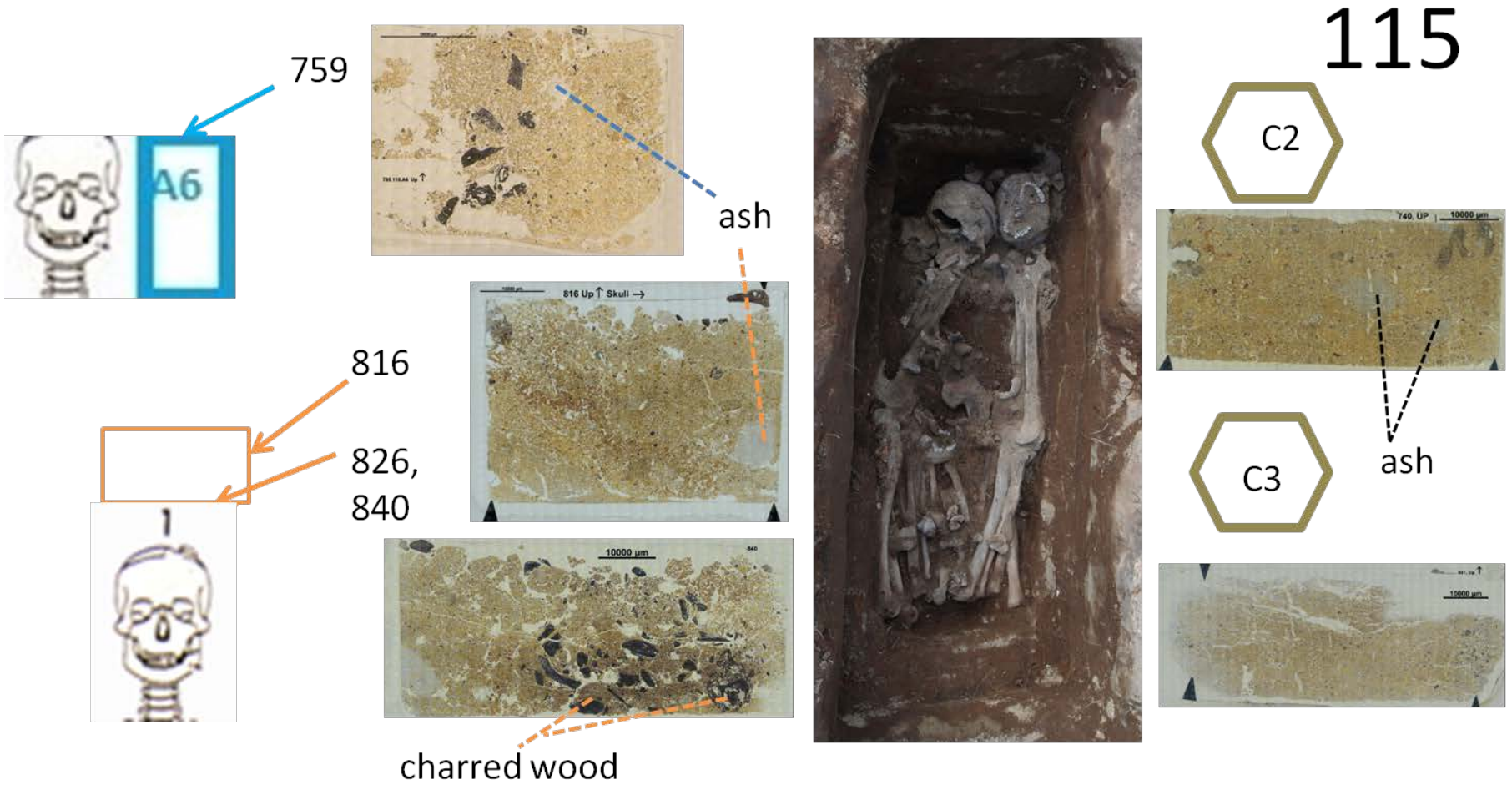

c)

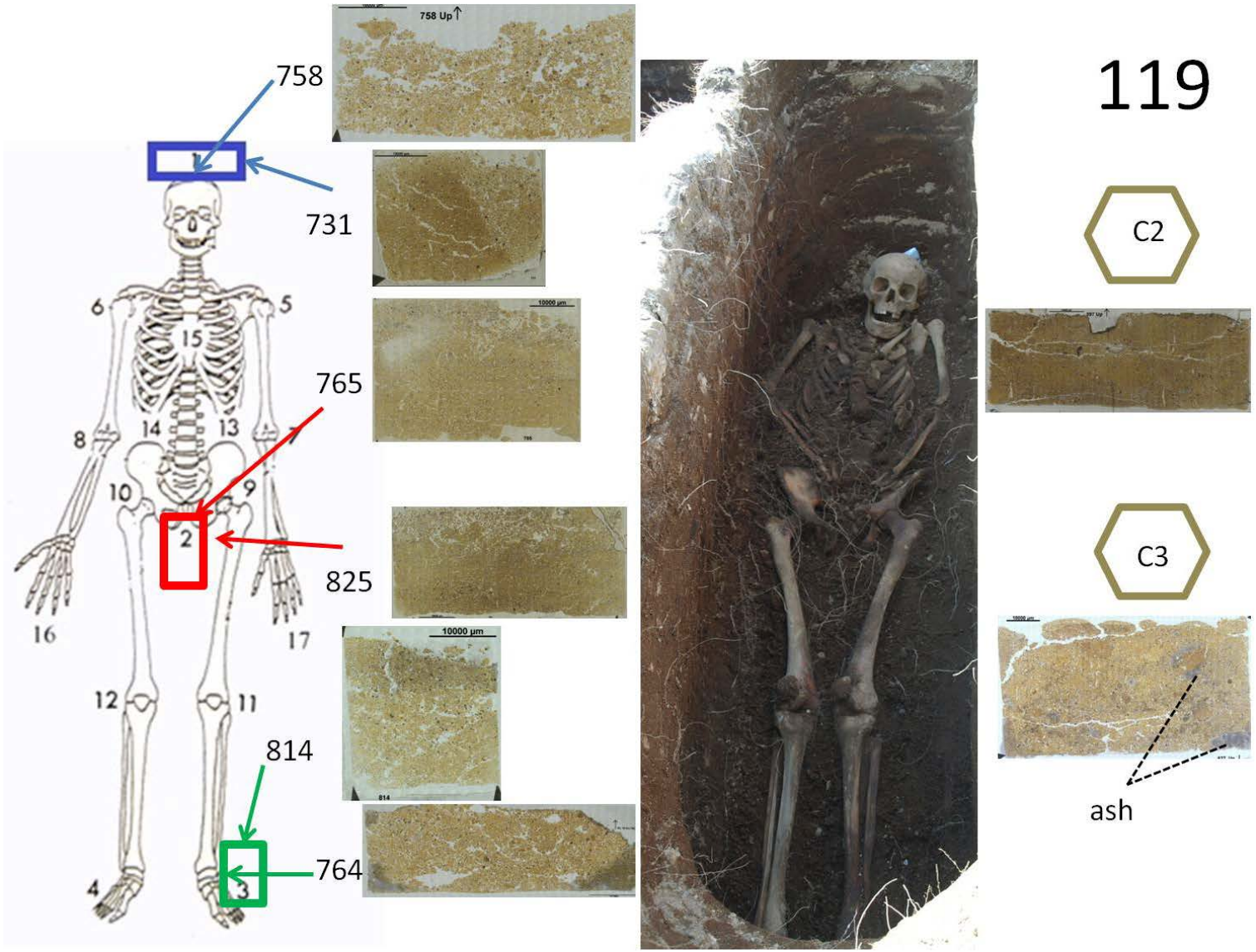
758
731
765
825
814
764
758 Up
10000 µm
814
119
C2
C3
ash
1
2
3
4
5
6
7
8
9
10
11
12
13
14
15
16
17

d)

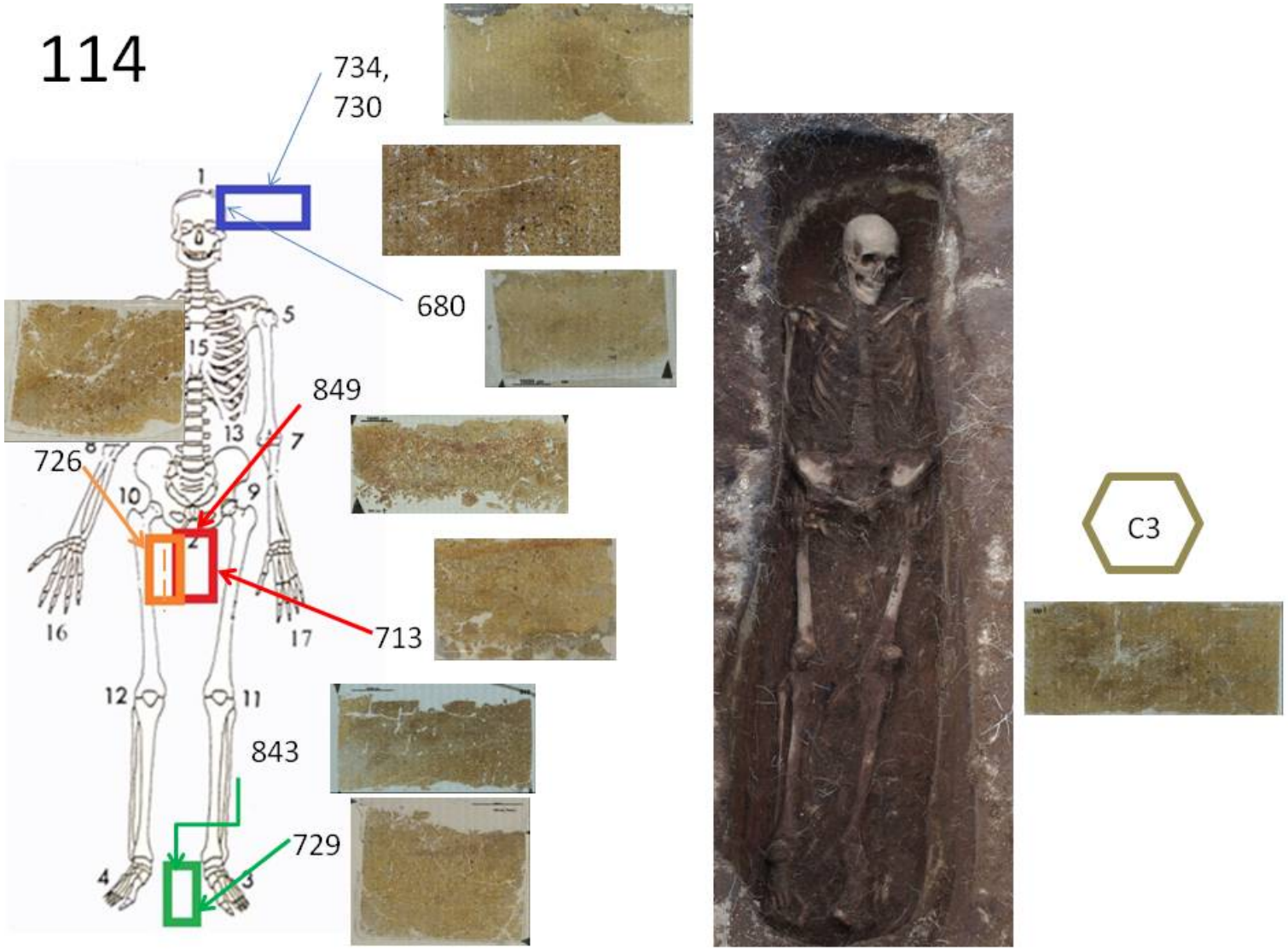
114
734,
730
680
849
726
713
843
729
C3
1
5
15
13
7
8
10
9
2
16
17
12
11
4
3

e)

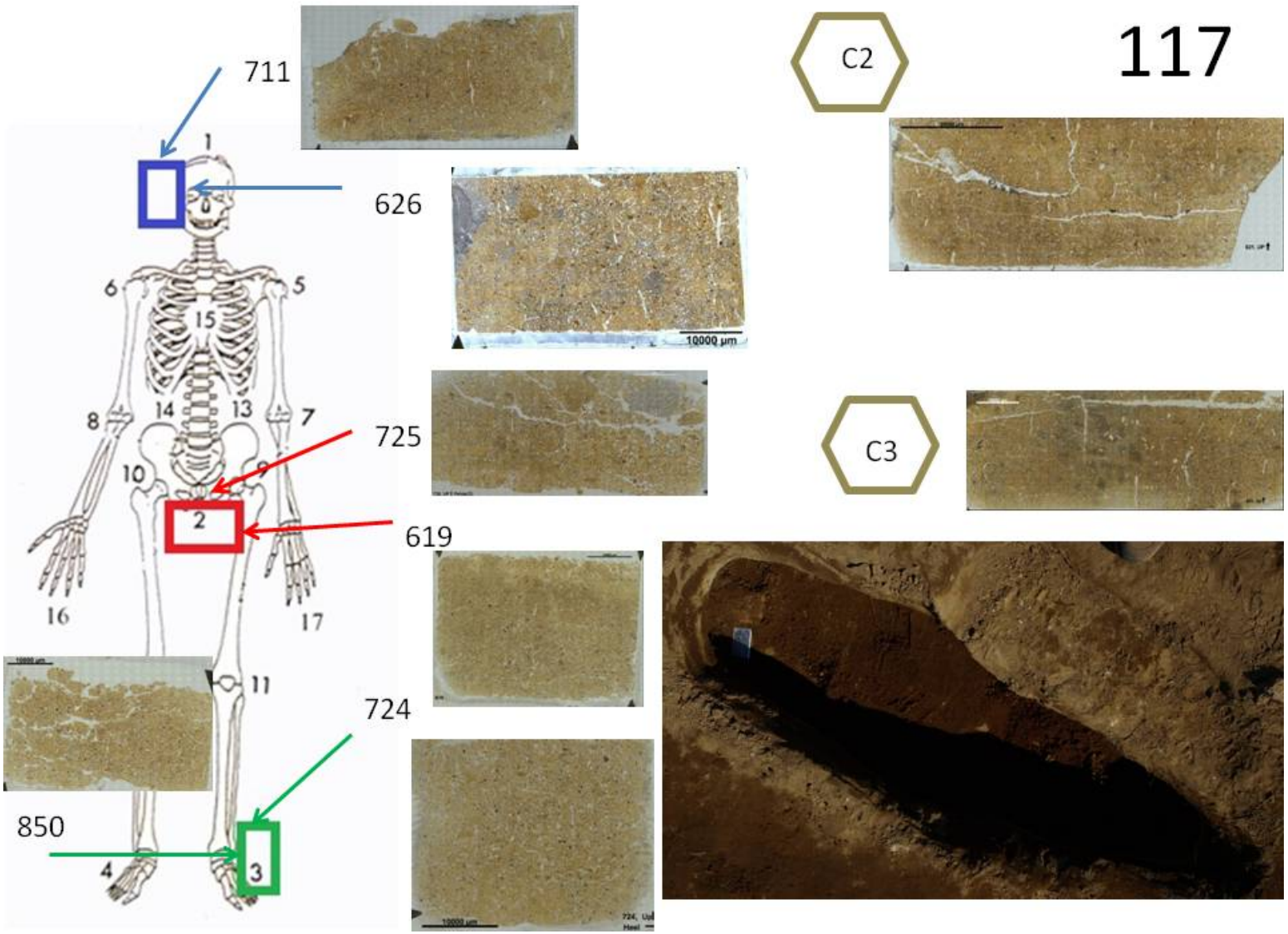

f)

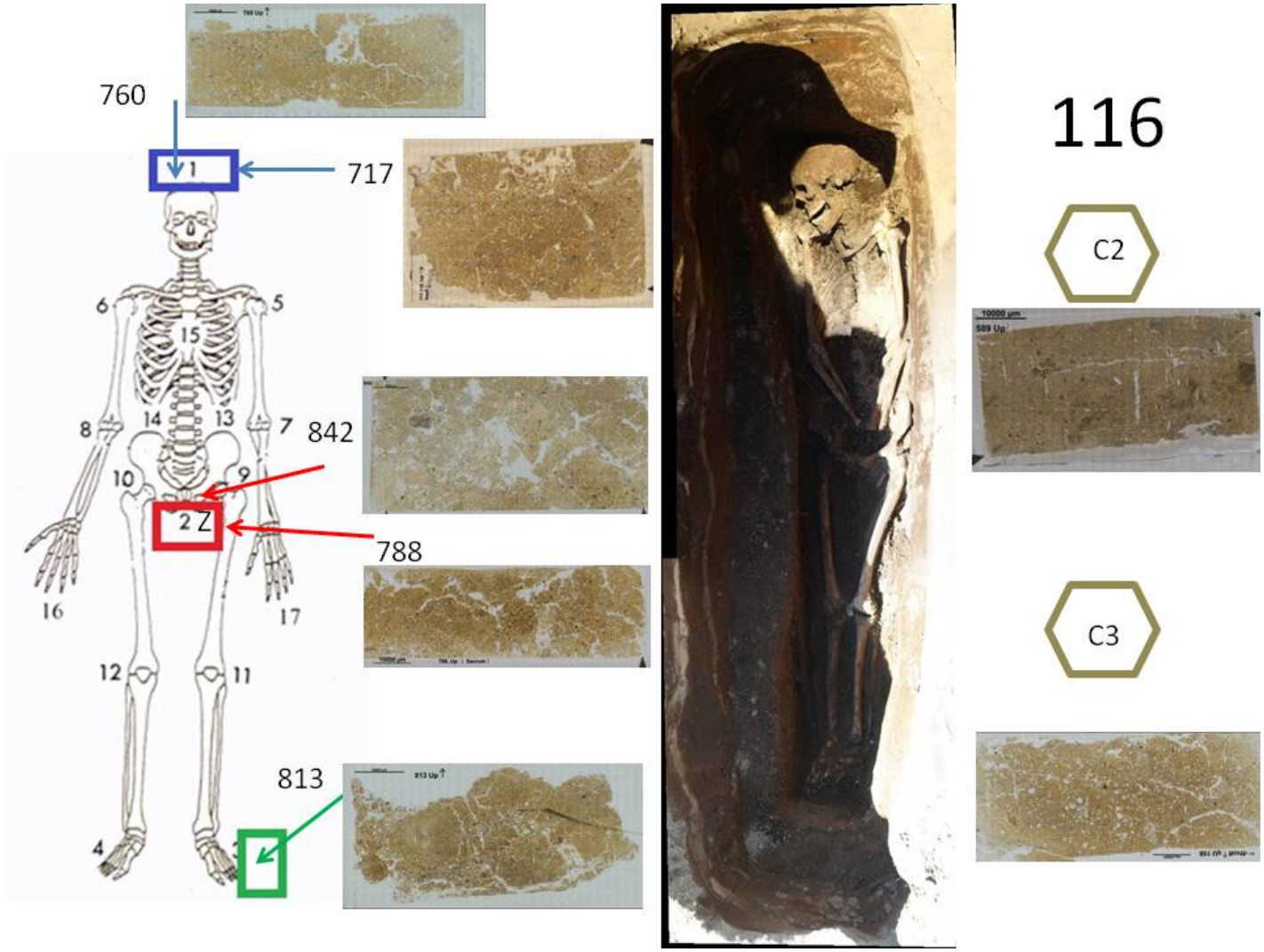

g)

Figure 4.9: Thin section locations and orientations within the graves relative to the skeleton. a) Grave 120. b) Grave 118. c) Grave 115. d) Grave 119. e) Grave 114. f) Grave 117. g) Grave 116.

4.2.2 Field observations

Each of the seven inhumations appeared during excavation to be in varying degrees of preservation, both in terms of completeness of the skeletal remains and in the physical state of the bones themselves. The sample adjacent to the sternum (S15) in GR 120 was reported to contain ash, and the left femur of GR 117 was described as having the 'texture of butter'. Inhumations in GR 114, 116, 117, and 119 were all fairly complete in their skeletal remains whereas GR 120 was moderately complete, and 115 and 118 were both reported as "jumble(s) of bones" by the member of the InterArChive team who sampled the grave (Figures 4.10 and 4.11). Indeed, the suggested interpretation of GR 115 in the field was that this disarticulated compact assemblage of bones may be evidence of skeletonisation of the individual prior to burial in this grave.

Figure 4.10: Relatively complete and articulated skeletal remains in GR 116.

Figure 4.11: Relatively incomplete and severely disarticulated skeletal remains in GR 115. Multiple skulls were found and a ring was present on one of the phalanges.

The skeletal remains in GR 114 were fairly complete, with a black line visible between the femurs and regions of very dark material both above the right foot and the upper right ribs. Dark organic rich sediment in and around the thoracic cavity in GR 114 was reported during excavation (SA2) and 119 (S15). Although only chemistry samples were collected for GR 114, SA2 and GR 119, S15, a micromorphology sample collected from the sediment near the thorax of another grave (GR 116) was assessed as this could have also contained trace amounts of similar deposits (Appendix III, skeleton sheets, GR 116, S2Z).

Ash lumps were reported as visible by the naked eye both within and surrounding the sternum on GR 117 (SA2) and GR 120 (S15 and SA1), leading to questions of whether this material could be observed and identified as such in the micromorphology and chemistry samples, and the extent and degree to which this ashy material had influenced the burial environment.

The main archaeological questions were whether the skeletonisation for GR 115 pre- or post-dated its burial at that location and the extent and nature of the supposed ash deposits. If skeletonisation was pre-burial in GR 115, why was a ring present on a finger (Figure 4.11)? The hypothesis currently proposed in this piece of work, is that this individual was not skeletonised, but was cut several times to create many small pieces which were then placed into the grave. GR 115 was sampled for micromorphology because the presence of multiple crania suggested that this burial was different from the other five (GR 114, GR 116-117 and GR 119-120) and to understand whether, accordingly, discernible traces of post-depositional processes affecting burial sediments of GR 115 were different from those of the other five graves.

At Hofstaðir, taphonomic processes had altered the wood and bone to various extents. Was the sediment pH the main contributor to the preservation of wood or were localised micro-environments a factor? Has wood been preserved in the same way across all graves examined at this site? Macro-scale observations during excavation suggested heterogeneity in the levels of degradation, resulting in visual damage to the structural integrity of bones from some of the skeletons. What specific conditions of the sedimentary environment facilitated these processes of decay and why had bone been preserved in different states and degrees of preservation across the site?

4.2.3 Thin section methods

Due to the nature of the research question regarding mineral weathering, a more systematic and detailed micromorphometrical approach was necessary and therefore point counting was also employed (Section 3.4.4) in addition to the standard micromorphological analysis (Section 3.4.2). For point counting, the material was viewed under both PPL and XPL, then identified and classed as belonging to one of the categories (point counting groups). Controls and tangential oriented sections from samples had a minimum of 1000 counts and perpendicular oriented sections a minimum of 3000 counts. Thin sections oriented perpendicular to the skeletal remains were point counted differently as perpendicular thin sections were split into smaller sub-sections with smaller incremental movements of the slide between counts compared to tangential oriented sections and controls (Sections 4.3.5.2 and 4.3.5.3).

Control and tangential oriented thin sections were point counted at 100 x magnification (10 x objectives) and at 5 mm intervals, except where the surface area of a thin section was too small to allow for greater than 1000 counts per thin section when operated at 5 mm intervals. For smaller thin sections, which occurred as a result of using the smallest of the three Kubiena sizes (Section 3.4.1), the interval of points was tailored to a value between 1000 and 300 µm which resulted in a total of greater than 1000 counts for each thin section. This method was executed on all thin sections produced from control samples (C1, C2 and C3 controls) as well as tangential sections from samples collected from the sediment near the body (S1t, S2t and S3t sections), in order to allow for comparisons to be made between the results from samples near the body against those from controls. Raw point counting tables are in Appendix III and point counting groups are listed in Table 6. The values listed in the results in Section 4.3.5 represent percentages of the frequency of the occurrence of each group calculated from the total count for each thin section or sub-division.

Table 6: Point counting groups. The types of materials allocated to each group and their abbreviated notations.

Group number	Types of materials	Abbreviation
1	tephra, rocks and minerals at weathering extents of 0 or 1	trm 0,1
2	tephra at weathering extent 2	t 2
3	tephra at weathering extent 3 or 4 (including opaque alteromorphs, poroalteromorphs, and other isotropic secondary phases as well as development of gel and fibro palagonite)	t 3,4
4	tephra at weathering extent 3 or 4 with iron accumulation resulting in a red (RL) and anisotropic (XPL) secondary product	t 3,4 fe
5	fine material	fine
6	voids	voids
7	nodules and coatings (including isotropic coatings by fine material)	nod & coat
8	organic material	OM
9	other (e.g. ash, excremental pedofeatures)	other

4.3 Thin section analysis

4.3.1 Summary of micromorphological observations

Micromorphological observations are described in detail in Appendix III and are summarised in Table 7. Size classes have been used to describe some of the features (Table 8), symbols to represent estimated abundance (Table 9) and terminology is discussed in Chapter 2. Most of the sediments in thin section displayed an undifferentiated b-fabric and an embedded (term after Courty *et al.* 1989) coarse to fine related distribution (Table 7). Voids present were mostly vughs, channels or chambers, with some vesicles and cracks were negligible (Table 7). Plant remains and fungi were present in controls and samples (Table 7). Amorphous organic matter was negligible in the sediments from the control profile but present in some of the burial sediments (Table 7). Thin layers of ash were observed in the some of the C1 controls and are interpreted as evidence of undisturbed aeolian deposits of volcanic ash (Figure 4.12). Ash was present in some of the samples and is discussed in Section 4.3.4. Tephra was present in samples and controls and is discussed in the following Section.

Table 7: Micromorphological observations, excluding tephra characteristics.[1]

TS	GR	S	µ-u	colour	c/f	b-f	r d	voids					pedofeature			inorganic					organic			
								ve	ch	cb	vu	cr	in	ma	no	T	I	N	t	o	AMO	ex	pl	o
715	C1	a	1 of 1	yellow-brown	25, 75	U	E	*	**	*	***	_	*		**	**	*	*	***	**	_	_	*	*
741	C1	bc	1 of 2	brown-yellow	90, 10	U	LC		**	*	***	_		****	**				*****	*	_	_	*	
741	C1	bc	2 of 2	orange-brown	15, 85	U	E	*	***	**		_		*	**	**	*	*	***		_	_	*	**
620	C1	de	1 of 2	orange-brown	20, 80	U	E		**	***	*	_		*	*	*		*	**	***	_	_	*	*
620	C1	de	2 of 2	brown-grey	90, 10	sp	E		***	***		_			*	*			**	*****	_	_	*	
623	C1	fh	1 of 2	medium brown	15, 85	U	E	*	**	**	*	_	*	***	**	**	*	*	**		_	_	**	*
623	C1	fh	2 of 2	pale grey	5, 95	sp	E	*	**	*	**	_			*	**			*	***	_	_		
599	C1	h-j	1 of 1	brown-orange	25, 75	U	E	*	*	***	*	_			**	**	**	*	***		_	_	**	*
727	114	C3A	1 of 1	orange-brown	25, 75	U	E	_	**	**	***	_	_	*	**	***	_	*	***	**	*	_	***	_
680	114	1t	1 of 2	brown-yellow	20, 80	U	E	**	**	***	**	_	_	_	**	***	*	_	***	_	**	_	**	**
680	114	1t	2 of 2	yellow-brown	40, 60	U	E	*	*	**	**	_	*	_	***	**	_	_	***	_	**	_	**	_
730	114	1p	1 of 2	orange-brown	25, 75	U	E	*	***	***	*	_	*	*	**	*	_	*	**	_	*	_	***	*
734	114	1p	1of 2	brown-yellow	20, 80	U	E	_	***	*	***	_	*	*	**	*	_	_	**	_	_	_	*	*
734	114	1p	2 of 2	orange-brown	45, 55	U	E	_	**	_	***	_	***	*	**	*	_	_	***	*	***	_	*	_
713	114	2p	1 of 2	orange-brown	25, 75	SP	E	_	***	**	**	*	_	**	*	**	_	*	**	**	*	_	_	**
713	114	2p	2 of 2	brown-yellow	20, 80	U	E	*	**	***	**	_	_	_	**	**	_	_	***	*	**	_	***	***
729	114	3/4t	1 of 2	brown-yellow	15, 85	U	E	*	**	***	*	_	_	*	***	**	*	_	**	**	_	_	**	_
729	114	3/4t	2 of 2	orange-brown	30, 70	U	E	_	**	**	***	_	**	**	**	*	_	*	***	**	_	_	*	*

[1] Abbreviations are as follows: sampling position (S) referenced as either tangential (*xxx*t), or perpendicular (*xxx*p), micro-unit (µu), ratio of coarse to fine components at 50µm limit (c/f), birefringence fabric (b-f), related distribution of coarse to fine components (r d), vesicles (ve), channels (ch), chambers (cb), vughs (vu), cracks (cr), intrusive pedofeatures (in), matrix pedofeatures (ma), nodules (no), tectosilicates (T), nesosilicates (N), inosilicates (I), tephra (t), other (o), amorphous organic matter (AMO), excremental pedofeatures (ex) and plant remains(pl). Estimated abundance uses symbols listed in Table 9.

843	114	3/4p	1 of 3	medium brown	30, 70	U	E	_	**	**	**	_	**	**	*	*	_	*	***	*	_	_	*	*
843	114	3/4p	2 or 3	brown-grey	55, 45	SP	E	**	*	**	*	_	***	***	*	_	_	*	***	_	_	_	*	*
843	114	3/4p	3 of 3	translucent	20, 80	U	LC	*	_	**	**	_	_	_	*		_	_	*****	****	_	_	_	*
726	114	16T	1 of 2	yellow	20, 80	U	E	_	_	**	**	_	_	_	_	***	**	*	****	**	_	_	*	_
726	114	16T	2 of 2	orange-brown	30, 70	U	E	_	***	*	****	_	_	**	**	*	*	*	***	*	*	**	**	_
740	115	C2	1 of 1	orange-brown	30, 70	U	E	_	**	*	***	_	***	**	**		*	*	***	***	_	_	*	*
826	115	1t	1 of 2	orange-yellow	70, 30	U	E	_	*	**	***	_	_	*	*	*	*	*	***	_	**	_	*	***
826	115	1t	2 of 2	brown-yellow	60, 40	SP	E	**	**	*	***	_	*	*	*	*	*	*	***	_	_	_	*	*
816	115	1p	1 of 3	brown-yellow	35, 65	SP	E	_	**	_	****	_	*	**	**	**	*	*	***	***	**	_	**	*
816	115	1p	2 of 3	brown-orange	70, 30	U	E	_	_	_	***	_	**	*	**	*	*	_	***	_	_	_	*	***
816	115	1p	3 of 3	brown-yellow	60, 40	U	E	_	**	*	***	_	_	*	**	*	*	_	***	*	_	_	*	*
759	115	A6	1 of 1	brown-yellow	35, 65	U	E	*	**	***	***	*	*	*	_	*	_	_	***	_	**	_	***	**
589	116	C2	1 of 1	orange-brown	35, 65	U	E	*	***	**	**	_	*	*	*	**	*	*	***	**	_	_	**	*
801	116	C3	1 of 1	orange-brown	20, 80	U	E	**	***	**	*	_	**	*	*	**	_	**	***	**	_	_	**	*
760	116	1p	1 of1	orange-brown	45, 55	U	E	*	***	***	***	_	**	*	*	*	**	*	***	_	**	_	**	*
717	116	1p	1 of 1	orange-brown	40, 60	SP	E	**	**	***	**	_	**	*	*	*	*	*	**	**	***	_	_	*
842	116	2zt	1 of 2	brown-yellow	40, 60	U	E	_	_	*	***	_	*	*	*	*	*	*	***	_	***	_	**	***
842	116	2zt	2 of 2	brown-yellow	40, 60	SP	E	*	*	**	**	_	*	_	*	*	**	*	***	_	*	_	*	*
788	116	2zp	1 of 1	orange-brown	45, 55	U	E	*	***	***	**	_	**	***	***	*	_	**	****	_	**	_	**	***
813	116	3(un)	1 of 1	medium orange	60, 40	SP	E	_	***	**	***	_	*	**	**	*	*	*	****	*	_	_	*	*

621	117	C2	1 of1	orange-brown	40, 60	U	LC	*	**	**	*	**	**	*	*	*	_	***	*	***	_	**	*
581	117	C3	1 of 2	brown-orange	45, 55	U	E	_	**	_	***	**	*	**	*	*	_	*	***	_	_	_	_	**
581	117	C3	2 of 2	grey	10, 90	U	E	_	**	**	**	_	_	_	_	*	_	_	**	_	*	_	*	_
626	117	1t	1 of 1	brown-orange	50, 50	U	LC	_	***	**	**	_	***	**	**	**	_	_	***	**	**	_	**	**
711	117	1p	1 of 1	yellow-brown	35, 75	U	E	_	***	**	***	*	**	****	***	**	_	*	***	**	**	_	**	*
725	117	2t	1 of 1	brown-yellow	40, 60	SP	E	_	**	*	***	_	**	***	*	*	_	_	***	**	**	_	*	_
619	117	2p	1 of 2	orange-brown	50, 50	U	LC	_	*	***	**	_	**	****	_	*	_	_	****	_	_	_	*	**
619	117	2p	2 of 2	pale yellow	40, 60	SP	E	_	_	**	***	_	_	***	**	**	_	_	****	**	_	_	_	_
724	117	3p	1 of 1	brown-yellow	50, 50	U	E	_	_	**	****	_	**	***	**	*		_	****	_	***	_	**	*
733	118	C2	1 of 1	orange-brown	25 75	U	E	*	**	*	**	_	***	_	**	*	*	*	***	_	_	_	**	_
732	118	C3	1 of 2	brown-orange	35 65	U	E	_	*	**	****	_	*	*	*	*	*	*	***	*	_	_	*	_
732	118	C3	2 of 2	dark orange	20 80	SP	E	_	*	**	***	_	*	*	**	*	*	*	**	_	*	_	***	*
597	119	C2	1 of 1	orange-brown	40, 60	U	E	_	***	***	***	_	**	*	*	*	*	*	**	*	*	_	**	*
627	119	C3	1 of 2	yellow-brown	30, 70	U	E	_	***	*	***	_	*	*	*	***	*	*	***	**	_	_	**	*
627	119	C3	2 of 2	brown-yellow	40, 60	U	E	_	*	_	***	*	*	*	*	**	*	*	****	_	_	*	*	*
758	119	1t	1 of 1	orange-brown	30, 70	U	E	*	***		***		***	**	**	**	*	*	****	_	*	_	*	*
731	119	1p	1 of 2	brown-yellow	25, 75	SP	E	_	**	***	**	_	*	*	*	**	*	**	***	*	_	_	**	*
731	119	1p	2 of 2	yellow-brown	25, 75	U	E	_	***	***	***	_	*	**	*	*	_	**	***	_	*	_	*	*
825	119	2yt	1 of 5	brown-orange	10, 90	U	E	***	_	_	***	_	*	**	*	*	_	_	***	*	***	_	_	***
825	119	2yt	2 of 5	brown-yellow	5, 95	U	M	**	**	*	_	_	_	_	_	_	_	_	*	_	_	_	_	*
825	119	2yt	3 of 5	brown-orange	30, 70	U	E	*	*		***	_	*	_	*	*	_	*	***	_	_	_	*	*
825	119	2yt	4 of 5	brown-yellow	15, 85	U	E	**	*	**	**	_	_	_	*	*	*	*	*	_	**	_	*	**
825	119	2yt	5 of 5	orange-brown	25, 85	U	E	*	**	***	*	_	*	*	**	*	*	*	***	_	*	_	*	*
765	119	2yp	1 of 1	brown-yellow	30, 70	U	E	**	**	***	*	_	**	*	**	**	*	*	***	***	**	_	*	***

764	119	3t	1of 1	yellow-brown	35, 65	U	E	_	***	**	*	_	*	**	**	**	*	*	****	*	***	*	*	**
814	119	3p	1 of 2	orange-brown	30, 70	U	E	_	**	*	***	*	_	**	*	*	*	_	***	_	*	_	*	*
814	119	3p	2 of 2	brown-yellow	20, 80	U	E	*	**		*	_	*	*	**	*	*	*	***	*	_	_	*	_
625	120	C2	1 of 1	yellow-brown	20, 80	U	E	*	**	***	**	_	*	*	*	***	_	_	***	**	_	_	*	*
800	120	C3	1 of 2	orange-brown	40, 60	U	E	**	**	*	*	_	***	_	*	*	*	*	***	_	_	_	**	*
800	120	C3	2 of 2	brown-orange	30, 70	U	E	**	_	*	***	_	**	*	*	*	*	*	***	_	_	_	***	_
767	120	1t	1 of 1	brown-yellow	40, 60	SP	E	**	**	***	*	_	**	**	***	**	_	**	***	**	*	_	**	**
718	120	1p	1 of 1	brown-yellow	45, 55	SP	E/LC	_	**	**	**	_	**	***	**	*	**	**	***	***	**	_	*	**
824	120	2xt	1 of 3	brown-orange	30, 70	U	E	*	***	*	**	_	**	*	**	**	*	*	***	_	_	_	*	_
824	120	2xt	2 of 3	pale yellow	10, 90	U	E	_	*	*	***	_	_	_	_	*	_	_	*	_	_	_	_	**
824	120	2xt	3 of 3	brown-yellow	25, 75	U	E	**	*	*	**	_	*	*	*	**	*	_	***	_	_	_	*	***
716	120	2xp	1 of 2	brown-yellow	20, 80	U	E	_	**	***	***	*	**	**	**	**	**	_	***	*	*	_	_	*
716	120	2xp	2 of 2	yellow-brown	35, 65	SP	E	_	*	*	***	**	*	**	**	*	**	*	***	**	*	_	_	*
766	120	4yt	1 of 1	yellow-brown	35, 65	SP	E	*	**	**	***	_	*	**	**	**	_	**	***	*	_	_	*	*
739	120	4yp	1 of 1	yellow-brown	40, 60	U	E	*	*	**	***	_	*	*	**	**	*	*	****	*	*	_	**	*
753	120	A1	1 of 1	orange-brown	45, 55	U	E	*	*	**	***	_	***	***	*	**	*	*	***	**	*	***	***	***

Table 8: Relative size categories used in tables of observations. All sizes listed in the table are in micrometres. Bone fragments, as inorganic materials of biological origin, have been allocated into the relative size category along with other listed inorganic materials (rocks, minerals and volcanic glass) and not that of the remainder of the organic inclusions. This is due to the range of sizes of bone fragments observed at this site.

Type	Small/Thin	Medium	Large/Thick
coating	<10	10--30	>30
nodules	<30	30--100	>100
rocks, minerals, volcanic glass, bone	50--100	100--200	>200
excremental pedofeatures, and organics*	<100	100--500	>500

Table 9: Symbols used to represent estimated abundance (estimated using charts of Bullock *et al.* 1985) in tables of observations.

Estmated abundace	Symbol
<1%	_
1-2%	*
2≥5%	**
6-10%	***
11-20%	****
21-30%	*****
31-40%	******
>40%	*******

a)

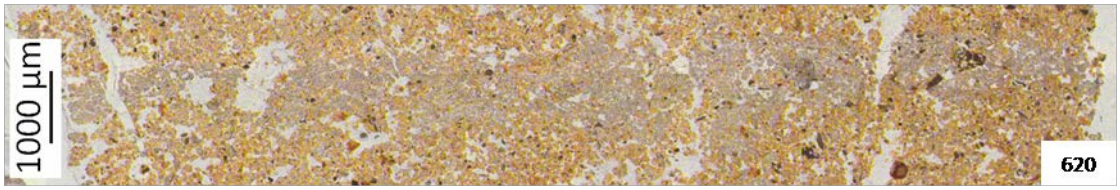

b)

Figure 4.12: Intact tephra layers. a) A 1 mm thick tephra layer observed in a section from a sample from the control profile (C1DE, TS 620, PPL). b) A *c.*1 cm thick tephra layer with undulating upper and lower boundaries from the control profile (C1FH, TS 623, PPL). The images are oriented with their upper part toward the top of the image.

4.3.2 Tephra characteristics

Tephra was observed at a range of textures, colours and sizes (Appendix III). Vesicular, non-vesicular, vitric and hypocrystalline tephra were present in controls and samples, and had a green, grey or brown isotropic vitric matrix when not heavily weathered (Figure 4.13) which weathered to a dark grey, red (Figure 4.14) or opaque material (Figure 4.15). Vesicles in vesicular tephra never exceeded 25% estimated abundance of a grain's volume. Phenocrysts in hypocrystalline tephra never exceeded 30% estimated abundance of a grain's volume. Types of minerals present as phenocrysts in hypocrystalline were feldspars, olivine and pyroxenes. Types of weathering patterns observed were linear (Figure 4.16), pellicular and dendritic. Gel- and fibro-palagonite (Figure 4.17) were observed in the samples and controls and gibbsite in the samples (Figure 4.18) and are interpreted as products from the weathering of tephra.

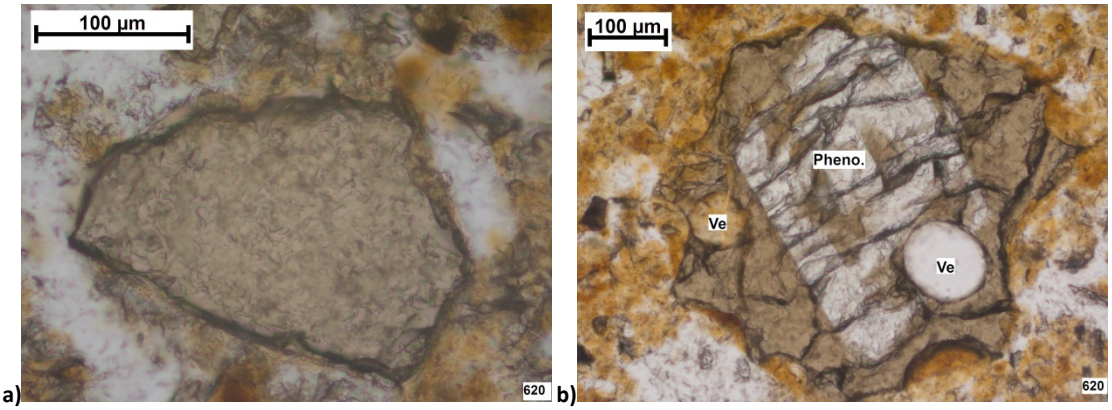

Figure 4.13: Fresh (weathering extents 0-1) tephra. a) Fresh non-vesicular vitric tephra (TS 620, C1, PPL). b) Fresh vesicular (Ve) hypocrystalline (Pheno.) tephra (TS 620, C1, PPL).

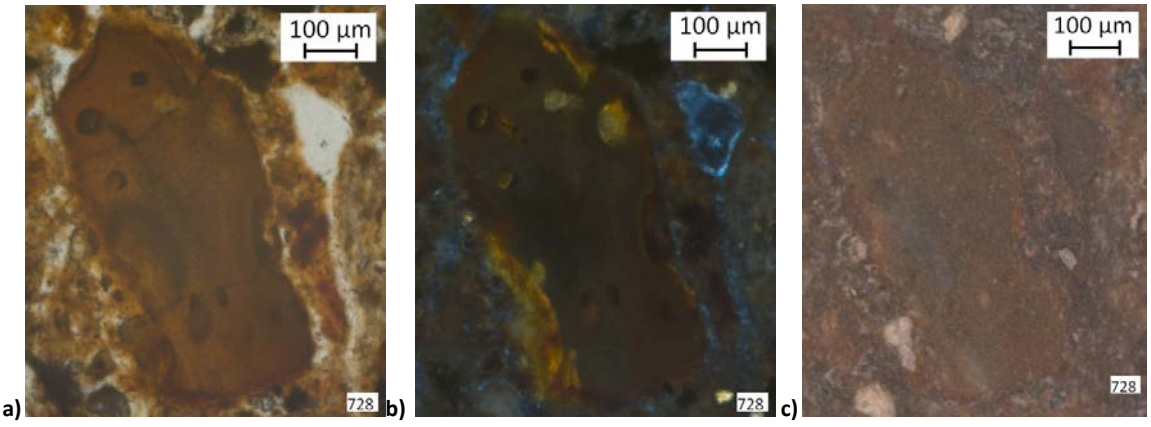

Figure 4.14: Iron rich alteromorph formed through the weathering of vitric tephra from the top of the control profile (C1A, TS 728), images taken under a) PPL, b) XPL, c) RLDF.

a) 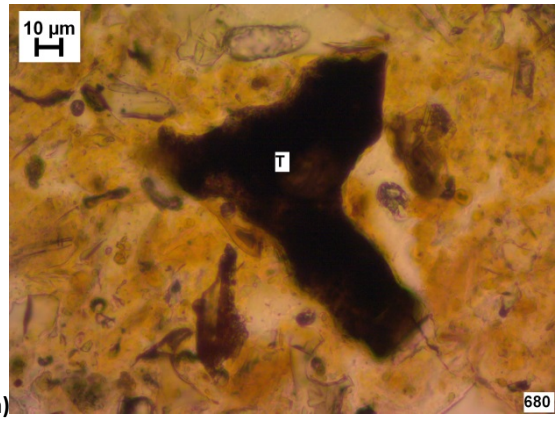

b) 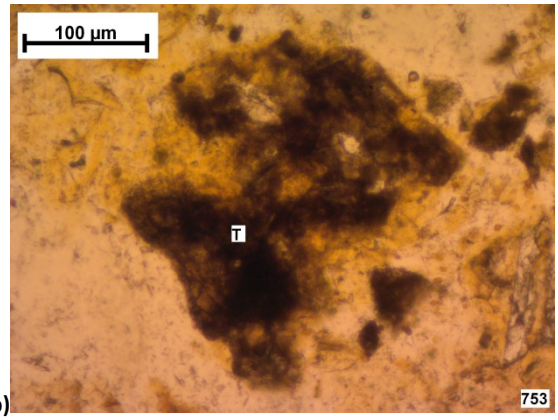

Figure 4.15: Heavily weathered tephra. a) Heavily altered vitric tephra with clear edges (TS 680, S1, GR 114, PPL). b) Heavily altered hypocrystalline tephra with diffuse edges (TS 753, SA1, GR 120, PPL).

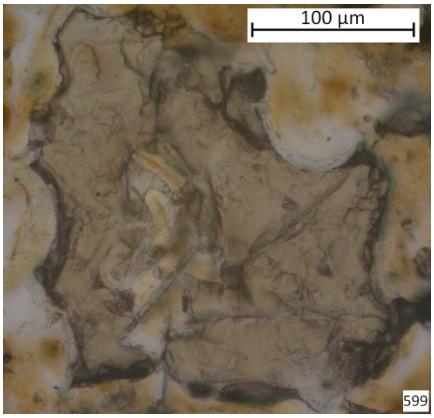

Figure 4.16: Vitric tephra with irregular linear weathering pattern from the control profile (C1FH, TS 599, PPL).

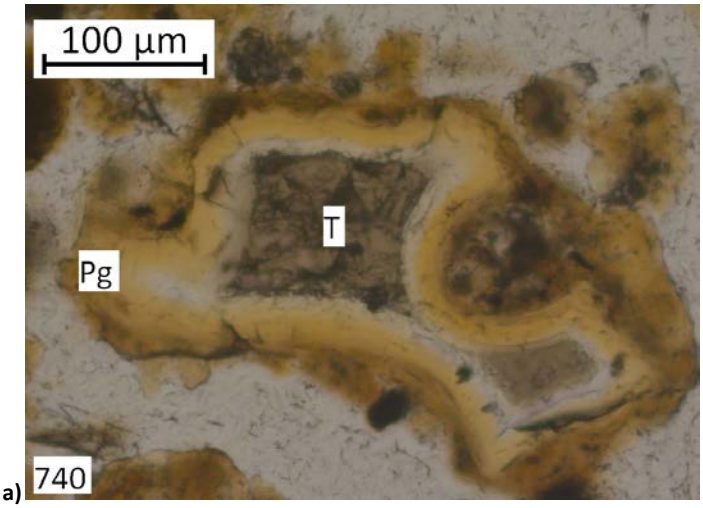

a)

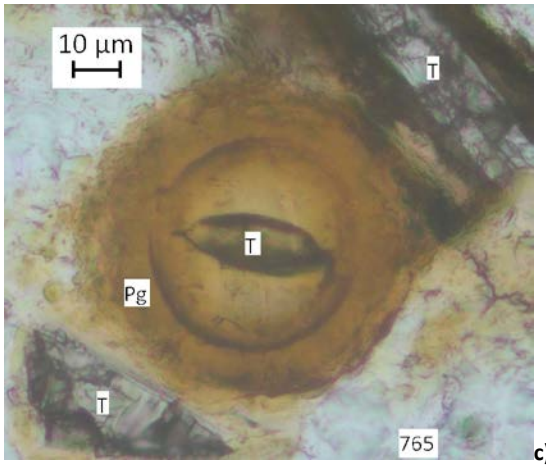

b)

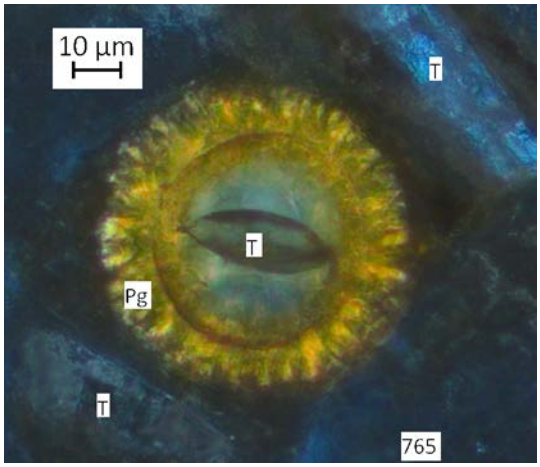

c)

d)

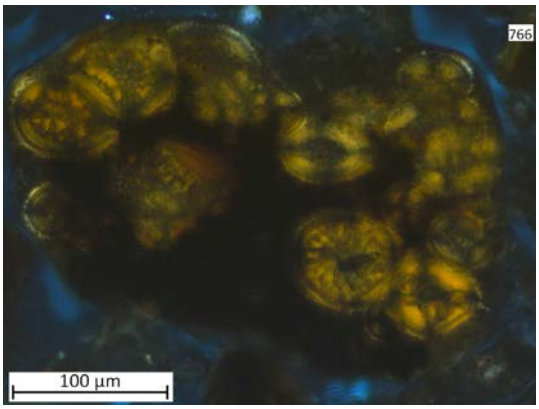

e)

Figure 4.17: Examples of palagonitization occurring on the volcanic silicates in thin sections from the grave sediments at Hofstaðir. a) Gel palagonite (Pg) forming as a hypocoating around a fragment of tephra (T) (GR 115, C2, TS 740, PPL). b) Fibro palagonite (Pg) developed through the weathering of a tephra fragment (T) (GR 119, S2, TS 765, PPL). c) XPL view of image b). d) Highly weathered tephra material showing opaque and anisotropic orange colours (GR 120, S4, TS 766). e) XPL view of image d).

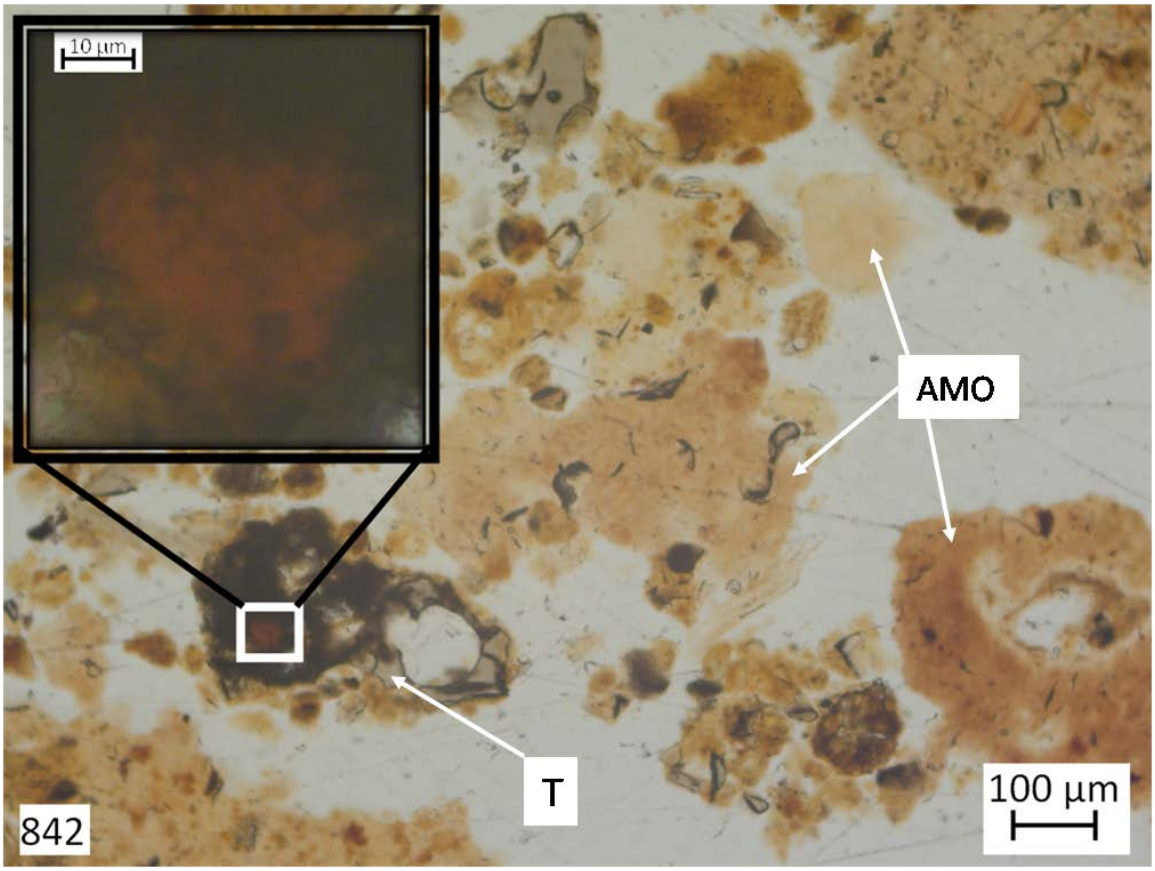

Figure 4.18: A grain of tephra (T) surrounded by amorphous organic matter (AMO) (GR 116, S2, TS 842, PPL). The volcanic glass has a isotropic red inclusion composed mainly of iron (by SEM-EDS analysis) which is consistent with the characteristics of haematite (inset at top left).

4.3.3 Biota in the sediments

Sclerotia were observed from bulk environmental (Section 4.1.3) and thin section (Table 7) analyses and are interpreted as evidence of fungal populations in the grave sediments. Fungal remains were observed in thin sections with a strong distribution both to amorphous organic material and to highly weathered tephra (Figure 4.19). Such distributions are interpreted as evidence of a relationship between fungi and the decomposition of organic matter and between fungi and the weathering of tephra. Significantly, observation of a micro-contextual spatial relationship as seen in Figure 4.19 is only possible with the technique of micromorphology. Experimental studies have suggested that microorganisms exert a strong influence on mineral weathering (Thorseth *et al.* 1992, 1995; Staudigel *et al.* 1995) through biotic processes. Endolithic organisms are those that inhabit a hard substrate (Gadd 2007). Some endoliths are able to bore directly into their substrates while others require the addition of a chemical agent (Tapanila *et al.* 2004 as cited in Tapanila 2008). Saprophytic fungi are some of the smallest endolithic heterotrophs (Tapanila 2008, 11). Studies on Archaean submerged tephras from ocean environments have shown convincing evidence for the bioerosion of volcanic glass by endoliths through hyphal boring into the silicates (McLoughlin *et al.* 2007 and 2008, 373).

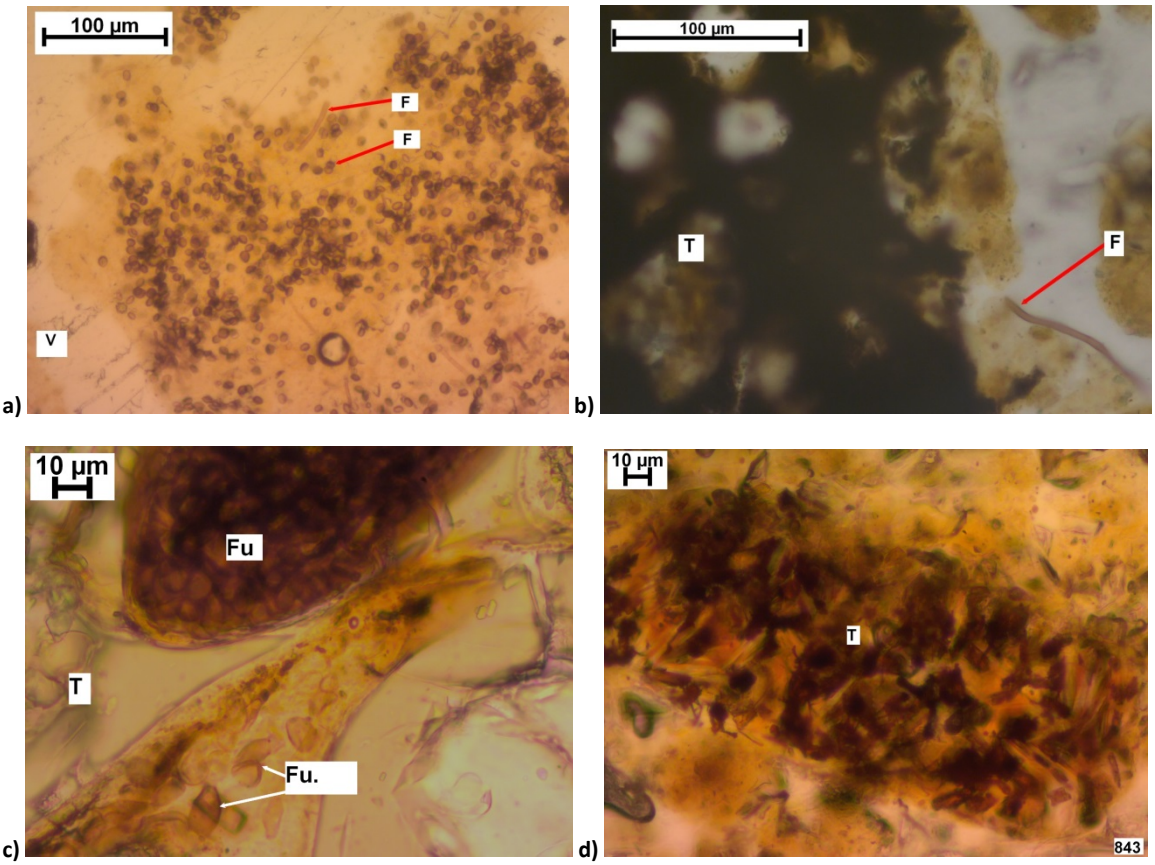

Figure 4.19: Tephra in close contact with fungal remains. a) organic matter and with fungal remains (TS 842, S2, GR 116). b) Heavily weathered tephra (T) with fungal hyphae (F) (GR 119, S2, TS 765, PPL). c) Weathered tephra (T) with fungal spores (Fu. sp.) (GR 114, S1, TS 680, PPL). d) Fungal remains have contributed to the creation of a kata-alteromorph from tephra (T) (GR 114, S3, TS 843, PPL).

4.3.4 Ash

Evidence of ash aggregates around the inhumations was present in GR 117 and 120 and in some of the other sampled graves in the skull and pelvis areas and but not near the feet. This can be seen most clearly in Table 7 by the observation of ash-related material in thin sections from all seven graves. Ashy material was observed during excavation at the sternum area of the skeleton in GR 117 and collected as an additional sample (SA2), as well as in GR 120 (S15 and A1). The excavators were confident in identifying this material as ash, but not as to its origins (volcanic or anthropogenic) or its significance in relation to the possible differences between GR 117 and 120 and the other graves. Did this appear only on GR 117 and 120 because they are in some respect different from the other five graves or was the ash preserved exclusively in these two graves?

4.3.4.1 Ash and bone in GR 120

The skull tangential thin section from GR 120 (TS 767) had mostly chamber voids, some excremental pedofeatures and some ash aggregates which were large and irregular in shape. A few remains of fresh roots, strongly referred to voids, support an interpretation of heavily bioturbated and also heavily weathered sediments, including identification of an example of a red coloured iron-rich alteromorph. The corresponding perpendicular thin section (GR 120, TS 718) had a weakly speckled b-fabric, 10% abundance of ash (Table 7), some of which occurs as two large aggregates at the edge furthest away from the skull, and while the bone remains were unburnt, there was some melted silica (which could not be identified with confidence as either anthropogenic or geological). Two large (2-3 cm) ash aggregates at the edge furthest from the skull were the only ash remains in the whole of the thin section and occur along the same vertical plane as each other (Figure 4.9a). Their common stratigraphic position supports their emplacement during the burial, perhaps the sprinkling of ash around the periphery of the head, rather than their transport to the skull area by, for example, bioturbation.

Sediment adjacent to the rib bones (GR 120, S1, TS 753) showed horizontal banded layers of yellow bone to opaque bone to ash (Figure 4.20d). The black micro-layer (opaque in thin section) was positively identified as bone from its optical characteristics and SEM-EDX analysis (Figure 4.20a-c and Appendix III). This sequence of materials and the boundaries between them supports the interpretation of the bone in these sediments opacitised *in situ*. TS 753 and 851 both contained some fungal remains and, unique to this sample, some (10% in TS 753 and 15% in TS 851) small red (PPL and XPL) spherules mainly composed of iron and located within the fine material (Figure 4.20). Although these spherules have a biaxial structure (Figure 4.20c) they differ from the calcareous spherulites often seen in micromorphological studies and attributed to faecal materials as the spherules seen in TS 753 and 851 have negligible amounts of calcium and a high concentration of iron and oxygen (Appendix III). The layers of yellow, opaque, and yellow materials (Figure 4.20d) at the top of TS 753 are interpreted as bone which has been altered by post-burial degradation which has partially altered its colours. The change in colour of the internal part of the bone fragment is attributed to microbial action which has altered the more porous part more rapidly than the more dense exterior bone (Chaplin 1971, 16-18 in Lyman 1994, 421). Investigations on bone porosity and the processes affecting bones in soils and sediments in temperate European climates have suggested the significance of pores at the sub-micron scale and the role of microbial attack in the diagenesis of bone and subsequent increases in porosity (Hedges 2002). Although the Overton experimental project had no evidence of uncooked bone with signs of microbial attack after 32 years of burial (Nielsen-Marsh and Hedges 2000) successive studies have emphasized that the rate of microbial attack on buried bone is established in its first 500 years of burial (Hedges 2002).

No microbial tunnels were observed in the bone and fungal borings should be visible in thin section (Chapter 2) whereas bacterially induced cracks and fissures (nanometer scale) would not be visible. There was, however, clear evidence of past fungal activity in this sediment (sclerotia in TS 753). The evidence of a lack of tunnels into the bone and the clear preference of the microbes for the internal bone, while leaving the cortex relatively untouched, suggests bacterial rather than fungal action is the principle cause for the change in opacity. The altered inner part of the bone fragment in sample GR 120 (SA1, TS 753) could suggest differences in groundwater and acidity levels in its proximity.

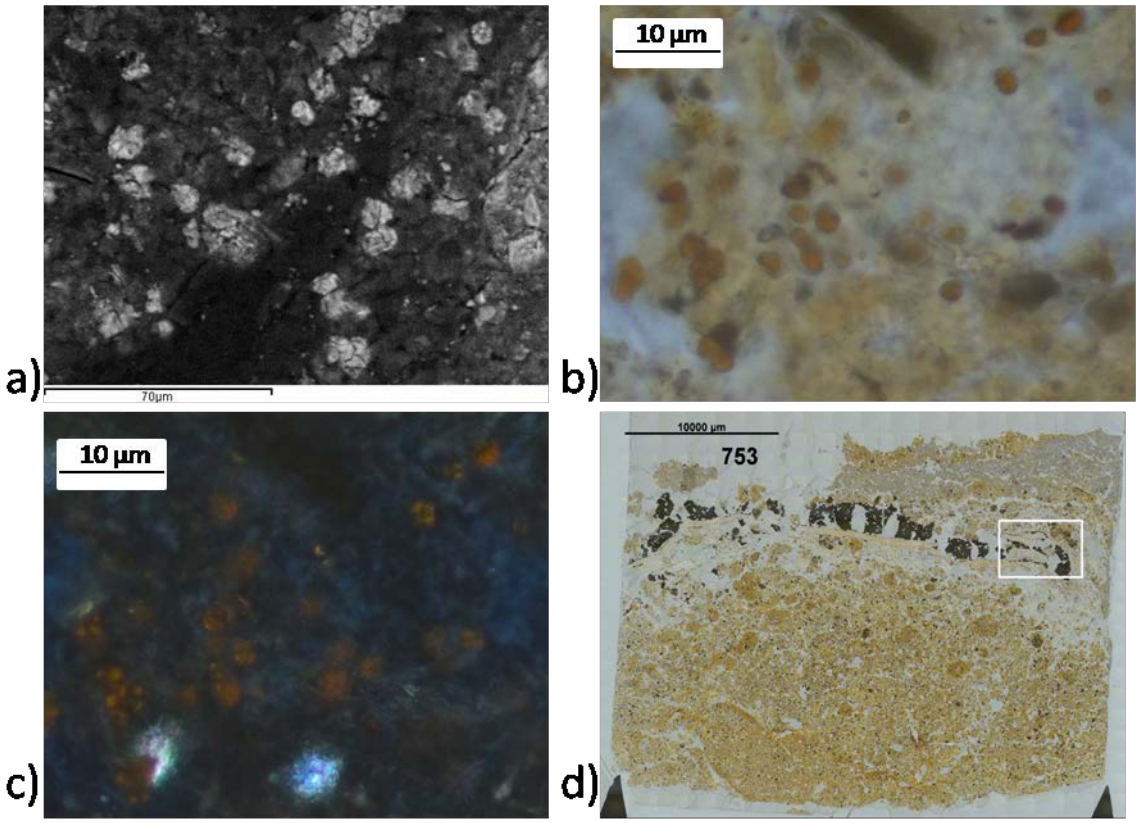

Figure 4.20: Red anisotropic iron-rich spherules associated with bone (TS 753, SA1, GR 120). (a) SEM image, x1.84k. (b) optical microscope (PPL). (c) (XPL). (d) Mosaic of TS 753 with the location of analysed area shown in (a-c) (white box) (PPL).

4.3.4.2 Ash in graves 114, 115, 116, 117 and 119

The C3 control for GR 114 (TS 727) was taken horizontally in line with the upper torso and just above the boundary of the lower grave fill and the sediment covering the skeletal remains. The thin section had a void modal average of vughs, and 5% abundance of ash aggregates making it quite similar to the sections from the pelvic and skull samples from grave GR 120. An abundance of fresh root remains was seen in transverse section (Appendix III) and interpreted as a result of a high level of bioturbation in this area (GR 114). No micromorphology sample was collected from the pelvis region either from above (*i.e.* S2X) or at (*i.e.* S2Y) the plane of the skeleton for GR 114. The sacral

sample for this grave was collected below the sacrum (TS 713, S2Z). A sample from the sediment around the hands, which were folded across the pelvis (TS 726, S16Y) had comparatively few voids (10%) and little ash (2%). The distribution of vugh shapes voids and ash in samples S2 and S1 of GR 114 are interpreted as the vertical displacement of ash by bioturbation.

TS 713 showed a decrease in ash with increasing distance from the sacral area in GR 114 (5% in micro-unit 1 compared to 2% in micro-unit 2) (Table 7). The most common (61/78) type of b-fabric in these sediments was undifferentiated, except for micro-unit 1 TS 713 where it was speckled (Table 7), probably in relation to the presence of disaggregated and disturbed ash. The absence of phytoliths in the ash of this sediment strengthens the interpretation that this ash was volcanic rather than wood ash. Micro-unit 2 of TS 713 had severely degraded wood present, interpreted as from the coffin base (Figure 4.21, Figure 4.22). Analysis of coffin remains at Hofstaðir by Py-Gc indicates them to be largely coniferous woods (chemistry team of the InterArChive Project). It is suggested that biota caused post-burial disturbance to the sediments in GR 114.

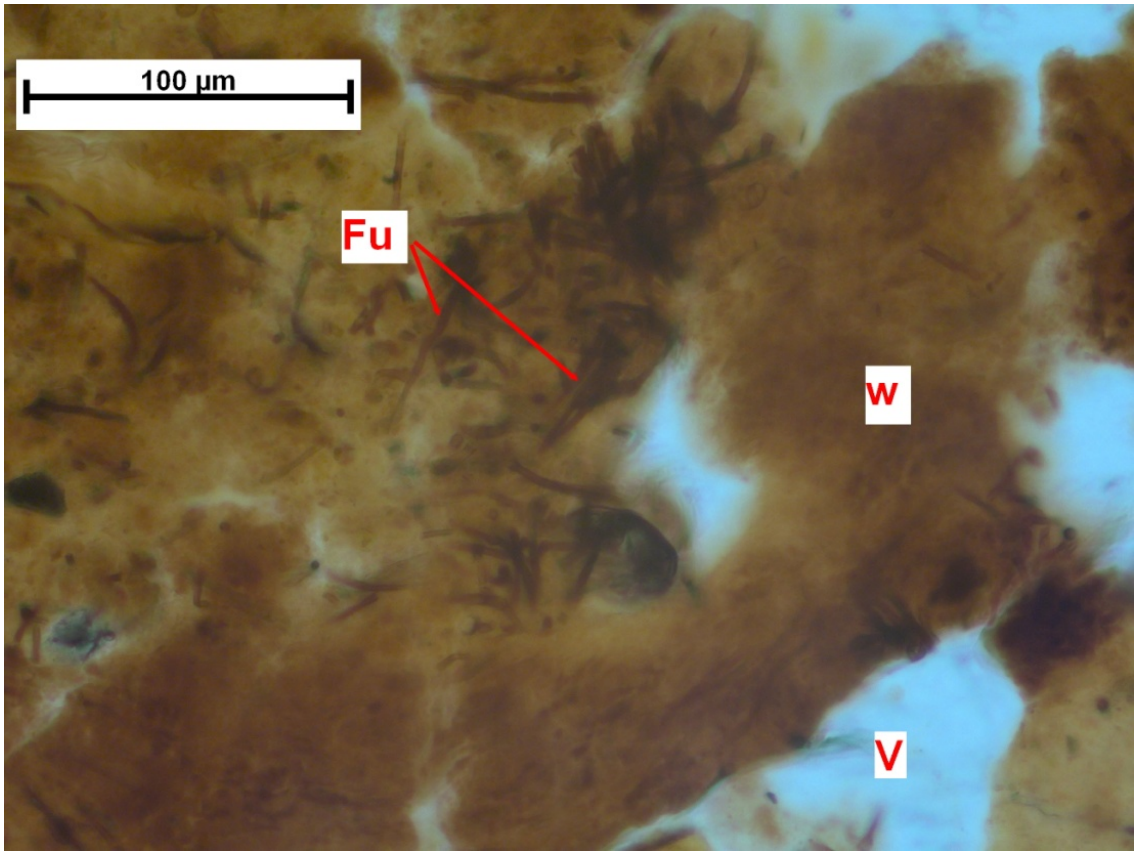

Figure 4.21: Fungal remains (Fu) and woody materials (W) surrounded by voids (V) in sediment from a pelvis adjacent sample (GR114, S2, TS 713, PPL).

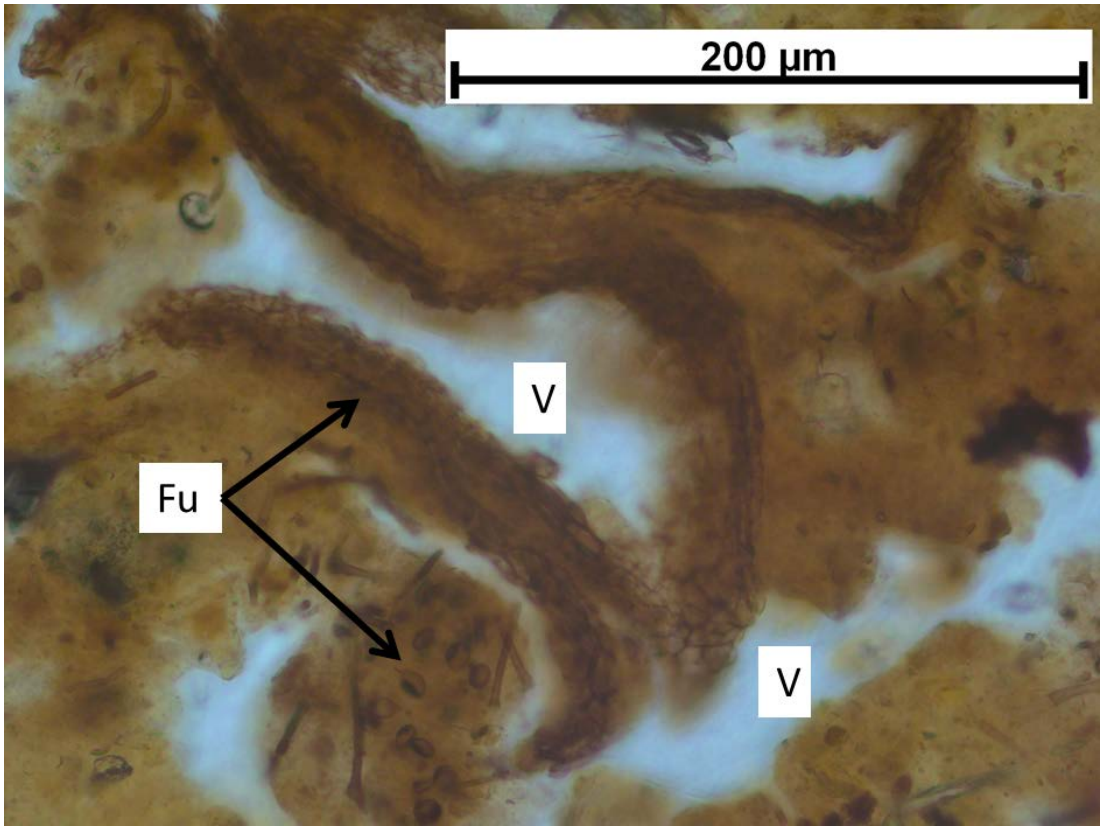

Figure 4.22: Fungal remains (Fu) surrounded by voids (V) in sediment from a pelvis adjacent sample (GR 114, S2, TS 713, PPL).

The upper grave fill in GR 115 (C2, TS 740) contained a comparatively large abundance of ash (15%) and most of its voids were vughs (Table 7). Meanwhile no ash was recorded from the sections of either skull (TS 816, 826 or 759). The skull sampled as SA6 (TS 759) had a 10% abundance of large angular opaque plant remains. The cellular structure of the material in TS 759 was indicative of a plant origin and the large angular forms of either a disruption *in situ* which had led to breakages of a large fragment into several smaller ones, or a primary deposition of this material. A history of these plant remains as a tertiary deposit or significant movement within the sediment would have resulted in more rounded, if not also smaller, fragments of charcoal (Schiffer 1987, 58-64 for use of terms primary, secondary and tertiary depositional histories, and Delvigne 1998, 388 for discussion of charcoal rounding in transport). The lack of ash in grave GR 115, despite only skull samples having been collected for micromorphological analysis, is seen as a notable difference between this and the other six graves.

The lower grave fill control in GR 116 (C3, TS 801) contained 5% abundance of ash small aggregates, a void modal average of channels and chambers, and 5% abundance of large excremental pedofeatures in a strongly linear basic distribution, which along with a partially developed granular microstructure (Table 7) and are interpreted as evidence to suggest that this unit was heavily bioturbated. By contrast, the skull perpendicular section (S1, TS 717) had a weakly speckled b-

fabric, along with ash in 5% abundance and having retained its high order interference colours considerably better than the ash aggregates from the surrounding graves. Phytoliths were absent from the sediment and the ash in this sediment is interpreted as volcanic. There was some bone (15% abundance) which, although it still displayed a ropey internal fabric in PPL, had weathered enough to lose its first order grey interference colours and so appeared isotropic in XPL. The presence of radial goethite crystals, a form common in wet environments, on some of the heavily weathered (*i.e.* weathering extents 3 or 4) tephra grains lends further support for the impacts of chemical weathering processes associated with an abundance of iron and aluminium ions in solution. The highly crystallized radial form of this goethite accretion supports its formation as an authigenic mineral.

The S2 sample tangential section from GR 117 (TS 725) had 5% abundance of ash aggregates with a banded distribution of horizontal oriented lenticular voids. The perpendicular section from the same sample (TS 711) exhibited 5% excremental pedofeatures, most of its voids were vughs, and ash was present as aggregates in 2% abundance with a strongly clustered basic distribution and a perpendicular referred distribution to the skull.

The lower grave fill control in GR 119 (C3, TS 627) had most of its voids as channels and vughs, a few roots (2%) and a few small excremental pedofeatures (2%) (Table 7) and are interpreted as evidence to suggest slight disturbance by bioturbative agents. The abundance of ash (5%) was greater than that of the C3 controls from other graves and reflects only a few quite large grains that appear as white aggregates (Figure 4.9d). By contrast, the upper grave fill (C2, TS 597) had an almost even abundance of channel chamber and vugh voids, and a feature that originally might have comprised very finely laminated micro-units, although the boundaries between them were no longer discernible. The mixing was attributed to an effect of mixing by sediment flora and fauna activities, represented through the proxy evidence of excremental pedofeatures (5% abundance) which have preserved their strong linear basic distribution, and thus cannot pre-date the mixing of the micro-layers. The sacral perpendicular section (S2p, TS 765) contained some ash aggregates (10%) which although have a moderately clustered basic distribution and there are a few (5%) medium excremental pedofeatures which have a strongly clustered basic distribution. The evidence in the S2 sample is interpreted as evidence to suggest that the disturbance by bioturbation extended across both the samples and the controls in GR 119.

4.3.5 Point counting

Point counting was carried out on all thin sections from Hofstaðir, assigning features to one of a total of nine possible categories, hereafter referred to as groups (Section 4.2.3). The nine groups

used in the point counting are listed in Table 6, and the results from the C1 controls are summarized in Figure 4.23.

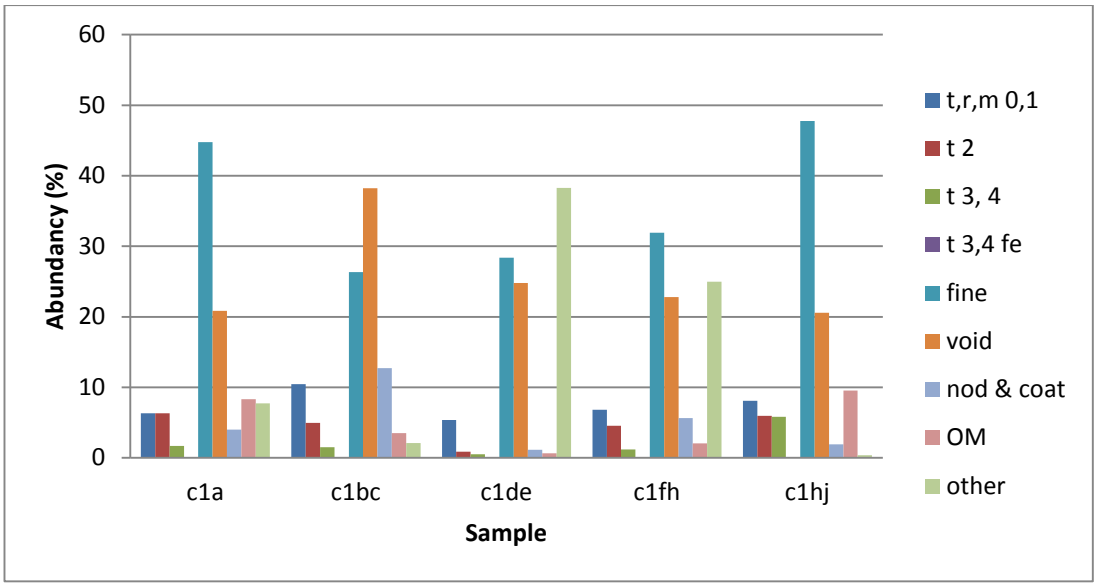

Figure 4.23: Summary results of point counting from C1 thin sections.

4.3.5.1 Controls and tangential oriented thin sections

The four tephra point counting groups were used to calculate the extent of tephra weathering expressed as a weathering ratio for each thin section. The ratio compared the relative amounts of the of heavily weathered (extents 3 and 4) to less weathered (extents 0, 1, and 2) tephra (ratio=(t3+t4)/(trm0+t1+t2)). Table 10 reports the weathering ratio for each of the C1 controls together with the percentage values. As such, higher values reflect more heavily weathered tephra and *vice versa*. This ratio used the percentage results of the point counting rather than the raw "counts" data and results are summarised below (Table 11).

Table 10: Results of tephra point counting on C1 controls to assess extent of weathering of tephra.[2]

tephra weathering	C1a	C1bc	C1de	C1fh	C1hj
t,r,m 0,1	6.327	10.471	5.392	6.843	8.095
t 2	6.327	4.941	0.899	4.562	5.952
t 3,4 bo	1.698	1.529	0.513	1.2	5.833
t 34 fe	0	0.118	0	0	0
total t	14.352	17.059	6.804	12.605	19.88
total t34	1.698	1.647	0.513	1.2	5.833
trm01% of Tt	44.08445	61.38109	79.2475	54.28798	40.71932
t2% of Tt	44.08445	28.96418	13.21282	36.19199	29.93964
all t34% of Tt	11.8311	9.654728	7.539683	9.520032	29.93411
ratio of 34 to 01&2	0.134187	0.106865	0.081545	0.105217	0.42
ratio of 34 to 01&2 (2dp)	0.13	0.11	0.08	0.11	0.42

Table 11: Weathering ratio of tephra from intra-grave controls (C2 and C3) and tangential thin sections for GR 114-120. Grey squares indicate absence.

Grave	C2	C3	1a	2a	3,4a
114		0.31	0.64	1.34	0.75
115	0.52	0.35	1.32		
116	0.34	0.39	0.57	1.67	1.38
117	0.48	0.44	0.89	0.83	1.18
118	0.42	0.3			
119	0.31	0.43	1.07	1.46	1.42
120	0.21	0.54	1.14	2.24	1.5

Figure 4.24 has a characteristic u-shape curve and this trend in the C1 profile is suggested to have been caused by an increased level of weathering in the upper horizons due to root activity in this grass-covered sheep grazing site (C1A, TS 715; Figure 4.7), lower level of biological activity in layers (C1DE, TS 620) and the older lower deposits (C1HJ, TS 599) having been heavily affected by the processes of weathering. The greater level weathering of the tephra in the lower deposits is inferred as an effect of the increased age of the lower deposits which were sealed by the Hekla tephra layer (Section 4.1) compared to the stratigraphically higher ones. The tephra present in the C1 profile had an irregular linear weathering pattern (Figure 4.16) and is interpreted as evidence suggesting a trend of increasing weathering ratio with depth after the topsoil (Figure 4.24). It is suggested that the sediment in the control profile is composed of relatively undisturbed tephra layers varying in thickness and content (Figure 4.12), which have been preserved due to their low

[2] Abbreviations used are as follows: tephra, rocks or minerals at weathering extent 0 or 1 (t,r,m 0,1), tephra weathered to extent 2 (t,r,m 2), tephra weathered to extent 3 or 4 exhibiting a dark colour and isotropic (t 34 bo), tephra weathered to extent 3 or 4 and exhibiting a red colour and anisotropic (t 34 fe), and tephra (t).

levels of sediment biota and pedoturbation. The interpretation that the C1 controls suggest an increased weathering with depth and are relatively undisturbed by bioturbation is supported by the literature. Previous studies on tephra weathering in andosols (Section 4.1.2) suggest that tephra weathers with irregular linear weathering patterns and exhibits a gradual increase in weathering extents down a profile from fresh (0) to highly altered (4) volcanic glass.

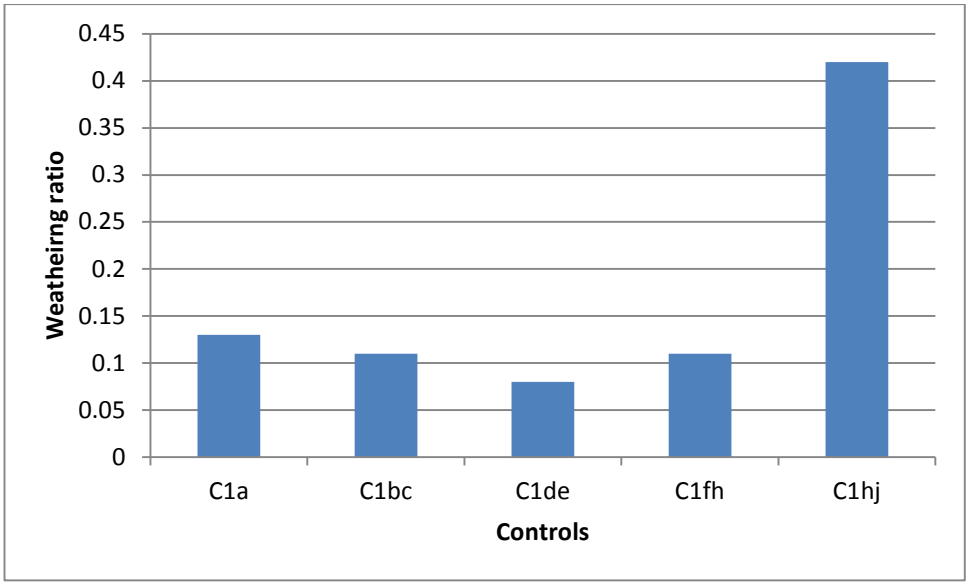

Figure 4.24: Tephra weathering ratio across the C1 profile from the top sediment (C1A) to the base (C1HJ).

4.3.5.2 Pilot study on perpendicular oriented thin sections

A pilot study was performed in order to assess the potential of point counting to reveal differences in the weathering ratio with increasing distance from the skeletal remains. The pilot study, using TS 619 (GR 117, S2p), entailed sub-division of the surface area into 1 cm intervals starting from the side closest to the pelvis (Figure 4.25). The results of the different weathering extents in Table 12 suggested a potential for interpretations of changes occurring in correlation to increasing distance from the decomposing body (Figure 4.26) and are discussed in the following sections.

Figure 4.25: TS 619 (GR 117, S2p) with 1 cm sub-divisions. The vertical black lines delineate the sub-divisions while the diagonal black line highlights the boundary between the two micro-units present within TS 619. The top of the thin section is at the top of the image and the pelvis is towards the right of the thin section.

Table 12: Abundance of different extent of weathering of tephra in pilot study of TS 619[3].

Tephra in thin section 619	s1	s2	s3	s4
trm01	12.727	17.143	16.667	7.143
t2	11.818	15.238	8.889	11.111
t34 bo	6.364	11.428	5.555	19.048
t34 fe	0	0	0	0

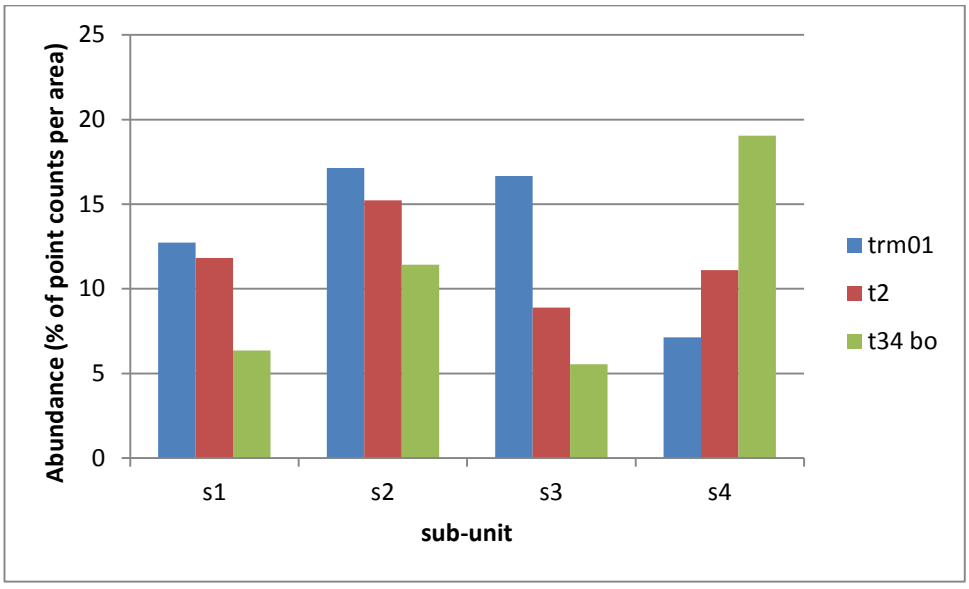

Figure 4.26: Weathering of tephra across 1 cm sub-sections of TS 619.[3]

[3] Abbreviations used are as folllows: tephra, rocks and minerals at weathering extents 0 or 1 (trm01), tephra at weathering extent 2 (t2), tephra at weathering extent 3 or 4 to a dark isotropic material (t34bo), tephra at weathering stage 3 or 4 to an iron rich alteromorph (t34fe), sub-division 1 (s1), sub-division 2 (s2), sub-division 3 (s3), sub-division 4 (s4).

4.3.5.3 Perpendicular oriented thin sections

Based on the potential of the results indicated by the pilot study (Section 4.3.5.2) this point counting method was modified and expanded. The intervals were halved and the numbering of the sub-sections reversed. The surface area was divided into six sub-divisions, each sub-section measuring 0.5 cm wide, starting from the side of the thin section closest to the skeleton (Figure 4.27). Each of these sub-sections was point-counted to a minimum of 500 counts. This method was employed to allow comparisons to be made between sub-sections at increasing distance from the skeletal remains. Where total size of a perpendicular thin section was less than 3 cm, some of the sub-sections have no data.

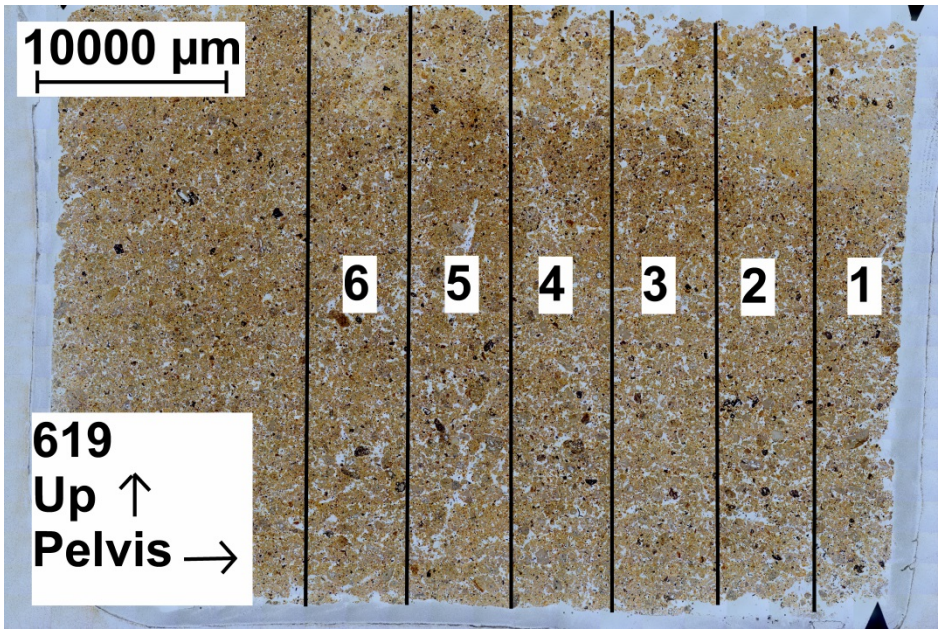

Figure 4.27: TS 619 (GR 117, S2p) with sub-divisions at 0.5 cm intervals from the edge of the thin section closest to the body. The top of the thin section is at the top of the image and the pelvis was towards the right.

The interpretation of the results in Table 11 suggests that weathering extents are higher in the tangential oriented sections from samples than in the controls (Section 4.3.5.1). Weathering ratio from tangential sections were compared those from the sub-divided sections of the perpendicular thin sections from the samples (Table 13) to assess weathering and proximity to the skeletal remains at the micro-scale. The interpretation of the evidence from the sections from 2Y samples in Table 13 suggests a trend of increasing weathering towards the skeleton. Sample 2 from GR 120 was collected from the sediment in the horizontal plane above the sacral region of the skeletal remains (S2X), and the thin section had plant remains (Table 7) which are interpreted as degraded

coffin wood. The S2Z sample from GR 116, S2X sample from GR 120, and S3/4 sample from GR 114 were collected in a different location relative to the foot bones compared to the S2Y samples from the other graves. The analyses of the tangential and perpendicular thin sections from the S2Z sample of GR 116 have a consistently high ratio, and are interpreted as due to the sample being collected underneath the plane of the sacrum. The results from the tangential and perpendicular thin section from S2 of GR 120 differ from the more general trend by consistently displaying high weathering ratios. This is also interpreted as evidence of a difference in the plane (x, y or z) of the sample referred to the skeleton. The interpretation of the evidence of the location of the samples in the graves (Figure 4.7 and Figure 4.9) and the trends in Table 13 suggest a pattern of increased tephra weathering closer to the skeletal remains.

Table 13: Weathering ratios from the tangential (t) and perpendicular (p) oriented thin sections from samples of the sediments adjacent to the a) skull, b) sacral, and c) foot regions within the seven graves sampled. Grey cells represent no data.

a)

	S1 t	S1 p sub-1	S1 p sub-2	S1 p sub-3	S1 p sub-4	S1 p sub-5	S1 p sub-6
GR 114	0.64	0.36	0.49	0.71	0.31	0.25	0.35
GR 115	1.32	0.5	0.6	0.66	0.45	0.33	0.88
GR 116	0.57	1.08	1.04	1.28	0.78	0.68	0.72
GR 117	0.89	0.62	0.96	0.94	1	0.7	1.05
GR 118							
GR 119	1.07	2.32	1.97	1.02	1.2	1.43	0.73
GR 120	1.14	1.46	7.3	1.31	1.49	0.64	

b)

	S2 t	S2 p sub-1	S2 p sub-2	S2 p sub-3	S2 p sub-4	S2 p sub-5	S2 p sub-6
GR 114	1.34	2.48	2.57	2.27	1.16	1.2	0.61
GR 115							
GR 116	1.67	4.3	4.16	6.53	2.89	2.81	
GR 117	0.83	0.86	0.7	0.43	0.28	0.27	0.22
GR 118							
GR 119	1.46	1.44	1.5	5.09	2.4	1.05	1.56
GR 120	2.24	1.47	1.77	2.24	1.88	2.44	2.35

c)

	S3,4 t	S3,4 p sub-1	S3,4 p sub-2	S3,4 p sub-3	S3,4 p sub-4	S3,4 p sub-5	S3,4 p sub-6
GR 114	0.75	1.94	1.74	1.17	1.09	0.86	1.06
GR 115							
GR 116	1.38						
GR 117	1.18	1.42	1.75	1.5	1.31	1.84	1.75
GR 118							
GR 119	1.42	5.5	5.46	1.57	1.94	1.62	
GR 120	1.5	3.95	0.56	0.92	2.38	1.21	0.93

The weathering ratio from the foot sample of GR 120 in Table 13 is different to this sample position from the other graves. The deviation from the trend for the second and third sub-divisions (sub-3 and sub-4 in Table 13) of the perpendicular samples is suggested to be because GR 120 was further away from the other graves and much closer to the turf wall. The ratio of the tangential section from the foot sample of GR 114 is lower than for the other graves. GR 114 foot sample was collected from between the two feet, rather than between a foot and the grave cut as in the other graves. It is suggested that the weathering rate of the tephra in the thin sections of the foot sample from GR 114 (Table 13) was affected by the location of the sample. Micro-scale sediment dynamics, especially regarding porosity as decreased aerobic levels could decrease fungal activity and could alter the permeability of sediment solutions. Hence, the difference in sediment conditions between the feet compared to between a foot and the coffin are suggested to have had an effect on tephra weathering and are expressed in the tephra weathering ratio.

4.3.6 Tephra weathering in samples and controls

The weathering ratios of the controls differ to those of the samples (Table 11) and fungi were present in thin sections from the samples and in the top sediment (C1A) (Table 7). The difference in the tephra weathering between controls and samples are interpreted as evidence to suggest that the burial has affected the biotic mineral weathering in the samples (Figure 4.28). In the graves of Hofstaðir the biotic weathering component of the tephra weathering process can be seen through an isomorphous phase with a dark grey colour in PPL (Figure 4.15).

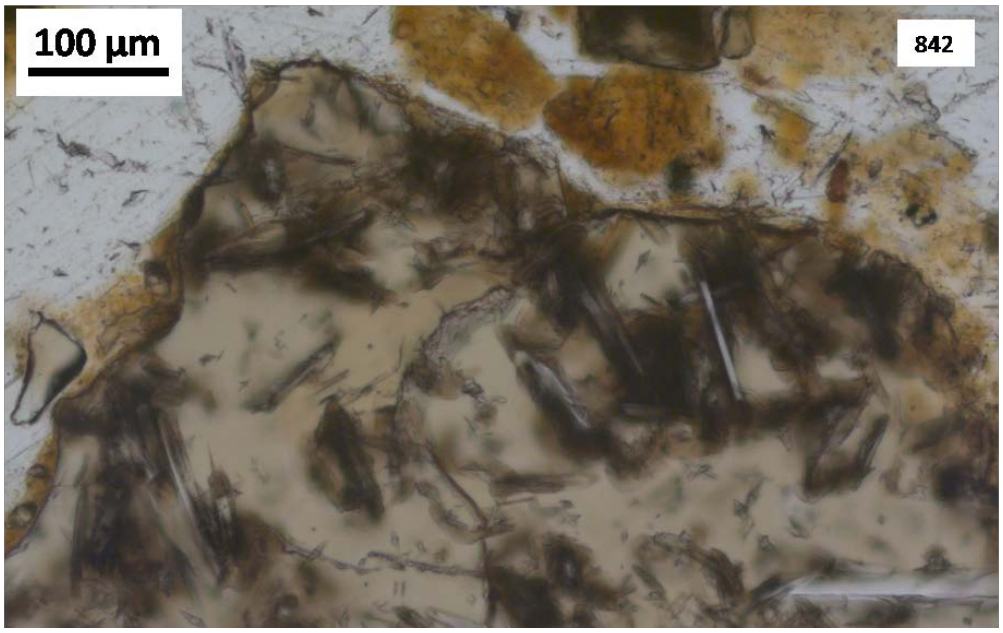

Figure 4.28: Tephra showing biotic weathering by exploiting dendritically into irregular fractures at the periphery of a fragment (TS 842, S2, GR 116, PPL).

The tunnels in the tephra are interpreted as tubules which remain after the fungal remains have been removed and suggest that that hyphae have bored directly into tephra (Figures 3.29 and 3.30), directly affecting the mineral weathering. The increasing weathering ratio from controls to samples in Table 11 is interpreted as evidence to suggest an increase in the weathering rate from the controls to the graves sediments. Greater amounts of material identified as fungal remains were observed in burial sediments compared to controls (Table 7). It is suggested that the increased levels of highly weathered tephra in the burial sediments is partially attributed to the elevated levels of fungal activity in these sediments compared to the controls.

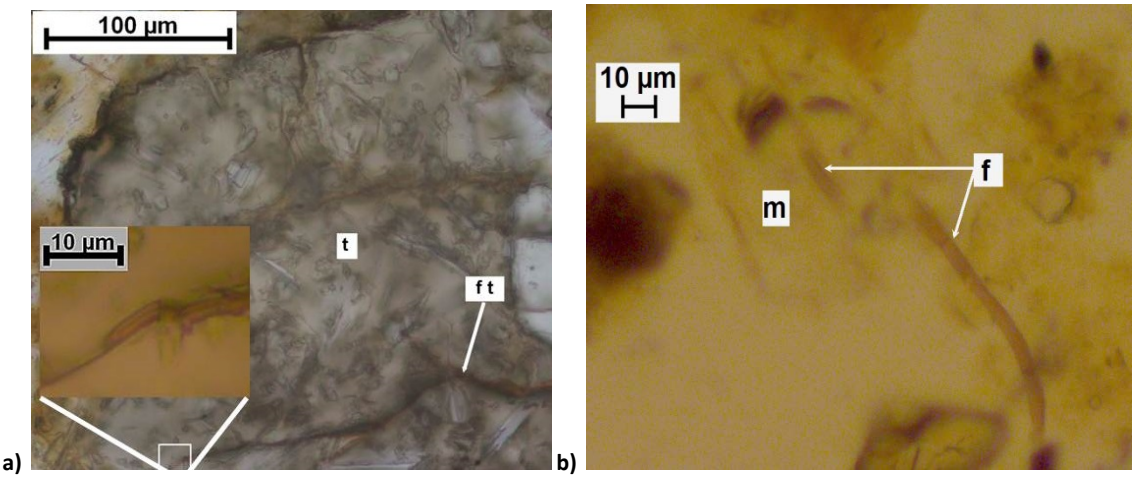

Figure 4.29: Fungal boring visible into tephra and colourless silicates. a) Fungal remains in a planar void (f t) with hyphae (inset) in tephra fragment (t) (TS 842, S2, GR 116, PPL). b) Fungal hyphae (f) in colourless silicate mineral (m) (TS 842, S2, GR 116, PPL).

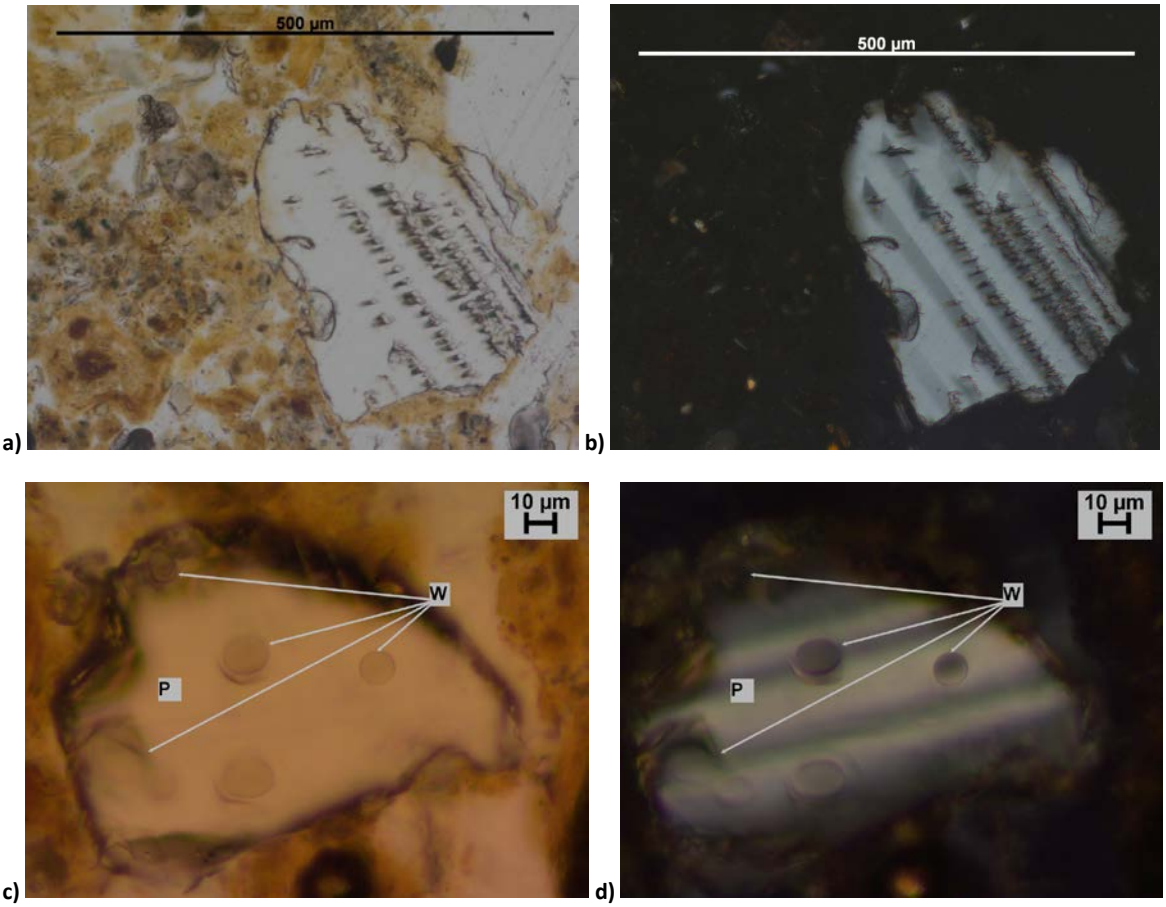

Figure 4.30: Plagioclase with speckled weathering. a) plagioclase with speckled weathering pattern congruent to polysynthetic twinning, attributed to abiotic weathering (PPL). b) XPL view of image a). c) plagioclase (Pg) with speckled weathering (W) pattern which do not appear to line up with polysynthetic twinning, attributed to biotic weathering (GR 120, C3, TS 801, PPL). d) XPL view of image c).

The weathering ratios of tephra in the controls and the samples (perpendicular and tangential thin sections) is represented in Figure 4.31 and increases from left to right across the graph as weathering ratios increase. The weathering ratio for the tephra within the samples (S1, S3,4 and S2) was greater than from the controls (C1, C2 and C3) and suggests a localized increase in the weathering process with proximity to the human remains. Identification of mineral specific weathering effects on the tephra is suggested to have potential as a proxy indicator of past fungal activity. This potential use could increase the length of time during which organic matter could be recorded from the archaeological record *via* proxy data, and indicate the detailed (cm to mm) spatial distribution of such activity. Preservation of such distributions could enable archaeologists to infer the location of buried remains in a grave.

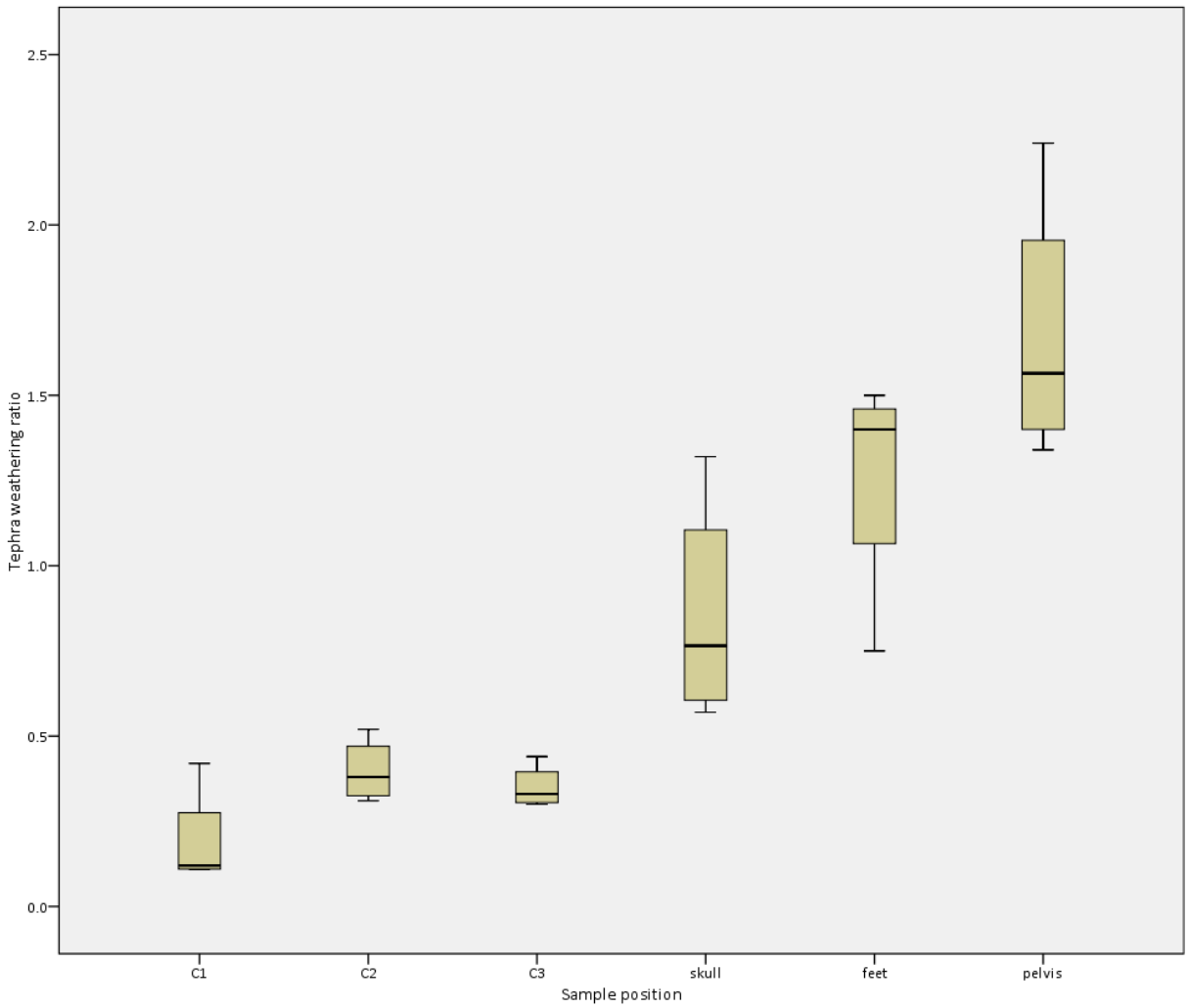

Figure 4.31: Weathering ratio from point counting analysis of tephra in thin sections from controls (C2, C3) and samples (S1, S2 and S3,4) of all seven graves sampled (GR 114-120). Values are lower from the controls (C2 and C3) at the left side of the graph compared to those from the samples near the skull (S1), feet (S3 or S4) and sacrum (S2) at the right of the graph. Box and whisker plots show medians and upper and lower interquartile ranges which do not overlap between controls (C1, C2 and C3) and samples (skull, feet and pelvis).

4.4 Interpretation and discussion

4.4.1 Mineral weathering

Tephra weathering patterns and extents from the samples are suggested to differ from the controls because of the presence of the burials in the graves (Figure 4.31). The interpretation of an effect on mineral weathering by the decomposition of a body is inferred from considering the weathering processes of the sediment conditions and processes in the control sediments.

The volcanic glasses, or tephra, were observed to be fragmented as a result of the exploitation of irregular linear weathering patterns to form fissures or fractures that were filled with an isotropic coating surrounding the tephra fragments. Studies have shown that this isotropic coating is formed by the movement of Al and Fe ions in the sediment, these being “liberated from the weathering of

other primary minerals" (such as tecto-, neso-, and inosilicates) (Jongmans *et al.* 1995, 341). Tephra deposits in soils often exhibits a general trend towards desilification, especially down a sediment profile. The yellow to orange anisotropic fine materials associated with the tephra cannot be definitively identified as either palagonite or allophane without further sub-microscopic techniques (Gérard *et al.* 2007). The strongest relationship between the exchange of ions during palagonitization is the loss of Si and Al accompanying gain in Ti (Staudigel and Hart 1983). Both gel- and fibro-palagonite were observed in the thin sections from the graves sampled at Hofstaðir (Figure 4.17). Palagonite is widely accepted as the first stable alteration product of tephra (Hay and Iijima 1968). The alteration of volcanic silicates through stages of palagonitization is well researched and documented (see review by Stroncik and Schmincke 2002) and easily observable at the scales of magnification offered by the light microscope. Despite earlier attempts to classify the two forms of palagonite into two distinct groups, gel-palagonite and fibro-palagonite (Peacock 1926) it has now been shown that these two materials are merely different phases of palagonitization, with the gel stage progressing towards the more crystalline fibro-palagonite phase (Stroncik and Schmincke 2002).

Gibbsite was observed and interpreted to have formed as an weathering product of tephra which was near to amorphous organic matter in a sample from these graves (Figure 4.18). This form was present in some of the samples but absent from the controls and it is suggested that the cause of such a distribution is related to the higher organic matter content in the samples compared to the controls. Studies suggest tephra can weather to produce gibbsite as a secondary product and that the presence of gibbsite within a context can be utilised to infer the most desilicated stage having been reached in a micro-scale environment (Jongmans *et al.* 1995, 341). The progress of tephra weathering described in Jongmans *et al.* (1995) supports the suggestion that in the C1 controls at Hofstaðir it was weathered mostly by abiotic transformations, and in samples with evidence attributed to biotic weathering processes. The graves at Hofstaðir were buried in a young andosol (Section 4.1) and the analysis of tephra weathering at the site was suitable for study as volcanic silicates have low thermodynamic stability and "are more reactive than associated primary mineral assemblages" (Stroncik and Schmincke 2002, 680)."

4.4.2 Discussion: archaeological questions and thin section analyses

Three main topics were raised in relation to observations during the excavation of the seven graves at Hofstaðir (Section 4.2.1). These were the location of ash, the multiple skulls in GR 115, and proxy evidence of decomposition. The interpretations are based on the results of Table 7 and the analyses in Section 3.3 and estimated abundances stated are those based on Bullock *et al.* (1985, 24-25).

4.4.2.1 Summary of ash in the graves

Assessment of the results of the micromorphological observations concerning the presence of ash (Section 4.3.4) is interpreted as evidence to suggest that opaque wood remains in some graves and aggregates of volcanic ash inferred as disturbed by bioturbation. Ash and blackened bone were present in the sediments from GR 120 and the opacity of the bone is interpreted as evidence of microbial activity as a post-depositional process (Section 4.3.4.1). The interpretation of the results of the micromorphological analyses are not consistent with the suggestion of a burning of materials in GR 120. Evidence of post-burial disturbance by biota is inferred from the remains of fungi in GR 114 in the degraded coffin wood layer (Section 4.3.4.2).

Evidence from GR 114, GR 116 and GR 119 is interpreted as supporting the suggestion of localised blackening of materials in the torso area in these three graves in addition to GR 120. Hence, the interpretations of the location of the ash in GR 117 and 120 do not suggest a difference of the activities related to the burial of these inhumations but to differential preservation, despite similarities in deposition of the burial with GR 114, 116, and 119. There is an absence of similar evidence from the thin section analysis of controls from GR 118, although no micromorphology samples were collected from this grave.

The interpretation of the evidence in GR 115 does not suggest that there is a relationship between the distribution of ashy materials and distance from the skeleton. This grave has some ash present in the upper grave fill (C2) and is interpreted as evidence of the disturbance by the grave cut. The ash aggregates in the C2 are not consistent with an interpretation as evidence of bioturbation by fauna within the grave sediments as such activities would have left traces in the C3 control located between the grave and the C2 control.

4.4.2.2 Burial sediment of the multiple burial in GR 115

The field notations of GR 115 listed this grave as different from the others (Section 4.2.2) because of the presence of multiple inhumations and the disarticulation of the skeletons (Figure 4.11). The interpretations of the distribution of ash are described in Section 4.3.4. The remains in this grave are suggested to have been skeletonised prior to burial in order for them to have been compacted in such an anatomically disarticulated manner. However, a ring was present on one of the fingers (Figure 4.11).

The skull which was sampled as S1Y sample from this grave is hereafter referred to as Skull#1, while the skull which was sampled as an SA6Y sample is hereafter referred to as Skull#2. The tangential thin section (S1Y, TS 826) of Skull#1 was slightly different in colour to that of skulls from other graves

with a slightly more orange tint to the sediment in TS 826, micro-unit 1. Across both the tangential (TS 826) and perpendicular (TS 816) sections of Skull# 1, the b-fabric was weakly speckled and with 1st order yellow interference colour rims on the pyroxene grains. The weakly speckled b-fabric compared to the undifferentiated b-fabric common in the sections from this site is interpreted as evidence of mixing of ash into the micromass as a result of disturbance in this grave sediment. The peripheral weathering patterns and lower order rims of the pyroxene grains supports interpretations of more advanced sediment weathering in this grave. Vughs were the most common type of voids in the thin sections from the S1 samples (from both Skull#1 and Skull#2) in this grave, similarly to those in the S1 positions in the other graves.

Micro-unit 1 of the tangential section from Skull#1 (S1Yt, TS 826) had an abundance of strongly clustered fungal remains in inclined related distribution to the isotropic, irregularly shaped, pale yellow amorphous organic matter interpreted as degraded bone material. The lower micro-unit (TS 826.2) from this sample contained moderately developed yellow-brown granular peds covered in loose fungal spores, which increased in abundance and size towards the corner of the thin section closest to the skull and lower edge. Micro-unit 1 of Skull#2 (SA6, TS 759) had highly speckled weathering on the tephra, some with adjacent anisotropic red material at the weathered edges. Bone and opaque plant remains were present in TS 759 in the area of the section furthest away from the skull and absent in the area of the section closest to the skull. This is interpreted to suggest that either these degraded bone fragments were not from this skull and from a different bone (Figure 4.11) or they had been heavily displaced. The weathering of the tephra in this grave was similar to that of GR 114 (Table 12).

The interpretations of the observations described above do not support a suggestion that the remains in GR 115 were different in terms of the decomposition processes compared to the other six graves. Hence, it is suggested that these remains were only partially skeletonised prior to burial and were subjected to a greater degree of disruption post-mortem than the other six bodies. The skeletons could have been disturbed primary burials that were reburied compactly, the compact nature of the burial visible in the photograph of the remains (Figure 4.11) both in terms of placement and abundance in relation to the size of the grave cut.

4.4.2.3 Proxy evidence for decomposition processes of human remains

Two questions raised during excavation concerned the potential of proxy evidence for recognising where organic matter was originally present and devising a strategy to access such information. The preservation of very fine tephra layers in the control sediment profile (C1A-FH) are interpreted as evidence of preservation of the aeolian deposition and negligible disturbance by sediment fauna

(Section 4.3). The degradation process at Hofstaðir is represented by evidence of past fungal activity in an andosol which have limited soil fauna (Section 4.1). The results of the thin section analyses of these graves are encouraging for the potential of mineral weathering to act as proxy evidence of sediment processes related to inhumation burials. In particular, the interaction between fungal organisms and readily weathered silicates such as volcanic glass hold considerable promise. Future work could research the role of other sediment microbes (Figure 4.32) in mineral weathering processes. The effects of bacteria on tephra weathering could be investigated to better elucidate the exact processes and rates by which the tephra weathering differs in graves sediments to non-grave sediments (Figure 4.31). Future work could entail a more extensive comparison between grave and non-grave sediments related to tephra weathering, perhaps with a wider variation of climates and different tephra types. Once the processes by which these effects on the sediments are more fully understood, research could progress into using these sediment differences to aid in answering questions such as whether a body in a grave was fleshed or skeletonised at the time of burial.

Figure 4.32: Microbe associated with tephra (HST-11, GR 116, S2Z, TS 842, PPL).

Interpretations of the evidence of the weathering ratios of the control sediment profile (C1A-FH), the C2 and C3 controls and the samples (S1, S2, S3) (Tables 11 and 13) suggest that weathering extents and patterns of sediment mineralogical materials can act as proxy evidence of human remains (Figure 4.29). This could be useful to archaeologists in future who have found a grave cut and decomposition has advanced so that no visible trace of the body remains. Silhouettes in graves have been recorded at archaeological sites and their elemental signatures discussed (Section 2.3). It has suggested black deposits on and adjacent to bone from graves in the UK were the result of

magnetotactic bacteria producing linked chains of crystalline deposits (Linford 2004, 2005). The blackened bone present in the samples from Hofstaðir could be the result of bacterial actions and its presence suggests that such post-burial change to bone is possible in andosols. In future work blackened bone, such as at Hofstaðir, could be investigated in relation to microbially linked chains of sub-microscopic (*c.* 100 nm) magnetite and where such material is found, this could aid in interpretations of hydrological changes over time across the site, such as water fluctuations within a grave (Section 2.3).

Interpretations of the results of the tangential and perpendicular thin sections has not been as encouraging in relation to identifying proxy evidence for the location of the body at a smaller scale and a greater level of detail compared to the results of the samples and the controls. However, the interpretations do suggest some trends that would benefit from additional studies of archaeological graves from sites on volcanic sediments (Chapter 8).

4.5 Conclusion

The analysis of the results from the study of the thin sections from the micromorphology samples collected at this site have been effective in answering the questions raised on site during the excavation, especially in terms of the trace scale proxy evidence of human remains and micro-contextual relationship between the organic matter and sediment minerals. The results from the study at Hofstaðir have been particularly positive, in relation to the role that volcanic silicates can play as proxy evidence for post-depositional formation processes of the archaeological record.

Chapter 5. Case study: Al Khiday, Sudan

5.1 Introduction

The site of Al Khiday offers an insight into the archaeology and site formation processes of the Nile region ranging from the Mesolithic to Meroitic periods (Usai *et al.*, 2010a). The Meroitic age of the archaeology was supported through radiocarbon dating of charcoal and shell materials (Usai *et al.* 2010a and Salvatori and Usai 2009). The site discussed in this chapter (site code 16D4) is one of several in the area reviewed by Usai *et al.* (2010a). The cemetery site of 16D4 is located on the western bank above the White Nile floodplain, south of present day Omdurman, Sudan (Figure 5.1) and carbon dating of shells from the sediments place the graves well within the Middle Mesolithic period (6678 and 6255 1σ cal BC, 7002 to 6213 2σ cal BC; Salvatori *et al.* 2011).

Figure 5.1: Map of the area of the site with inset (adapted from Google Maps © 2014).

For much of the Holocene the climate of the region has been arid, with wind as the prime natural force of sedimentary erosion (Gamri 2004). Several lakes existed to the west of the site during the early Holocene (Usai 2014). These bodies of water were seasonally present around the time of the Mesolithic occupation of the region and were created by the cyclical flooding of the Nile (Williams

and Adamson 1980, Adamson *et al.* 1982, Williams *et al.* 1982, Cremaschi *et al.* 2006, Williams 2009, Zerboni 2011). Micromorphology of the sites in the region of the graves has been discussed by Zerboni (2011). Micromorphological analysis of the sediments in the pits at site 16D4 revealed the groundmass to include microsparite, burnt and unburnt bones and calcite pseudomorphs (from wood ash), leading to their interpretation as Mesolithic fire pits and indicating the use of fish and molluscan resources by the inhabitants (Zerboni 2011).

Previous work on the site revealed 154 graves belonging to either Mesolithic, Neolithic or Meroitic phases of occupation at the site (Salvatori *et al.* 2011). The six graves discussed in this chapter belong to a larger collection of 70 graves from the Mesolithic period of use, that were distinguished from the other graves at the site by their elongated, prone body positions and lack of grave goods, excepting grave (GR) 153 (*ibid*).

5.1.1 Mineral surface micro-textures

The sediment surrounding the graves was primarily composed of sand grains. SEM and SEM-EDS analysis of quartzose sand grain surface textures has been shown to aid in determining the origins, weathering and transport histories of the grains (Mahaney 2002, 9-10 and 172). Diagenetic effects on quartz grains are particularly useful in "the interpretation of grain modification following deposition" (Mahaney 2002, 186). Although surface micro-texture analysis should ideally be conducted on loose grains mounted on stubs for SEM analysis (Krinsley and Doornkamp 1973), rather than in a polished section, thin sections have some uncut and unpolished grain surfaces encased in resin.

5.2 Materials and methods

5.2.1 Excavation and sampling

The excavation at site 16D4'11 revealed several shallow graves, some of which were sampled for organic chemical and micromorphological analyses by the InterArChive project team. On the basis of stratigraphic sequence, the excavators tentatively suggested the six graves sampled for micromorphology (Table 14) to be late Mesolithic (Usai *et al.* 2010a). Full implementation of the InterArChive sampling protocol (Usai *et al.* 2014) was not possible due to the advanced level of exposure of the skeletal remains at the time of sampling: intra-grave controls (C2 and C3) could not be obtained.

Confidence that the samples represent the original sediment that was adjacent to the Mesolithic human remains is compromised by subsequent Meroitic pits and animal burrowing. The loose friable nature of the sediment and its transport to the UK prior to impregnation may have caused some disturbance in the Kubiena tins. For this reason, the thin sections from the site have not been labelled to reflect their orientations relative to the skeletal remains or the direction of the ground surface. The locations of the micromorphology slides across the graves are listed in Table 14 and Figure 5.2.

Table 14: Thin section (TS) numbers for the micromorphology samples and the control.

	GR 142	GR 147	GR 148	GR 149	GR 150
Sample	**Thin section number**				
S1					391
S2		418, 419	437		
S3					375
SA1-$_n$	389, 390			386	

Control	**Thin section number**
C1	376

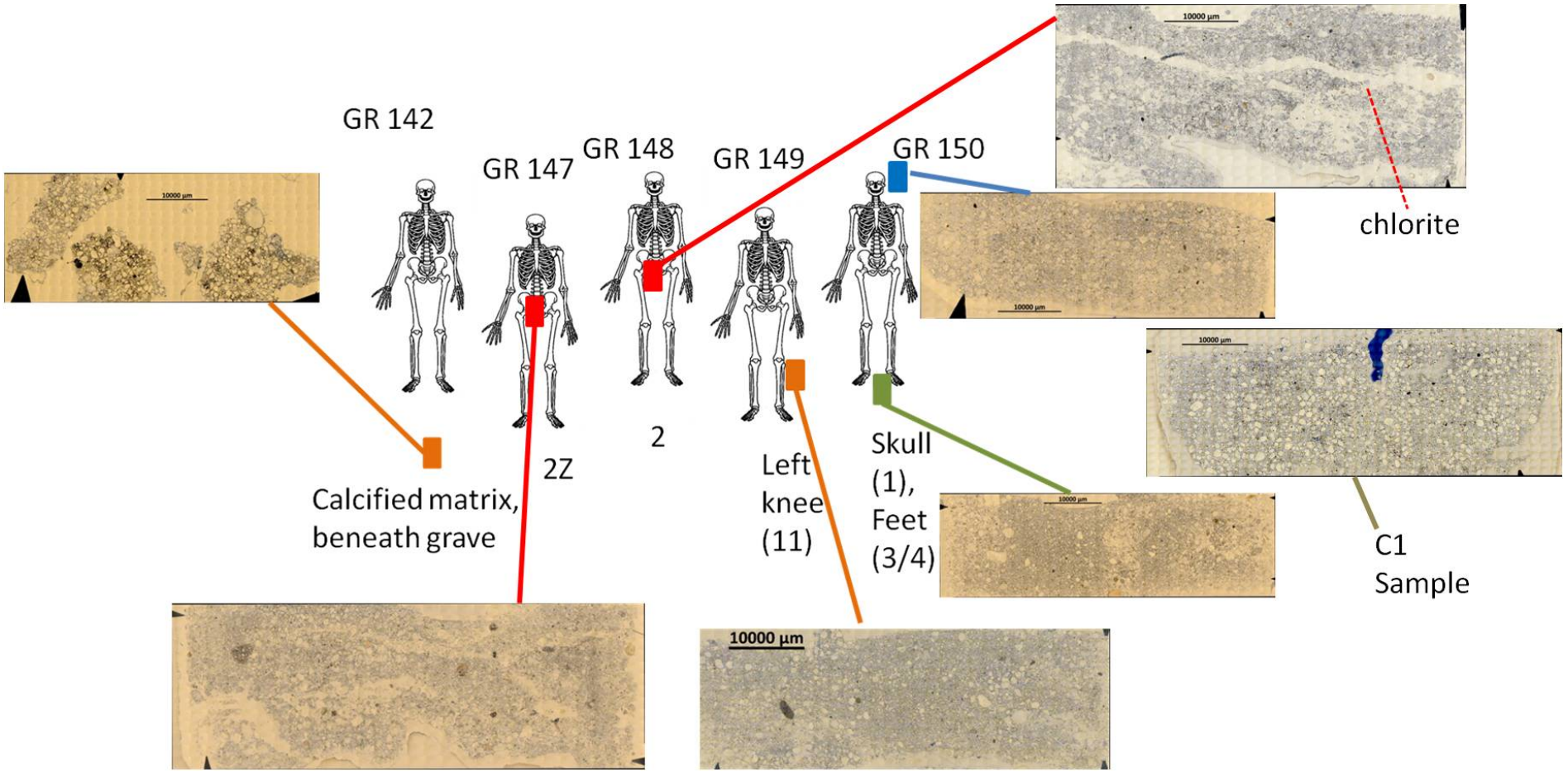

Figure 5.2: Locations of the micromorphology samples from the graves with mosaic images (PPL) of thin sections[4]. The samples collected for each grave are listed below each skeletal image.

[4] The layout of the graves is numerical only and does not relate to the inter-grave distribution as excavated at the site.

5.2.2 Field observations

Previous reports on the formation (Salvatori *et al.* 2011) and micromorphology (Zerboni 2011) of site 16D4'11 discussed the roles of calcite recycling and the effects of intercutting by later (Meroitic period, c.8th century BC to 4th century AD) pits. The Meroitic graves have in some cases eradicated the archaeological evidence of part or all of some of the earlier Mesolithic graves, including the five graves in Figure 5.2. This activity destroyed large parts of the skeletal remains of GR 150. However, the Meroitic activities partially protected the Mesolithic graves from the detrimental effects of post-depositional wind erosion by creating a resistant barrier which was relatively well preserved compared to the surrounding friable sandy sediments (Usai *et al.* 2010a and Zerboni 2011).

The calcite concretions within the sediments (Salvatori *et al.* 2011) are part of the natural state of the sediment and are typical of arid sediments and sediments (Duchaufour 1982, 75). It has, however, been subjected to repeated cycles of dissolution, migration in solution and re-precipitation. This has not only had an effect on the sediments themselves but also on the bones from these graves. In particular, the calcite recycling and re-crystallization had a detrimental effect on the collagen in the bones, preventing their use in radiometric dating (Salvatori *et al.* 2011). The effect of the recycling on the mineral constituents of the bones has not been as thoroughly assessed and is discussed in the following sections.

5.2.3 Thin section methods

The micromorphology slides were described utilizing the methodology described in Chapter 3 and description sheets for each micro-unit are provided in Appendix IV, including mineral identification and mineral weathering (Chapter 3 and Section 5.1.1 this chapter). Surface micro-textures were described using the terminology of Mahaney (2002).

5.3 Thin section analysis

A striking distinction between the micromorphology samples, both in block form and in thin section, was the traits of Sample S2 from GR 148 (TS 437 and TS 438) and to a lesser extent S2Z from GR 147 (TS 418 and TS 419). The pelvis adjacent samples (S2Z, GR 147 and S2, GR 148) were discernible from the other samples in hand specimen (Figure 5.2) by a lesser amount of coarse sand (size range 1-2 mm after Wentworth 1922).

5.3.1 Summary of micromorphological observations

Micromorphology observations are described in detail in Appendix IV and are summarised in Table 15. The C1 control (TS 376) contained well rounded sand-sized quartz grains with few accessory minerals and no channel or chamber voids (Table 15). By contrast, the thin sections from the pelvic area of GR 148 had semi-rounded (SR) quartz grains, accessory minerals and channel and chamber shaped voids. Accessory minerals observed included amphiboles, chlorite, glauconite and carbonates. The sample of the calcified matrix beneath GR 142 (SA1, TS 389 and 390) had an intergrain aggregate coarse to fine related distribution with the calcitic matrix filling the spaces between the coarse (<50 µm) sand grains. Bone fragments were observed both in the intra-grave samples and in the control (C1, TS 376). The interpretation of the presence of bone fragments in the control (TS 376) suggests that this sediment is from a part of the site that had been affected by the creation of the later (Meroitic) pits which inter-cut the graves. Examination of thin sections in hand specimen suggested an increased proportion of fine to coarse material in the pelvis adjacent samples (GR 148 and GR 147).

Table 15: Micromorphological observations of basic attributes and estimated abundance (Bullock *et al.* 1985).

GR	S	TS	c/f (50µm)	Related distribution	Void types	Quartz (%)	Feldspars	Accessory minerals	Bone (%)	Fungal traces in bone	Mineralisation of bone
control	C1	376	98/2	single population	vughs	80	microcline	amphiboles, (chlorite)	1	none	none
142	A1	389	40/60	intergrain aggregate	channels, vughs	55	none	carbonate, chlorite	0	N/A	N/A
142	A1	390	40/60	intergrain aggregate	channels, vughs	50	none	carbonate	0	N/A	N/A
147	2Z	419	70/30	linked & coated	channels, chambers	50	none	glauconite, chlorite, amphiboles	5	Wedl tunnels	discoloured rims
148	2	437	80/20	intergrain aggregate	channels, vughs	70	none	carbonates, glauconite, chlorite	5	Wedl tunnels	rhombohedral structure
148	2	438	80/20	intergrain aggregate	channels, vughs	70	none	amphiboles, chlorite, carbonates, glauconite	5-10	Wedl tunnels	rhombohedral structure
149	11	386	75/25	intergrain aggregate	vughs	60	none	amphiboles, CPX, chlorites, carbonates	0	N/A	N/A
150	1	391	75/25	coated	vughs	70	none	(amphiboles), (carbonates)	5	(fungal traces on quartz)	discoloured rims
150	4	382	80/20	linked & coated	vughs	80	none	CPX, (chlorites), carbonates	5	none	none
150	4	375	80/20	linked & coated	vughs	80	none	(CPX), chlorites, carbonates	5	none	discoloured rims

5.3.2 Quartz grain surface texture

The surfaces of the quartz grains in the thin sections were analyzed to identify post-depositional formation processes within the graves at Al Khiday. Mineral weathering has been primarily discussed in this site analysis using the terminology of Delvigne (1998) (Chapter 3). However, as additional terminology exist and were diagnostically indispensable in the discussion of the surface micro-textures of quartz grains (Mahaney 2002, 27-30) this is employed as an accompaniment.

The control (C1, TS 376) contained rounded quartz grains with low relief and some v-shaped percussion cracks (Figure 5.3). By contrast, the quartzite grains from the sand fraction of the sediments in the samples displayed intra-mineral fractures (terminology after Delvigne 1998) which were often exploited by iron-rich precipitates (Figure 5.4) and dissolution etching (Figure 5.5), with acicular formations of iron-rich (SEM-EDS) precipitates on grain surfaces (Figure 5.6).

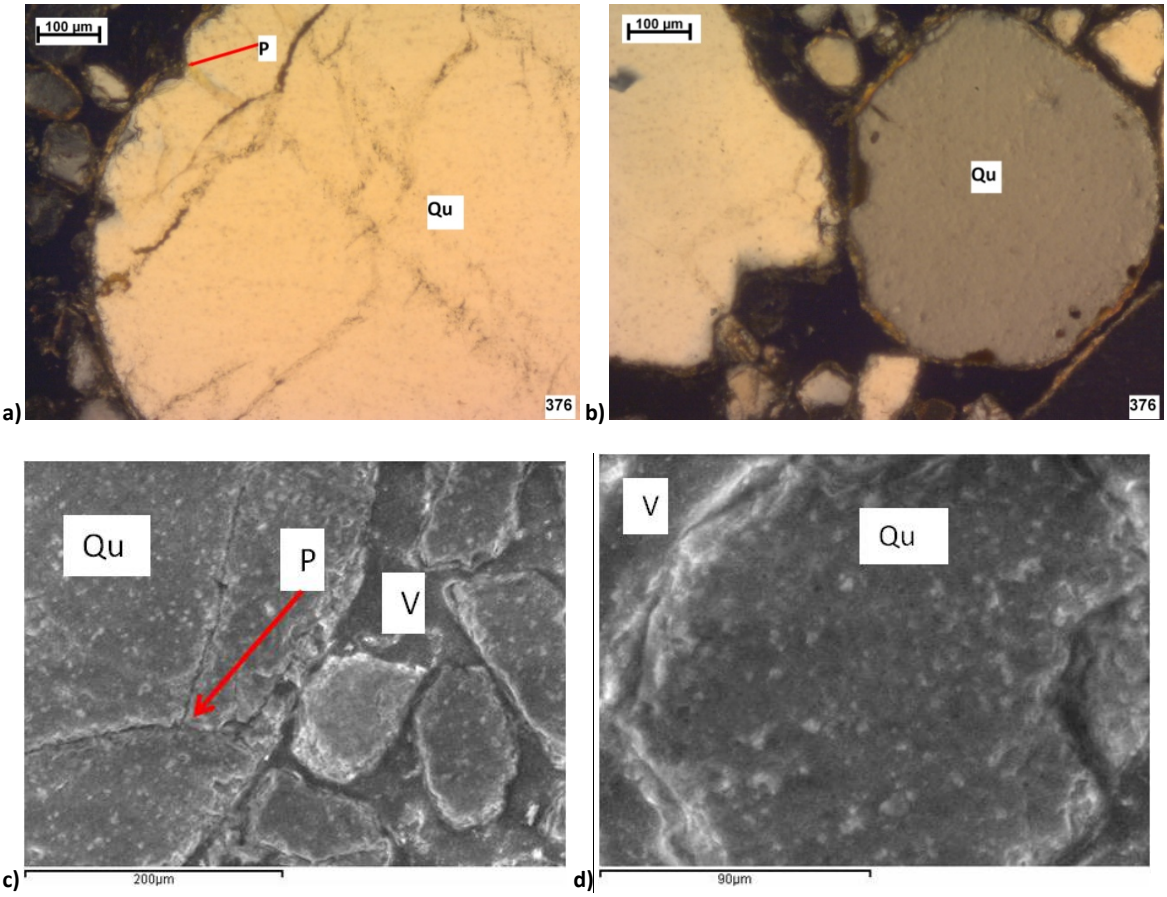

Figure 5.3: Weathering of sand-sized quartz grains from the control. a) V-shaped percussion mark (P) on a sand sized quartz grain (Qu) (C1, TS 376, XPL). b) Well-rounded sand sized quartz grain (Qu) (C1, TS 376, XPL). c) Quartz (Qu) sand grains showing sub-rounded shape and v-shaped percussion (P) marks (C1, TS 376, SEM secondary detector mode/ VPSE). d) Low relief surface microtexture of a sand sized quartz grain (Qu) (C1, TS 376, SEM secondary detector mode/ VPSE).

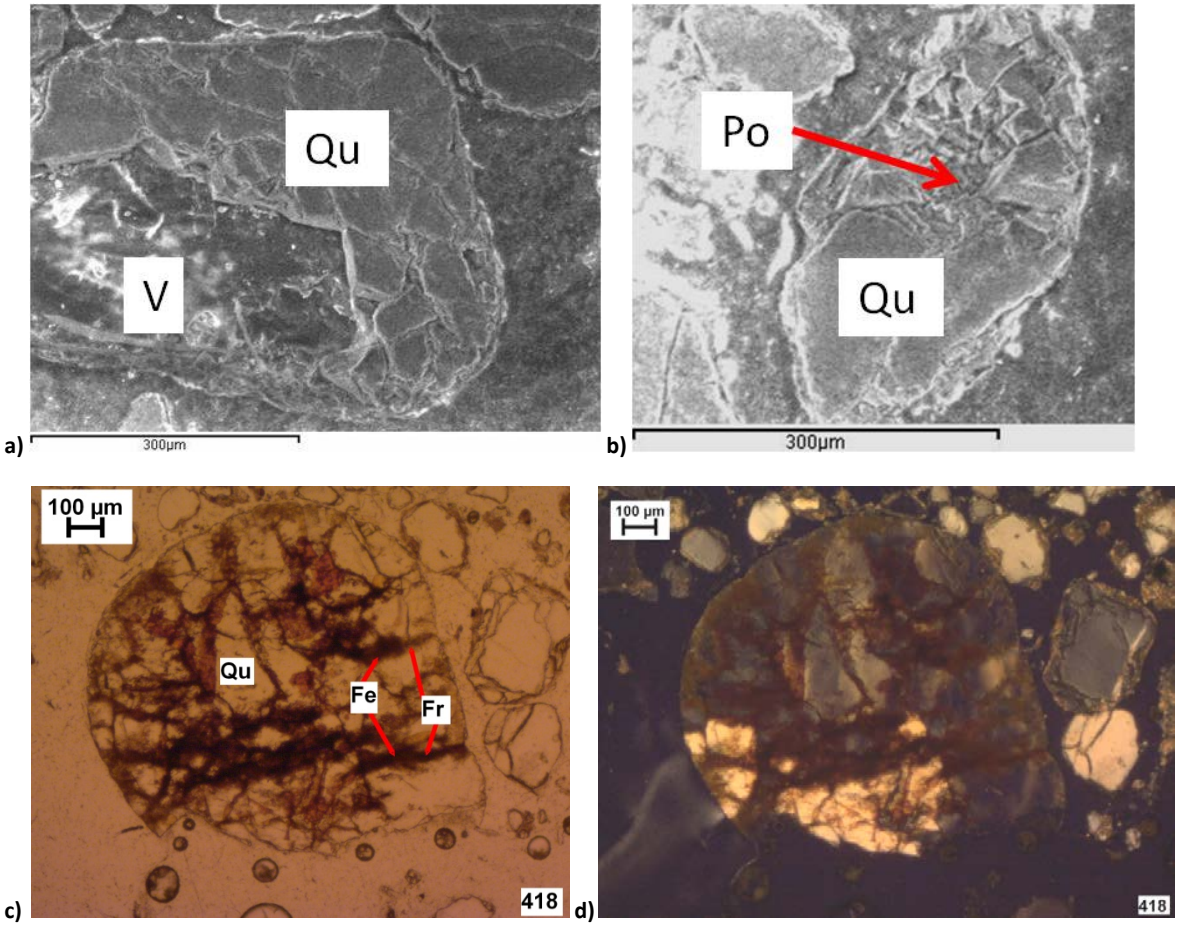

Figure 5.4: a) Quartz sand grain (Qu) with intense fracturing and mineral alteration with the lower half of the grain replaced by a void (V) (GR 148, S2, TS 437, SEM secondary detector mode/ VPSE). b) Quartz sand grain (Qu) with heavy inter-mineral fracturing resulting in the creation of a central pore (Po) in the upper centre of the grain (GR 148, S2, TS 437, SEM secondary detector mode/ VPSE). c) Quartzite grain (Qu) with heavy fracturing and iron-rich precipitate (Fe) accumulated inside the fractures (Fr), -the circles along the base of the frame are resin bubbles and are an artefact of slide manufacturing, (GR 147, S2Z, TS 418, PPL). d) XPL view of image c).

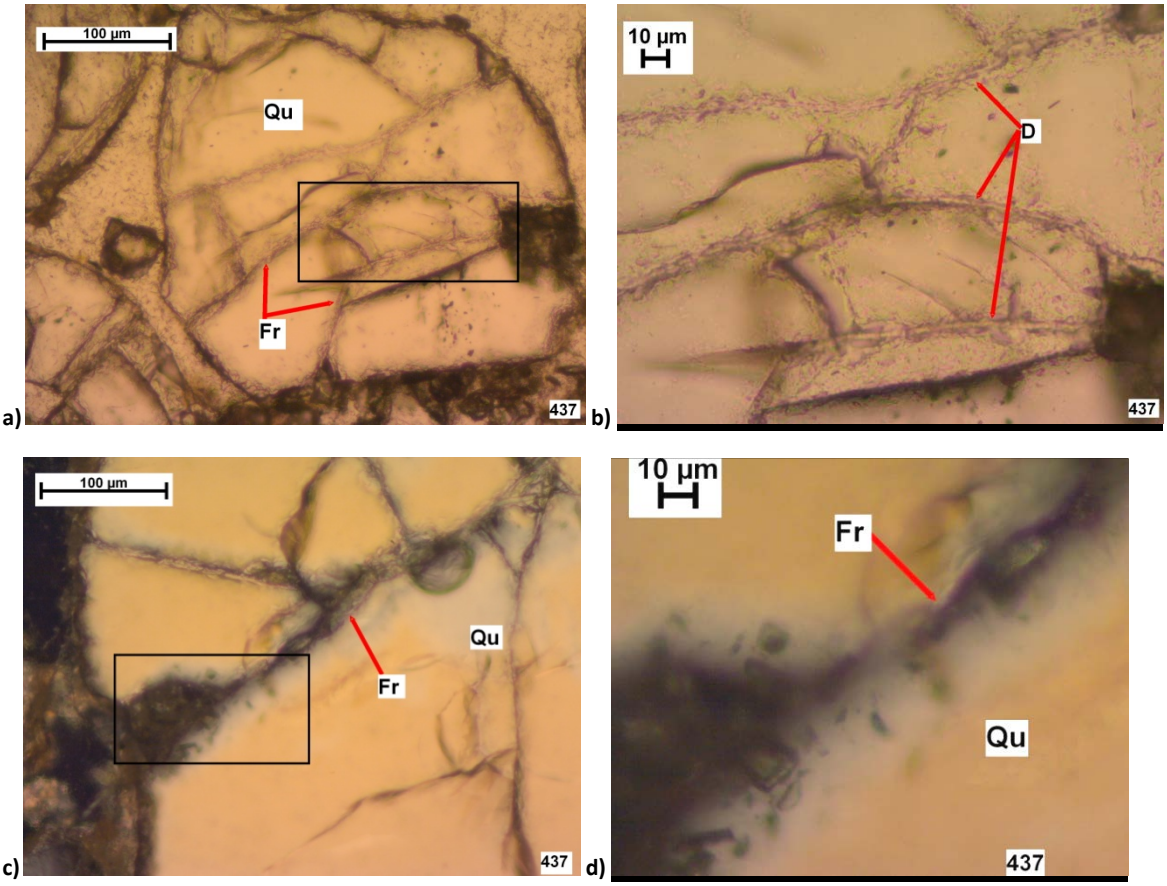

Figure 5.5: Weathering of sand-sized quartz grains from intra-grave thin sections. a) Quartz grain (Qu) with intra-mineral fractures (Fr) and linear dissolution etching (GR 148, S2, TS 437, PPL). b) Detail of a) as outlined by black box on image a), showing further chemical dissolution (D) occurring along the fracture lines (PPL). c) Quartz grain (Qu) with intra-mineral fractures (Fr) and dissolution etching along exterior fracture and intra-mineral fracture (GR 148, S2, TS 437, XPL). d) Detail of image c) as shown by black rectangle in image c) (GR 148, S2, TS 437, XPL).

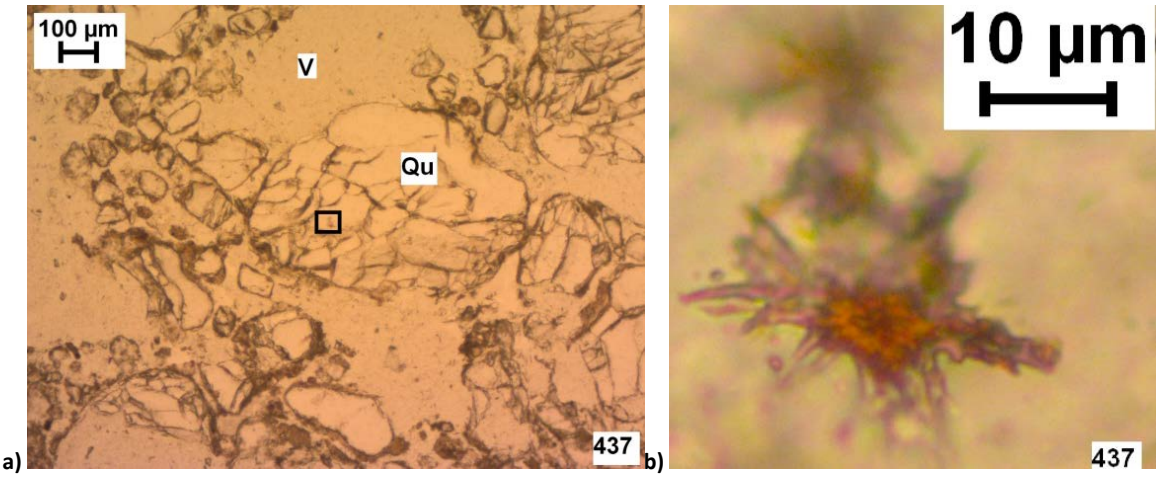

Figure 5.6: Acicular forms of an iron-rich precipitate on a quartz grain. a) Iron rich precipitate (black rectangle) on a quartz grain (Qu) surrounded voids (V) (GR 147, S2, TS 437, PPL). b) Inset (black rectangle) from image a), detail of iron rich crystalline material of an acicular morphology (GR 147, S2, TS 437, PPL).

5.3.3 Accessory minerals

The mineral fractions of the thin sections were dominated by quartz and feldspars (Table 15) and were accompanied by amphiboles, clinopyroxene, blue-coloured minerals and glauconite as accessory minerals. Identification of minerals was made using the methodology and references described in Chapter 2. The inosilicate minerals include members of the calcic amphibole tremolite-actinolite series and sodic amphibole glaucophane-reibeckite series, with the exception of hornblendes in GR 149 (GR 149, S11, TS 386). Phyllosilicate minerals observed included members of the glauconite group.

5.3.3.1 Amphiboles and clinopyroxene

Blue (PPL) amphiboles exhibiting pleochroism (PPL) and upper-1st to mid-2nd order interference colours were observed in GR149 (S11, TS 386), 147 (S2Z, TS 418 and 419), and 148 (S2, TS 437 and 438). The thin sections of these graves showed blue (PPL) amphibole cleaved minerals with dark blue-green to lilac to colourless pleochroism (Figure 5.7), and with blue to colourless pleochroism (Figure 5.8). No amphiboles exhibiting blue pleochroism were observed in the control (C1, TS 376). Amphiboles, with the exception of anthrophyllite-gedrite, can be separated into three series or groups of minerals: the cummingtonite series (cummingtonite-grunerite), tremolite series (tremolite-actinolite/ferroactinolite) and the sodic amphibole group (glaucophane-reibeckite) (Klein and Hurlbut 1998, 495). Confident identification of these minerals to group level, based on optical characteristics in transmitted light microscopy is supported by the literature (*ibid*, 488-489). Identification of minerals to the sub-group level should include some additional methods of analysis such as XRD, SEM, EDX, or TEM.

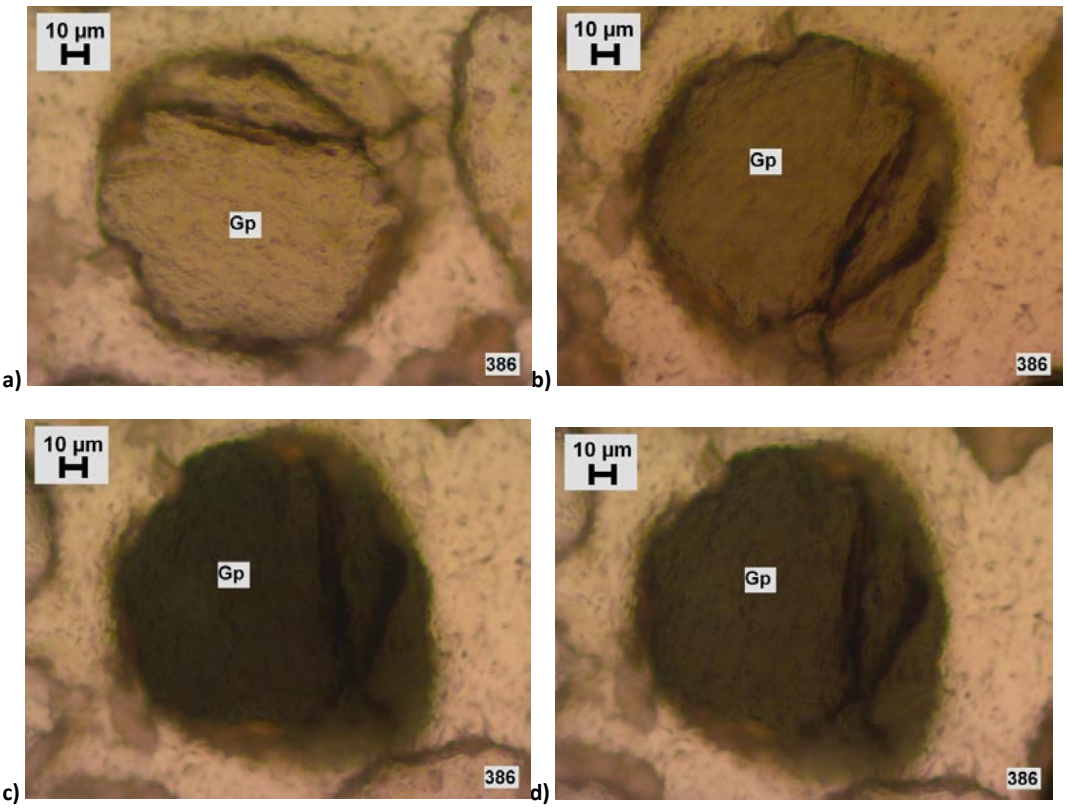

Figure 5.7: Mineral grain displaying cleavage typical of amphibole minerals with pleochroism ranging from a) colourless to b) lilac to c) dark green to d) blue-green colours (GR 149, S11, TS 386, PPL).

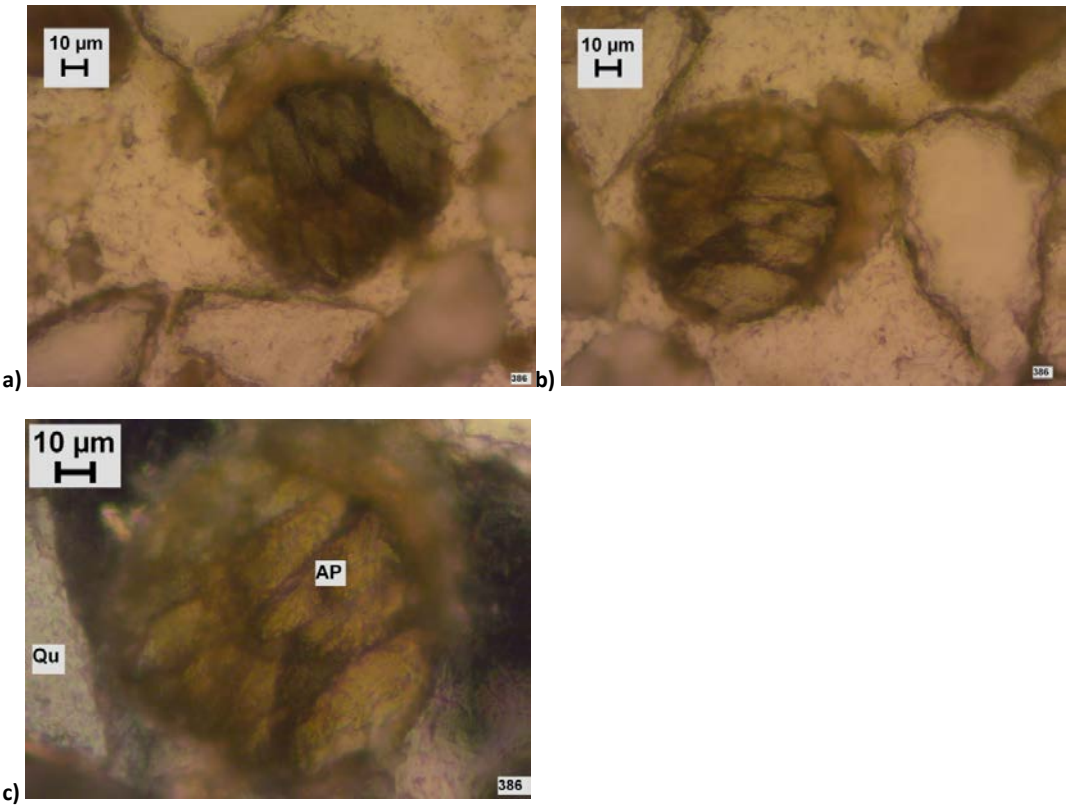

Figure 5.8: Pleochroic mineral with amphibole cleavage angles. a) Mineral grain displaying darkest colours in PPL (GR 149, S11, TS 386, PPL). b) mineral grain in image a) rotated to show lightest colours in PPL (GR 149, S11, TS 386, PPL). c) Mineral grain in image a) and b) displaying upper first order interference colours (GR 149, S11, TS 386, XPL).

Calcic amphibole minerals, the tremolite-actinolite series, were identified in GR 147 (S2Z, TS 418 and 419), 148 (S2, TS 437), and 149 (S11, TS 386 and 381) and absent in the control (Table 15). Some of the sodic-calcic amphiboles identified in the sediments from the knee (GR 150, S11, TS 386) and pelvic (GR 147, S2Z, TS; GR 148, S2, TS) samples are tentatively identified as glaucophane (based on their lilac-colourless pleochroism (PPL) and 0.088-0.022 birefringence values (XPL)) (MacKenzie and Guilford 1980, 49) (Figure 5.9), and some are tentatively identified as tremolite (based on their green-colourless pleochroism (PPL) and 0.025-0.026 birefringence values (XPL)). Diopside in thin section is distinguishable from tremolite-actinolite minerals by habit and colour, diopside having the characteristic hornblende cleavage angles (56 and 124 degrees) and colours of pleochroism (brown/green in PPL) (MacKenzie and Guilford 1980, 46-47). These optical traits of diopside can be compared to those of the tremolites which have green-colourless pleochroism (PPL) (MacKenzie and Guilford 1980, 45). The blue-green pleochroic amphiboles in these graves were not identified as hornblendes in these graves (Table 15). Calcic and sodic amphiboles are connected by a solution series which allows for the existence of transitory minerals (*e.g*. winchite) (Smelik and Veblen 1992). This relatedness of the series and their ability to both take columnar habits results in difficulties differentiating the glaucophane-reibeckite series and tremolite-actinolite mineral series in thin section, on the basis of optical microscopy analysis alone (Gaines *et al.* 1997, 237-238). Hence, the amphibole minerals in the samples and controls are classified as sodic-calcic amphiboles and further sub-classifications are tentative.

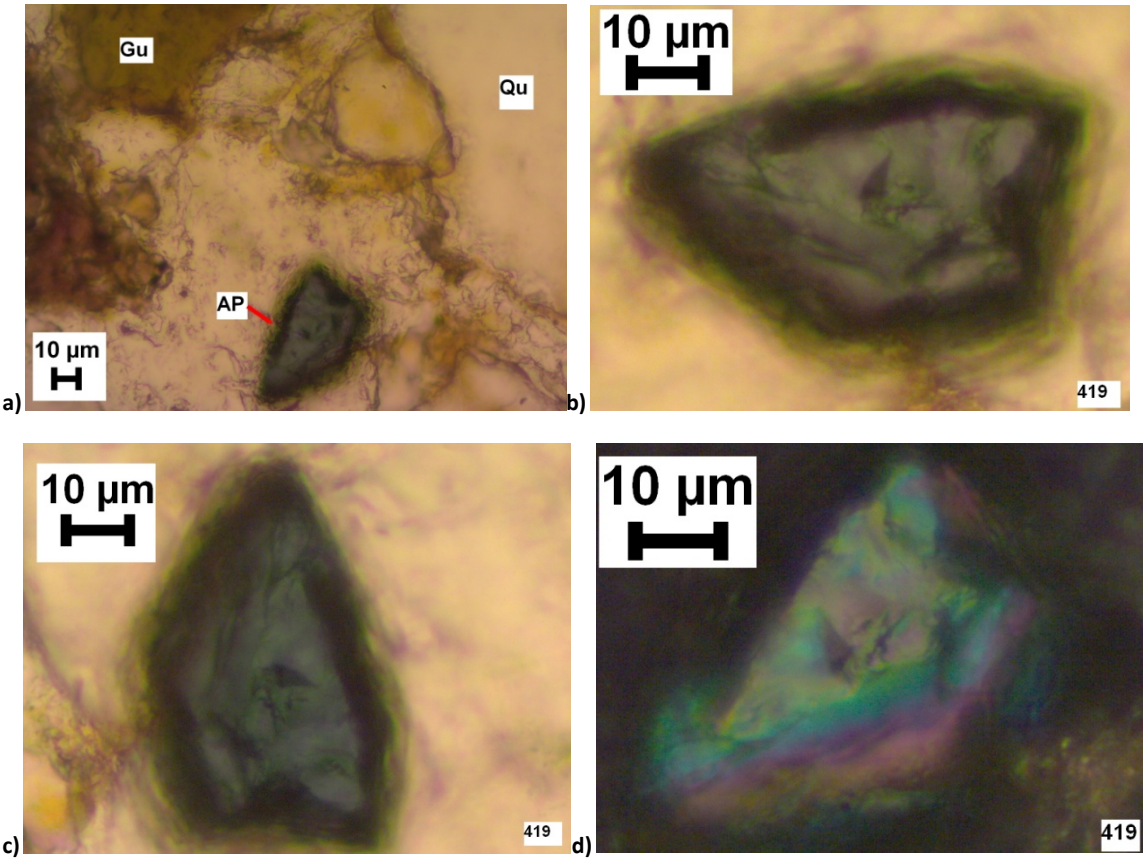

Figure 5.9: Amphibole mineral tentatively identified as a member of the glaucophane series. a) Amphibole (AP) mineral shown in context with neighbouring glauconite (Gu) and quartz (Qu) (GR 147, S2Z, TS 419, PPL). b) Detail of amphibole shown in image a) (AP), rotated to show weakest pleochroism (GR 147, S2Z, TS 419, PPL). c) Detail of amphibole shown in image a) (AP), rotated to show strongest pleochroism (GR 147, S2Z, TS 419, PPL). d) Detail of amphibole shown in image a) (AP), displaying 2nd order interference colours (GR 147, S2Z, TS 419, XPL);

Hornblendes were present in GR 149 and were identified by yellow to brown pleochroism and masked interference colours (Figure 5.10), and 126 and 54 degree cleavage which differentiate the amphiboles/hornblendes from the pyroxene families of the inosilicates (MacKenzie and Adams 1994, 16). Hornblendes were observed in the sediments of GR 149 (SA1, TS 386; Figure 5.10). Minerals displaying these optical properties were not observed from any other grave or the control. The variety of amphibole minerals between different sediment samples could be related to the range of sediments within the site and highlights the necessity of more than one control to represent such variability in the types and frequencies of the components of the non-grave sediments in the area. Additional controls collected from sediments above, adjacent to and below the graves, to represent both intra-layer and inter-layer differences would add more information on the materials in the neighbourhood.

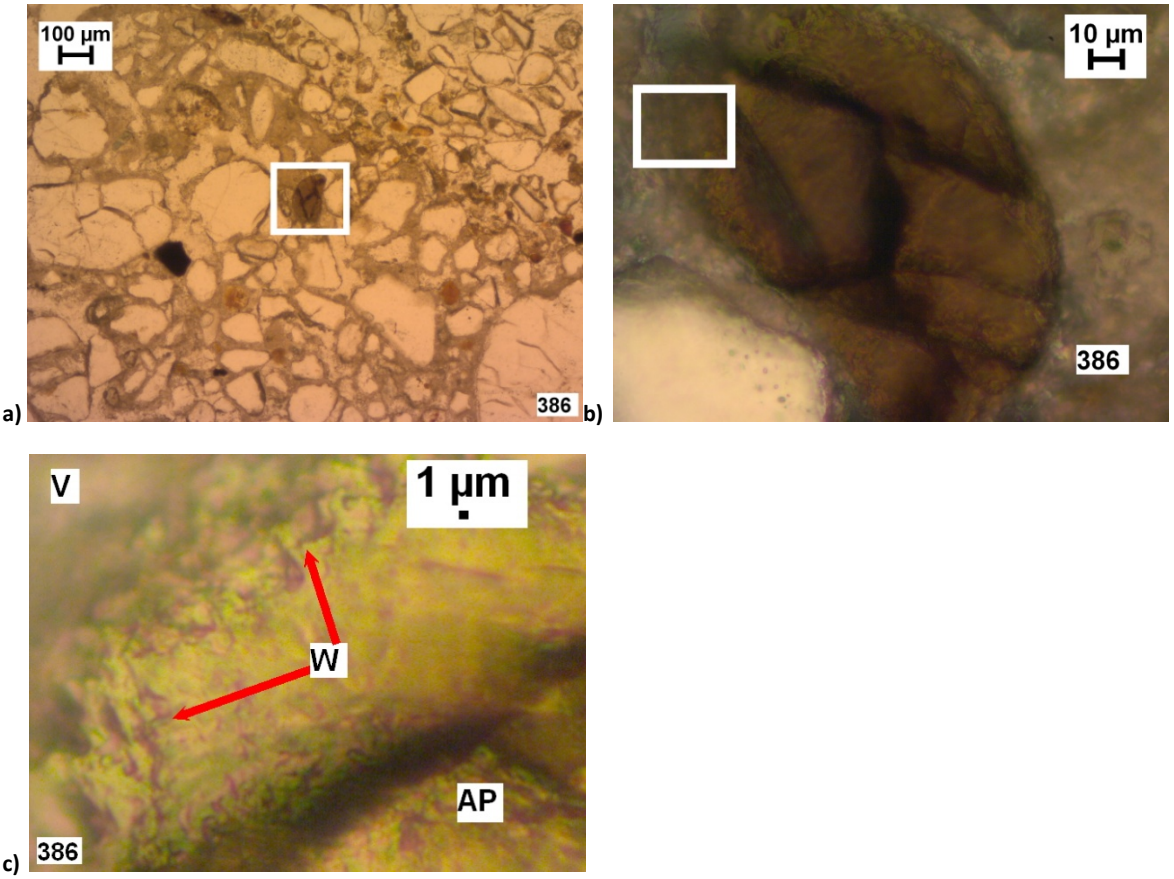

Figure 5.10: Brown pleochroic amphibole. a) Hornblende in a fine material of calcium carbonate (GR 149, S11, TS 386, PPL). b) inset (white rectangle) from image a), the hornblende grain has been rotated to show maximum pleochroic colours (GR 149, S11, TS 386, PPL). b) Hornblende grain showing maximum interference colours (GR 149, S11, TS 386, XPL). c) Detail white rectangle in image (a) of the amphibole grain's edge (AP) and void (V), with edges appearing to have been affected by wedging effect (Chapter 2) (GR 149, S11, TS 386, PPL).

GR 149 was different from the other graves by the observation of hornblendes and a few grains of clinopyroxenes (GR 149, S11, TS 386). The clinopyroxenes in this thin section were small (<50 µm) and heavily weathered (weathering extent 3, 75-97.5% altered) to an iron-rich material (as determined by SEM-EDS spectra) (Figure 5.11). The only other thin section with clinopyroxenes was the sample of the calcified matrix beneath the graves (GR 142, SA1, TS 389 and TS 390).

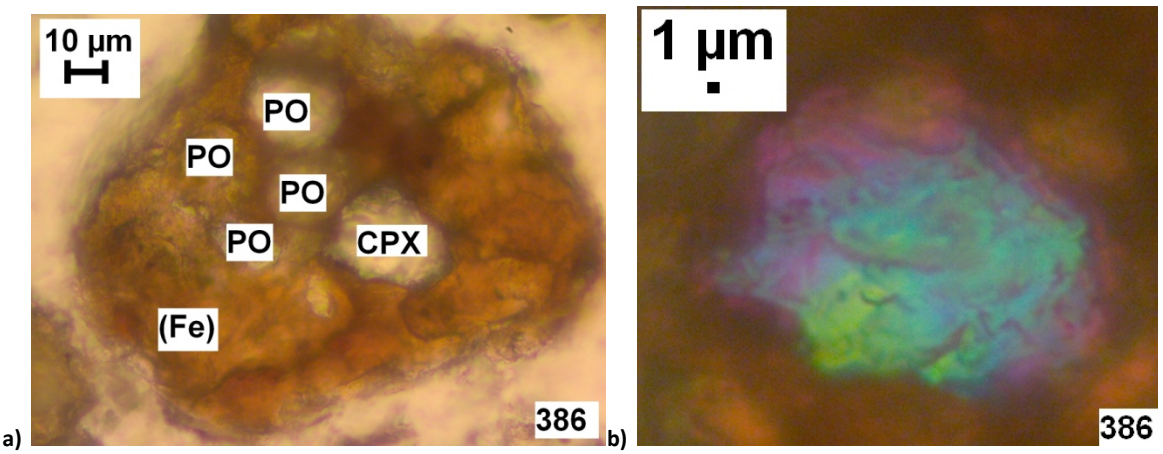

Figure 5.11: Intensely weathered clinopyroxene group mineral. a) clinopyroxene (CPX) mineral weathered to produce an iron rich material (Fe) including the production of secondary pore spaces (PO) (GR 149, S11, TS 386, PPL); b) detail of remaining primary mineral (CPX) in image (a) displaying second order interference colours (GR 149, S11, TS 386, XPL).

5.3.3.2 Glauconite and blue coloured minerals

Blue coloured minerals were present in GR 149 (S11, TS 386) in the groundmass (Figure 5.12b) and along the edges of aggregates (Figures 5.2 and 5.13). The colours of these minerals could suggest that they are either chlorites or vivianite. However, although chlorite minerals are often identifiable by their blue to light blue pleochroism (PPL) and anomalous blue to isotropic interference colours (XPL) in transmitted light microscopy (MacKenzie and Adams 1994, 46-47) they are not know to form in sediments at the scale visible with the light microscope. The blue minerals were tentatively identified as vivianite based on their colour, sheet-like structures, and distributions along the edges of aggregates. Vivianite has been found in graves and is a blue colour when oxidised. Occurrences of vivianite in archaeological sediments and its oxidation process are reviewed in McGowan and Prangnell (2006). Glauconite, identified by its green colour, grainy appearance in XPL and lobate morphology, was present in GR 147 (S2Z, TS 419) and 148 (S2, TS 437 and 438; Table 15). The glauconite in GR 147 and 148 displayed a well-rounded form (Figure 5.14), suggestive of considerable physical weathering and possible transport since the time of their mineralogical formation (Fanning *et al.* 1989a, 583-584).

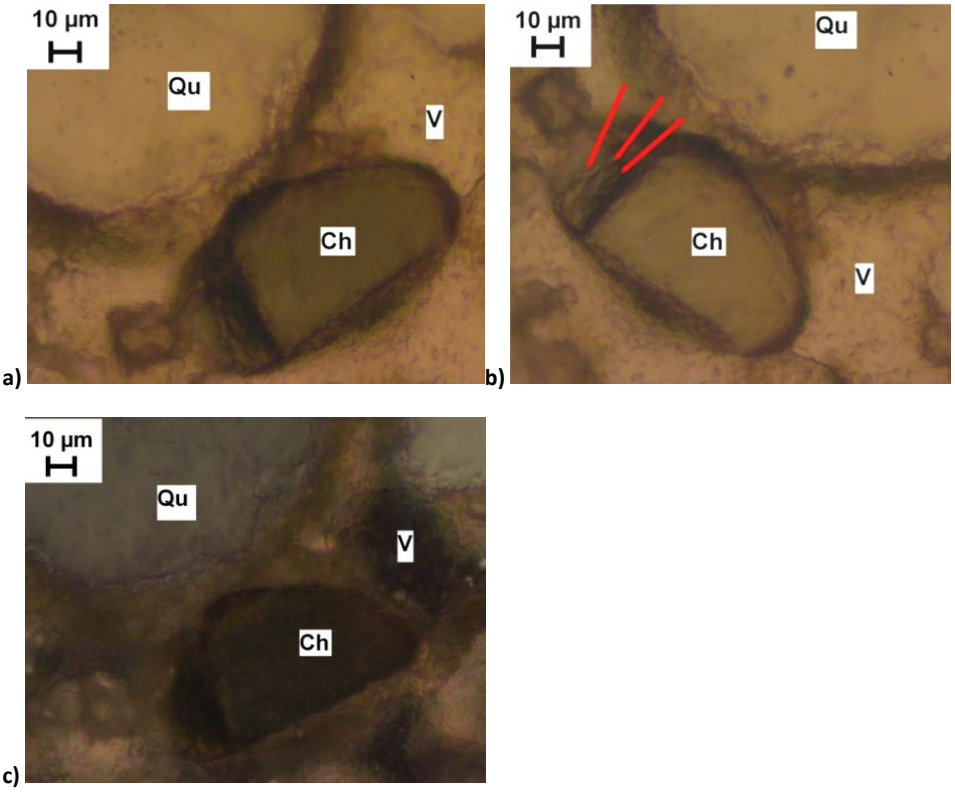

Figure 5.12: Blue (PPL) pleochroic mineral with sheet-like structure. a) Pleochroic blue to colourless mineral (Ch), shown at darkest blue colours (GR 149, S11, TS 386, PPL). b) Mineral grain shown in a) rotated to show colourless colours and sheet-like structure typical of phyllosilicate minerals (GR 149, S11, TS 386, PPL). c) Mineral grain shown in a) and b) displaying anomalous interference colours (GR149, S11, TS 386, XPL).

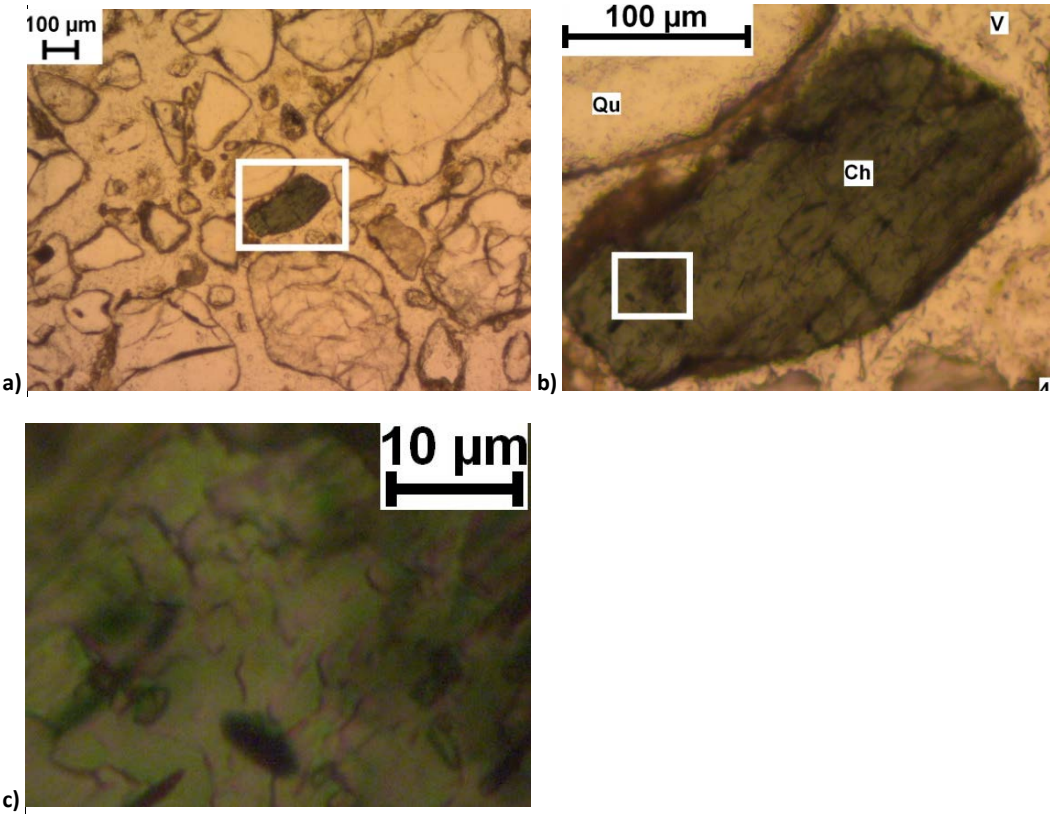

Figure 5.13: Blue-green coloured mineral grains in thin section from GR 147. a) Blue-green coloured mineral grain (TS 418, Sample 2Z, GR 147) (PPL). b) Detail of inset in image (a), with void (V) blue-green mineral (Ch) and quartz (Qu) (PPL). c) Detail of inset in image (b) showing platy structure (PPL).

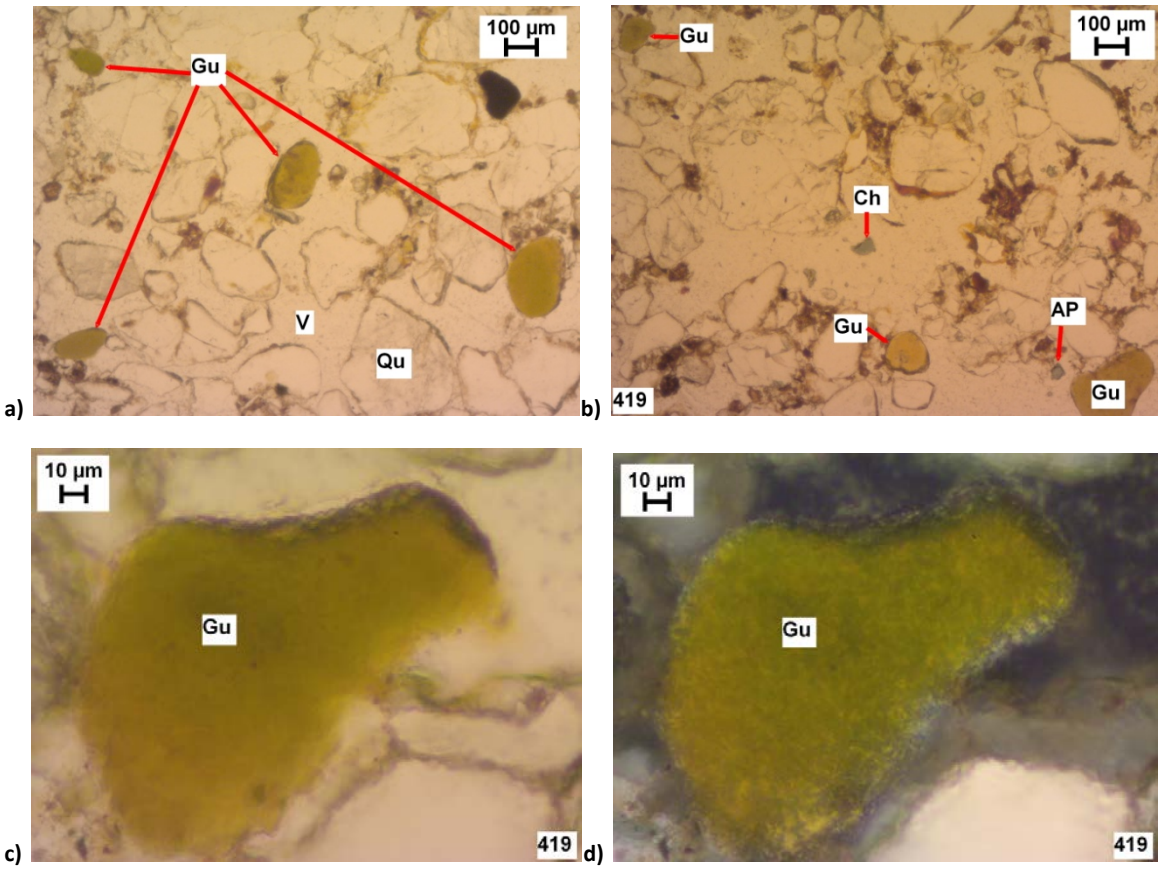

Figure 5.14: Glauconite in thin section. a) Glauconite (Gu) in a porous (V) sandy (Qu) sediment (GR 147, S2Z, TS 419, PPL). b) Glauconite (Gu) in a sandy sediment accompanied by blue (PPL) amphibole (AP) and blue isotropic mineral (Ch) minerals (GR 147, S2Z, TS 419, PPL). c) Glauconite (Gu) grain shown in detail, showing yellow-green colours (PPL) (GR 147, S2Z, TS 419, PPL). d) XPL view of image c), showing yellow-green speckled anomalous interference colours (XPL) (GR 147, S2Z, TS 419, XPL).

5.3.4 Bone fragments

Bone was present in sections from the control (C1, TS 376) and samples (GR 147, 148 and 150). Both anisotropic (Figure 5.15a) and isotropic bone materials were present in samples (Figure 5.15b). First order grey interference colours are typical for unburnt bone in cross polarized light (Karkanas and Goldberg 2010, 524). Fragmented bone materials observed in thin section from some of the graves (GR 147) displayed a strong retention of the birefringence property (Figure 5.15a) of unburnt bone interpreted as the preservation of the apatite component while others (GR 148) appeared to have lost this optical property (Figure 5.15b). Some samples had a mixture of both isotropic and anisotropic bone fragments (GR 150, S4).

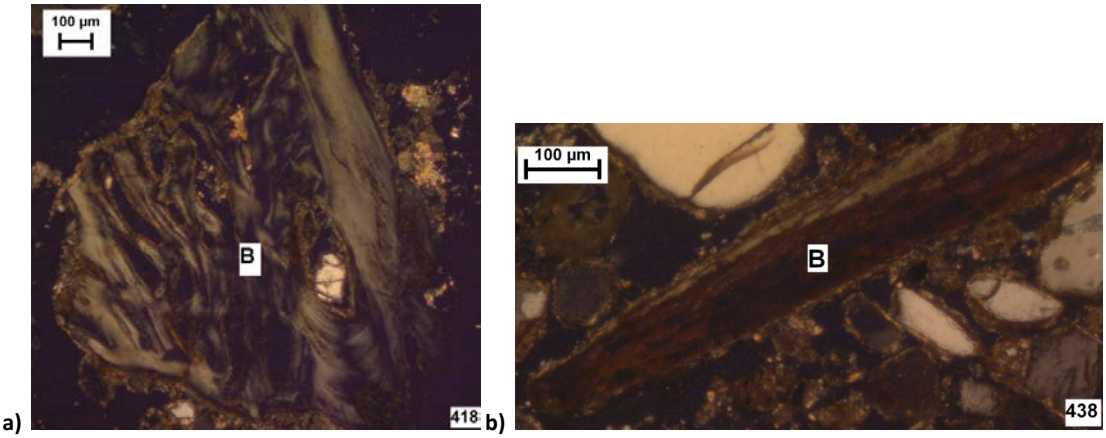

Figure 5.15: Bone fragments from samples. a) Bone with first order grey interference colours (GR 147, S2Z, TS 418, XPL). b) Bone without first order grey interference colours (GR 148, S2, TS 438, XPL).

Some bone fragments contrasted in colour (PPL) from their exterior to interiors (Figure 5.16a and c). A colourless area surface of the fragments, differing from the yellow coloured (PPL) internal area (Figure 5.16a and c), was interpreted as a product of post-depositional processes.

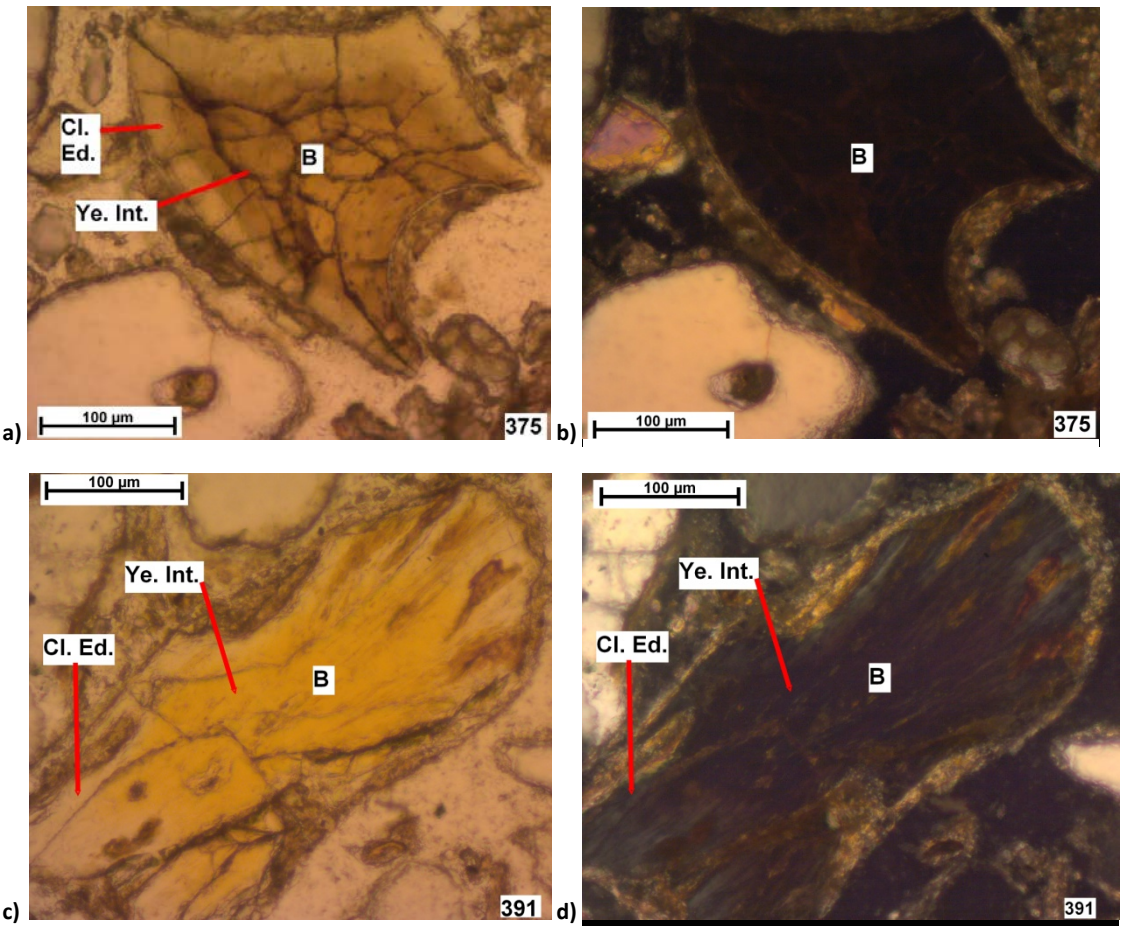

Figure 5.16: Bone fragments with variation in colour. a) Bone fragment (B) with colourless edges (Cl. Ed.) and yellow interior (Ye. Int.) areas (GR 150, S4, TS 375, PPL). b) XPL view of image a). c) Bone fragment (B) with colourless edges (Cl. Ed.) and yellow interior (Ye. Int.) areas (GR 150, S1, TS 391, PPL). d) XPL view of image c).

A fragment of bone from GR 148 (S2, TS 438) displayed a change in internal morphology along an open fracture (Figure 5.17a). Along this part of the fragment a rhombohedral internal structure predominated (Figure 5.17b), interpreted as evidence of the mineralization of the bone. Tunneling in bones (Figure 5.18a and c) was seen in samples from GR 147 and 148 (Table 15), and interpreted as remains of past fungal activity. The fungal remains were reddish pink in colour (PPL) and had a branched structure (Figure 5.18b and d).

a) 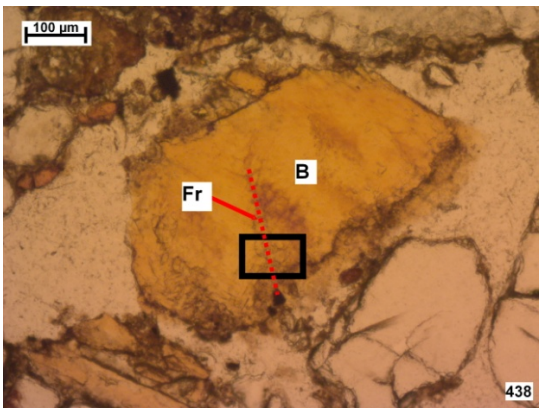

b) 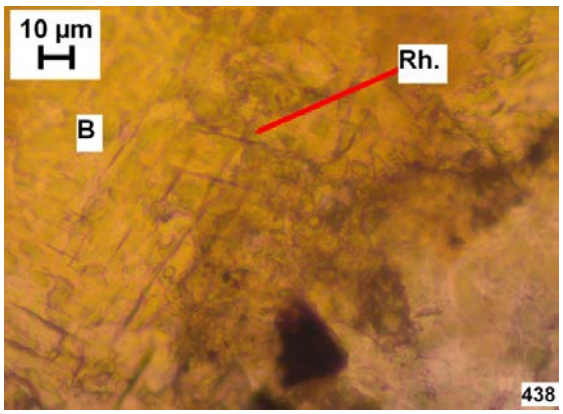

Figure 5.17: (a) Bone fragment (B) displaying change in internal morphology along a fracture (Fr) which runs from the edge of the fragment in the lower half of the frame towards the upper left corner of the frame (shown by red dashed line) (GR 148, S2, TS438, PPL). (b) Detail of bone (B) in image a) as shown by black rectangle in image a), the rhombohedra structure (Rh) can clearly be seen in the centre of the frame (GR 148, S2, TS438, PPL).

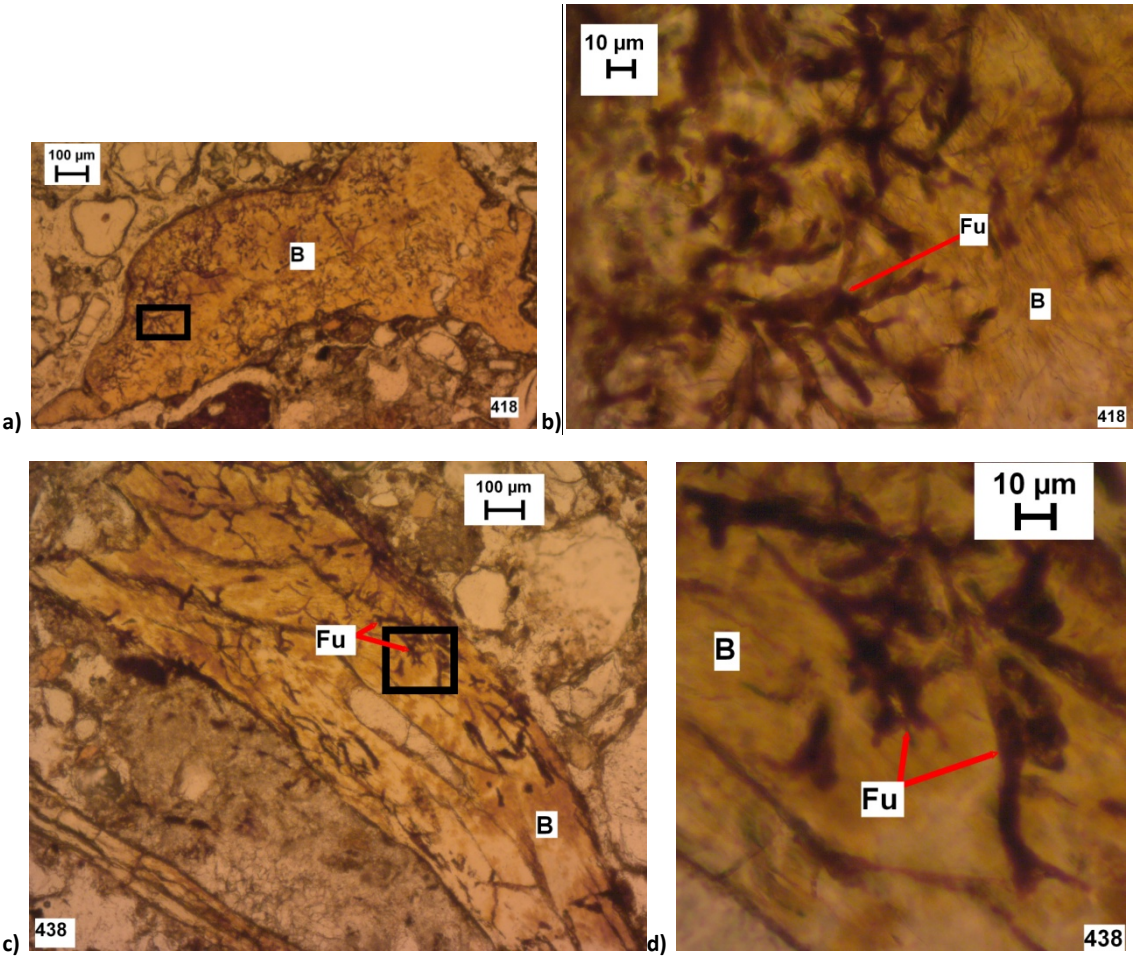

Figure 5.18: Fungal traces in association with bone fragments. (a) Fungal traces (Fu) in bone fragment (B) (GR 147, S2Z, TS 437, PPL). (b) Detail of inset (black rectangle) in image a) (GR 147, S2Z, TS 437, PPL). (c) Fungal traces (Fu) in bone fragment (B) (GR 148, S2, TS 438, PPL). (d) Detail of inset (black rectangle) in image c) (GR 148, S2, TS 438, PPL).

5.4 Interpretation and discussion

5.4.1 Quartz grain surface textures

The low weatherability of quartz (Goldich weathering sequence, Goldich 1938), makes quartz ideal for studying long term changes or those formed as a result of processes in the distant past (Mahaney 2002, 215). Surface micro-textures (Krumbein and Pettijohn 1938; Krinsley and Doornkamp 1973) of sand sized (64-2,000 µm, after Wentworth, 1922) quartz grains were assessed (Section 5.1.1). The intense intra-mineral fracturing and dissolution features along fracture lines, in combination with chemical etching seen as dissolution surface micro-textures, did not match the surface micro-textures seen in the control. The V-shaped percussion cracks viewed on the quartz sand grains in the control (C1, TS 376) are typical indicators of fluvial erosion. In combination with the well-rounded shape of the grains (Figure 5.3) they match to previous analyses of sand grain surface textures from Nile sediments (Mahaney 2002, 97). Features on the quartz sand grains in

the intra-grave thin sections suggested that, at least a part, of their weathering history was related to subaerial weathering processes (specific micro-textural surface features have been discussed as evidence of subaerial weathering processes in Mahaney 2002, 186).

Intra-grave samples had polygonal cracks (Figure 5.19a) but lacked other micro-textures indicative of aeolian weathering (Mahaney 2002, 69), such as parallel ridges and elongate depressions (*ibid*). Polygonal crack microfeatures are known to form as a result of chemical weathering such as occurs with the recrystallization of salts (Lucci and Casa 1968, Krinsley and Doornkamp 1973, Le Ribault 1975, Krinsley and McCoy 1978, Mahaney 2002, 70).

The effects of the recrystallization of surrounding calcium carbonate rich matrix material adjacent to those grains with intense chemical dissolution pit surface micro-textures was seen on some quartz and quartzite grains from samples (Figure 5.21). Hence, due to their accompanying microfeatures (crescent gouges and dissolution pits) the polygonal cracks on the grains from the samples are interpreted as evidence of chemical weathering processes. The sand-sized quartz and quartzite grain surface micro-textures on grains from the samples include microfeatures indicative of a complex weathering history suggesting that aeolian weathering was followed by intense sub-aerial weathering processes.

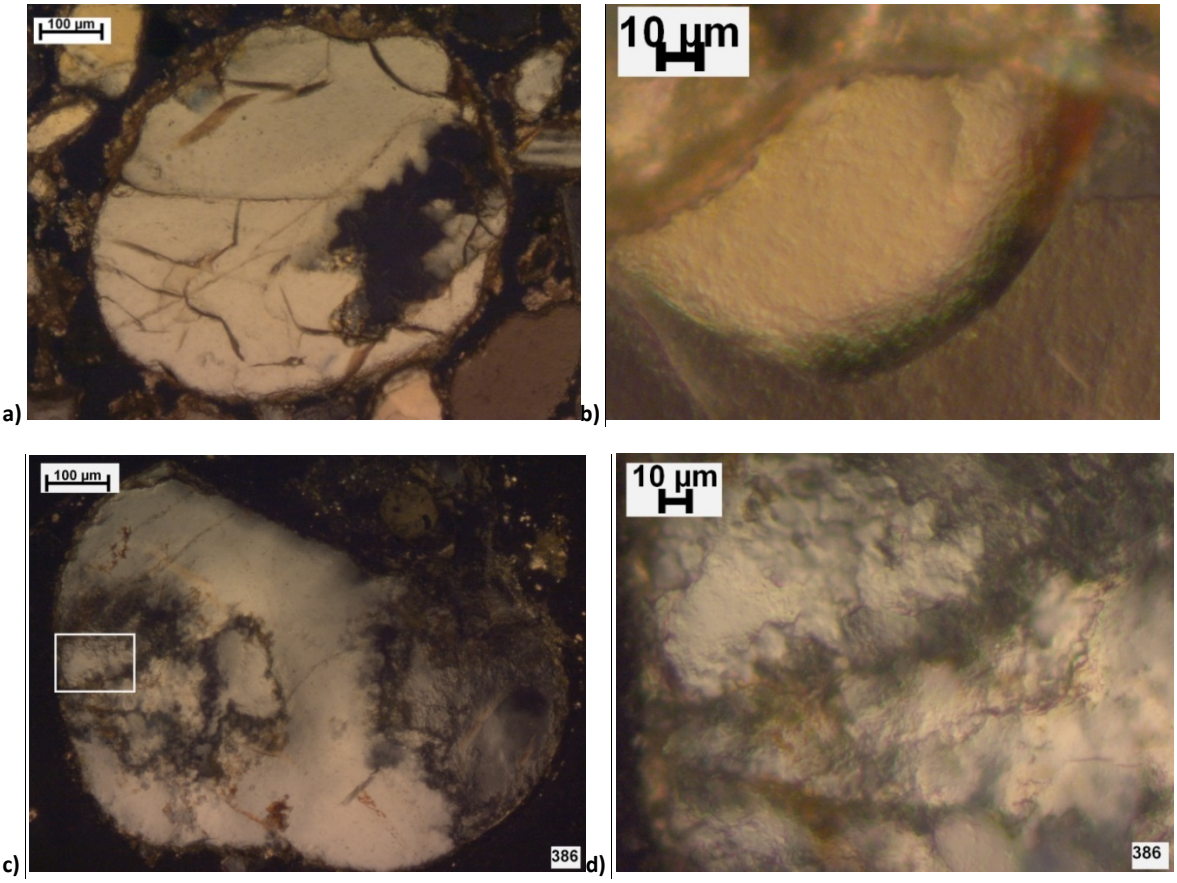

Figure 5.19: a) Quartzite sand grain with bulbous edges representative of eolian weathering visible as preweathered microfeatures overwritten by later polygonal cracks (lower left of grain), crescent gouges (upper right of grain), and chemical dissolution etching (middle right of grain), (GR 150, S1, TS 386, XPL). b) Quartzite sand grain with crescentic gouges. Crescent gouges can be formed through chiselling action of bladed fragments typical of mass wasting deposits (Mahaney 2002, 29), (GR 150, S1, TS 386, XPL). c) Quartzite sand grain with intensive chemical dissolution (GR 150, S1, TS 386, XPL). d) Detail of image c) shown by white rectangle in image c) (GR 150, S1, TS 386, XPL).

Previous studies have demonstrated the interpretation of past events through the study of surface microfeatures of loose quartz sand grains (Mahaney and Andres 1996, Mahaney 2002). Furthermore, subaerial weathering processes within sediments suggest that "diagenetically altered sediments may add an important dimension to interpretations that are made about sediment mineral weathering" (Mahaney 2002, 186). Thereby, the investigation of sand quartz grains from grave sediments may provide useful information in future studies by displaying discernible differences in the weathering patterns and extents between non-grave sediment minerals and grave sediment minerals. Such studies should include SEM analysis of unimpregnated grains as well as a more representative collection of controls in order to facilitate a firmer interpretation of whether the burial assemblage has affected the micro-scale properties of the quartz mineral grains in the burial sediments at Al Khiday. A group of controls more representative of the variability within the sediments outside of the grave cut could have included controls from several depths (including that of the burial) within the sediments outside the graves to allow for comparisons

between controls and interpretations of inter- and intra-layer variability in the non-grave sediments at the site.

5.4.2 Fungi

Fungal traces were present within some of the bone fragments seen in thin section from the intra-grave sediments in GR 147 and 148 (Section 5.3.4). Some opaque (PPL) and isotropic (XPL) features were also present (Figure 5.20) adjacent to some of the mineral fragments within a thin section from GR 150 (S1, TS 391). Unique to this thin section, the opaque material had a clustered basic distribution (Bullock *et al.* 1985, 35; Figure 5.20a-c) that was not an artefact of manufacture of the thin section. These opaque features (Figure 5.20c), showed some similarities in optical properties including dimensions, form, and external morphology to fungal spores in thin sections from other archaeological sites examined in this study (Figure 5.20d). The differences in colour and sharpness (between Figures 5.20d and c) may have been due to the features having been preserved as trace fossils, representing proxy signals for the presence of the fungal remains.

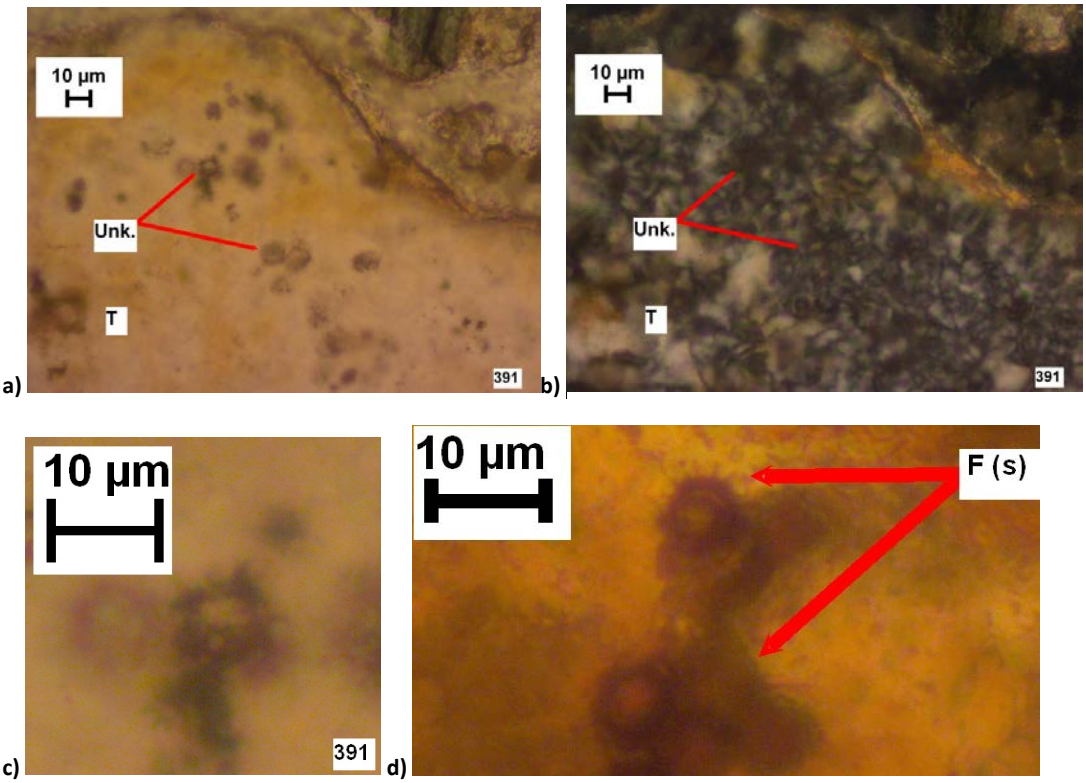

Figure 5.20: Tectosilicate with unidentified trace materials on surface, compared to fungal spores in thin section from a Swedish sediment (Chapter 7, Section 7.8). (a) Tectosilicate (T) with unidentified opaque materials (Unk.) clustered in the surface of the grain (GR 150, S1, TS 391, PPL). (b) XPL view of image a) showing the isotropic optical characteristic of the unidentified material (Unk.) (GR 150, S1, TS 391, XPL). (c) Detail of image a) showing the well rounded shape and reticulate external morphology of the unidentified material. d) Fungal spores (F(s)) observed in thin section from the archaeological investigation into the grave sediments at Sala Vastmaal (Chapter 7, Figure 7.14) (RAA51, GR 5914, C3, TS 861, PPL).

5.4.3 Bone weathering

Bone fragments from the graves sampled displayed a variety of optical characteristics which may be related to post-burial diagenetic processes and the weathering of the bone material, including trace evidence of fungal activity and mineral replacement processes. Fungal attack by Wedl tunneling (Wedl 1864 in Hackett 1981) was observed on the bone fragments from the pelvis adjacent samples (GR 147, S2Z, TS 437 and GR 148, S2, TS 438). Wedl tunnels are a common feature of post-depositional processes affecting to human archaeological bone (Jans *et al.* 2004), occurring most commonly without the explicit remains of the fungi (Jans 2008). The fungal driven changes to the bone most likely occurred in the archaeological context (term archaeological context after Schiffer 1972) as the environmental conditions necessary for fungal growth were not present at the site at the time of sampling.

Fungal attack may in turn have been inhibited on some fragments from samples where the edges had altered into a protective rim (Section 5.3.4). The discoloured exterior edges of the bone fragments as were seen in GR 150 (GR150, S1, TS 391 and GR 150, S4, TS 375), have are interpreted as secondary weathering product rims, hypo-mineralised in the sense of the bone's native mineral apatite (Figure 5.16). Previous literature has discussed how the protein component of the bone fragments at Al Khiday has been heavily altered (Salvatori *et al.* 2011). The bone fragments from GR 150 with such altered rims have no morphologically discernible microbial effects. From thin section observations the weathering processes appear to be limited to mechanical damage, along with some iron oxide depositions (Figure 5.16). Fungal attack may have been inhibited on fragments where the edges had altered into a protective mineralized rim.

A second type of bone effect observed in a thin section of GR 148 (S2, TS 438) affected the internal structural arrangement of the material along a fracture (Figure 5.17). The changes to this bone fragment along a fracture may have exposed the interior of the bone. Hence, the protein component may have been completely removed and the mineral component altered from hydroxyapatite to a calcium carbonate rich material that assumed the crystallographic rhombohedral structure characteristic of calcite ($CaCO_3$). Such chemical affects on the bone may have occurred due to conditions matching those required by the "recrystallization window" (Berna *et al.* 2004) in conjunction with calcite mobility from the transitory calcrete horizon (Zerboni 2011). Previous studies suggest that a process of recrystallization would include quartz sand grains as "a variety of processes including contamination with quartz and secondary carbonates and ionic substitution from the sediment solutions are responsible for these postmortem chemical alterations (on bone)" (Pate *et al.* 1989, 303). At Al Khiday, mineral substitution of bone apatite by a secondary carbonate mineral while maintaining the original external bone morphology (Weiner

2010, 115 for discussion of the pseudomorphic cast issue), could have occurred due to the fracture being narrow and deep.

5.4.4 Discussion of micromorphological observations and field observations

Duricrusts (hard pans of precipitated materials within sediments and sediments) can be composed of siliceous deposits (silcretes), calcic deposits (calcretes), or a mixture of the two (Nash and Shaw 1998, Wanke and Wanke 2007). Calcretes are authigenic precipitated deposits of carbonates which are mainly composed of calcite (Wang *et al.* 1994), widely reported from around the globe and have been well studied in the pedogenic literature (Gile 1961; Goudie 1983). The sediment described by the excavators at Al Khiday as a "calcium carbonate cement" deposit, is hereafter interpreted and referred to as a calcrete.

5.4.4.1 Calcrete

The calcic concretion found below the graves at site 16D4'11 (GR 142, SA1, TS 389 and GR 142, SA1, TS 390), had "separated and engulfed" (Robins *et al.* 2012, 1897) the quartz sand grains into a groundmass of pedogenic carbonate (Figure 5.21). This suggests that the development of a petrocalcic horizon at this site could be inferred as stage 3 or higher of the six-stage petrocalcic horizon model (Gile *et al.* 1965, Netterberg 1969, Bachman and Machette 1977, Watts 1978, Wieder and Yaalon 1982, Robins *et al.* 2012). At this stage of petrocalcic sediment horizon formation, further development of the calcic micromass may induce cracking or exploitation of pre-existing fractures of quartz sand grains (Robins *et al.* 2012).

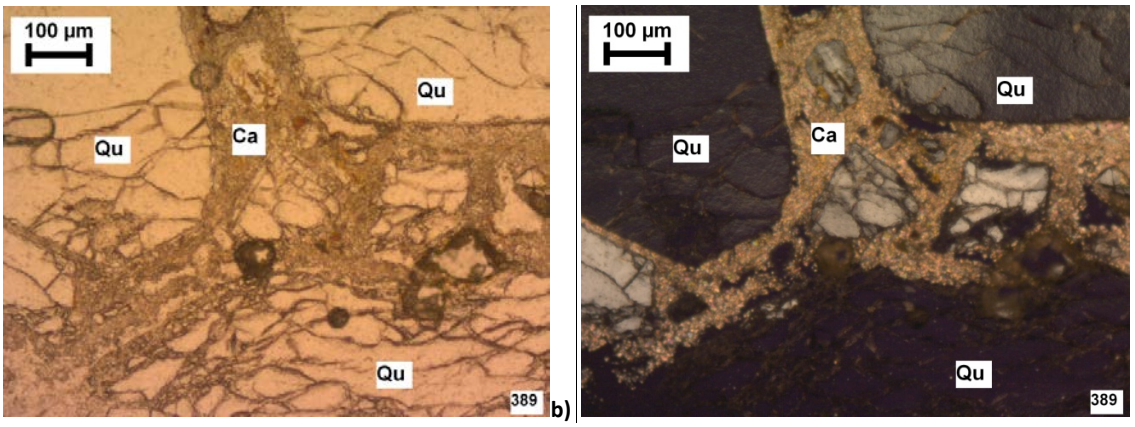

Figure 5.21: (a) Sand-sized quartz grains (Qu) with cracks surrounded by a calcitic (Ca) micromass (GR 142, SA1, TS 389, PPL); (b) XPL view of image a) (GR 142, SA1, TS 389, XPL).

The level of the authigenic calcic precipitate in the profile may have risen and fallen over time. Such changes in calcrete levels across a profile are commonly ascribed to changes in environmental conditions such as alternating wet/dry cycles (Alonso *et al.* 2004). Evidence to support such changes at Al Khiday was observed in thin sections from samples adjacent to the skull and pelvis areas (GR 150, S1, TS 386 and GR 147, S2Z, TS 418).

The skull adjacent sample (GR 150, S1, TS 386) displayed evidence of a former induration with an over–saturated carbonate solution, despite a lack of calcium carbonate micromass (at the time of excavation) compared to that present in the samples from underneath the graves (GR 142, SA1, TS 389 and 390). The presence in the grave sediments of euhedral rhombs of fourth order interference coloured minerals lining solution channels and neighbouring heavily altered quartz grains (Figure 5.22a) in TS 386 is considered as evidence for a calcrete that had been present at this higher level. This interpretation is supported by further evidence (a euhedral carbonate mineral grain within the fine material coating a quartz grain) of this process in a thin section from under the pelvic area of GR 147 (GR 147, S2Z, TS 418; Figure 5.23). Carbonate rhombs in sediments have been shown by Watts (1980, 671) to be indicators of calcrete genesis /diagenesis. The chemical dissolution features observed on the non-polished edges of the quartz grain in thin section (Figure 5.22b) are interpreted to have formed by the dissolution of silicates exposed to oversaturated carbonate solutions followed by periods of intense evapotranspiration. The formation mechanism has been comprehensively discussed and modelled by Wang *et al.* (1994).

a) 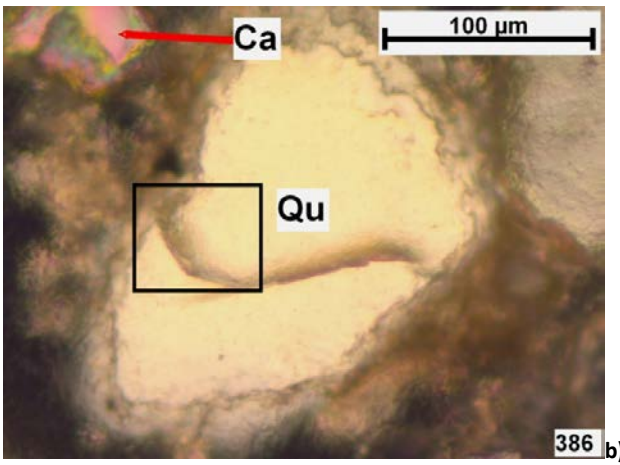

b) 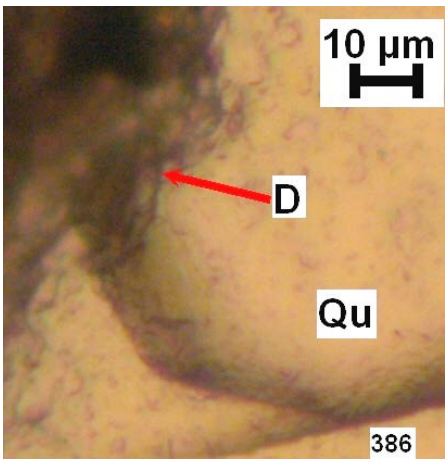

Figure 5.22: a) Quartz sand grain (Qu) with intense chemical dissolution along grain edges and a rhombohedral structured calcitic mineral (Ca) visible in the upper left corner of the image frame displaying fourth order pink and green interference colours (GR 150, S1, TS386, XPL). b) Detail of dissolution weathering (D) impact on quartz grain surface (Qu) image a) shown by black rectangle in image a) (GR 150, S1, TS386, XPL).

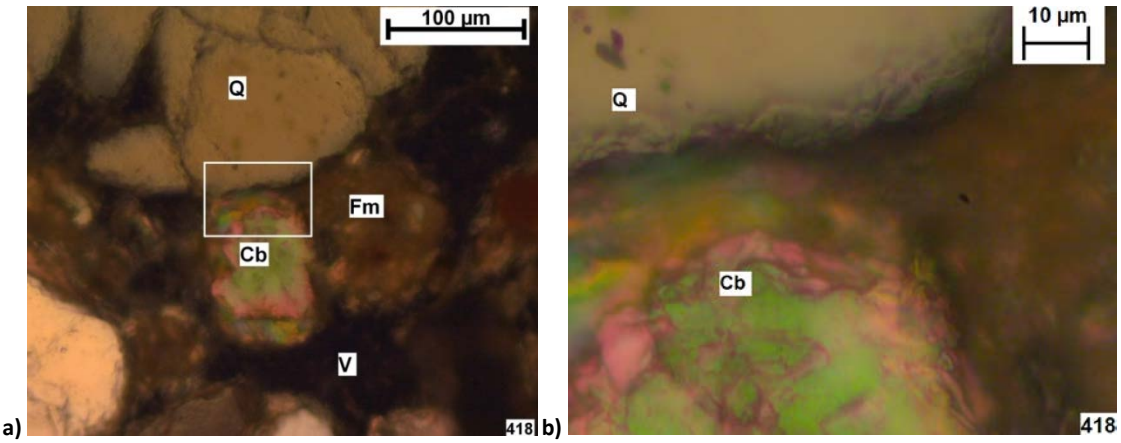

Figure 5.23: Carbonate mineral within a coating on a quartz grain. a) Quartz grain (Qu) and adjacent fine material (Fm) adjacent and carbonate mineral (Cb) with neighbouring by voids (V) (GR 147, S2Z, TS 418, XPL). b) Detail of image a), displaying fourth order interference colours of the carbonate (Cb) mineral grain adjacent to a quartz grain (Q) and fine material (Fm) (GR 147, S2Z, TS 418, XPL).

The formation of pedogenic calcium carbonate occurs in a range of sediment environments (Gile *et al.* 1966) and can occur in various levels of induration, from calcic nodular or pendant forms to petrocalcic horizons (Bachman and Machette 1977) depending on how advanced the accumulation has developed. In arid climates the role of evaporation is judged more influential on the formation of calcic horizons than vegetation, the effect of vegetation being linked to the role of CO_2 in sediment solutions (Duchaufour 1982, 75). Hence, the formation of intra-mineral cracks in the quartz sand grains from the grave sediments at Al Khiday (Figure 5.5) cannot be causally positively attributed to either calcrete formation or to the post-depositional effects of the inhumed corpse without further analyses. Although the abiotic processes necessary required for pedogenic calcrete formation are well known and are understood to be positive feedback loops, the involvement of biotic are not well defined, beyond the assertion they are influential (Robins *et al.* 2012).

5.4.4.2 Calcrete pedogenesis and bone fragments

At the Al Khiday site, the pedogenesis of a calcrete sedimentary layer situated below the graves has developed to a massive extent (massive pedostructure, see Stoops 2003), and it is interpreted that epigenetic replacement of bone minerals has commenced in some of the bone fragments (Section 5.4.3). Calcium carbonate may replace other minerals by a process of "epigenesis", where the profile has dried out and the concretions are massive in arid environments (Ruellan 1976, Duchaufour 1982, 75). Comparison of the diagenetic alterations to the bone fragments from grave sediments against those from sediments below the graves could not be determined as bone was absent from the sample of the calcic micromass below the graves (GR 142, SA1, TS 389/ 390). Hence, alteration to bone fragments by epigenesis of calcium carbonate cannot be confidently

determined from these six micromorphology samples at Al Khiday. However, sediment mineral evidence suggests that the petrocalcic horizon may have been at a higher level in the sediments in the past compared to the level at which it was recorded during the excavation of these graves.

The vertical movement of petrocalcic horizons and calcic concretions within a sediment is a widely accepted sediment process and is influenced by climate (wetting/ drying) and soil chemistry (Duchaufour 1982, 74). It is suggested that the calcic epigenetic replacement of the bone mineral in grave sediment GR 148 (S2, TS 438; Figure 5.17) could have been an effect of the calcic concretion, occurring as a result of the close proximity of the bone fragment to calcrete in the past, despite the latter being located below the graves at the time of excavation.

5.4.5 Mineral weathering

Thin section analysis of the mineral fraction of the sediments revealed various orders of silicate minerals and redoximorphic precipitates (Table 15). The silicate fraction contained tectosilicates, inosilicates and phyllosilicates. The inosilicates comprised calcic-sodic amphiboles and the phyllosilicates glauconite. The amphiboles are interpreted to have been affected by the presence of the adjacent inhumation, in relation to their mineral diagenesis and weathering pathways (Section 5.3.3.1). By contrast, the glauconite is interpreted to be a natural component of the sediments, *i.e.* lithogenic/pedogenic in origin (Section 5.3.3.2).

5.4.5.1 Amphiboles, hornblende and clinopyroxene

Based on sediment mineral inter-relationships, ranging from quartz and calcite to glaucophane, the presence of sodic-calcic amphiboles in the burial sediments may relate to the calcite cycling and calcrete vertical movements in the profile. It has been suggested that vertical movements of calcretes in sediment profiles, caused by variations in environmental conditions over time, can lead to calcitic coatings on quartzose sand grains (Nash and McLaren 2003) and the formation of euhedral carbonate-rich minerals lining voids (Watts 1980). Evidence for both processes were observed in the thin sections from Al Khiday (Figure 5.21).

It is suggested that the presence of colourless minerals with blue interference colours (Figure 5.24) are sodic-calcic amphiboles, and their presence in the pelvic and knee samples may be related to the presence of a corpse.

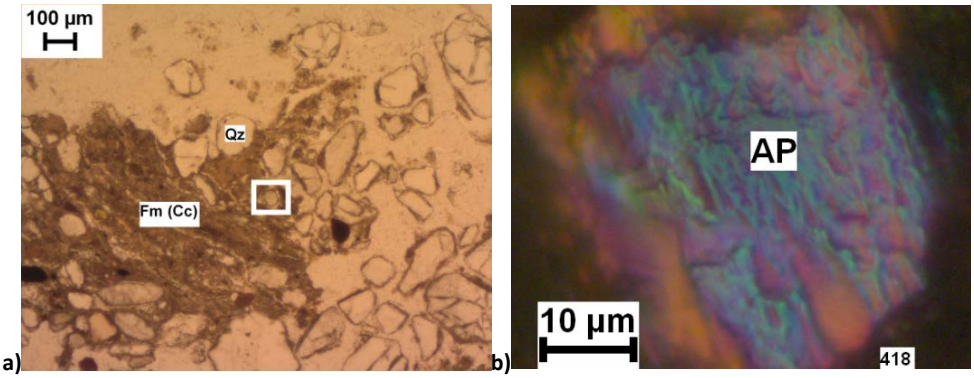

Figure 5.24: Amphibole mineral adjacent to calcium carbonate-rich fine material and quartz. a) Amphibole mineral (white rectangle area) adjacent to calcium carbonate-rich fine material (Fm(Cc)) and quartz grains (Qu) (GR 147, S2Z, TS 418, PPL). b) Detail of amphibole grain (AP) in image a), displaying columnar structure and lower 2nd order interference colours (GR 147, S2Z, TS 418, XPL).

The influence of the inhumation on the weathering of minerals is interpreted from the differing weathering pathways of the clinopyroxenes, as evidenced in the knee sample (GR 149, SA1, TS 386) and the sample from the calcrete beneath the graves (GR 142, SA1, TS 390) (Section 5.4.4). The clinopyroxene minerals from the grave sediments displayed evidence of ferralitic weathering pathways, while those from the calcrete sample displayed evidence of iron leaching weathering pathways (Figure 5.25).

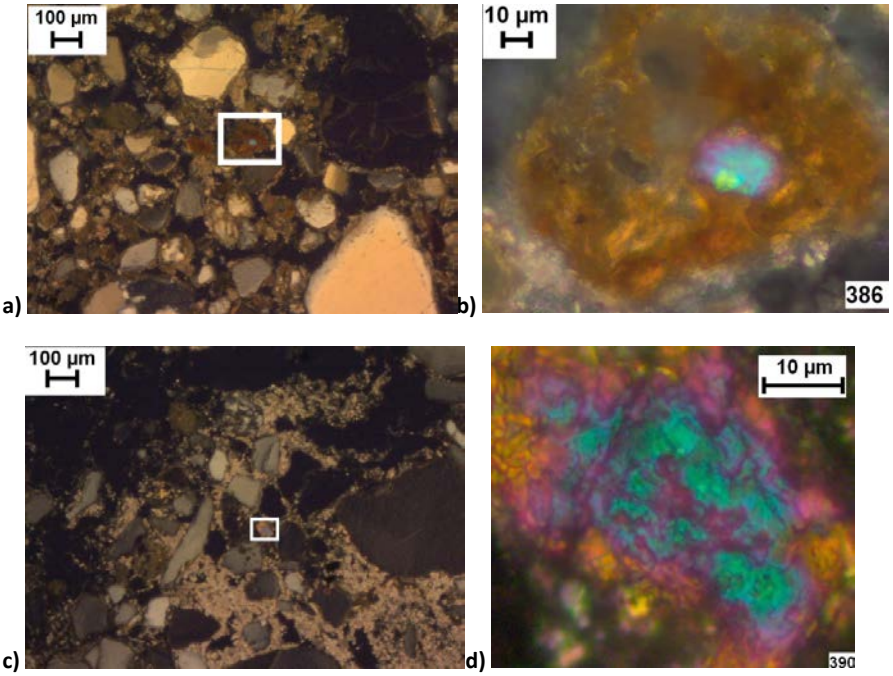

Figure 5.25: Clinopyroxene grains displaying differential weathering pathways between grave (a and b) and non-grave (c and d) sediments. a) Clinopyroxene as an accessory mineral in a sandy sediment matrix (GR 149, SA1, TS 386, XPL). b) Detail of inset (white rectangle) in image a) displaying pellicular weathering pattern and the creation of an iron-rich material as a product of weathering. c) Clinopyroxene as an accessory mineral in a calcitic groundmass cementing sand sized quartz grains (GR 142, SA1, TS 390, XPL). d) Detail of inset (white rectangle) in image c) displaying second order green interference colours, the edges have been affected by the wedging effect (GR 142, SA1, TS 390, XPL).

It is suggested that there is a difference in the weathering pathways of the inosilicate accessory minerals in the sediments of the graves to those in the control. Reduced conditions in the grave sediment are inferred as related to the microbes associated with the decomposition of the body. This explanation is supported by the experimental work of Buss *et al.* (2007) which attempted to replicate the effects of bacteria (*Bacillus* sp.) on hornblende minerals. They showed an increase in Fe and Al release from silicates in samples exposed to the bacteria than in their controls (Buss *et al.* 2007). Wilson (2004) demonstrated that in the upper part of the sediment profile, where the sediment minerals were exposed to organic ligands and increased accumulation of organic material, the sediment microbiota had a greater impact than abiotic pedogenic factors on the weathering of the sediment minerals. The graves at Al Khiday were not cut into the uppermost part of the sediment at the time of burial and it is suggested that the inclusion of the human remains acted similarly to topsoil roots in terms of a presence of organic matter.

Based on the observations from the limited dataset of six micromorphology samples at Al Khiday, it is suggested that there is a difference in the mineral weathering in the intra-grave burial sediments and the control. However, in view of the small frequency of non-quartz minerals in the sediments, a larger dataset would be required in order to form a stronger conclusion.

5.4.5.2 Glauconite

Glauconite was present in the samples and absent in the control (Table 15). Glauconite is an iron potassium phyllosilicate mineral that is widespread in sandstones and limestones and often forms in shallow marine environments (Tucker 1981, 188-189). The glauconite pellets seen in these graves exhibited the lobate form and grainy internal morphology (Figure 5.14) typical of geologically formed mineralogical glauconite (Wilson 2013, 156). Thus, the glauconites at Al Khiday were formed prior to the burials and are lithogenic in origin. The recognition of a geological origin of the glauconite (rather than an *in situ* formation through mineral weathering) is strengthened by the argument that authigenic glauconite is unstable when in association with calcite in calcretes (Krumbein and Garrels 1952; Watts 1980). Thus, any authigenic pellets would have been removed by pedogenic processes in areas beyond the reach of the micro-scale sediment conditions caused by the decomposition the skeletal remains.

The presence of glauconite in burial sediments and absence in the control (Table 15) may not be due to post-depositional effects but could have been a misleading result caused by too small a dataset for this rarely occurring (<5% estimated abundance; estimated abundance charts of Bullock *et al.* 1985, 24-25) mineral in these thin sections. Interpretation of the formation and role of

glauconite in the burial sediment environment at Al Khiday is inconclusive and would benefit from further sampling. If in future studies, the effects of reducing conditions on glauconite are further defined then the presence of this mineral with the characteristics of glauconite that had been exposed to reducing conditions could be used to infer reducing conditions and therefore used as evidence to suggest body decay conditions. Laboratory experiments have shown that this mineral can form in sediments at the boundary of redox zones in alkaline (pH 8.5) sediments (Harder 1980), and can become altered due to the activities of associated iron-oxidizing bacteria when combined with $FeSO_4$ and K-bearing minerals (Ross *et al.* 1982; Fanning *et al*. 1989a, 606). These factors could strengthen future interpretations of glauconite in burial sediments, such as the sediments at Al Khiday, which were alkaline (evidenced by the periodic formations of calcretes as reported in Salvatori *et al.* (2011)), prone to redox variations (the mobilization of iron and a climate of alternating wet/dry seasons leading to redox is discussed in Zerboni (2011)) and contained K-bearing minerals (*e.g.* microcline, Table 15). Furthermore, glauconite was only present in thin sections from samples collected from the pelvic region (S2, GR 147 and S2, GR 148), and was absent from all other sampling positions (Table 15).

The interpretation of the spatial occurrence of glauconite in the samples from Al Khiday being limited to the area of the pelvis is tentative, being limited by the small dataset gathered at this site. The interpretation that the glauconite in these sediments was formed by geological processes is supported by the literature, with the studies of Geptner and Ivanovskaya (2000) on the authigenic formation of glauconite *in situ* through the action of weathering of quartz grains. They deduce that mineral degradation caused by the activities of bacteria release Si anions (Yakhontova *et al.* 1983), which are then reused in the formation of authigenic glauconite (Geptner and Ivanovskaya 2000). In their case, the glauconite is formed expressly at the expense of the quartz and deposited in fissures and cracks within the quartz grains as a secondary mineral, directly affecting the quartz internal morphology without changing the total volume of the quartz. Such isomorphous changes would create an iso-septo-alteromorph which is at dissonance with the combined pellicular and irregular linear weathering pattern and iron-rich secondary products within the meso-alteromorphs observed in the thin sections from Al Khiday (Appendix IV).

5.4.5.3 Blue-green coloured minerals

Blue-green coloured minerals were identified in samples and not in the control (Table 15). Identification of such blue coloured minerals would require additional sub-microscopic techniques such as XRD, however based on optical properties they are suggested to be either chlorite or vivianite and the >10 µm blue-green minerals present along the edges of aggregates in samples from this site have been tentatively identified as vivianite (Section 5.3.3.2). Formation of chlorite

in soils and sediments has only been as shown by the presence of very small interstratified deposits in the clay (<2 μm) fraction (Slaughter and Milne 1960). Vivianite was interpreted to have formed post-depositionally in voids in the deposits of the turf mound at the Gokstad ship burial (Macphail *et al.* 2013). The blue coloured minerals in the grave sediments from Al Khiday (Figure 5.12) could have been related to the post-depositional processes in the graves, although further evidence would be needed to confirm this.

5.5 Conclusion

The micromorphological evidence gathered from the thin section analysis of the grave sediments at Al Khiday suggests that a suite of complex pedological and microbial post-depositional processes have affected them over time. The sequences of carbonate and silicate dissolution and precipitation events within the sediment have impacted on the human remains and the sediments adjacent to them. Thus, the possible post-depositional proccesses on the sediment minerals caused by the effects of decomposition of the deceased individual may have been overwritten by the subsequent effects of calcrete genesis/diagenesis within these sediments.

While the calcrete genesis/diagenesis processes that are often associated with harsh, arid desert climates have degraded some of the archaeology through a recycling of the materials (calcitic features), these same processes have also been the agents of preservation of other types of archaeological information, such as bone. The bone fragments, where they have not been altered through calcium carbonate epigenetic transformations (Figure 5.17), have been well preserved. Well preserved bone fragments have retained their external morphology and internal structural integrity, and also retain records of attacks by fungal organisms (Figure 5.18).

Excepting an ivory bracelet in one grave (GR 153) no grave goods were found associated with the larger group of 70 graves at Al Khiday (16D4, Section 5.1) including the graves discussed in this chapter. Studies have suggested that vivianite in graves could be linked to the degradation of iron-rich metal grave goods (Ern *et al.* 2010). Hence, the presence of vivianite observed in thin sections from these graves could suggest that metal grave goods were deposited with the burials but have degraded in this sandy and permeable sediment. Thin section analysis from the current dataset from Al Khiday are not able to contribute further information to that of the excavation reports (Salvatori and Usai 2005, Cremaschi *et al.* 2006, Usai *et al.* 2010a, Salvatori *et al.* 2011, Zerboni 2011, Usai 2014) regarding ritual, procedure for grave rilling relative time of filling process with respect to the burials, or the provenance of the materials of the grave fills.

Perhaps the most intriguing processes evidenced in the thin sections from Al Khiday are those relating to the diagenesis of bone fragments and to the distributions of glauconite and vivianite. The wealth of information on the diagenetic pathways of the bone fragments from the graves, and the preservation of proxy data of presumed Mesolithic fungi within bones is promising. If, in future studies, the thin section observations on bone fragments were to be combined with a comprehensive analysis of the weathering pathways and surface micro-textures of loose sand quartz grains, and further research was made into the possibility of glauconite as a marker for past inhumations, grave sediments could prove to possess a strong potential for geoarchaeological research.

Chapter 6. Case study: Tel Qarassa, Syria

6.1 Introduction

The site of Tel Qarassa is located in south west Syria within the district of As Suwaydā (Figure 6.1). It was excavated in 2009 and 2010 by a team funded by the Spanish Institute of Cultural Heritage (Ibáñez *et al.* 2010) during which time samples were collected on behalf of the InterArChive team by A. Balbo, according to the protocol designed by the InterArChive team (Chapter 3 and Section 5.2). The site would have been contemporary with a nearby lake (Ibáñez *et al.* 2010). The area of the burials in this Chapter corresponds to zone 2, area EF101 of the site reports (Ibáñez *et al.* 2010; Balbo *et al.* 2012) (Section 6.2). The site contained buildings of PPNB (pre-pottery Neolithic B) age which, post-abandonment, were used for burial purposes, followed by the burning and collapse of a wooden roof (Ibáñez *et al.*, 2010). The burials have been dated to the 9th millennium BC (9100 ± 60 BP) from carbon AMS dating of a legume (*Leguminosae* seed) (Santana *et al.* 2015). The three PPNB stone buildings were found within deposits of two main unit types, the first being a yellow-red adobe sediment that was overlain by the second, a fine-grained dark grey ashy sediment with small basaltic clasts (Balbo *et al.* 2012). The basaltic clasts may have been from eruptions from the volcanic activity of the basaltic Harrat-Ash-Shamah volcanic field (Figure 6.2) which extends across a wide stretch of the Arabian plate including southern Syria (Krienitz *et al.* 2007).

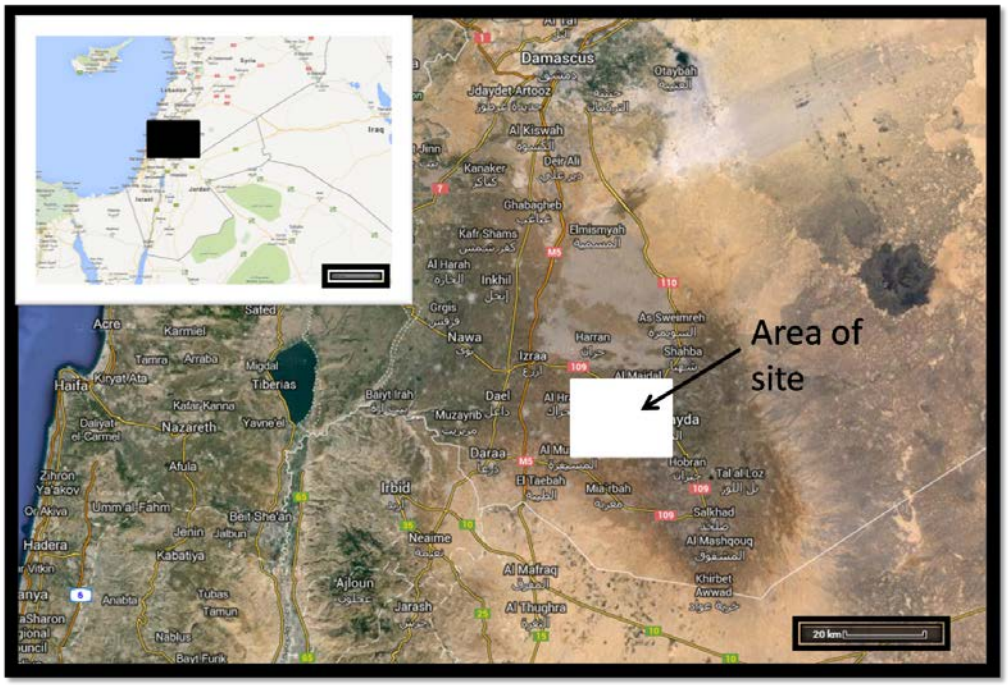

Figure 6.1: Map of the location of the archaeological site Tel Qarassa, with inset showing wider geographical context (images adapted from Google maps ©2014). The As-Safa is visible as a dark circle to the northeast of the site as part of the Harrat-Ash-Shamah volcanic field.

Xererts are sediments which are often young and from basaltic rocks (WRB). The local geology around Tel Qarassa is young (Quaternary) and mainly basaltic (Figure 6.3). Basaltic clasts in sediments have been found to weather discriminately, starting with glass (if present) and then phenocrysts (Bain and Russell 1980). Eggleton *et al.* (1987) suggested that the weathering of the phenocrysts could be described as olivine, pyroxene, plagioclase and then K-feldspar, as although plagioclase may start before pyroxene, it progresses slower and so persists longer. Although the sequence of the weathering of basalt is well established, there may be alternative pathways by which the phenocrysts produce a selection of clays and iron oxides as secondary mineral products. Trajectories of mineral weathering in the sediments from Tel Qarassa are investigated in this chapter. The aim was to discern if patterns could be identified through comparison of samples against controls to investigate whether post-depositional processes related to the secondary burial of a skull cache inhumation left trace evidence in the surrounding sediments.

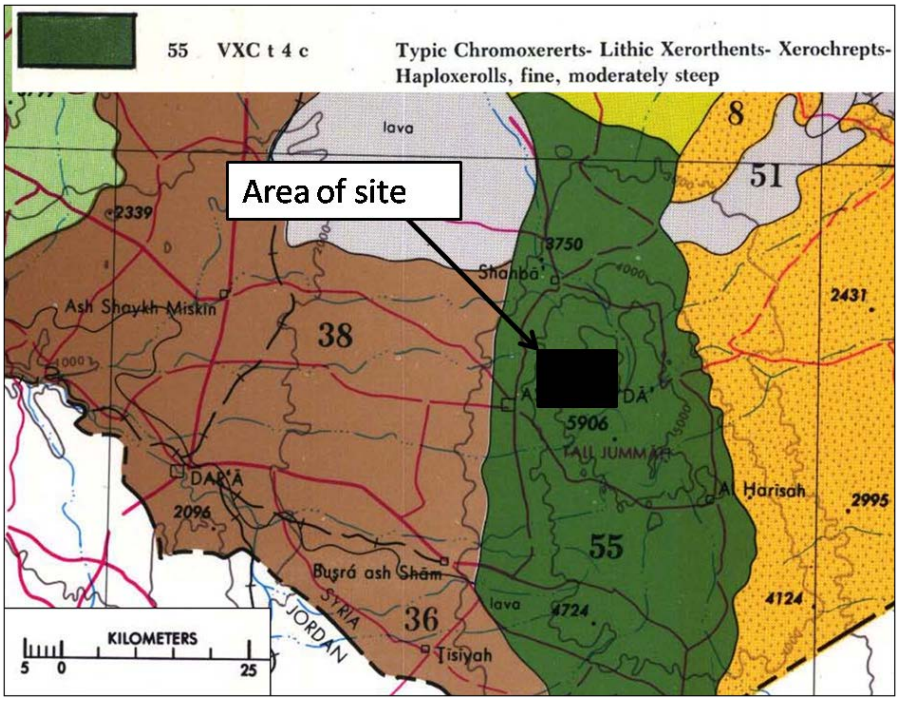

Figure 6.2: Sediment map of south west Syria (adapted from Ilawi 1985 accessed *via* Panagos *et al.* 2011). The site is located within the area identified in green as a typic chromoxerert, which is bounded by an inceptisol (brown) to the west and an aridisol (yellow) to the east. Chromoxererts are vertisols, which are clay rich sediments prone to shrink-swell and cracking. Inceptisols are young immature sediments. Aridisols are sediments with little sediment moisture and often are freely draining.

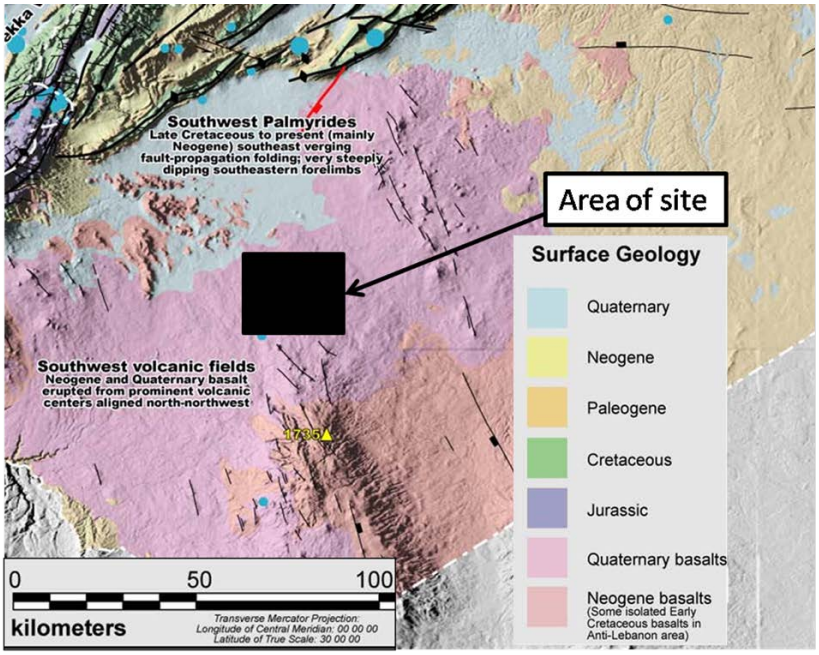

Figure 6.3: Geological and tectonic map of south west Syria, the site is located within the Quaternary basalts area identified as the "Southwest volcanic fields (Neogene and Quaternary basalt erupted prominent volcanic centers aligned north-northwest)" (adapted from Brew 2000 accessed *via* Cornell University Geoscience Information pages).

6.2 Materials and methods

6.2.1 Excavation and sampling

The area sampled for the InterArChive team centres on a skull cache in House Three within Zone 2 (QZ2, site code EF101). The site control (C1; Table 16) was collected from the west face of a trench dug near the south slope of Tell North. The skulls were arranged in a reniform-shaped deposit and the sampling methodology created for the InterArChive project (Chapter 3) was modified for application at this site. Human remains are referred to by skeleton numbers (SK) in this chapter, rather than by grave numbers as in other chapters (*e.g.* Chapters 4, 5, and 7). No C2 control was collected, two grave fill controls (C3 and C3b) and skull adjacent samples (S1 and SA1, inside the skull) were collected (Table 16b; Figures 6.4 and 6.5). The C3 control was collected from the deposit overlying the burial deposit and is the infill of a later pit (Ibáñez *et al.* 2010). As such the C3 control is not from sediment directly related to the burial and hence it has been studied, along with the C1 control, as a representation of the variety of different sediments present at this site. The other intra-grave control (C3b) was a deposit assessed by Ibáñez *et al.* (2010) to be contemporaneous with the burial and spatially adjacent to the two clusters of skull bone remains (Figures 6.4 and 6.5). The skulls were grouped into two areas with large rocks separating SK 4, SK 8 and SK 3 from SK 2, SK 5 and SK 1 (Figure 6.4). A detailed osteological analysis of the crania is reported in Santana *et al.* (2012).

Table 16: Micromorphology controls (a) and samples (b) collected at Tel Qarassa for the InterArChive team.

a)

Sample	Description	Thin Section Numbers
C1	C1, taken from West profile of the Tell	959
C3	C3, possible secondary intrusion of sediment from Chalcolithic reshaping of the Tell	1113, 1018
C3b	C3b, taken from between the two main skull caches. Original material associated with burial.	1239

b)

Skeleton Number	Sample	Thin Section Numbers
SK 1	1	971, 965, 952
SK 2	1	958, 991, 1001
SK 3	1	960, 954
SK4	A1	961, 1009
SK 5	1	970, 956
SK 8	1	957, 1112

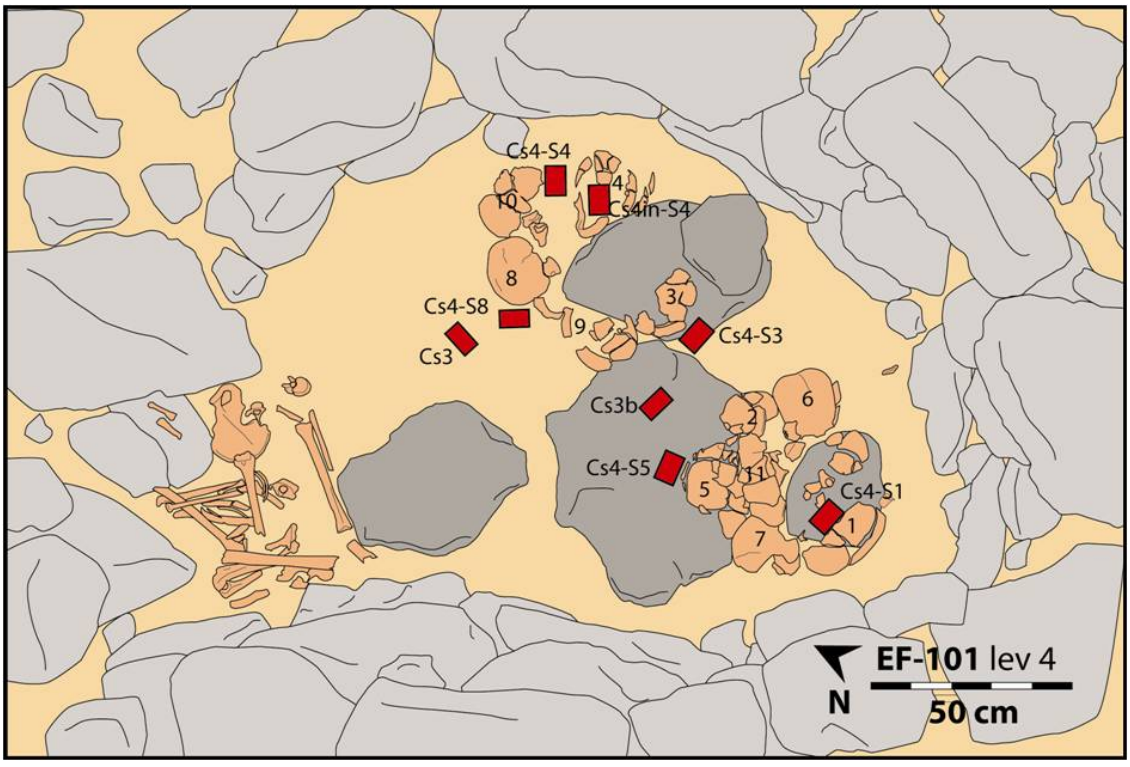

Figure 6.4: Drawing of skeletal remains and surrounding archaeological features. Annotations indicate the position of the micromorphology samples: C3 control, C3b control, and samples (S1) from the 6 skulls sampled (SK 1, SK 2, SK 3, SK 4, SK 5, and SK 8) (Balbo *et al.* 2012). The location of the sample from the sediment surrounding the skull from SK 2 is not shown on this figure as it was not known (sample was collected by a third party, Section 6.1).

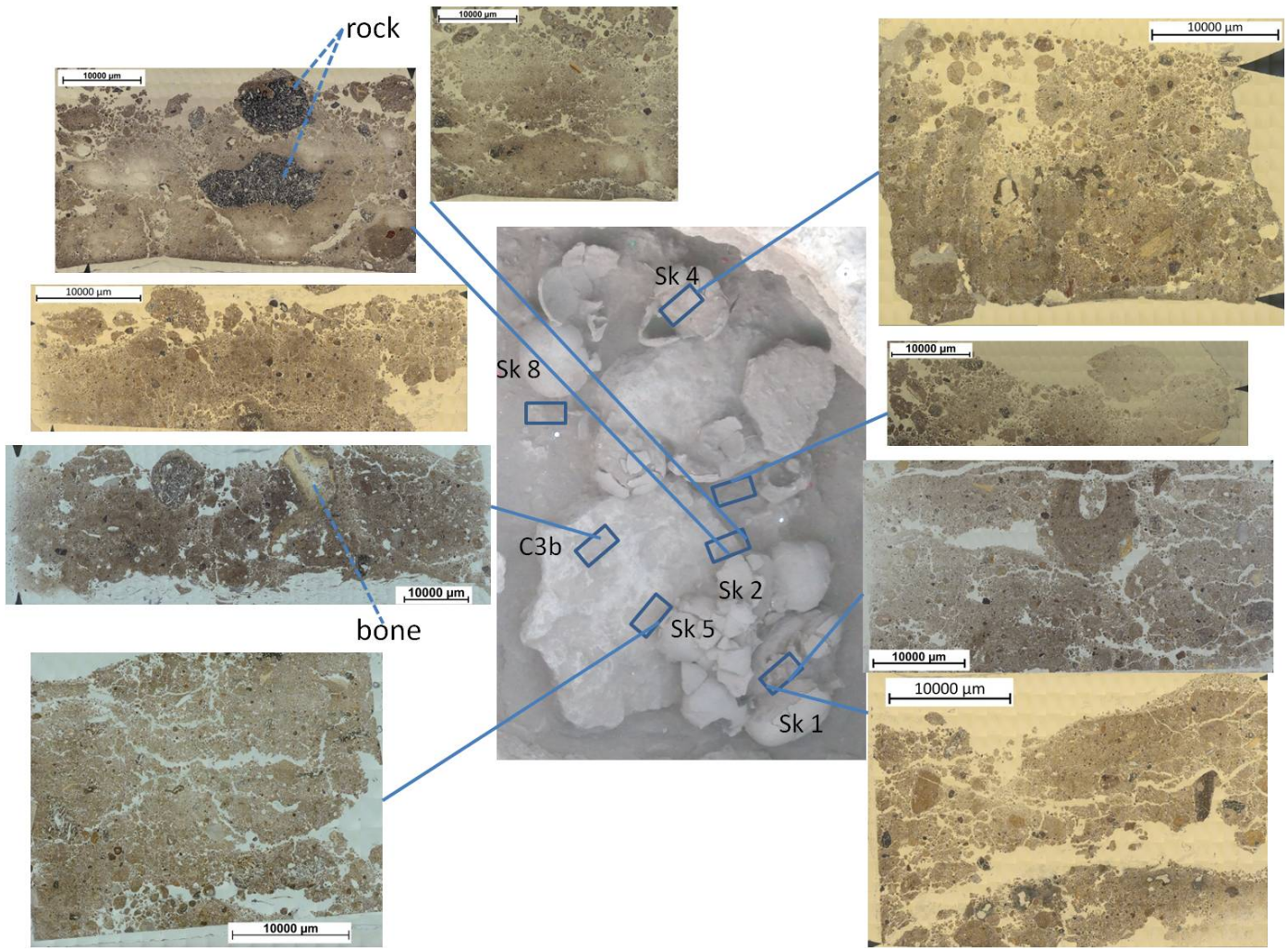

Figure 6.5: Location of skulls and thin sections.

6.3 Thin section analysis

The micromorphology slides were described utilizing the methodology described in Chapter 3, including mineral identification and mineral weathering. Macroscale visual observation showed that the largest rock fragments within this collection of thin sections were in the controls rather than in the samples (Figures 6.6 and 6.7). A full collection of mosaic images for all thin sections studied from Tel Qarassa is available in Appendix I.

a)

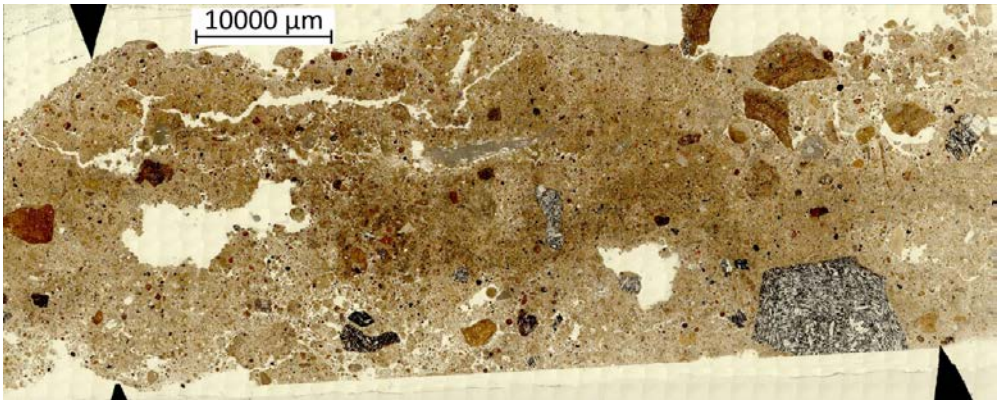

b)

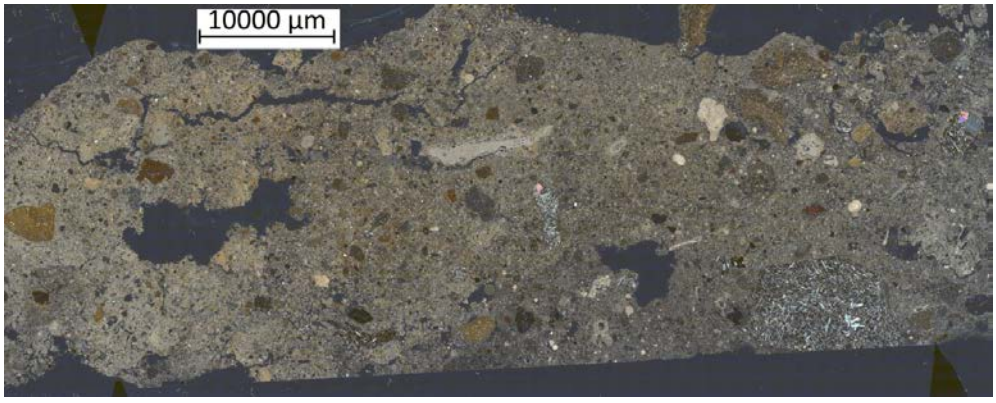

Figure 6.6: Mosaic image of TS 959 (C1), a) PPL and b) XPL. Note the relative sizes between this figure and the following figure, especially in relation to the large rock fragment at the bottom right of the mosaic of the C1 (Figure 6.6) compared to the largest rock fragment visible in the skull adjacent sample (mid-right in Figure 6.7).

a)

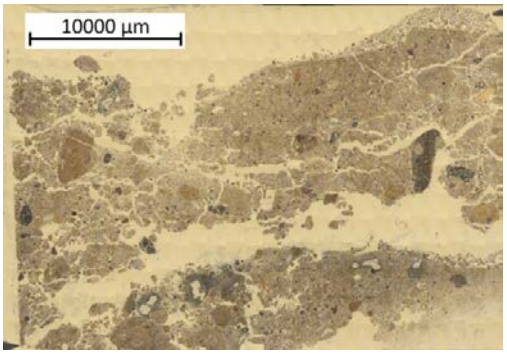

b)

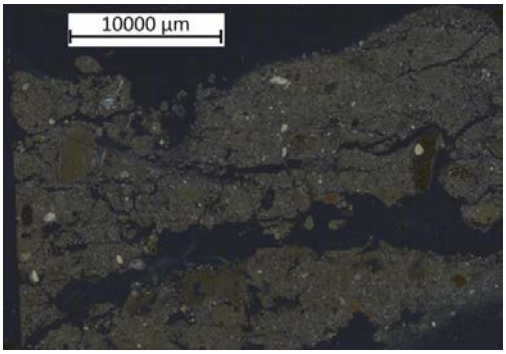

Figure 6.7: Mosaic image of TS 971 (SK 1, S1), a) PPL and b) XPL.

6.3.1 Summary of micromorphological observations

Detailed micromorphological observations are given in Appendix V and are summarised in Table 17. The related distribution of coarse to fine materials was embedded, b-fabric cristallitic and ped microstructure granular in all thin sections (Table 17). Basaltic clasts and mineral grains were observed embedded in the sediment matrix in the controls and the samples (Table 17). The most common types of voids in the samples and controls were vughs, channels and chambers (Table 17). Plant, bone and shell remains were present in some of the thin sections (Table 17). Red anisotropic and pale grey with high order white interference colours pedofeatures were observed in controls and samples (Table 17). Excremental pedofeatures were observed in controls and samples (Table 17).

Table 17: Results of micromorphological analysis. Symbols have been used to represent abundance recorded using the estimated abundance charts of Bullock *et al.* (1985).[5]

[5] **The symbols used in the table are as follows: 0≥1 = _, 1-2 = *, 2≥5 = **, 5≥10 = ***, 10≥20= ****. The limit used in determining the relative proportions of the coarse to the fine material (c/f ratio) is set at 50 µm. This summary table has been abridged (for the full version see appendix), by the removal of columns which contained no variation across all of the thin sections, this includes the categories of: b-fabric (cristallitic), limpidity (speckled), related distribution of coarse to fine materials (embedded) and type of pedostructure (granular). Also categories with no positive recorded values (i.e. an abundance >0) from these observations have been removed (quasi-coatings, amorphous organic matter, and phyllosilicates). Pedofeatures are divided into two categories: pedofeatures related to voids, grains and aggregates and pedofeatures not related to voids, grains or aggregates, thereby respecting the primary division of pedofeatures in soil thin sections as listed in Stoops, 2003. Size ranges used for peds are as follows: very small (50-1000 µm), small (1000-2000 µm), medium (2000-5000 µm), and large (5000-10000 µm). Abbreviations used are as follows: thin section (TS), sample (S), vesicles (Ve), channels (Ch), chambers (Cb), vughs (Vu), cracks (Cr), hypocoatings (Hypo.), infillings (Infil.), excremental pedofeatures (Excr.), tectosilicates (Tecto), inosilicates (Inos), nesosilicates (Neso), pseudomorphs composed by carbonate rich material (CO3 pseu.), level of development (level of develop.). *NB*: unknown abundance has been denoted by "?" in the cells listing inosilicate and nesosilicate abundance for TS 956 (SK 5), this is due to the high extent of weathering in this section which has produced iron-rich alteromorphs which cannot be confidently traced back to their primary mineral in a manner which enables discernment between pyroxenes (clinopyroxene or orthopyroxene) from olivine.**

TS	S	colour (PPL)	c/f ratio	sorting	Voids					Pedofeatures related				Pedofeatures not related			Inorganics					Biological				Peds	
					Ve	Ch	Cb	Vu	Cr	Intrusive		Matrix		Nodules		Excr.	Minerals				Rock	plant	bone	Other		level of	size
										Fe-rich	CaCO3-rich	Hypo.	Infil.	Fe-rich	CaCO3-rich		Tecto	Inos	Neso	Other	Basalt			shell	CO3 pseu.	develop.	range
959	C1	pale orange	15, 85	unsorted	_	***	*	**	_	*	*	*	_	*	***	*	*	*	*	_	**	**	*	*	*	weak	very small,
1113	C3	pale grey yellow	30, 70	poorly sorted	_	*	*	**	_	*	**	*	_	**	*	*	**	*	*	_	****	*	*	_	*	very weak	very small
1239	C3b	medium orange	20, 80	unsorted	_	**	***	*	_	_	*	*	_	*	_	*	*	*	*	_	***	**	***	_	_	weak	very small
965	Sk 1	yellow brown	30, 70	unsorted	_	***	**	**	_	_	_	*	***	*	*	*	**	*	*	_	**	*	*	*	_	weak	small
1001	Sk 2	yellow grey brown	10, 90	unsorted	_	**	*	***	_	_	*	*	_	*	*	**	**	_	_	*	*	*	*	_	_	moderate	small, medium, large
954	Sk 3	medium yellow	35, 65	unsorted		*	*	****	_	_	*	**	_	**	*	_	***	*	*	_	**	**	**	_	*	moderate	very small,
1009	Sk 4	medium orange	25, 75	unsorted	_	*	**	***	_	_	*	**	_	***	_	*	***	*	*	_	*	*	**	_	*	weak	very small
956	Sk 5	medium yellow	30, 70	unsorted	*	***	*	***	_	_	_	*	_	**	*	*	***	*-?	?	*	**	*	**	_	_	very weak	small, medium
1112	Sk 8	yellow grey	25, 75	unsorted	_	*	_	***	*	_	_	*	_	*	*	*	**	*	*	_	**	*	*	_	_	weak	small, medium

6.3.2 Bone fragments

Fragments of bone were present in controls and samples (Table 17). Bones were identified by their colours (pale yellow) interference colours (ropey first order greys) and structure (osteological canals). Bone fragments observed in the site control (C1, TS 959) showed evidence of a nematoblastic (needle morphology) crystalline substance within the intra-bone spaces (Figure 6.8a and b) and a thick coating of fine-grained calcitic material (Figure 6.8g). Some of the bone fragments from samples were coated in calcitic material (SK 5, S1, TS 956, Figure 6.8d and SK 4, SA1, TS 961, Figure 6.8e) and others were not (SK 1, S1, TS 965,Figure 6.8d and TS 961, SK 4, SA1, TS 961, Figure 6.8f).

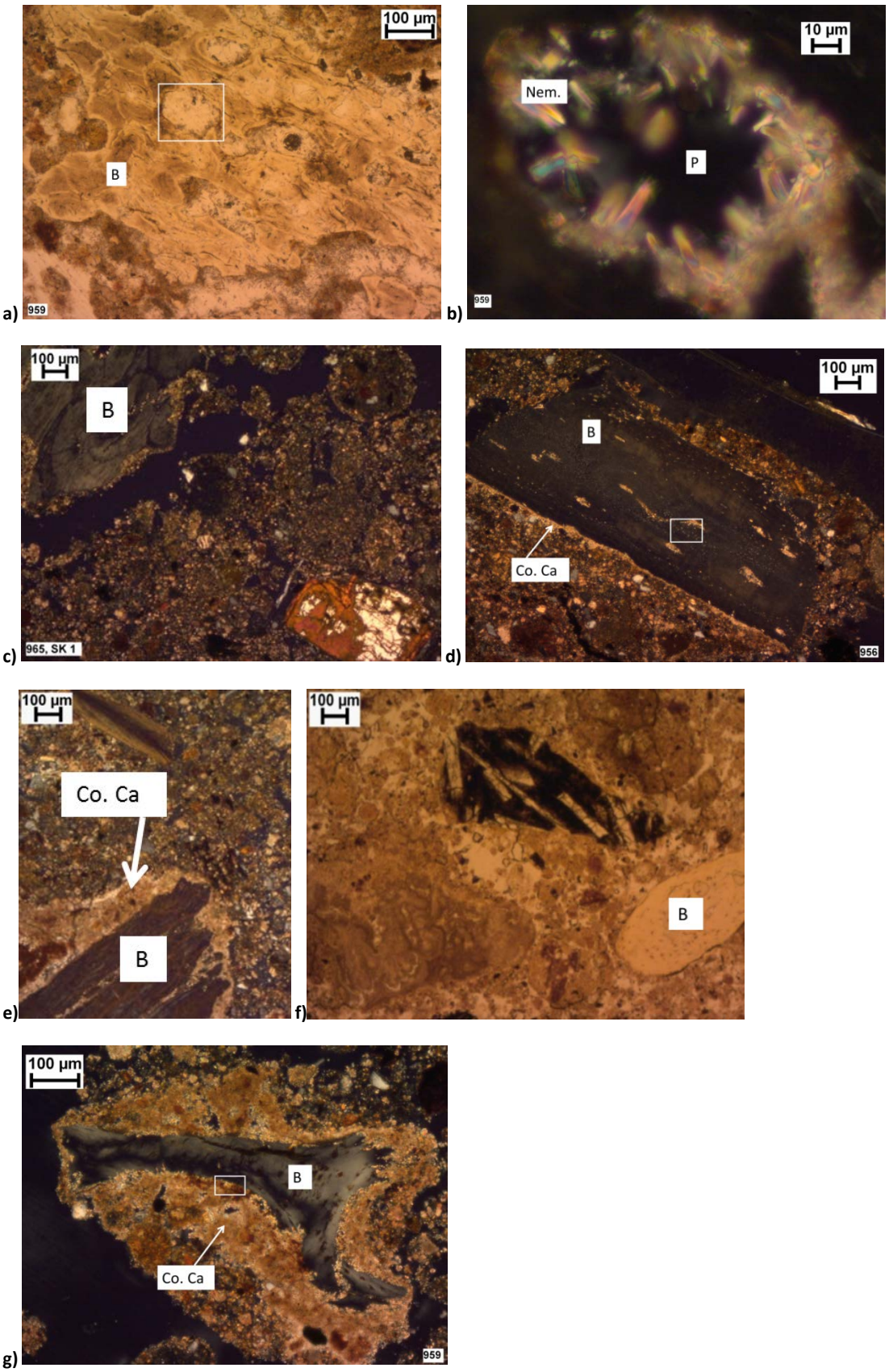

Figure 6.8: Bone fragments in thin section from controls and samples. (a) Bone fragment (B) from site control (C1, TS 959, PPL). (b) Detail from inset (white rectangle) in image a) showing nematoblastic texture (Nem.) in intra-bone pores (P) (C1, TS 959, XPL). (c) Bone fragment (B) from skeletal adjacent sample without calcitic coating (SK 1, S1, TS 965, XPL). (d) Bone fragment (B) from skeletal adjacent sample with thin calcitic coating (Co. Ca) (SK 5, S1, TS 956, XPL). (e) Bone fragment (B) from TS from sediment inside a skull with thick calcitic coating (Co. Ca) (SK 4, SA1, TS 961, XPL). (f) Bone fragment (B) from sample from sediment inside a skull without calcitic coating (SK 4, SA1, TS 961, PPL). (g) Bone fragment (B) from site control with thick calcitic coating (Co. Ca) (C1, TS 959, XPL).

6.3.3 Biota in the sediments

Excrement pellets were present in the controls and the samples (Table 17). Excrement pellets were identified by their characteristic shape (cylindrical, ovate or circular), colour (brown), clustered basic distribution and inclined related distribution to channel and chamber voids (distribution terminology after Bullock *et al.* 1985). Channel and chamber shaped voids with excremental pellets (Figure 6.9) were interpreted as proxy evidence for past biota.

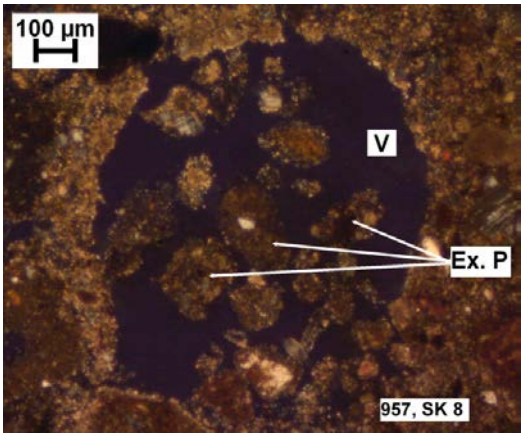

Figure 6.9: Void (V) with excremental pellets (Ex. P) (S1, SK 8, TS 957, XPL).

6.3.4 Rock and mineral weathering

The rock fragments present in the sections (Table 17) differed in terms of their phenocryst frequencies (Appendix V) and their contents and weathering is summarised in Table 18. Basaltic clasts were coated in iron-rich and carbonate-rich coatings in some samples and the C3 control (Table 18). Phenocrysts in the basaltic clasts included plagioclase, olivine, and pyroxene and are discussed in the following sections. Some clasts were more silicic than others, denoted by higher ratios of feldspar to ferro-magnesian silicates which exhibited a range of sizes (Appendix V). Direct quantitative comparisons of phenocrysts are not considered to be reliable given the low abundance and the impact on size appearance in thin section due to the plane of cut through the material (Stoops 2003, 11-32). Weathering extents and patterns of phenocrysts and embedded mineral grains differed between samples and controls (Table 18). The weathering of the phenocryst minerals and the production of their secondary products can be assessed reliably following the terminology of Delvigne (1998) (Chapter 3). Mineral weathering can be ascertained despite the unknown variable of a random plane of cut (Delvigne 1998, 56-57) and has been considered separately as their origin from the basaltic clasts within the corresponding *gefüge* (Chapter 3) is not certain.

Table 18: Mineral weathering patterns and extents of mineral grains both within basaltic clasts and embedded within the sediment micromass from the sediments observed in thin section.[6]

[6] **Abbreviations used are as follows: thin section (TS), skeleton (SK), sample (S), opaque (op.), non-matrix cappings (capp.), non-matrix coatings other than cappings (coat.), plagioclase (PG), pyroxene (PX), olivine (OV), glauconite (Gc), chlorite (Ch), acanthomorphic (ac.), small (sm) (<250 µm), medium (med) (250-1000 µm), and large (lr) (>1000 µm). Coloured squares indicate presence of cappings and coatings (columns 4-7) and opaque products (columns 14-17).**

TS	SK	S	Rock Fragments														Embedded minerals	
			Coatings to basalt				Basalt phenocrysts				Glassy groundmass weathering		op. product morphology				Primary (PX&OV) weathering	Other
			CO_3-rich		Fe-rich		PG weathering		PX & OV weathering									
			capp.	coat.	capp.	coat.	extent	pattern(s)	size	extent	extent	colour					extent	type
959	C1	C1					1	linear	sm	1	2(/1)	brown, grey					2 (/1)	/
1113	C3	C3					1	linear	med	2	1	op., grey					3	/
1018	C3	C3					1	ac.	sm to med	1	2(/3)	brown, yellow					2	/
1239	C3b	C3b					1	linear	sm to med	2/1	2/1	grey, op.					2 (/1)	AP, Ch
958	2	1					2	ac., linear	med	1	2	brown, yellow					3/4	AP
991	2	1					1	ac., linear	sm to med	2 (/1)	2	brown, grey					3 (/2)	AP
1001	2	1					1	ac., linear	sm	2 (/3)	3	op., grey					2	AP
965	1	1					1(/2)	linear	sm to med	3	2	grey, op.					2 (/3)	/
971	1	1					1	ac., linear	sm	2 (/1)	2(/3)	brown, grey					3	AP , Ch
956	5	1					1	ac., linear	sm to lr	3/2	4	op.					3	AP
970	5	1					1	ac., linear	sm to med	2 (/3)	2	brown, grey, red					2	/
957	8	1					2	linear	sm to med	3/4	2	op., grey					3/4	AP, Ch
1112	8	1					1	linear	sm	3/4	2	grey, op., yellow					3	/
954	3	1					2	linear	sm to med	3/4	2(/3)	op., red					3/4	AP
960	3	1					2	linear	sm	3/4	3	op.					3/4	AP
1009	4	A1					1 (/2)	ac., linear	sm to med	3	3(/4)	op., red					3/4	AP
961	4	A1					1	ac., linear	sm	3/4	3/4	op.					3	AP, Ch, Gc

6.3.4.1 Plagioclase phenocrysts

The types of plagioclases present had either simple or polysynthetic twinning (the calcic to sodic plagioclases, respectively) (Figure 6.10 and Appendix V). The weathering patterns observed included trans-mineral fractures as well as a combined peripheral and irregular linear pattern and an acanthomorphic ('fish-bone') pattern (Table 18). An acanthomorphic weathering pattern producing acantho-septo-altermorphs from feldspars is less common on simple twinned plagioclase than on those of multiple twinning (Delvigne 1998, 242). However, the occurrence in basalts is not undocumented, and studies have shown that this pattern may even be seen on weathered pyroxenes infilled by iron-oxyhydroxide deposits (Delvigne 1998, 242).

Red coloured deposits having red interference colours, possibly iron-rich minerals, were observed in the septa of altered plagioclases in the controls (C1, TS 959 and C3, TS 1018). By contrast, the intra-mineral cracks of plagioclase phenocrysts in the samples (SK 1, 2, 3, 4, 5, and 8) were filled by an opaque material. The difference in infill material within the secondary pore spaces of the plagioclase phenocrysts of the controls and the samples is interpreted as evidence of variability in the types or rates of post-depositional processes that affected these sedimentary micro-environments. Studies by Soubrand-Colin *et al.* (2005) in sediments where transmineral fractures and/or acanthomorphic weathering has occurred through dissolution and removal of the silica-rich plagioclase materials, have shown these areas to be commonly infilled with a colourless isotropic material and stained by iron-rich precipitates from sediment solutions or clays (Soubrand-Colin *et al.* 2005). Where weathering has proceeded and drainage conditions have been good iron-rich minerals can deposit in the septa of plagioclases (Delvigne 1998, 104-105).

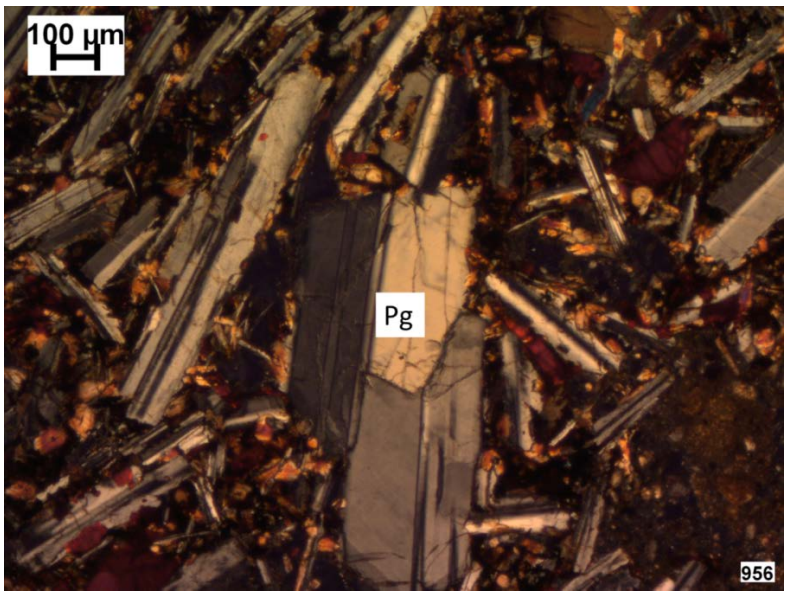

Figure 6.10: Plagioclase (Pg) phenocrysts in basalt from the sediments surrounding SK 5, containing plagioclases of both simple and polysynthetic twinning (SK 5, S1, TS 956, XPL).

6.3.4.2 Olivine and pyroxene phenocrysts

Most of the intra-clast olivine and pyroxenes had weathered to extent two or greater in the samples, contrasting with the controls (C1, TS 959 and C3, TS 1018) and one thin section from SK 2 (S1, TS 958). The olivine exhibited irregular weathering patterns with a red and orange coloured anisotropic secondary product (Figure 6.11), interpreted as iron-rich (red colours displayed in OIL). This secondary product is interpreted as iddingsite, a common iron-rich alteromorph after olivine (Stoops *et al.* 1979). In most observations from the thin sections, the morphology (external shape) of the olivine crystals was affected, leading to holo-alteromorphs rather than pseudomorphs. An exception was recorded from a grain in TS 1009 (SK 4, SA1), where the euhedral form was preserved, forming an early stage pseudomorph after olivine. Alteration of forsterite olivine in basalts to produce an alteromorph of iddingsite and with exsolution of magnesium from the rims and within exploited intra-mineral fractures has been well studied by Eggleton *et al.* (1987). The work of Eggleton *et al.* (*ibid*) provided clear evidence linking observations from optical and sub-micron level microscopies to support a genetic relationship between these minerals. The studies by Delvigne (1998) and Eggleton *et al.* (1987) support the interpretation that the olivine has altered and iddingsite has formed as part of alteration processes in the rock fragments. Hence, the contrast between the alterations in the basaltic clasts in the grave sediment from SK 4 and the holo-alteromorph in the other samples (SK 2, 3, 5, and 8) is interpreted as variability within a sediment and not as evidence of pedological processes.

The pyroxenes were altered to red and orange coloured anisotropic minerals (Figure 6.12) which are interpreted as iron-rich, similar to the type of alteration affecting the olivine. This is interpreted as the effect of alteration resulting from geological processes and not from pedogenesis.

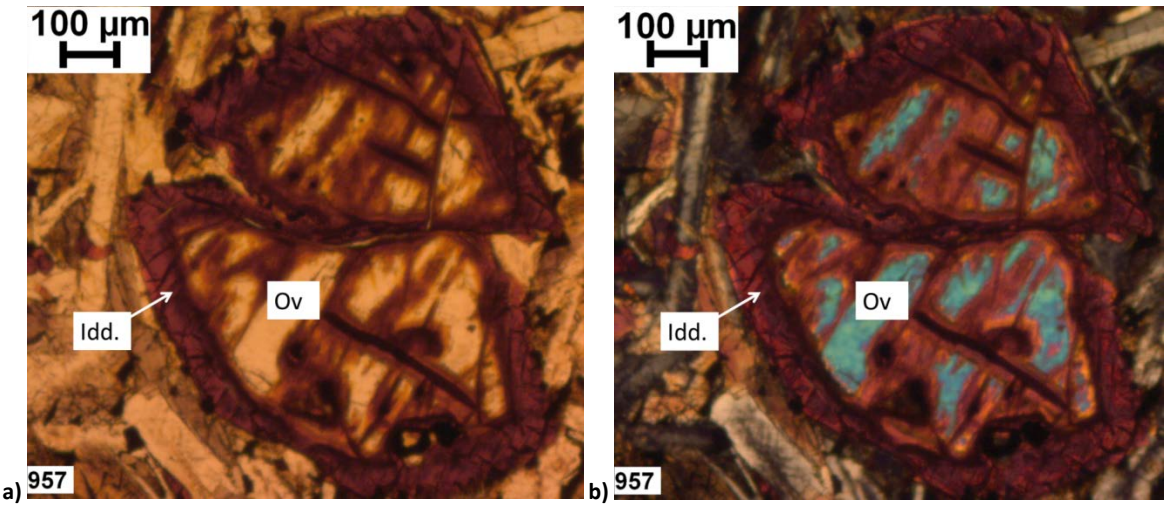

Figure 6.11: Olivine (Ov) within basalt from the sediments adjacent to SK 8 (S1, TS 957), a) PPL and b) XPL. The associated iddingsite (Idd.) is interpreted as due to alteration, and not as a result of weathering occurring in the sediments.

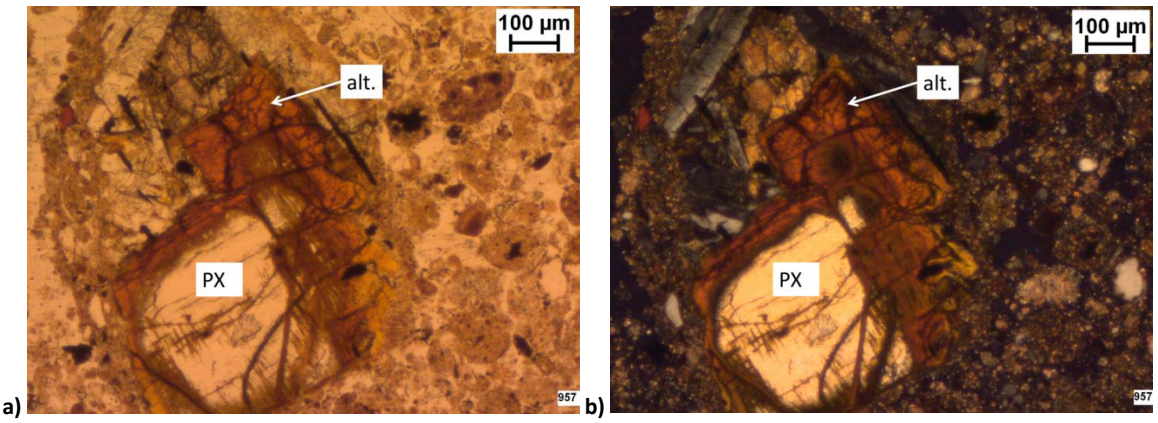

Figure 6.12: Pyroxene (PX) grain altered to an iron-rich alteromorph (alt.) in basalt from sediments adjacent to SK 8 (S1, TS 957), a) PPL and b) XPL.

6.3.4.3 Glassy groundmass in the basaltic clasts and opaque materials

A glassy groundmass was present in different proportions within the basaltic clasts of the controls and the samples (Table 18). The variations were most notable in the estimated abundance ratio of the glassy groundmass to plagioclase phenocrysts. The colours of the glassy groundmass ranged from moderate grey-green to pale grey-green and pale grey to moderate grey (Figure 6.13).

The colours of the glass's alteration products ranged from dark red to dark brown to pale yellow, the opaque forms being the most frequent alteration products (Table 18). The dark red coloured alteration product was present in samples SK 4 (SA1, TS 1009), SK 3 (S1, TS 954) and SK 5 (S1, TS 970). The anisotropic yellow-coloured crystalline alteration product was present in three sections, TS 1018 (C3), TS 958 (SK 2, S1) and TS 970 (SK 5, S1). A dark brown coloured alteration product was present in samples of SK 1, SK 2 and SK 5(SK 2, S1, TS 958; SK 5, S1, TS 970; SK 2, S1, TS 991; and SK

1, S1, TS 971) and absent in samples of SK 8, SK 3 and SK 4. Yellow and dark brown coloured alteration products were absent in samples from SK 3, 4 and 8, and in the controls. An opaque material was common in samples and controls.

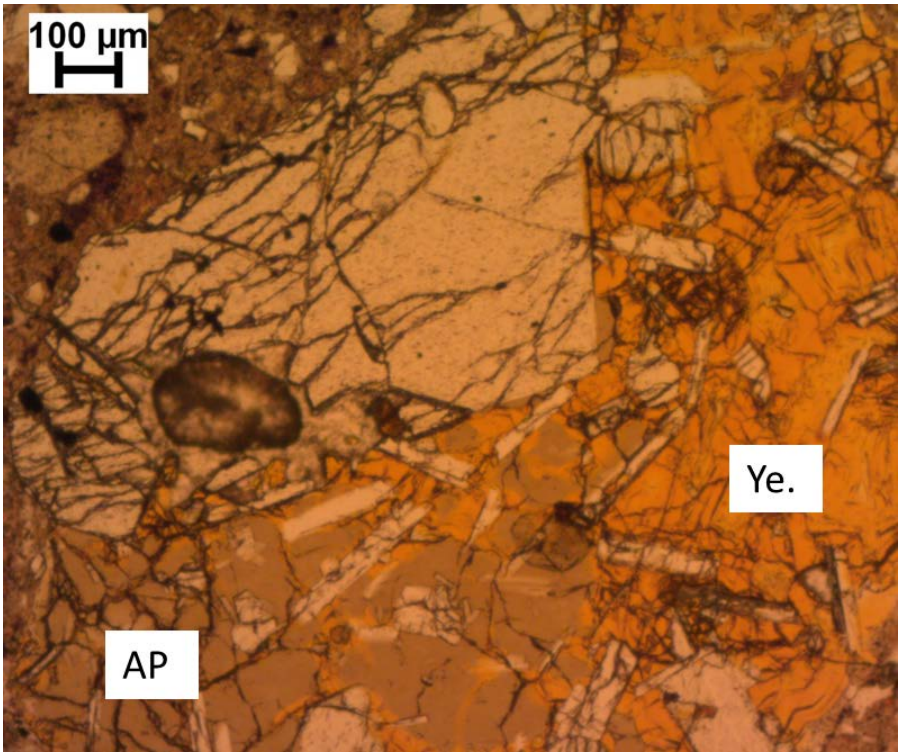

Figure 6.13: Glassy groundmass displaying grey colours and altering to a yellow coloured product in basalt from the sediments surrounding SK 1 (SK 1, S1, TS 965, PPL).

The morphology of the opaque materials within basaltic clasts contrasted between samples and controls (linear and circular and linear, respectively). These were present adjacent to feldspars within the basaltic clasts. These geological secondary products were opaque in PPL, XPL, OIL and RLDF (dark field reflected light). They frequently exhibited right-angled shapes (linear, crosses, or cubes; Figure 6.14) in the samples and controls (Table 18). In the C1 and C3 controls they also exhibited circular or spherical forms (Table 18). Although the opaque secondary mineral exhibits cubic morphology, it can be established that it is not pyrite by the lack of colour in OIL (pyrite displays bronze colours in OIL). Based on its opacity and diagonal cubic form it is tentatively identified as a member of the spinel group. The spinel group minerals share a common structure rather than sharing a common elemental formula. They are commonly oxides or hydroxides, the central O^{2-} anion according the common structure (Battey and Pring 1997, 213). The other morphologies observed (linear and crosses) could be interpreted as reflecting tightly packed linear or cubic forms, the overall cross form being due to the constraints imposed by the inter-mineral secondary pore spaces within the clasts.

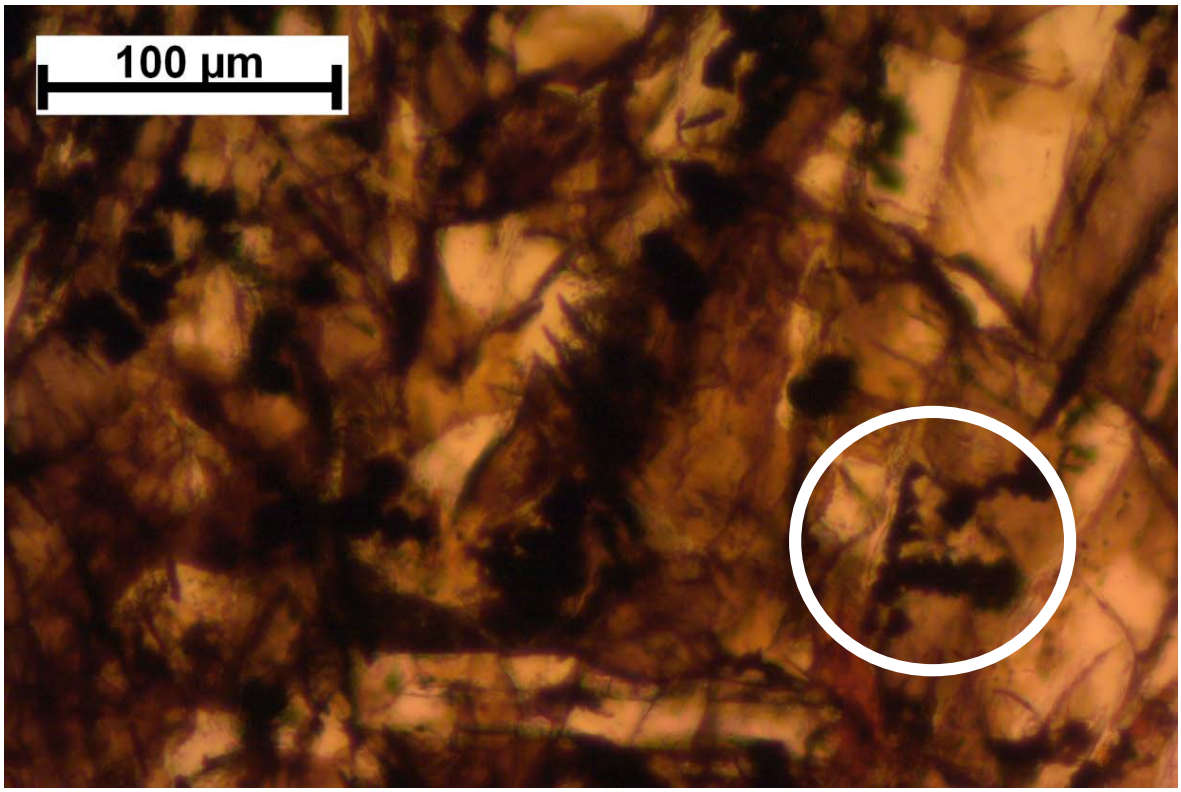

Figure 6.14: Opaque secondary products, displaying diagonal cubic morphology (circled in white) (SK 8, S1, TS 1112, PPL).

Magnetite is commonly present with some ferromagnesian silicates, including olivine (Delvigne 1998, 110 and Eggleton *et al.* 1987) and amphiboles (Mackenzie and Adams 1994, 40). An omission solid solution relationship exists between magnetite and maghemite (Battey and Pring 1997, 216). Although both magnetite and maghemite can be biotically formed (Gaines *et al.* 1997, 229), maghemite (rather than magnetite) forms in environments with a limited supply of oxygen (Skinner and Jahren 2005, 128). Based on the formation parameters of magnetite and maghemite, the opaque secondary product in these thin sections could be used as a possible indicator of past levels of aerobic/anaerobic conditions. Hence, the secondary product can be interpreted as magnetite (Fe_3O_4) based on its colour and morphology. Magnetite can be oxidized to form maghemite (gamma-Fe_2O_3), which has a diagonal cubic form. The tentatively identified maghemite in the samples which display a cubic structure is suggested to probably be an oxidation product of secondary magnetite.

Sediment biota can affect oxygen levels in sediments through their respiration (Laanbroek 1990) and the processes of mineralization and weathering (Van Breemen *et al.* 1983; Mulder *et al.* 1994). The presence of excremental pedofeatures (Figure 6.9) ascribed to bioturbation (Bullock *et al.* 1985), indicates that sediment fauna were present in the grave sediments (Section 6.3.3). However,

the current dataset from Tel Qarassa presents such a range of sediment variability that a relationship between aerobic microbial activity in the grave fill and a contrasting mineral weathering between the controls and the samples would require future research (Chapter 9).

6.3.4.4 Sediment minerals in the groundmass

Minerals in the groundmass included olivine, pyroxene and glauconite (Table 18). Moderately weathered pyroxenes and moderately to heavily weathered olivines were present in the micromass in the samples and controls. These mineral grains showed similar weathering patterns to their counterparts within the basaltic clasts. The pyroxenes and the olivines both exhibited pellicular and irregular linear weathering patterns, the former being mostly weathered to extent two or greater and the latter to extent three or greater. By contrast, the olivines in the C1 and C3 controls and SK 5 and 2 had a weathering extent of two (Table 18) though they exhibited greater extents of weathering than their counterparts within the clasts present in the same thin section. This is consistent with the lower reactive surface area of mineral grains contained within the rock fragments and encased by sodic-calcic plagioclases, which are less susceptible to weathering (according to the weatherability sequence of Goldich (1938), which is based on the magmatic reactive series of Bowen (1928)). However, evidence such as the yellow fragment of oriented clay which could be a fragment of a surface crust (Figure 6.15) suggests there may be a complex sequence of sedimentary events (Figure 6.15) and that any weathering observed may not necessarily linked to the time in the grave fill sedimentary environment.

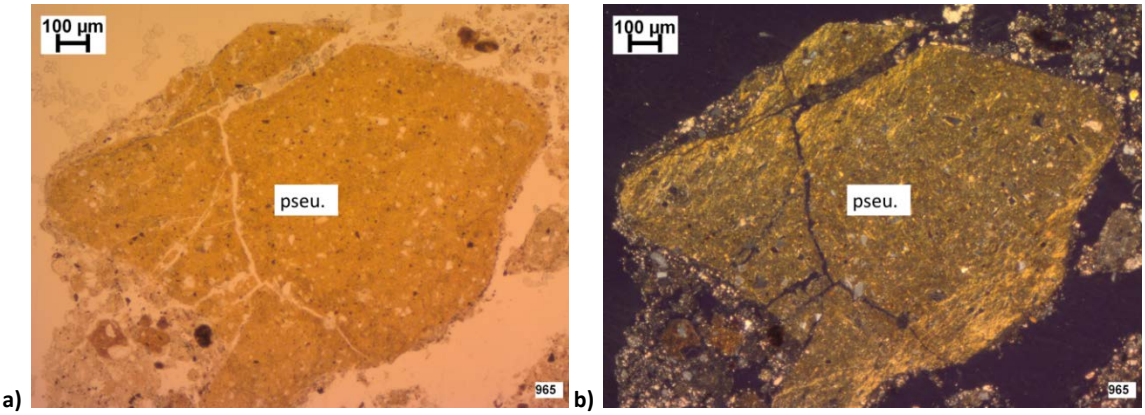

Figure 6.15: Yellow coloured material with smooth edges and fractures from sediment adjacent to a skull, possibly a fragment of orientated clay (SK 1, S1, TS 965), shown in a) PPL and b) XPL.

Minerals exhibiting pale blue to medium blue pleochroism, mid to high second-order interference colours, small dimensions (<10 µm) and poorly expressed cleavages were identified as amphiboles.

They were present in the groundmass in samples (SK 2, 3, 4, 5, and 8) but not in the C1 and C3 controls (Table 18). They were present in the groundmass in thin sections of samples containing some of the more heavily weathered pyroxenes and olivines (in the groundmass and basaltic clasts) and absent from the less weathered sediments (*e.g.*, C3, C1 and SK 2) (Table 18). The distribution of amphiboles is interpreted as evidence of the variability in the burial sediments rather than authigenic formation through accelerated weathering of the primary minerals.

A mineral grain in one thin section (SK 4, SA1, TS 961) was identified as glauconite (Figure 6.16) by its characteristic green and yellow speckled colours (PPL) and interference colours (XPL) (Mackenzie and Adams 1994, 128) along with a rounded (term after Wentworth 1919) form. Glauconite (Section 5.4.3) is commonly found in sediments of marine origin and is formed from the tests of foraminifera (Odin and Matter 1981). Glauconite has been shown to undergo weathering in sediments, notably *via* substitution of the Fe cations (Johnston and Cardile 1987), mainly by Al to produce Al-glauconite and eventually illite (Ireland *et al.* 1983). Based on correlations between light microscopy observations and Mössbauer spectral analyses, Fanning *et al.* (1989b) argued that the colours (PPL) of glauconite in thin section can indicate the oxidation state of the Fe component. According to Fanning *et al.* (1989b) the yellow-green colour, as observed in TS 961 (SK 4, SA1), is characteristic of more oxidized conditions and blue-green colours of more reducing conditions.

a)

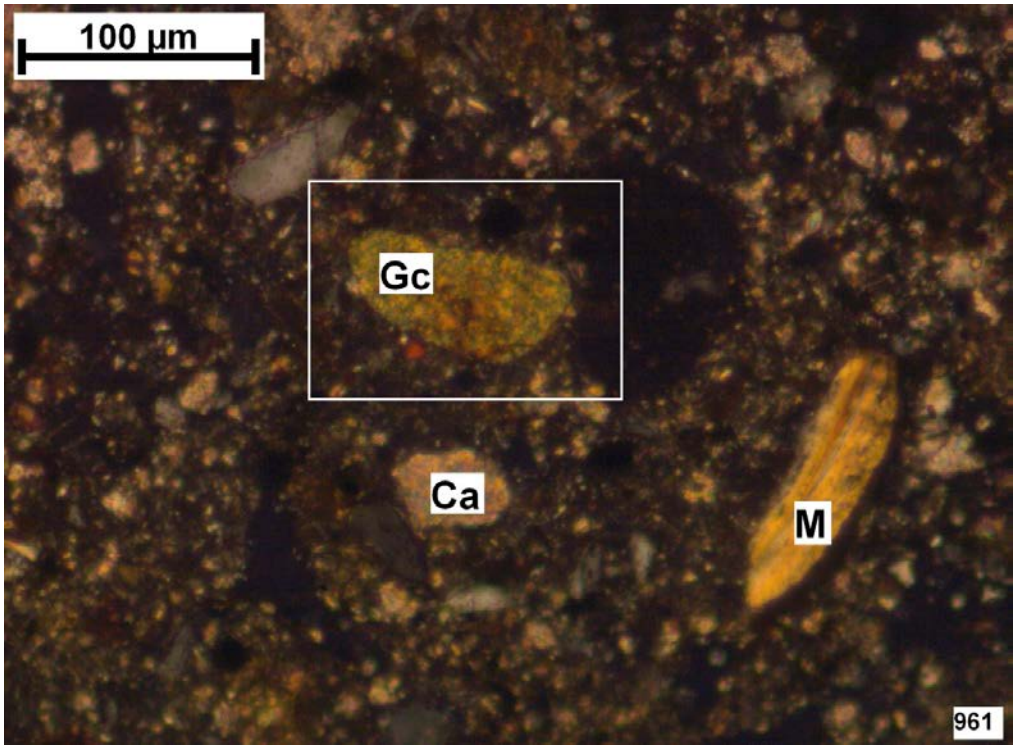

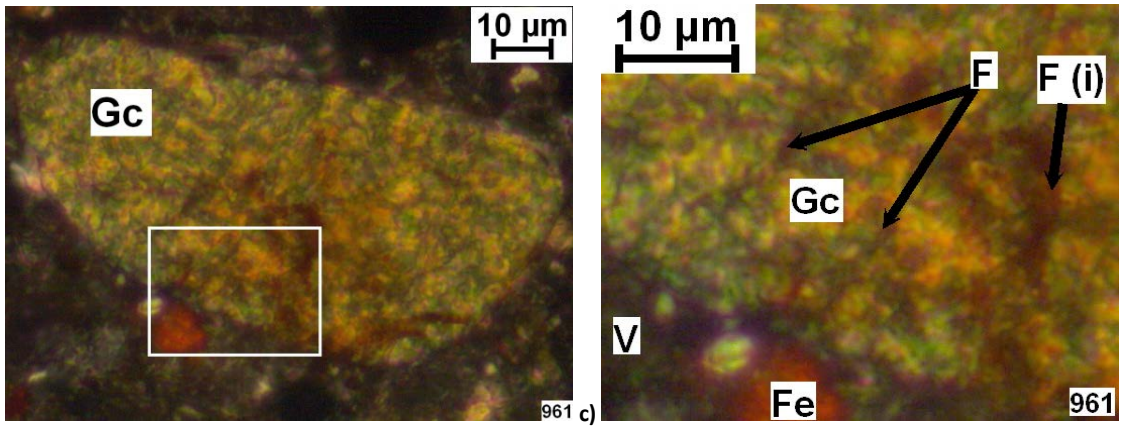

Figure 6.16: Glauconite. (a) Glauconite (Gc) in groundmass adjacent to carbonate- rich material (Ca) and yellow micaceous material (M) (SK 4, SA1, TS 961, XPL). (b) Detail of inset from image a). (c) detail of inset from image b), at the edge of the glauconite (Gc) near the void (V) and iron-rich material (Fe), showing weathering fractures (F), some of which have been infilled (F(i)). The 'up' direction (i.e. the direction of the ground surface) is at the top of the photomicrographs.

The slide TS 961 represented the only sediment from within a skull (SK 4, A1) at this site. For this reason, a duplicate thin section was made from the same sample block and cut at the same angle (TS 1009). Glauconite was absent in TS 1009 suggesting a low frequency within the intra-cranial sediment of SK 4. There are three main interpretations for the presence of glauconite in SK 4 (TS 961, SA1): authigenic formation, localised preservation due to unique pedogenic processes, or that it is a marker of an allogenic deposit which was brought into the burial area. Due to the low frequency of observations of glauconite from these burial sediments, further sampling would be required before such an interpretation of events could be reasonably asserted with a greater degree of confidence.

The evidence from the micromorphological analysis at Tel Qarassa does not support an authigenic formation for the glauconite in SK 4. Glauconite has been formed in sediments from solutions at near surface conditions, slightly alkaline pH and redoximorphic conditions (Velde and Odin 1975, Harder 1980). Hence, if glauconite had formed from solution as a secondary mineral it would be expected to be in the clay fraction and more abundant in the other sediments from the burial cache that display a greater abundance of pedofeatures attributed to redoximorphic conditions (*e.g.* iron nodules and/or micro-laminated nodules Bullock *et al.* 1985) (*i.e.* SK 1, S1; SK 2, S1). The evidence of weathering of the glauconite in TS 961 includes fractures, infillings, and an iron-rich accumulation at the lower boundary (Figure 6.16b and c). Glauconite is known to weather to clays *via* Al for Fe substitution leading to the production of illite (Thompson and Hower 1975, Johnston and Cardile 1987). Such a pattern of weathering is evidenced by the high levels of clay minerals in a sediment, though determination if it is of illite composition would require XRD analysis. The evidence that the glauconite grain observed in SK 4 (SA1, TS 961) was neither small (*c.* 100 µm) nor situated in the sediment groundmass adjacent to a large void or excremental pedofeature (Figure 6.16) does not

support an interpretation attributable as a remnant from a faecal pellet from earthworm activity either in its cast (Canti 1998, Canti and Piearce 2003) or in its in calcite crystals (Gago-Duport *et al.* 2008). If the crania of SK 4 had previously been deposited in a different sediment before its deposition in the skull cache in House 3 (Figure 6.5) it could have remnant glauconite that had remained semi-stable throughout its secondary deposit (*i.e.* burial zone EF101, House 3). The presence of glauconite in TS 961 is interpreted as evidence to suggest that either this is an indicator of an area with less intensive weathering to clays or an allogenic remnant from the primary deposit of this skull in a different sediment. Using this interpretation to consider a wider understanding of the burial it could be questioned as to which deposit this glauconite was transported from, as none of the controls from the site (C1, C3 or C3b) recorded glauconite in their thin sections. The archaeological implication of a previous burial of the remains of SK 4 is discussed in Section 5.4.

6.3.5 Basalt clasts and coatings

No Fe- or CO_3-rich coatings were observed on the basaltic rock fragments in the micromorphology samples of sediment adjacent to SK 8 or 3. By contrast the thin sections from the other samples (SK 5, 2, and 1) and from the grave fill control (C3) all contained Fe- or CO_3-rich coatings on the basalt clasts. The Control C3 (TS 1113 and 1018) contained both CO_3-rich and Fe-rich coatings, the former being the thickest and surrounding the Fe-rich coating (Table 18; Figure 6.17). In micromorphological studies, Fe-or CO_3-rich coatings on objects can infer impacts of past precipitation events from a previously saturated sediment solution. The presence of the coatings is interpreted to suggest a change from an acidic to a more alkaline sediment environment over time. Iron-rich coatings were present on some of the basaltic rock fragments in samples from SK 1, and as cappings in SK 5 and 2. The lack of disturbance of the cappings in SK 5 and 2 indicates that they formed post-burial. The type and sequence of coatings in the Control C3 and in the sample from SK 2 provide evidence of similar and long term conditions within the sediment environment, whereas those of the samples from SK 1 and 4 reflect a late stage precipitation event from a previously mobile carbonate-saturated sediment solution. The coatings form barriers between the objects they cover and the sediment and could inhibit further weathering. Inhibition may arise not only by the reduction of the surface area exposed to a dynamic, possibly aerobic, environment (closed system versus an open system), but also by creating a physical barrier to microbes.

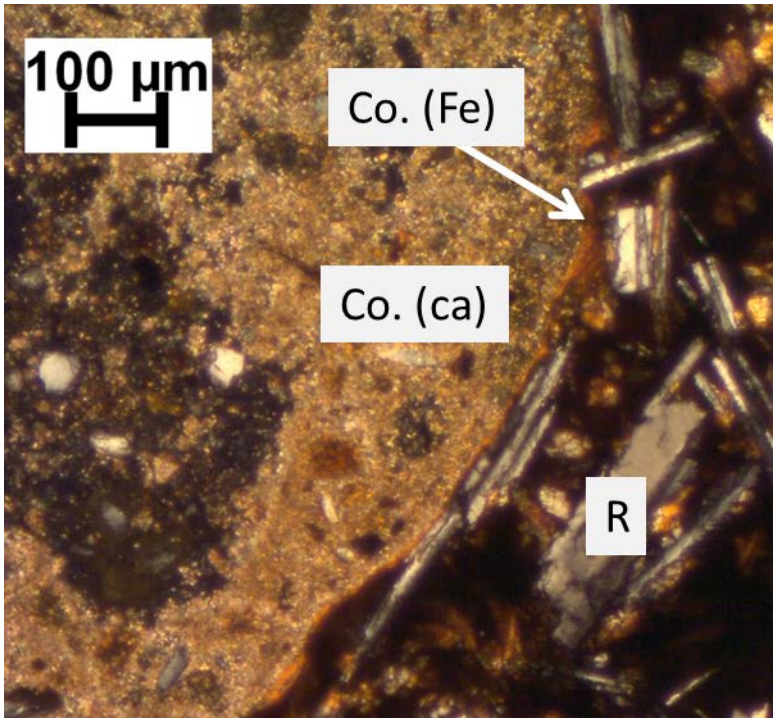

Figure 6.17: Basaltic clast (R) from a control sediment showing a thin iron-rich hypocoating (Co. (Fe)) followed by a thick carbonate-rich coating (Co. (ca)) (C3, TS 1113, XPL).

6.3.6 Summary of weathering and alteration processes

While weathering processes were prevalent, the rates and products of weathering differed between the controls and the samples and between samples. The extent of weathering in most sediments generally increases up a sediment profile, suggesting that the minerals in thin section from the uppermost layers of the Tell C1 control) would be more weathered than those from lower deposits (samples). However, the mineral weathering extents from controls and samples suggest that mineral weathering has progressed in both samples and controls. The trend in the weatherability of minerals in the Tel Qarassa samples and controls basaltic rock fragments is interpreted as olivine, pyroxene, to albite twinned plagioclases and is supported by the literature of mineral weatherability (Section 6.1). The weatherability sequence of minerals (Goldich 1938) reflects minerals that crystallized under the most extreme conditions (as identified by Bowen 1928) being the least stable in surface or near surface sediment conditions.

Opaque alteration products from phenocrysts were separated into two classes based on their morphologies; circular and linear in the controls and cubic and linear in the samples. The evidence of the presence of these two forms is interpreted as suggesting that the tentatively identified magnetite was present in the controls and maghemite had formed in the samples. Samples had a wider range of alteration products that did not reflect the typical weathering patterns of basaltic sediments. In addition to contrasts of the controls compared to the samples, there were also

differences observed in comparisons of the samples from different skulls, discussed further in Section 6.4.

6.4 Discussion: micromorphological observations and archaeological questions

6.4.1 Controls and samples

All three controls (C1, C3, and C3b) appeared to be constituted of similar sediments but with the site control (C1, TS 959) slightly less affected by weathering processes than the burial controls (C3, TS 1113 and TS 1018; C3b, TS 1239).

Some slight variation in micromorphological observations were observed in the controls (Table 17). This is attributed to the three controls (C1, C3 and C3b) having been from three different deposits (west profile of the Tell, later fill within intra-burial zone, and grave fill contemporary to the burial deposit, respectively). All three controls contained bone fragments and charred plant remains. The micromorphological evidence supports the field-based interpretation that the sediments exposed in the tell profile (*i.e.* C1) were largely composed of archaeological deposits formed by later activities on site (Balbo *et al.* 2010).

The C3b control (TS 959) had more in common with the samples than with the C3 control (TS 1113 and 1018). Although similarities between the two grave fill controls (C3 and C3b) could be seen, they were both observed to have been composed of similar types of sediment (fine grained sediment with few small basaltic clasts) which had been affected by bioturbation, and supporting the interpretation of the excavation report (Balbo *et al.* 2010) that the sediments that the C3b was sampled from were deposited during the burial and those of the C3 were not (Section 6.2).

Although both controls and samples were of similar types of sediment and affected by bioturbation there were distinct differences in the alterations of the minerals of these two groups of samples. Such differences included the different morphologies of the opaque materials within the basaltic clasts in the controls and samples, and are interpreted as evidence suggesting the sediment heterogeneity and variability within sediments at the Tell (Section 6.3).

6.4.2 Samples

The thin sections of samples from SK 1, 2, and 5 exhibited differences in the colours of their mineral weathering products compared to those in samples from SK 4 (SA1, TS 1009) and SK 3 (S1, TS 954).

The differences in colours are interpreted as evidence to suggest that different sediment processes affected the two distinct areas of the burial cache (skull group A and skull group B, Section 6.2.1).

The sample from SK 4 was described by the sampler as an intra-cranial sediment (Balbo *et al.* 2010). However, a complete cranium does not usually fill with sediment (Brothwell pers. comm.) and it is unknown at what stage this skull fragmented and sediment filled it. The movement of skeletal remains from a primary depositional area to a new site has been discussed in Neolithic archaeology. The presence of glauconite in the sediments from within the crania of SK 4 could be used to interpret the area of primary deposition of SK 4 as from an area outside Tel Qarassa zone 2, where glauconite sediments could be formed and found as sediments of an aqueous origin, perhaps closer to the edges of the documented paleo-lake (Section 6.1). Such an interpretation of past events is supported by the conclusions of Santana *et al.* (2012), that these skulls were brought to this cache (area EF101) as a secondary deposit, after they had first been deposited in a primary context long enough for some level of skeletonisation to have occurred. The archaeological report based on the osteological analysis from these skulls (Santana *et al.* 2012) makes a strong argument for the skulls of this cache to have been from the post-cranial (*i.e.* the parts of the skeleton below the head) skeletal remains excavated in zone 1 from the site. Based on the combination of the conclusions of Santana *et al.* (2012) and the evidence of glauconite in samples from near SK 4 (Section 6.3.4.4), future work including XRD analysis on the post-cranial burial sediments is recommended. The sediments adjacent to the post-cranial remains from zone 1 should be examined as to whether any glauconitic remnants (or other minerals of marine origin) could be identified.

6.5 Conclusion

The controls from Tel Qarassa (C1, C3, and C3b) differed from the samples (S1 and SA1). Differences in alteration of the rock fragments and minerals in these two groups of sediments are attributed to the heterogeneity of Tell sediment and not to the presence of the inhumed human remains and related post-depositional decomposition processes. In the sediments at Tel Qarassa, the weathering of basaltic clasts and their associated mineralogical assemblage was slightly more extensive in the samples than the controls, morphologically apparent *via* different pathways of alteration. The variation in alteration is reflected in differences in the shapes of the opaque minerals in the basaltic clasts (Section 6.3.4.3 and Chapter 9).

Reburial, especially of crania, is a known practice in archaeological burials of the Near East in the PPNB (Santana *et al.* 2015). Reburial of skeletal remains after skeletonisation was a frequent method of burial practice in this region at this time and skulls were often separated from the rest

of the skeleton (Santana *et al.* 2012 and 2015). The micromorphological analysis of the sediments from the skull cache in Tel Qarassa supports the interpretation as a secondary burial by the excavating team (Santana *et al.* 2012) and suggests that the lack of discernible patterns differentiating the control sediments from the samples could reflect the heterogeneity of Tell sediments in a small area. Previous micromorphological analyses of domestic deposits at the Tell site of Saar have shown differences in sediments when sampled systematically using a grid system at one to two metre intervals. The use of the InterArChive sampling strategy to investigate trace evidence in the burial sediments is perhaps not suited to the complex history of sediments of a secondary burial in a Tell.

Chapter 7. Case study: Sala Vastmaal, Sweden

7.1 Introduction

The archaeological site of Sala Vastmaal (site code RAA51) was a graveyard to the SW of the town of Sala (Västmanland), Sweden. The graveyard is on the edge of Quaternary deposited silts to the east (Appendix VI for 1:50,000 quaternary deposits map) and the ores which made the region famous for its silver mines to the west. Galena (lead sulphide), the predominant lead ore in the area, is sometimes associated with silver deposits (Geijer 1958; Amcoff 1984). In terms of sediment geochemistry, sulphur can be significant in terms in relation to sulphate-reducing bacteria (Coleman *et al.* 1993). Lead is relatively immobile within sediments and is toxic to many organisms (Goyer 1993). Southern Sweden, including Sala Vastmaal, has a high annual rainfall and temperate climate (average -3/+15C) (WMO). A NW/SE flowing stream ran across the NW corner of the graveyard and may have seasonally fluctuated and affected the hydrology of the site.

The graves were sampled by the InterArChive project team in 2011 within a Swedish excavation (SAU) led by Ylva Bäckström (Bäckström and Sundström 2010). The graves were aligned E-W within the southern boundaries of the contemporary churchyard, and dated from the 16th century (Carbon-14 dates, Bäckström and Sundström 2010, 24). Micromorphology samples and controls were collected according to the InterArChive sampling protocol (Chapter 2), grave numbers being prefixed with GR, and are referenced by their sample number and control number throughout this chapter. A pit was dug to sample across various sedimentary layers for the sampling of multiple site controls (C1 controls). Three C1 controls (C1A, C1B, and C1C) were collected, which correlated to surrounding sediment sequences of finely laminated deposits (Figure 7.1).

Figure 7.1: The C1 control profile with Kubiena tins in place for micromorphology sampling (C1A, C1B, and C1C).

7.2 Materials and methods

7.2.1 Excavation and sampling

Burial sediments were sampled from inhumations of three male adults, two females in their teens, and one infant (Tables 19 and 20). Except for GR 5926, all of the sampled graves had coffins, in some cases with fairly well preserved wooden remains still visible. The skeletons were in varying degrees of preservation and most appeared to have been prone, complete and articulated at the time of burial. Despite the protocol's (Chapter 3) stipulation of 2 controls per grave, only one intra-grave control was collected per grave because of the advanced stage of excavation by the time that the InterArChive project team arrived. One of the six graves, uncoffined GR 5926, had the skull missing and an orange metal collar was present at the top of the cervical vertebrae. The type of metal of the collar is unknown. However, if iron, the colour could be indicative of ferrihydrite or schwertmannite, suggesting exposure to acidic groundwaters, as reported in other mining sediments rich in sulphur (Bigham *et al.* 1996, Regenspurg *et al.* 2004, Zhu *et al.* 2016).

Table 19: Micromorphology controls (a) and samples (b).

a)

Grave	Control	Thin section number
n/a	C1A	874
n/a	C1B	975
n/a	C1C	976
5914	C3	887, 861
5926	C3	993
7464	C3	991
7519	C3	875
7555	C2	992

b)

Grave	Sample	Thin section number
5914	1	867, 995
	2	997, 996
	4	936, 907
	A2	906, 919
5926	2	877, 862
	4	920, 978
7464	1	935, 982
	4	876, 918, 981
	A1	921, 984, 994
7491	4	979, 968
	9	969, 977
7519	1	873, 888, 889
	13	908, 938, 917
	4z	985, 983
7555	1	872, 882, 881
	2	821, 860
	3x	905, 937, 980

Table 20: Orientations of thin sections relative to skeletal remains in S1, S2 and S3 samples. Grey cells indicate no data.

	Sample and orientation	S 1 t	S 1 p	S 2 t	S 2 p	S 3 t	S 3 p
Grave	5926			877	862	978	978
	5914	867	867	996	997	936	907
	7555	882	872	821	860	905	980
	7519	888	873	908	938	983	
	7464	982	935			981	876
	7491			977	969	968	979

Micromorphology samples were collected from near the skull, pelvis, or feet regions and additional areas in the graves (Figure 7.2). The C3 control from GR 5914 was collected from the fill directly above the pelvis close to sample S2 from this grave (GR 5914). Two samples (S2 and SA1) from another grave (GR 7464) were also collected adjacent to each other. The additional sample (GR 7464, SA1) was collected from the sediment surrounding the coffin base adjacent to the left femur of the skeleton.

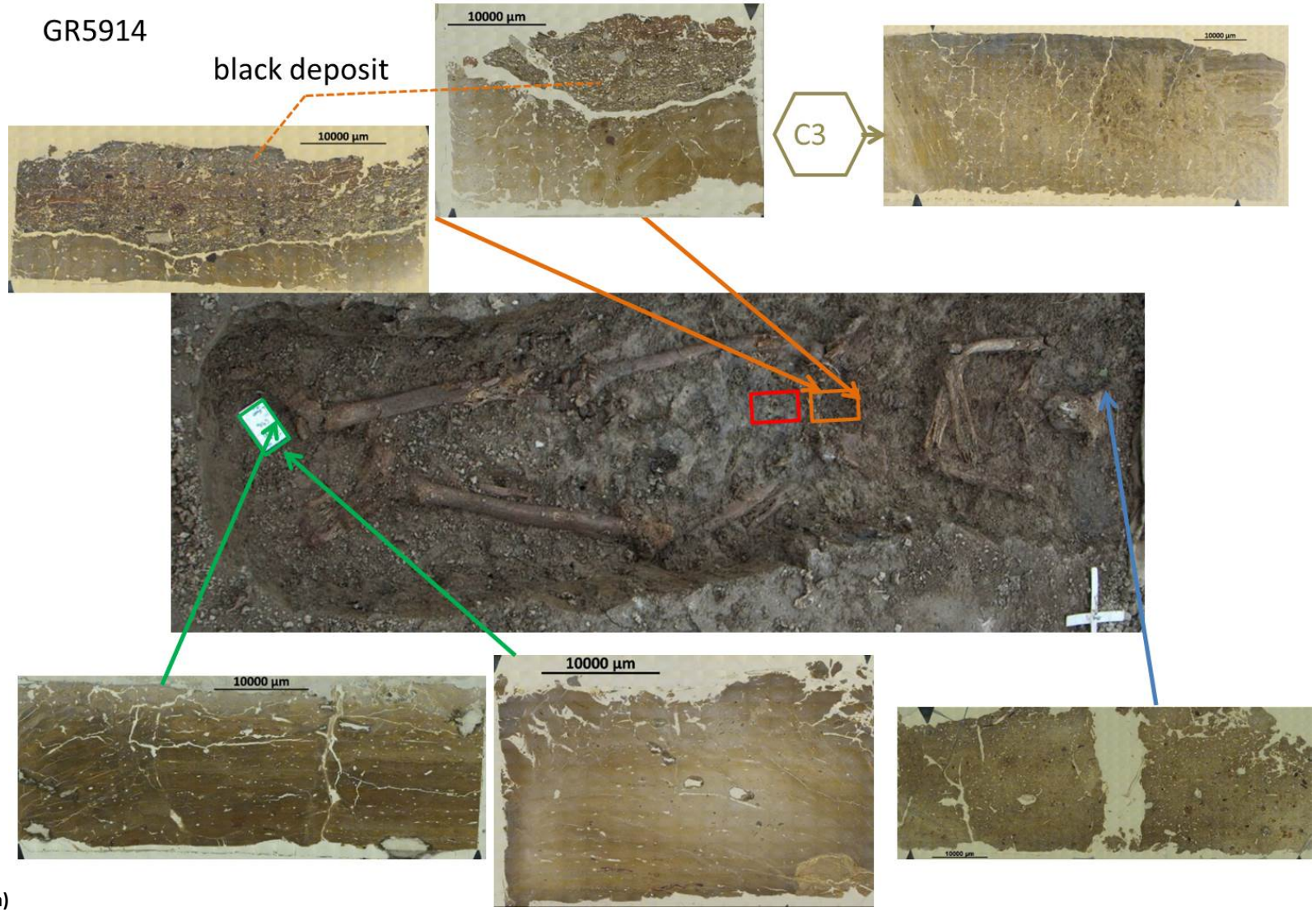
GR5914
black deposit
10000 µm
10000 µm
C3
10000 µm
10000 µm
10000 µm
10000 µm

a)

GR5926

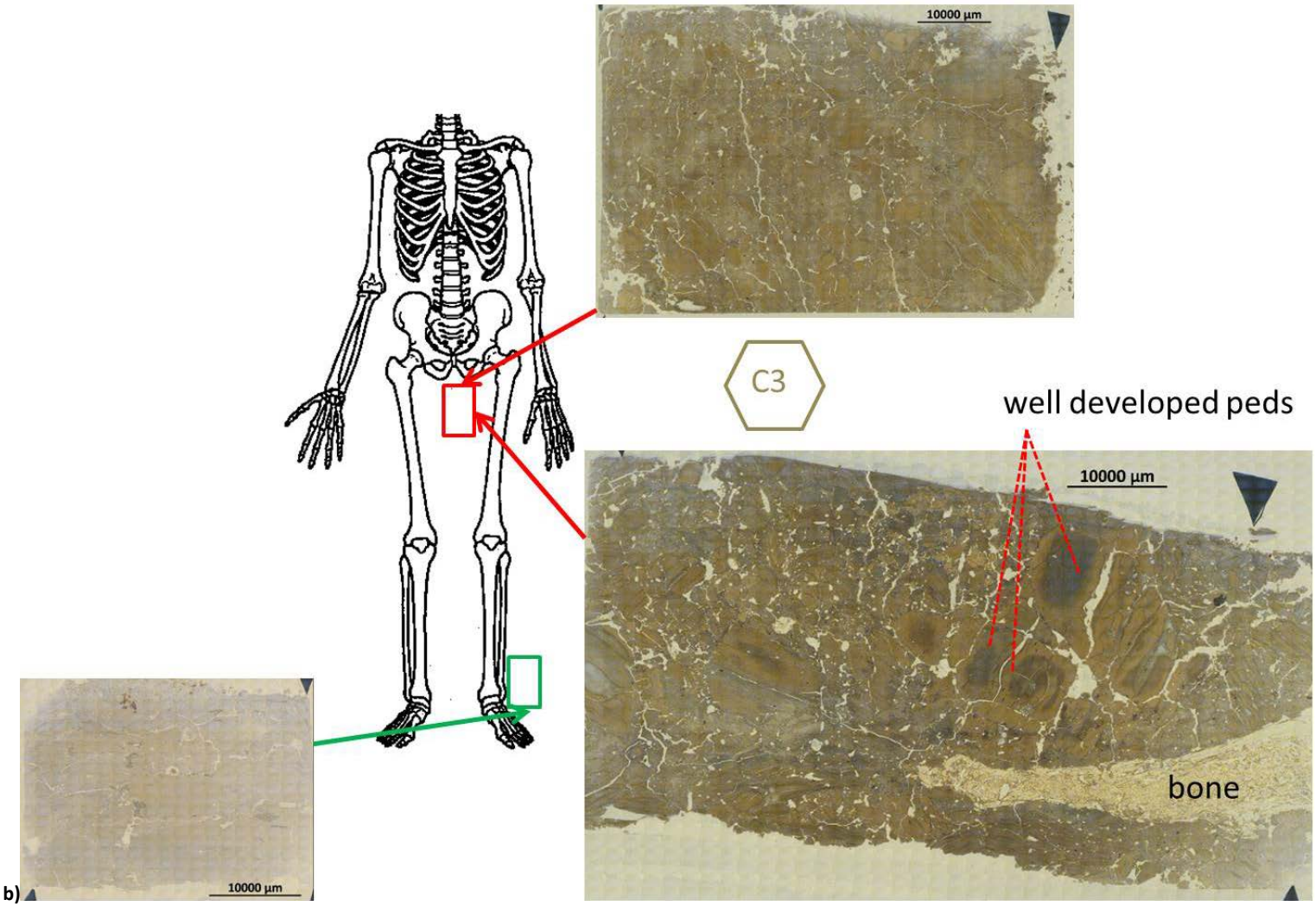

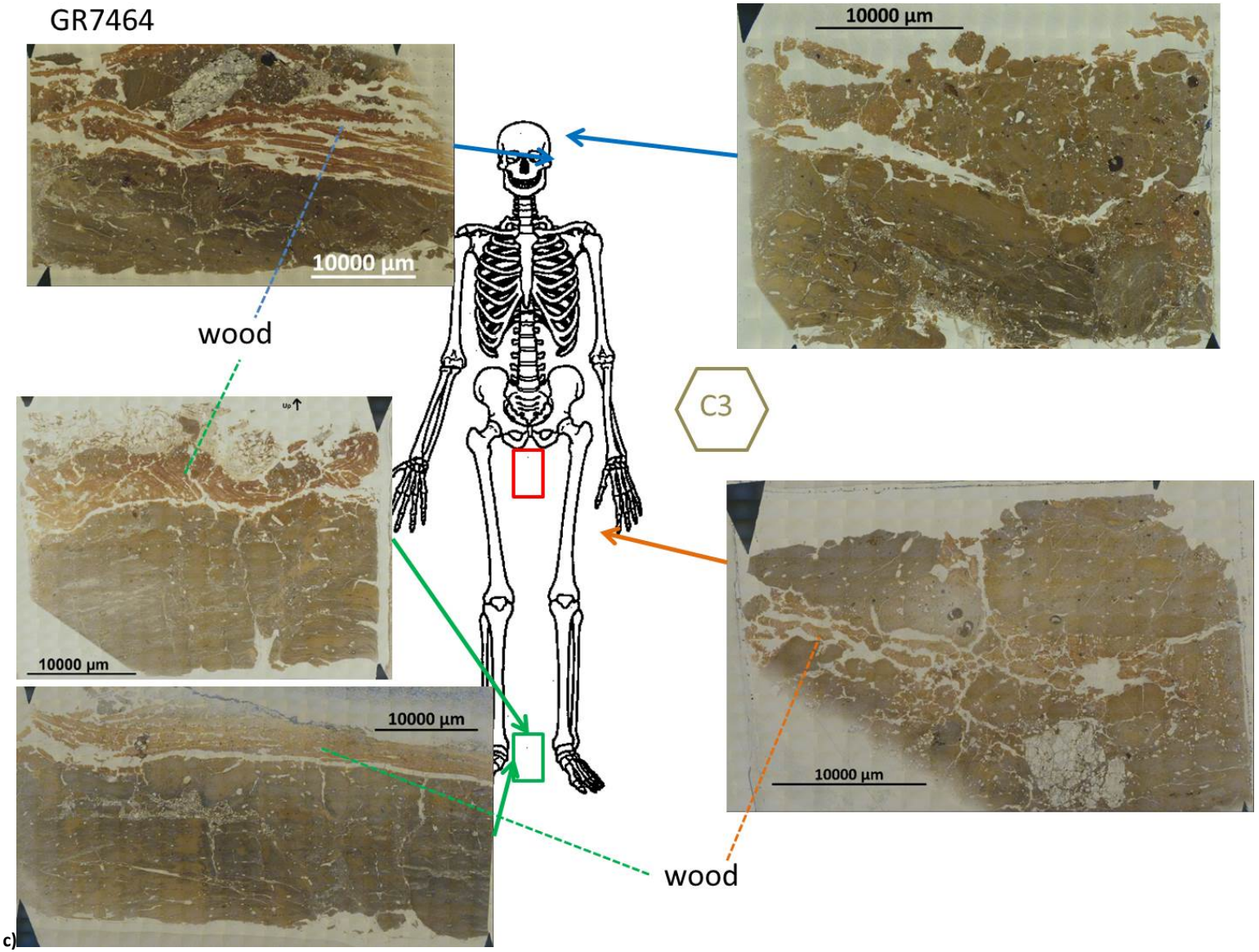
GR7464
10000 µm
wood
10000 µm
C3
10000 µm
10000 µm
10000 µm
wood

c)

GR7519

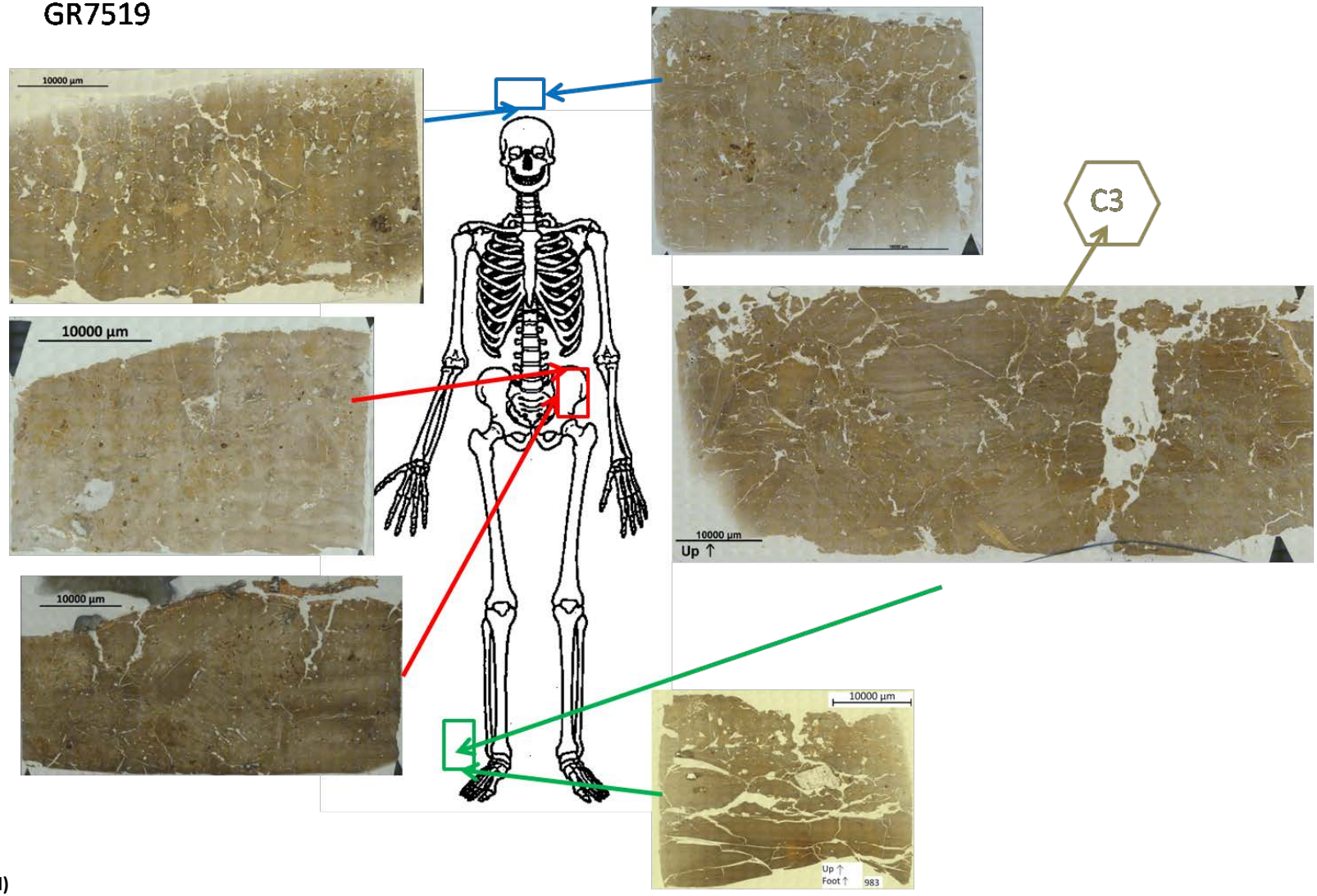

d)

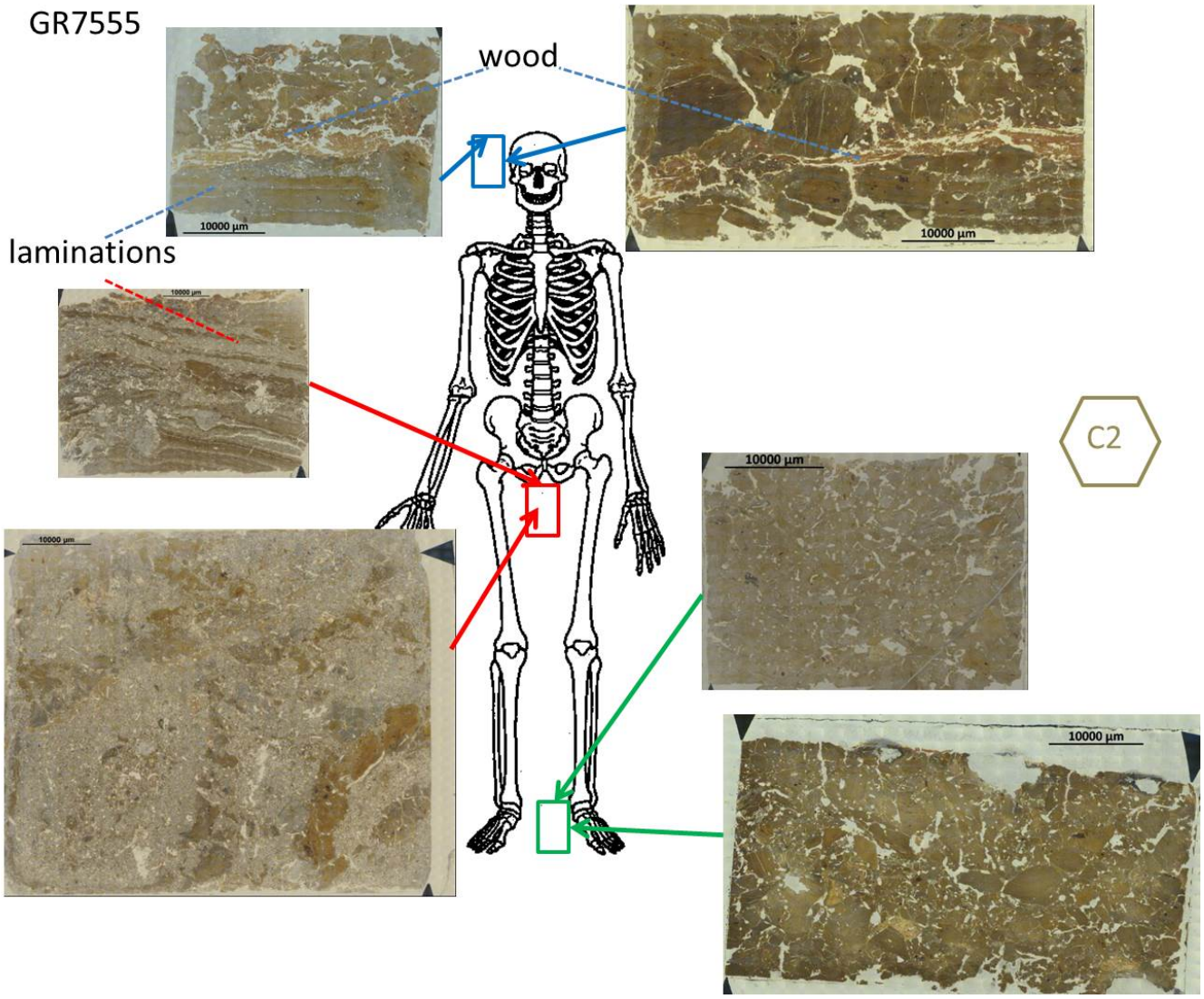
GR7555
wood
laminations
10000 µm
10000 µm
10000 µm
10000 µm
10000 µm
C2

e)

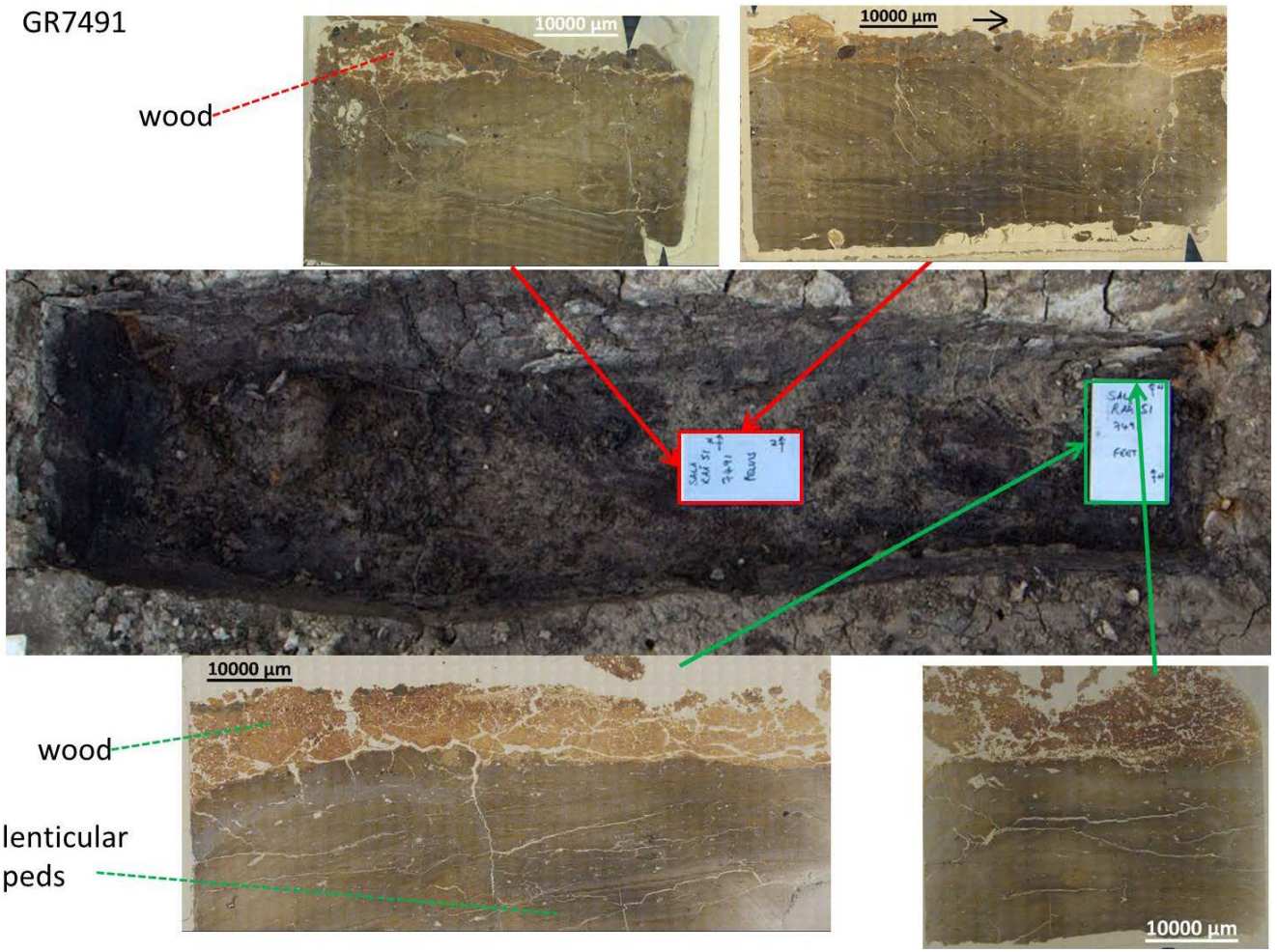

f)

Figure 7.2: Diagrams of thin section distribution throughout the six graves sampled at Sala Vastmaal. Where samples were taken the locations are illustrated in different colours according to sampling position number: sample (S)1 positions are shown in blue, S2 positions are shown in red, S3 and 4 positions are shown in green, and additional samples are shown in orange. a) Grave (GR) 5914. b) GR 5926. c) GR 7464. d) GR 7519. e) GR 7555. f) GR 7491.

7.2.2 Field observations

On excavating the pelvis for GR 7555 a strong smell of faecal material was noted during sampling by the member of the InterArChive team responsible for sampling, despite no apparent macroscopic differences between this sediment and that surrounding it. An unidentifiable black material was present between the femurs in GR 5926, as well as red material which could have been derived from textile (Appendix VI). The skull in GR 7464 was heavily fragmented (Figure 7.3).

Figure 7.3: Photograph of the crushed skull (lower half of photograph) within GR 7464, with sampling location of Kubiena tin (S1, GR 7464) represented by the white rectangle.

7.3 Thin section analysis

Micromorphology samples were processed, observed and described as detailed in Chapter 3. The micro-units are referred to by grave number (GR), sample position (S), thin section number (TS), and then micro-unit (µ-u) (Chapter 1). The material of Controls C1A, C1B, and from the top half of Sample C1C, contained finely laminated orange-brown sediments which continued laterally across the site (Figure 7.4a). The grave fills were lower in elevation than the finely laminated sediments and were at a stratigraphic level equal to the sediment in the lower half of the C1C control (Figure 7.4b).

a)

b)

Figure 7.4: Controls. a) Kubiena tin for C1C *in situ* at the base of Profile C1. b) Kubiena tin for C2 *in situ* within a grave, the finely laminated deposits are near the surface and the more homogenous deposit of the graves are visible at the right of the photograph.

7.3.1 Summary of micromorphological observations

The detailed thin section descriptions (Appendix VI) have been summarized in Table 21 and a summary interpretation of the deposits is given in Appendix VI. Most of the thin sections had multiple micro-units. Separate micro-units were identified in thin sections were there were

multiple sediments visible with different micromorphological characteristics (Chapter 3). The sediments in thin section had a range of coarse/fine related distributions (single population, embedded, or intergrain aggregate; terminology after Courty *et al.* 1989) and silicate minerals (tectosilicates, inosilicates or phyllosilicates; Table 21). The relative proportions of coarse to fine material were lower in the C1 controls compared to the C2 and C3 controls and the samples (Table 21). Fungal and bone remains were present in some of the samples but absent from the C1 controls (Table 21). The types of voids most common in the C1 controls were vesicles and cracks (Table 21). Vesicle shaped voids were less common in the samples than channel, chamber, vugh and crack shaped voids (Table 21).

Table 21: Summary of micromorphological observations

TS	GR	S	TS orient-ation	µ-unit	Colour (PPL)	C/F	Related distribution	Voids					Inorganics				Organics				Pedality
								ve	ch	cb	vu	cr	Silicate minerals			Other	AMO	Plant remains	Fungal remains	Bone	
													T	I	P						
874	n/a	C1A	n/a	1 of 3	grey-brown	2, 98	single population	*	*	*	*	**	_	/	/	/	/	/	/	/	apedal
874	n/a	C1A	n/a	2 of 3	brown-orange	2, 98	single population	*	**	*	_	**	/	/	/	/	/	_	/	/	apedal
874	n/a	C1A	n/a	3 of 3	brown-grey	2, 98	single population	*	/	_	/	*	/	/	/	/	/	/	/	/	apedal
976	n/a	C1C	n/a	1 of 2	grey-brown	2, 98	single population	*	*	/	/	*	/	/	/	/	/	/	/	/	apedal
976	n/a	C1C	n/a	2 of 2	grey-brown	10, 90	embedded	/	*	/	_	*	***	/	/	/	/	/	/	/	apedal
861	5914	C3	n/a	1 of 2	orange-grey	5, 95	single population	*	/	/	**	***	*	/	/	/	/	/	/	/	platy
861	5914	C3	n/a	2 of 2	yellow-grey	10, 90	embedded	*	**	**	_	*	**	/	/	/	/	_	/	/	sub-angular-blocky
995	5914	1	t	1 of 1	grey-brown	30, 70	embedded	/	**	**	**	_	*	/	**	**	_	***	/	**	apedal
867	5914	1	p	1 of 1	brown-grey	50, 50	embedded	/	**	**	*	****	**	_	*	*	*	**	**	/	apedal
997	5914	2	p	1 of 2	grey-brown	25, 75	embedded	/	*	**	*	_	***	**	_	/	_	***	*	/	apedal
997	5914	2	p	2 of 2	yellow-grey	5, 95	embedded	**	_	/	*	**	_	/	_	/	/	*	/	/	apedal
936	5914	3 & 4	t	1 of 1	orange-brown	5, 95	single population	**	*	*	*	**	*	/	/	/	/	_	/	/	sub-angular-blocky
907	5914	3 & 4	p	1 of 1	grey-orange	5, 95	single population	**	_	*	*	***	*	/	/	/	/	_	/	/	sub-angular-blocky
919	5914	A2	n/a	1 of 2	grey-brown	40, 60	embedded	/	*	**	***	**	**	*	*	**	**	***	*	/	apedal
919	5914	A2	n/a	2 of 2	grey-orange	5, 95	embedded	*	/	**	*	**	**	/	/	/	/	_	/	/	sub-angular-blocky
877	5926	2	t	1 of 1	grey-orange	20, 80	embedded	_	/	_	**	***	***	_	/	/	*	/	/	/	sub-angular-blocky
862	5926	2	p	1 of 1	orange-brown	20, 80	embedded	*	/	*	*	***	***	/	/	/	/	*	/	***	sub-angular-blocky
996	5926	2	p	1 of 2	grey-brown	30, 70	embedded	_	_	*	**	/	**	/	/	/	/	***	/	_	apedal
996	5926	2	p	2 of 2	yellow-brown	2, 98	single population	_	/	/	*	*	_	/	/	/	/	_	/	/	sub-angular-blocky
978	5926	4	p	1 of 3	yellow-brown	15, 85	embedded	/	_	_	*	**	**	*	_	/	/	*	/	/	apedal
978	5926	4	p	2 of 3	brown-grey	20, 80	intergrain aggregate	/	/	/	/	/	******	/	/	/	/	/	/	/	apedal
978	5926	4	p	3 of 3	yellow-brown	10, 90	single population	*	_	*	*	***	**	/	/	/	/	_	/	/	sub-angular-blocky

982	7464	1	t	1 of 3	grey-orange	10, 90	embedded	*	/	*	/	**	*	/	/	/	/	/	/	sub-angular-blocky
982	7464	1	t	2 of 3	brown-grey	40, 60	embedded	/	**	**	/	/	*****	*	**	***	*	**	*	/	apedal
982	7464	1	t	3 of 3	orange	80, 20	intergrain aggregate	/	***	**	/	****	*	/	/	/	****	******	***	/	n/a
935	7464	1	p	1 of 2	grey-orange	10, 90	embedded	_	/	/	/	**	*	/	/	/	/	/	/	/	sub-angular-blocky
935	7464	1	p	2 of 2	orange-grey	40, 60	embedded	*	*	**	*	/	*****	**	**	*	**	**	**	/	apedal
876	7464	4	t	1 of 2	grey-brown	70, 30	intergrain aggregate	_	**	_	**	*	**	/	*	/	***	*****	*	****	sub-angular-blocky
876	7464	4	t	2 of 2	grey-orange	25, 75	embedded	_	*	**	*	***	***	/	*	/	/	/	/	/	sub-angular-blocky
981	7464	4	p	1 of 3	brown-orange	50, 50	embedded	_	**	**	***	***	**	*	*	/	***	*****	*	***	apedal
981	7464	4	p	2 of 3	brown-orange	15, 85	embedded	*	/	_	/	***	**	/	/	/	/	/	/	/	sub-angular-blocky
981	7464	4	p	3 of 3	grey-orange	35, 65	intergrain aggregate	**	/	/	*	/	****	*	*	_	/	_	/	/	apedal
984	7464	A1	n/a	1 of 4	orange	35, 65	embedded	/	/	/	/	/	*	/	/	/	****	***	/	/	granular
984	7464	A1	n/a	2 of 4	yellow-brown	20, 80	embedded	**	*	*	_	**	*	*	*	*	**	**	***	/	sub-angular-blocky
984	7464	A1	n/a	3 of 4	grey-orange	5, 95	embedded	*	/	_	/	***	*	/	/	/	/	/	/	/	sub-angular-blocky
984	7464	A1	n/a	4 of 4	grey-brown	45, 55	intergrain aggregate	/	/	/	**	*	***	*	**	****	/	/	/	/	apedal
968	7491	3	t	1 of 3	orange-brown	40, 60	linked and coated	/	**	_	**	***	/	/	/	/	******	***	***	***	granular/lenticular
968	7491	3	t	2 of 3	brown-orange	10, 90	embedded	*	/	*	/	***	***	/	*	/	*	/	/	/	apedal
968	7491	3	t	3 of 3	green-grey	20, 80	embedded	/	/	*	_	***	***	/	*	/	/	/	/	/	lenticular
979	7461	3	p	1of 2	orange	80, 20	linked and coated	/	/	/	***	/	/	/	/	/	******	***	/	/	granular
979	7461	3	p	2 of 2	orange-brown	10, 90	embedded	_	/	*	/	**	**	/	*	/	/	/	/	/	lenticular
977	7491	9	t	2 of 4	grey-orange	30, 70	embedded	/	/	*	/	***	***	*	*	_	/	*	/	/	sub-angular-blocky
977	7491	9	t	3 of 4	yellow-brown	15, 85	embedded	/	*	*	/	**	*	/	/	/	/	/	/	/	apedal
977	7491	9	t	4 of 4	green-grey	15, 85	embedded	/	/	*	/	**	**	/	*	/	/	/	/	/	platy
969	7491	9	p	1 of 3	brown-grey	70, 30	intergrain aggregate	/	*	/	***	_	**	/	*	*	****	***	**	**	granular
969	7491	9	p	2 of 3	orange-brown	10, 90	embedded	**	*	**	/	**	**	/	*	**	**	/	/	/	sub-angular-blocky
969	7491	9	p	3 of 3	green-grey	10, 90	embedded	**	**	*	/	/	**	/	/	/	/	/	/	/	platy
977	7491	9	t	1 of 4	grey	70, 30	intergrain aggregate	/	*	*	***	**	**	*	_	/	*	******	/	/	apedal

875	7519	C3	n/a	1 of 1	grey-orange	5, 95	single population	**	*	*	*	***	*	/	/	/	/	_	/	/	sub-angular-blocky
888	7519	1	t	1 of 2	grey-orange	5, 95	single population	/	/	/	/	***	*	/	/	/	/	/	/	/	sub-angular-blocky
888	7519	1	t	2 of 2	grey-yellow	15, 85	embedded	**	**	*	*	*	**	/	*	/	/	_	/	/	sub-angular-blocky
873	7519	1	p	1 of 2	brown-yellow	2 ,98	single population	*	/	/	/	***	*	/	/	/	/	/	/	/	sub-angular-blocky
873	7519	1	p	2 of 2	yellow-grey	20, 80	embedded	/	*	**	**	*	**	/	/	/	/	/	_	/	sub-angular-blocky
983	7519	4	p	1 of 3	grey-yellow	5, 95	embedded	*	_	/	/	***	*	/	/	/	/	/	/	/	sub-angular-blocky
983	7519	4	p	2 of 3	brown-grey	25, 75	embedded	*	/	*	**	*	***	/	*	**	*	**	/	/	apedal
983	7519	4	p	3 of 3	brown-orange	20, 80	embedded	_	/	_	/	***	***	/	**	/	/	/	/	/	lenticular
908	7519	13	t	1 of 2	yellow-orange	5, 95	embedded	/	/	/	_	**	*	/	/	/	/	/	/	/	sub-angular-blocky
908	7519	13	t	2 of 2	grey-yellow	15, 85	embedded	*	_	_	**	**	**	/	/	/	**	/	/	**	apedal
908	7519	13	t	1 of 2	yellow-orange	5, 95	embedded	/	/	/	_	**	*	/	/	/	/	/	/	/	sub-angular-blocky
908	7519	13	t	2 of 2	grey-yellow	15, 85	embedded	*	_	_	**	**	**	/	/	/	**	/	/	**	apedal
938	7519	13	p	1 of 2	orange-brown	5, 95	embedded	*	/	/	_	***	*	/	_	/	/	/	/	/	sub-angular-blocky
938	7519	13	p	2 of 2	brown-grey	25, 75	embedded	*	*	**	/	*	**	/	/	/	*	*	_	/	apedal
938	7519	13	p	1 of 2	orange-brown	5, 95	embedded	*	/	/	_	***	*	/	_	/	/	/	/	/	sub-angular-blocky
938	7519	13	p	2 of 2	brown-grey	25, 75	embedded	*	*	**	/	*	**	/	/	/	*	*	_	/	apedal
882	7555	1	t	1 of 3	orange-brown	15, 85	embedded	/	**	*	**	*	**	*	*	/	_	/	*	/	sub-angular-blocky
882	7555	1	t	2 of 3	orange-grey	90, 10	intergrain aggregate	/	****	/	**	/	**	*	**	/	***	******	***	/	apedal
882	7555	1	t	3 of 3	grey-brown	65, 35	embedded	_	*	*	**	**	**	_	*	/	/	/	/	/	sub-angular-blocky
872	7555	1	p	1 of 3	orange-brown	35, 65	embedded	*	**	*	**	*	**	*	*	/	/	****	***	/	sub-angular-blocky
872	7555	1	p	2 of 3	yellow-grey	5, 95	embedded	/	/	/	*	***	*	/	_	/	/	/	/	/	platy
872	7555	1	p	3 of 3	colourless	90, 10	single population	/	/	*	/	/	******	**	*	/	/	/	/	/	apedal
860	7555	2	t	1 of 1	orange-grey	70, 30	intergrain aggregate	/	*	**	*	/	*****	**	***	*	/	/	/	/	apedal
821	7555	2	p	1 of 3	orange-yellow	80, 20	intergrain aggregate	/	**	_	*	_	***	_	**	/	**	******	***	/	apedal
821	7555	2	p	2 of 3	pale orange	70, 30	intergrain aggregate	/	/	*	*	/	******	**	***	**	/	/	/	/	apedal
821	7555	2	p	3 of 3	brown-orange	15, 85	embedded	/	/	*	/	**	**	/	/	/	/	/	/	/	lenticular
905	7555	3	t	1 of 1	orange-grey	20, 80	embedded	/	**	***	**	*	**	_	*	/	/	*	/	/	sub-angular-blocky
980	7555	3	p	1 of 2	orange-brown	10, 90	single population	_	/	*	/	***	**	/	/	/	/	/	/	/	angular-blocky
980	7555	3	p	2 of 2	grey-brown	40, 60	embedded	*	*	**	**	*	***	**	**	/	/	/	/	/	apedal

7.3.2 Lead and bone fragments

Bone fragments were present in thin sections from GR 5926, 7491 and 5914 (Table 21) and were analysed by SEM-EDS to assess their lead levels. Lead was present in bone fragments from GR 5914 (S1, TS 995) and absent in the bone fragments from GR 5926 and GR 7491 (Figure 7.5). Copper was found in bones from two graves, the adolescent female (GR 7464) and the infant (GR 7491), although only in traces amounts (<1%) in both (Figure 7.5). Copper is often found in association with galena and may have been liberated from the rock and solubilized in ground waters (Rivera *et al.* 2015).

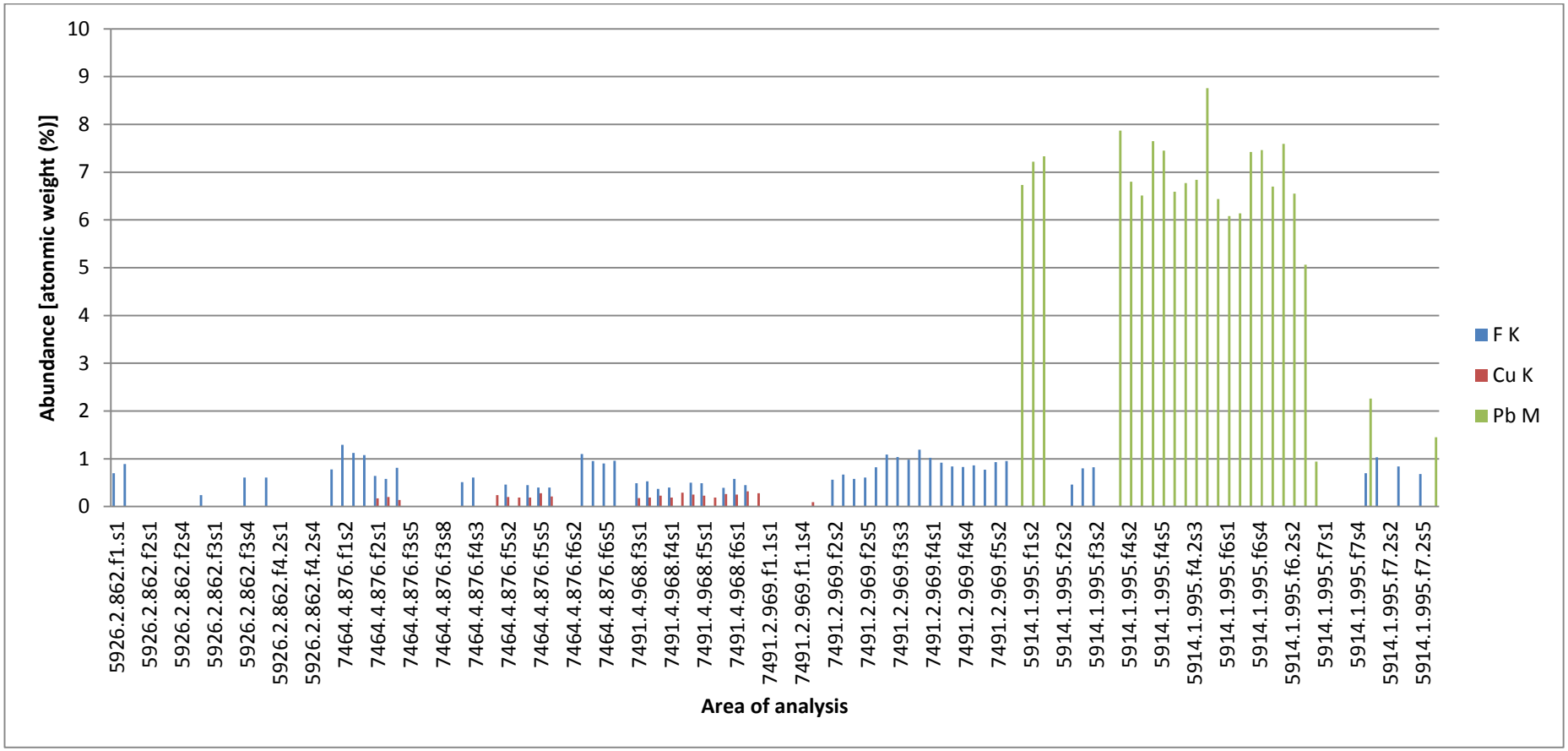

Figure 7.5: Lead, fluorine and copper levels obtained through SEM-EDS analysis of bone fragments from GR 5926 (S2), GR 7464 (S4), GR 7491 (S4 and 2), and GR5914 (S1). Results are ordered as analysed regions of bone fragments along the x-axis and are grouped by grave, as well as sub-divided by sample. Areas of analysis are described by grave number, sample number, thin section number, foci number and spectra number (*e.g.* "5926.2.862.f4s1" relates to GR 5926, Sample 2, TS 862, foci number 4, spectrum number 1).

Results from GR 5914 differ from the other five graves in the elemental composition of the bone fragments in the sediments (Figure 7.5). The bone fragments in TS 995 (GR 5914, S1) were analysed by SEM-EDS and contained lead in quantities that would have affected the individual's health (Figure 7.6). The lead content in the groundmass of the thin sections from GR 5914 was also different from the other graves (Table 21), making it possible that the lead in the bone could have been affected by post-depositional processes. Hence, lead levels in the groundmass, bone fragments and sediment adhering to bone fragments were measured by SEM-EDS analysis (Figures 7.6-7.8). The amounts of lead in the micromass and in the sediment adhering to the bones were lower than within the bones (Figures 7.6-7.8). The highest lead levels of these three types of materials were being in the bone (blue in Figures 7.9 and 7.10) suggests that it was incorporated during the lifetime of the individual. This interpretation is supported by osteological analyses of skeletons from the graveyard at Sala, which identified lead lines in the bones of some individuals (Bäckström and Sundström 2010).

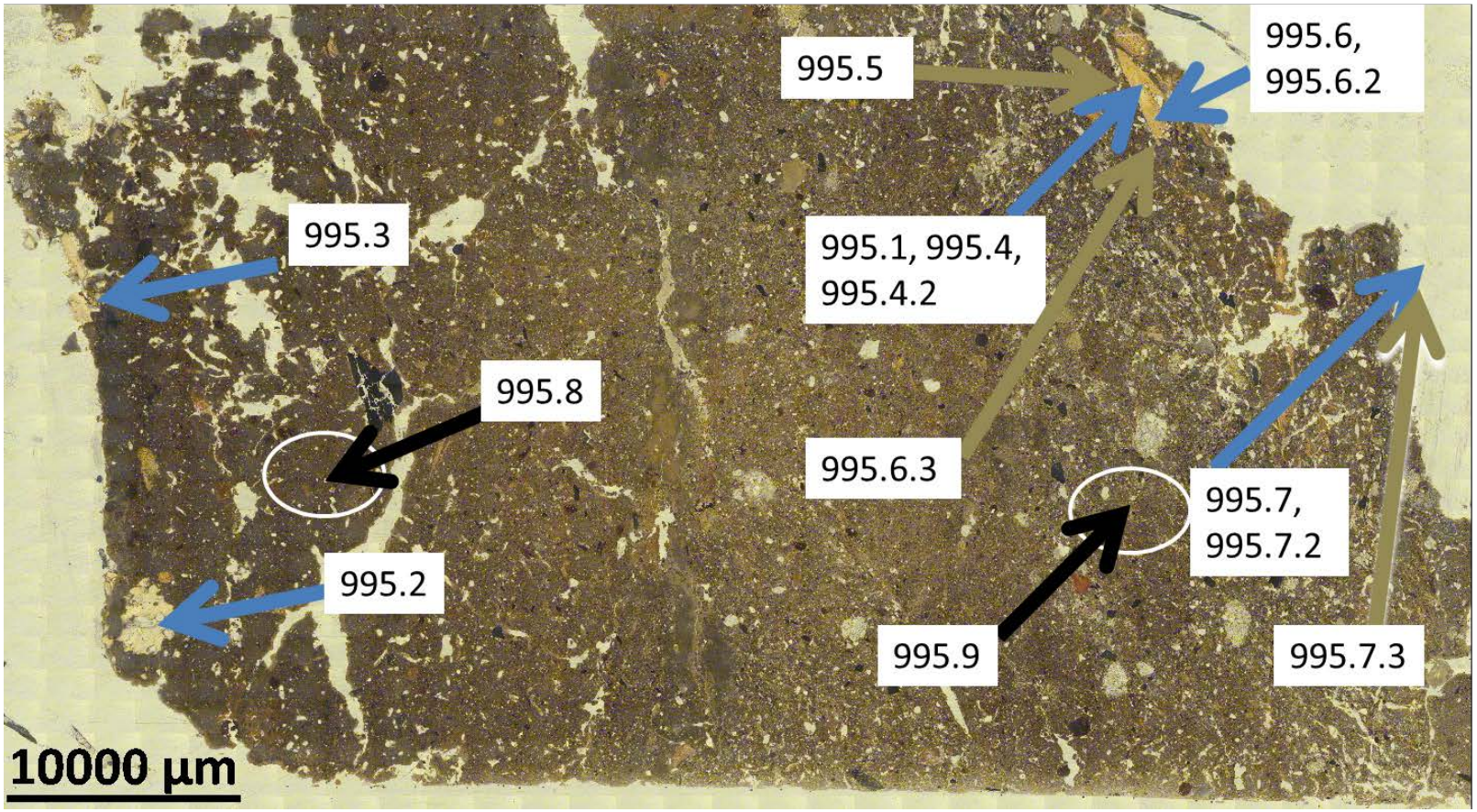

Figure 7.6: Mosaic image of TS 995 with annotations displaying the locations of the regions of interest in the SEM-EDS analysis (GR 5914, S1Zt, TS 995, PPL). As this sample was an S1Zt sample, this thin section was from a sample of sediment directly beneath the skull. In order to be cut tangentially to the skeletal remains from a sample below the skull, this thin section has been cut parallel to the plane of the ground surface, rather than perpendicular to the ground surface as is typical of thin sections. Although the skull was located above the position that this sample was collected from the bone fragments in this thin section could have moved downwards through the sediments due to fragmentation of the skull and sediment collapses within the grave fills below the skull. Measurements from regions of interest on bone are represented by blue arrows and those from sediment adjacent to bone fragments are represented by brown arrows. Measurements from the sediment micromass are represented by white circles and black arrows.

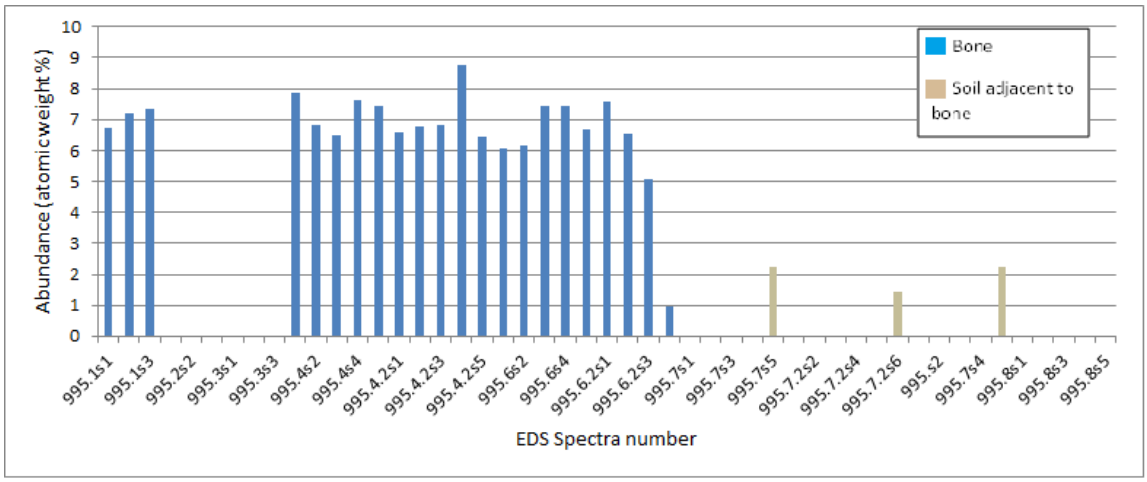

Figure 7.7: Results from SEM-EDS analysis of lead in bone fragments (blue) and in the sediment groundmass (brown) from the sample under the skull (GR 5914, S1Zt, TS 995).

a)

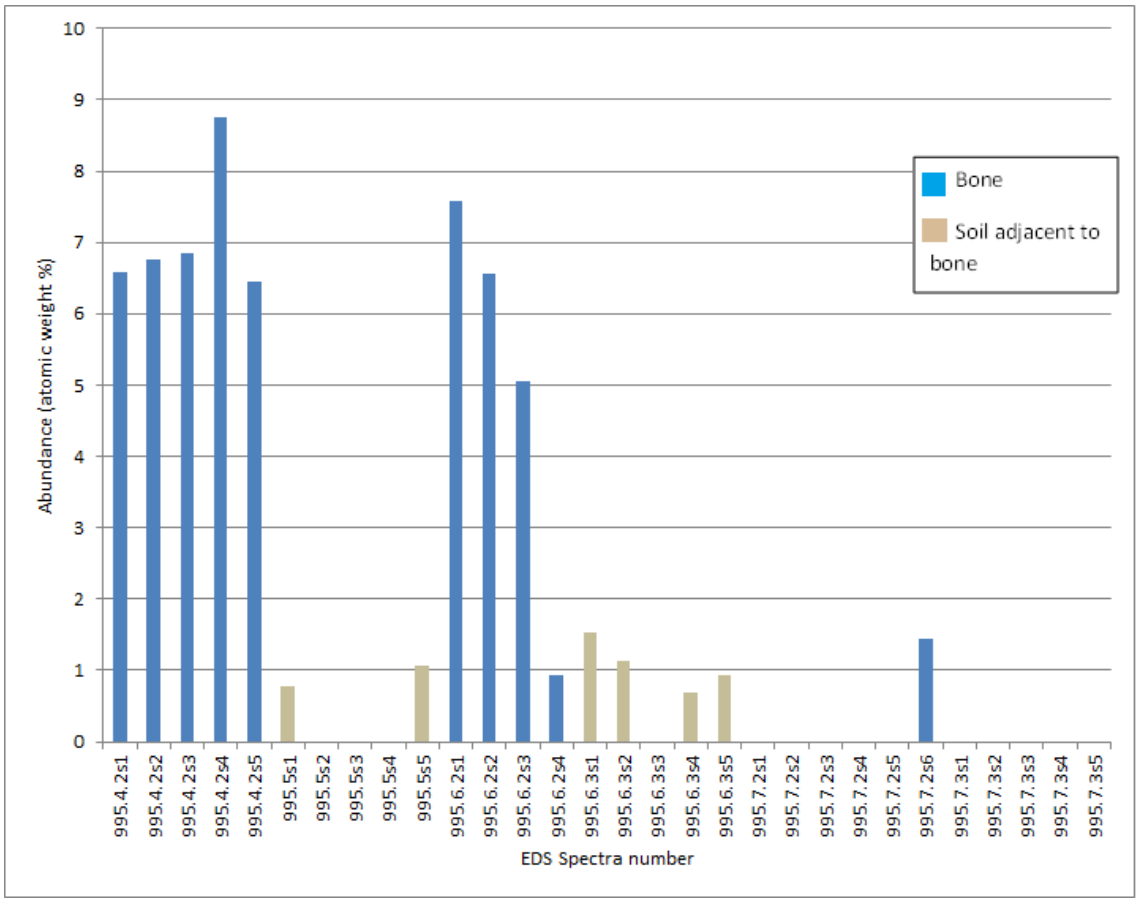

Figure 7.8: Lead levels in bones with their adjacent sediment (GR 5914, S1Zt, TS 995). Bone 995.4.2 (blue) and sediment 995.5 (brown), bone 995.6.2 (blue) and sediment 995.6.3 (brown), and bone 995.7.2 (blue) and sediment 995.7.3 (brown).

7.3.3 GR 5914

Sediments in thin section from GR 5914 differed from the other five graves. Thin sections from GR 5914 contained a rock fragment type unique to this grave (Figure 6.9), vesicular silica tephra (Figure 7.10a and b), pollen (Figure 7.10g) and unidentified red (PPL) material (Figure 7.10c and d). The vesicular structure of the silica-rich material (Figure 7.10e) may be interpreted as characteristic of phytoliths which had been heated to a high temperature. Charcoal was present in the black material above the sacral area of this skeleton (SA2, TS 919; Figure 7.2a). The black material from above the sacral area is different to the non-grave sediment in the C1 and is interpreted as evidence that this sediment was deposited into the grave during inhumation. Glass has been found in Scandinavian inhumations from this time period, although more often in cremations than in inhumation burials (Hunter 1975). Hence, the micromorphological observations indicate that the burial practice of GR 5914 was slightly different to the other five graves at Sala.

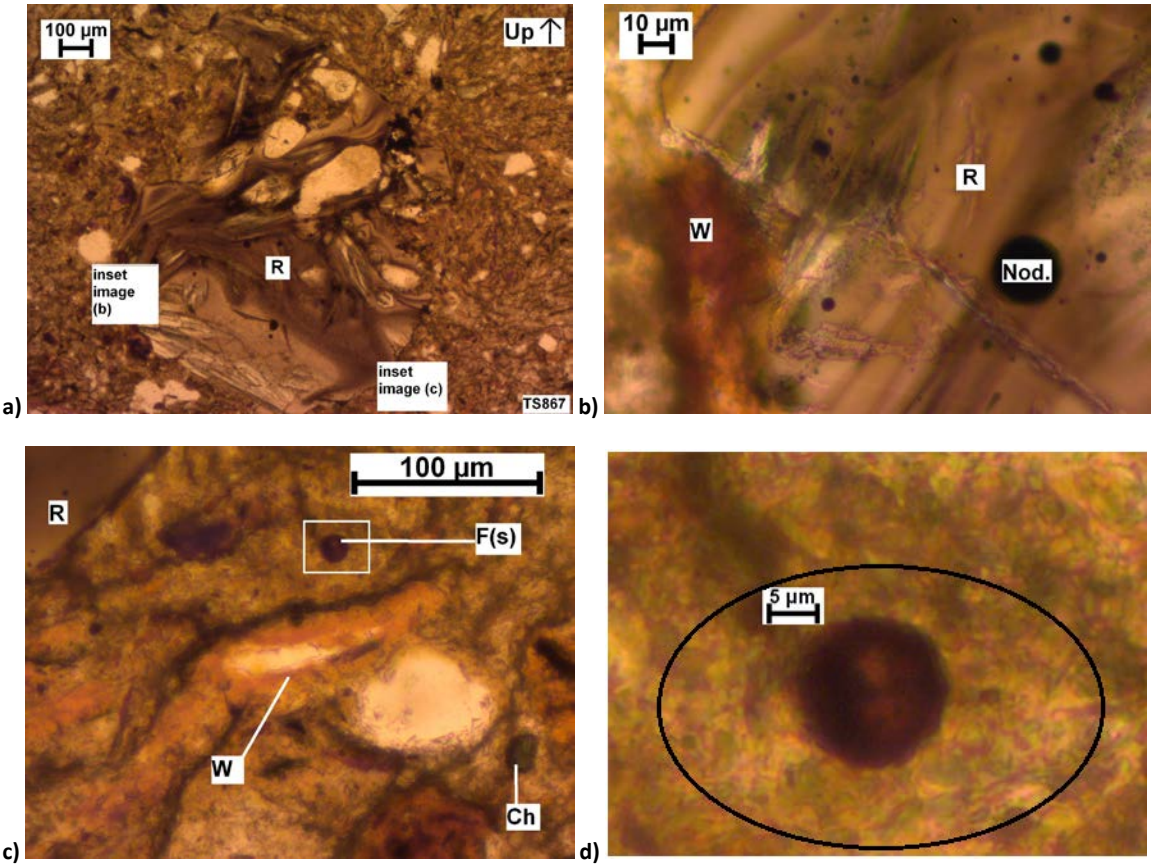

Figure 7.9: Rock fragment (R) of a type particular to this grave from the data set (GR 5914, S1p, TS 867, PPL). (a) Rock fragment (R) showing complex weathering patterns including speckled pattern avoiding the mica minerals and manganese-rich nodules and concentrated at the upper surface of the fragment. (b) Detail of image a), showing wood remains (W) adjacent to the edge of the rock fragment (R) and manganese-rich (manganese determined by SEM-EDS) nodules (Nod.). (c) Detail from image a): wood remains (W), fungal spores (F(s)), and chlorite (Ch) adjacent to the edge of the rock fragment (R). (d) Detail of image c), showing fungal spore situated in a depression of the surrounding fine material (depression shown by black ellipse annotation).

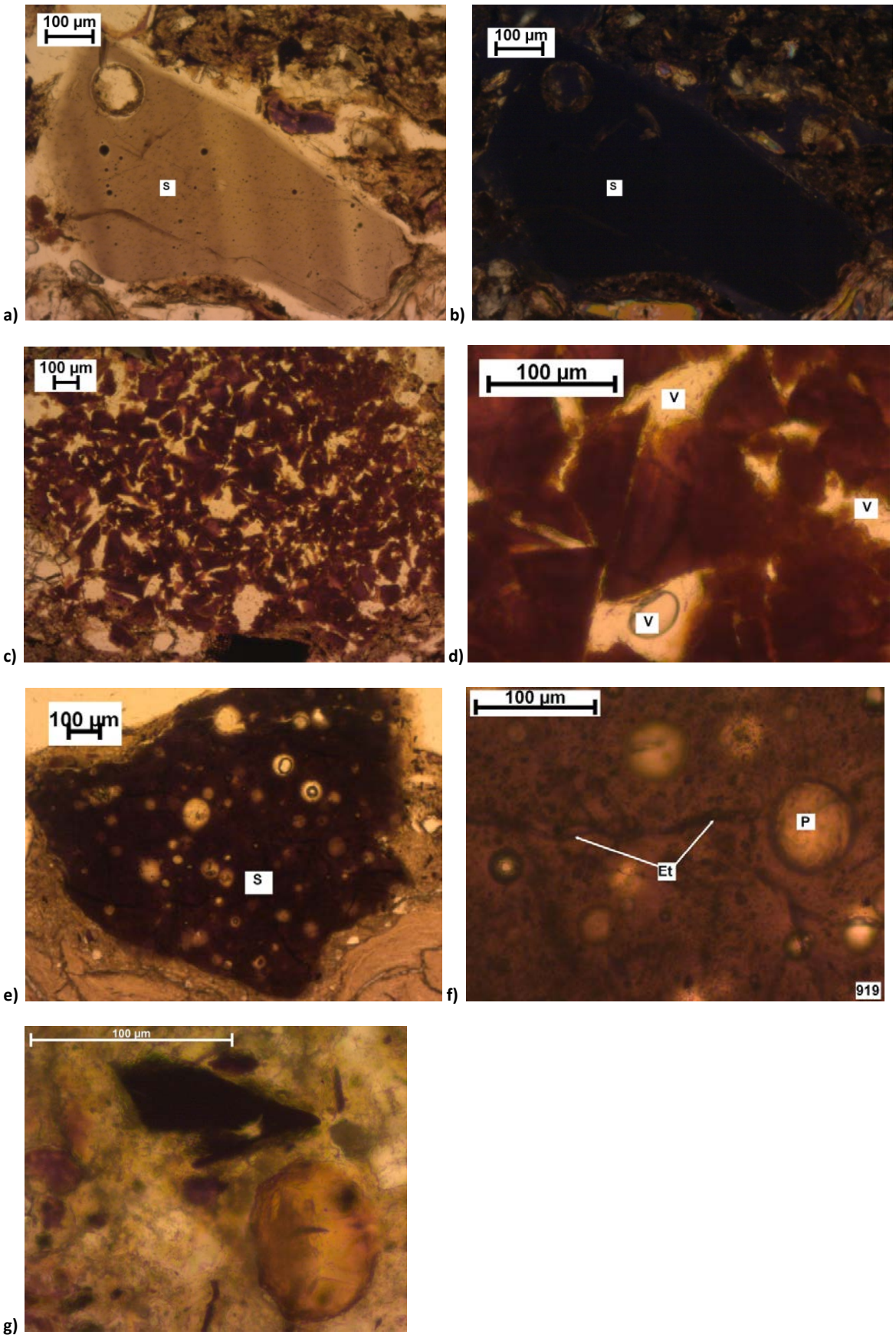

Figure 7.10: Materials in thin section from GR 5914. (a) Silicate (S), tentatively identified as melted phytoliths, (GR 5914, SA2, TS 919.1, PPL). (b) XPL view of image a). (c) Unidentified red material (GR 5914, SA2, TS 919.1, PPL). d) detail of image c). (e) Vesicular material (S) (GR 5914, SA2, TS 919, PPL). f) Detail of image e), pores (P) and etching (Et). (g) Pollen grain (GR 5914, SA2, TS 919, PPL).

7.3.4 Chlorite and muscovite

Chlorites were present in samples from all six graves (Table 21). Chlorite group minerals were identified in thin section by their blue pleochroic colours and anomalous blue interference colours or isotropic characteristics (MacKenzie and Adams 1994, 46-47). Although more detailed classification within this mineral group is possible based on optical properties (Saggerson and Turner 1982), firm identifications would require additional analyses such as XRD (Schaetzl and Anderson 2005, 73). Identifications of particular members of the chlorite group to discern intricate mineralogical differences between sediments have not been attempted in these grave fills.

Chlorite and biotite were present in some of the thin sections (Figure 7.11) and each exhibited a range of weathering extents (Table 22). The estimated abundance of chlorite from the samples and controls was greater (>*c.* 2% of the area of the micro-unit) in micro-units in samples of the pelvis (GR 7555, S2; GR 7555, S2 and GR 7491, S13) and feet (GR 7519, S4) sediments (Figure 7.11). Biotite weathering to form an iso-alteromorph was observed in a micro-unit from GR 5926 (Table 22), the only uncoffined burial, and was unique to this grave. Primary mica minerals (muscovite or biotite) in the controls were altered through the expansion of layers (parallel linear weathering pattern). Such expanded layers were later infilled (terminology after Delvigne 1998, 160; Chapter 3) by the surrounding groundmass as a part of the early stages of their transformation to clays (Figure 7.12).

Weathering of mica to form poro-meso-alteromorphs (with the formation of lenticular intra-mineral pores) or kata-alteromorphs (Bisdom *et al.* 1982) were present in the samples. No discernible differences were observed between weathering patterns of muscovite and sample positions S1, S2 and S3 (Figure 7.13). The evidence of the weathering patterns suggested that primary mica minerals in the samples had altered to forms *via* one of two pathways. No evidence of forms related to either of the two weathering pathways in the samples, was observed on primary mica minerals in any of the controls (C1, C2, or C3). The interpretation of the evidence of the weathering of the primary mica minerals suggests that they had weathered differently in the C1 controls to the samples.

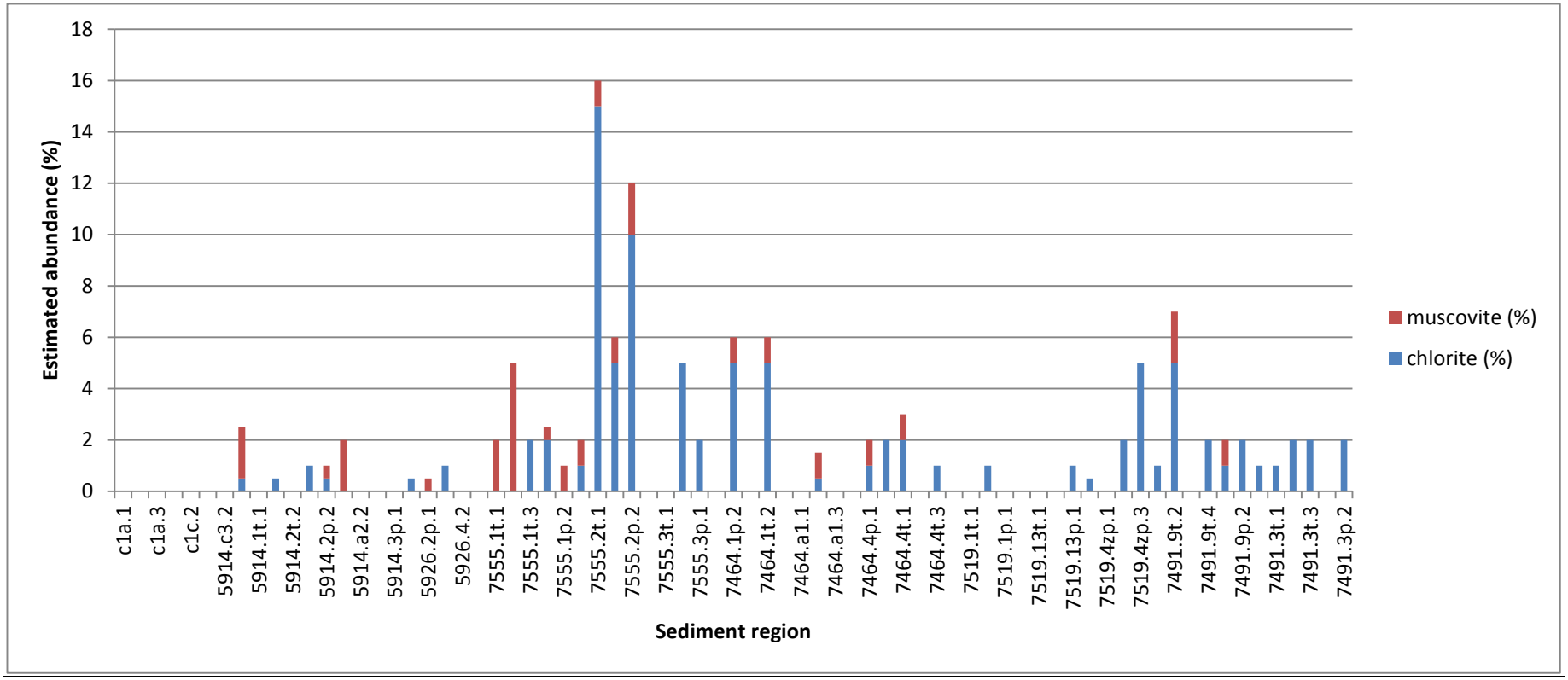

Figure 7.11: Distribution and estimated abundance of chlorite and muscovite and biotite in thin sections. Sediments are grouped as control sediments (C1) or grave number and sample number[7].

[7] Labels along the x-axis denote grave number, sample number, thin section orientation related to the body and micro-unit number (*e.g.* "5914.1t.1" relates to GR 5914, Sample 1, tangential oriented thin section and micro-unit 1 from that thin section).

Table 22: Biotite: estimated abundance, weathering extent and weathering pattern(s). Micro-units observed in thin section where no biotite was recognized have been omitted from this table.[8]

micro-unit	biotite (%)	weathering extent	weathering pattern
5914.1p.1	2	1	pellicular
5914.2p.2	0.5	2	pellicular
5914.a2.1	2	2	parallel linear with layer expansion forming meso- and kata-alteromorphs
5926.2p.1	0.5	3	complex: pellicular & parallel linear forming iso-alteromorphs
7555.1t.1	2	3	parallel linear forming kata-alteromorphs with chlorite along expanded layer spaces
7555.1t.2	5	3	parallel linear forming kata-alteromorphs with chlorite along expanded layer spaces
7555.1p.1	0.5	2	parallel linear and pellicular
7555.1p.2	1	3	parallel linear with expansion of sheet-like layers forming meso-alteromorphs
7555.1p.3	1	1	parallel linear with expansion of sheet-like layers forming meso-alteromorphs
7555.2t.1	1	2	complex: parallel linear forming phyllo-poro-alteromorphs, then intra-mineral pores altered to chlorite
7555.2p.1	1	2	pellicular (through 'tops and bottoms' weathered) and some parallel linear
7555.2p.2	2	2	complex
7464.1p.2	1	1	pellicular
7464.1t.2	1	2	parallel linear forming meso-alteromorphs with chlorite in the expanded layer spaces and some pellicular ('tops and bottoms')
7464.a1.2	1	1	pellicular
7464.4p.1	1	2	parallel linear forming phyllo-poro-kata-alteromorphs
7464.4t.1	1	1	complex: pellicular and parallel linear
7491.9t.2	2	2	parallel linear with layer expansion forming meso-alteromorphs
7491.9p.1	1	2	parallel linear with layer expansion forming meso-alteromorphs

[8] Micro-units are listed by grave, sample, thin section orientation and micro-unit number (*e.g.* "7491.9p.1" denotes GR 7491, Sample 9, perpendicular oriented thin section and micro-unit 1 from that thin section).

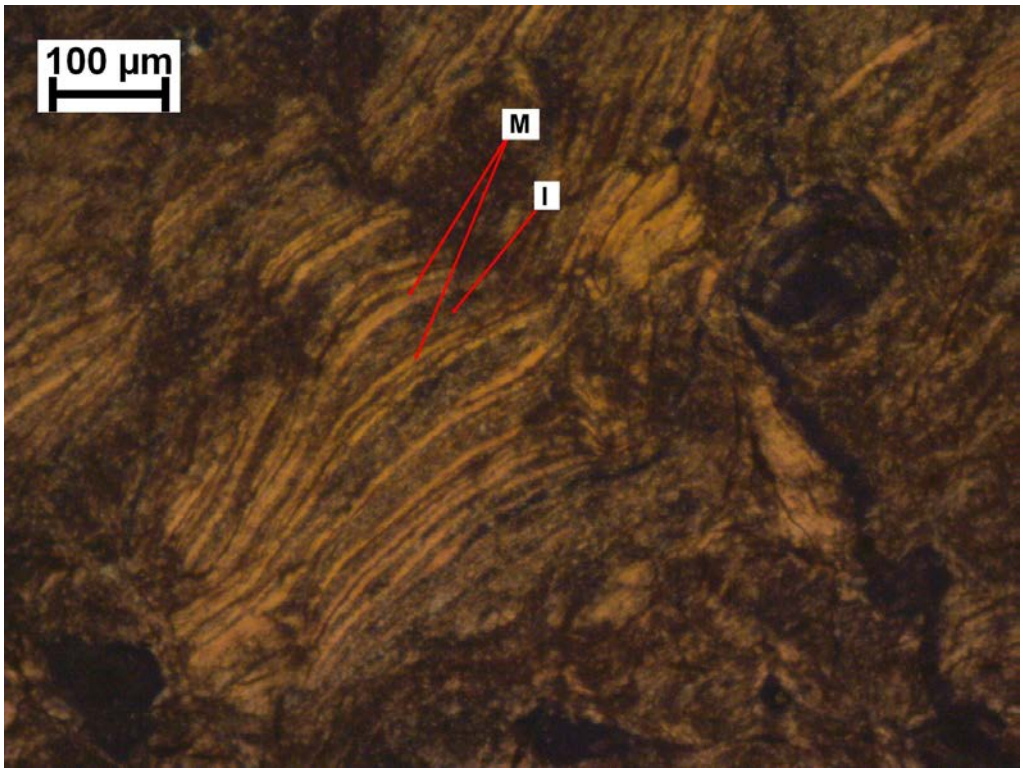

Figure 7.12: Holo-meso-alteromorph of biotite (M) showing expansion between sheet-like layers (I), following a parallel linear weathering pattern leading to the production of clays (GR 7519, C3, TS 875, XPL).

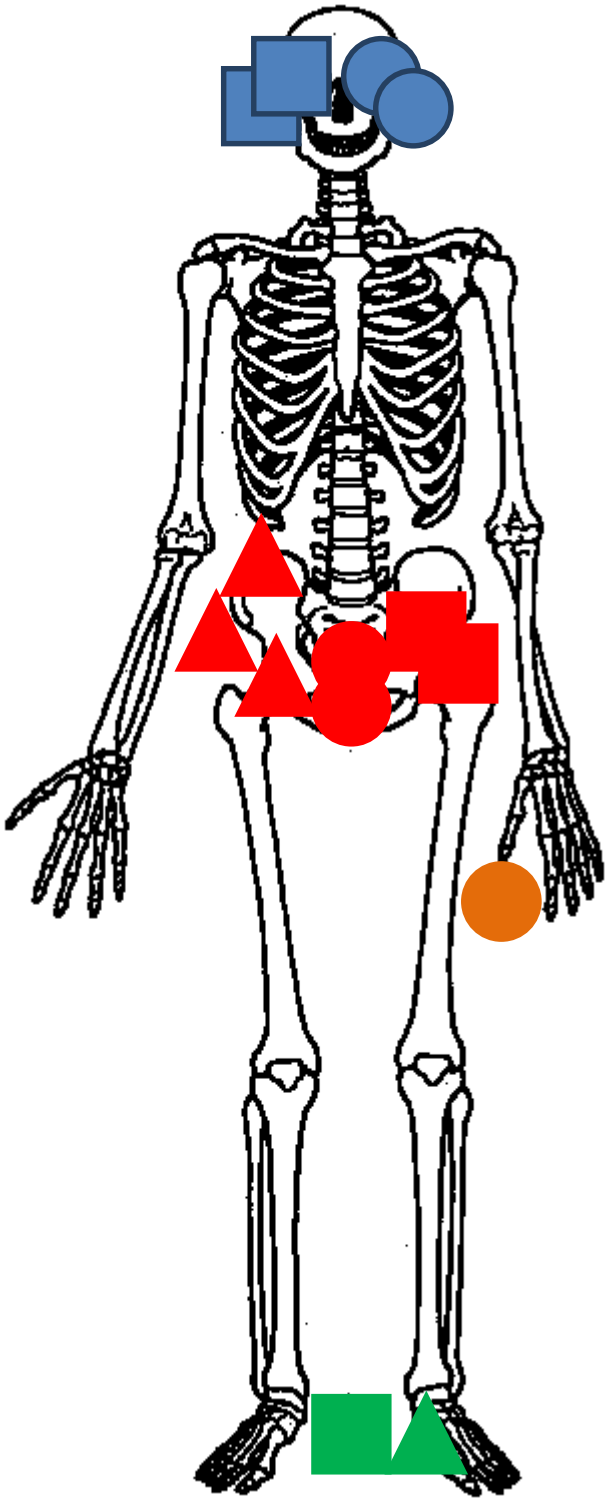

Key:

Circle= pellicular weathering pattern

Square= parallel linear weathering pattern

Triangle= complex weathering pattern

Figure 7.13: Skeleton image with shapes representing the spread of different types of weathering patterns observed affecting biotite in samples from all six graves. This figure is an illustration of the data listed in Table 22.

7.4 Interpretation and discussion

7.4.1 Fungi

Two distinct species of fungi were identified in the grave sediment thin sections (Figure 7.14). The shape and size of the fungal remains from GR 7555 (Figure 7.14c and d) allows their identification as *Sporotrichum pulverulentum,* a species which inhabits dead wood. *Sporotrichum pulverulentum* are white-rot fungi, saprophytic necrophytes of coniferous woods, found specifically with *Abies* (spruce) and *Pinus* (pine) in this area of Sweden (Eriksson, 1978). Fungal remains seen in Fe lined voids of GR 5914 (C3, TS 861; Figure 7.14a and b) were identified as macroconidia. The size and shape of the remains allows their identification as *Sepedonium*, which are saprobes of *Boletales* (mushrooms) (Sahr *et al.* 1999). The micro-contextual relationships between the fungal remains, void and coating (Figure 7.14a) are interpreted to suggesting the development of an iron-rich coating on the exterior surface of coffin fragment was subsequently colonised by a fungal growth that utilised the wood host until only the void, conidia, and an iron-rich coating remained. Previous studies have demonstrated that iron accumulations can be integral to the production of enzymes required by white rot for wood degradation (Paszczyński *et al.* 1986 and Tien and Kirk 1983). Hence, the possibility exists that observation of such fungal remains in thin section could serve to indicate that a coffin had been present (Chapter 9).

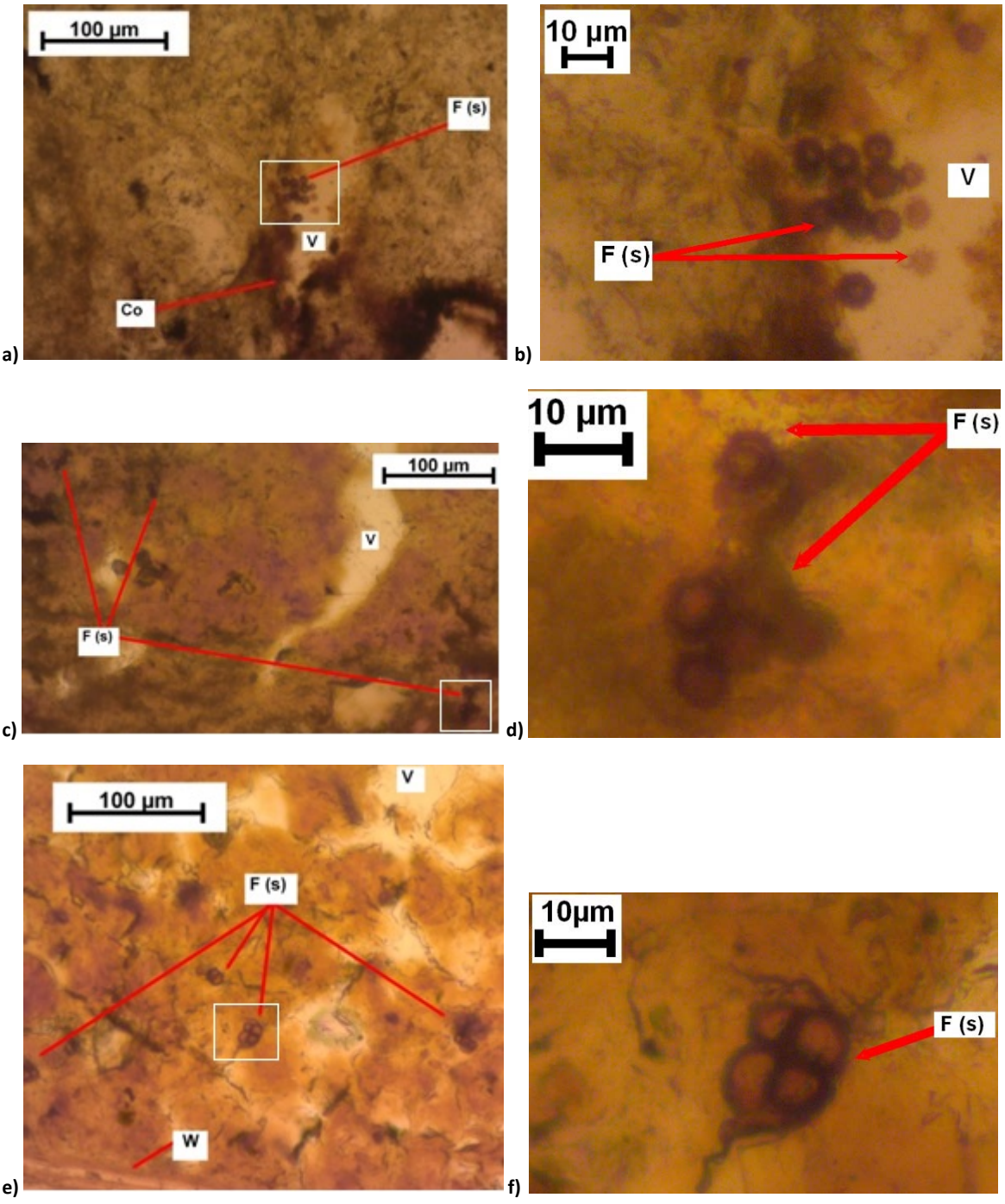

Figure 7.14: a) Fungal spores (F (s)) in void (V) with coating (Co) (GR 5914, C3, TS 861, PPL). b) detail of inset (white rectangle) in image a). c) Fungal spores (F (s)) adjacent to degraded coffin (GR 7555, C3, TS 982, PPL)[9]. d) detail of inset (white rectangle) in image c). e) Fungal spores (F (s)) with smooth exterior surfaces in a micro-unit with voids (V) and wood remains (W) (GR 7464, C3, TS 982, PPL). f) detail of inset (white rectangle) in image e).

The fungi and heavily weathered micas in the samples are inferred as related to the burial. The micro-contextual associations of the secondary micas and the fungi may be linked to Fe-

[9] Images (a) through (d) show fungal spores displaying spined and globose traits characteristic of macroconidia of fungi from the genus Sepedonium (best viewed in image b).

interdependency (*e.g.* by *Uredinales*, Voegele *et al.* 2009) and accumulations related to wood saprophytes (*e.g.* by *Basidiomycetes*, Fekete *et al.* 1989). Further investigations and research into the complex relationships between the body and wooden coffin, and the saprophytes that inhabit this type of sediment system could be useful in elucidating these interactions (Chapter 9).

7.4.2 .Chlorite and organic matter

The phyllosilicate minerals of a blue-green colour (PPL) (Appendix VI) were tentatively identified as members of the chlorite group by their colour, pleochroism, interference colour and structure, and are hereafter referred to as secondary chlorite(s) minerals (Table 21). At a micro-contextual level, the secondary chlorites exhibited strong radial referred distribution (referred distribution terminology after Bullock *et al.* 1985, 35) to the fungal remains, the amorphous organic material from degraded coffin wood and, on occasion, bone fragments (Figures 7.15-7.17). By contrast, the biotite, the primary mica mineral from which the secondary chlorite minerals are interpreted to have formed, was absent in sediments adjacent to the fungal remains and/or amorphous organic material from degraded coffin wood. Semi-quantitative analysis of chlorite, via a technique such as image analysis, could help confirm this spatial relationship. However attempts at this have not yet been successful (Sections 7.5.1.3 and 7.5.1.4). The association of the secondary chlorite with the fungal or plant remains and bone fragments may suggest a relationship between fungal saprophytes colonising the burial and the presence of chloritized biotite. Spatial relationships observed through micromorphological analysis did not show a relative causality of such two occurrences (of fungi respiration and biotite alterations), however the results may suggest that while the two are not linked in terms of cause and effect they are related as the sedimentological conditions under which fungi were more active were also favourable to the preservation of the chloritized biotite in contrast to the controls were fungal remains were not present and biotite present was observed weathering to clays.

Biotite was present at weathering extent one (2.5-25% altered) in a micro-unit (GR 7464, S4t, TS 981.2), where neither fungal nor plant remains were present (Section 7.4.1). This relationship between primary mica and organic materials was also observed with muscovite in the corresponding micro-unit from the perpendicular thin section from this S4 sample (GR 7464, S4p, TS 876.2). The inferred relationship between the chlorites and organic remains (Figure 7.16a-b) is supported by the presence of muscovite and biotite in micro-units where organic remains were absent.

The interpretation of the chlorite in samples from Sala as related to the alteration of biotite is supported by the literature: the transformation of chlorite to muscovite has been demonstrated

(Franceschelli *et al.* 1986) and sediment water is shown to have an active role in the process (Jahren and Aagaard 1989). Previous studies have detailed the processes that determine chlorite formation in rocks (Curtis *et al.* 1985), and the types of weathering patterns affecting muscovite and biotite in soils and sediments (Delvigne 1998). Primary chlorite has been suggested to weather readily to an aluminium-rich secondary chlorite in poorly drained sediments (Duchaufour 1982, 13) such as the heavy clay sediments at Sala (Section 7.1). The interpretation of the chlorites in samples from Sala as minerals formed through alteration and preserved in the soils through a lack of weathering to clays is supported by reports of well crystallized and relatively stable secondary chlorites (Gac 1968).

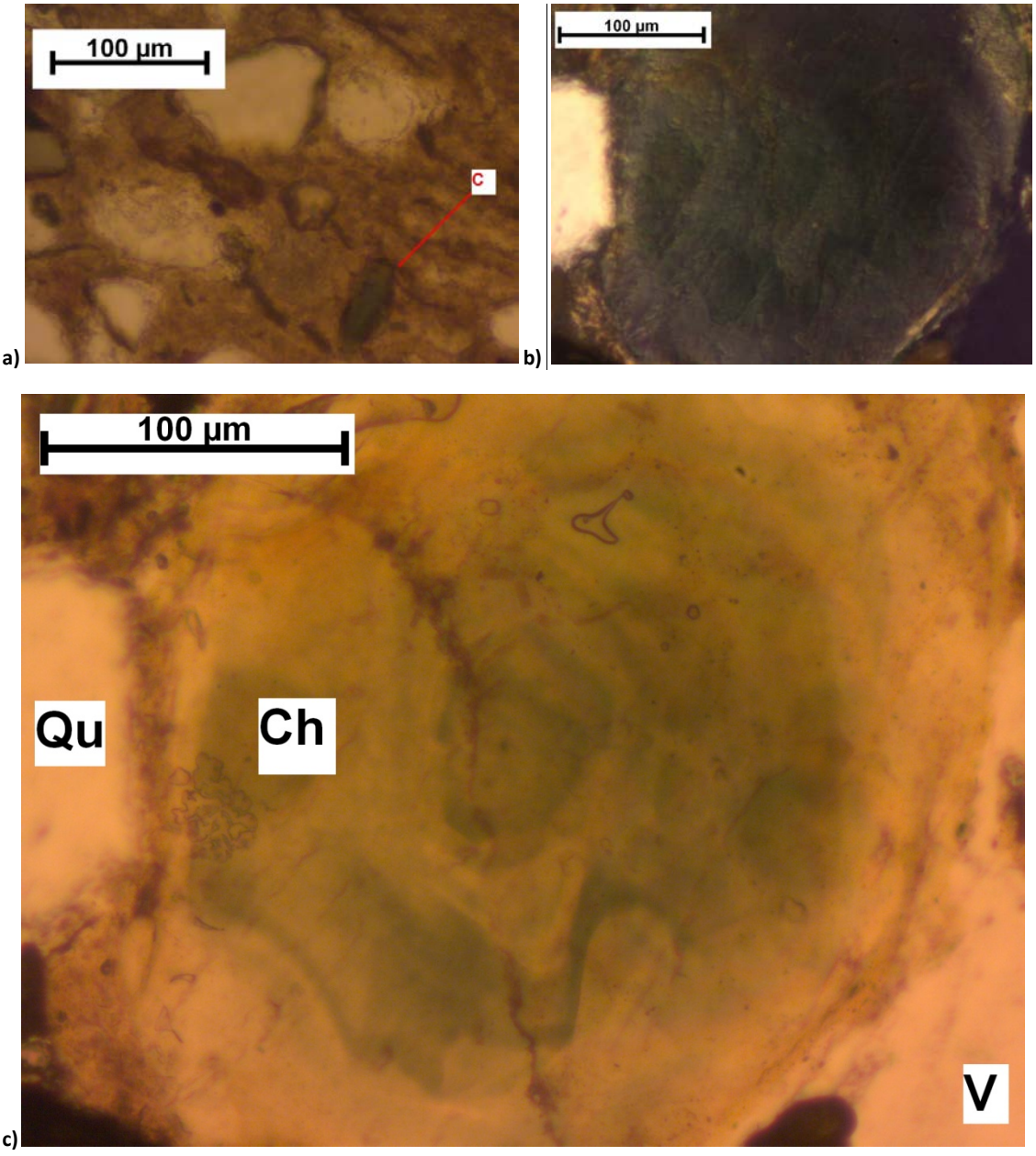

Figure 7.15: Chlorite in thin section from samples. (a) Secondary chlorite (C) with diffuse edges (GR 7555, S2, TS 821.2, PPL). (b) Chlorite (Ch) adjacent to quartz (Qu) and voids (V) (GR 5914, S1, TS 995) (XPL). (c) PPL view of image b) (GR 5914, S1, TS 995, PPL).

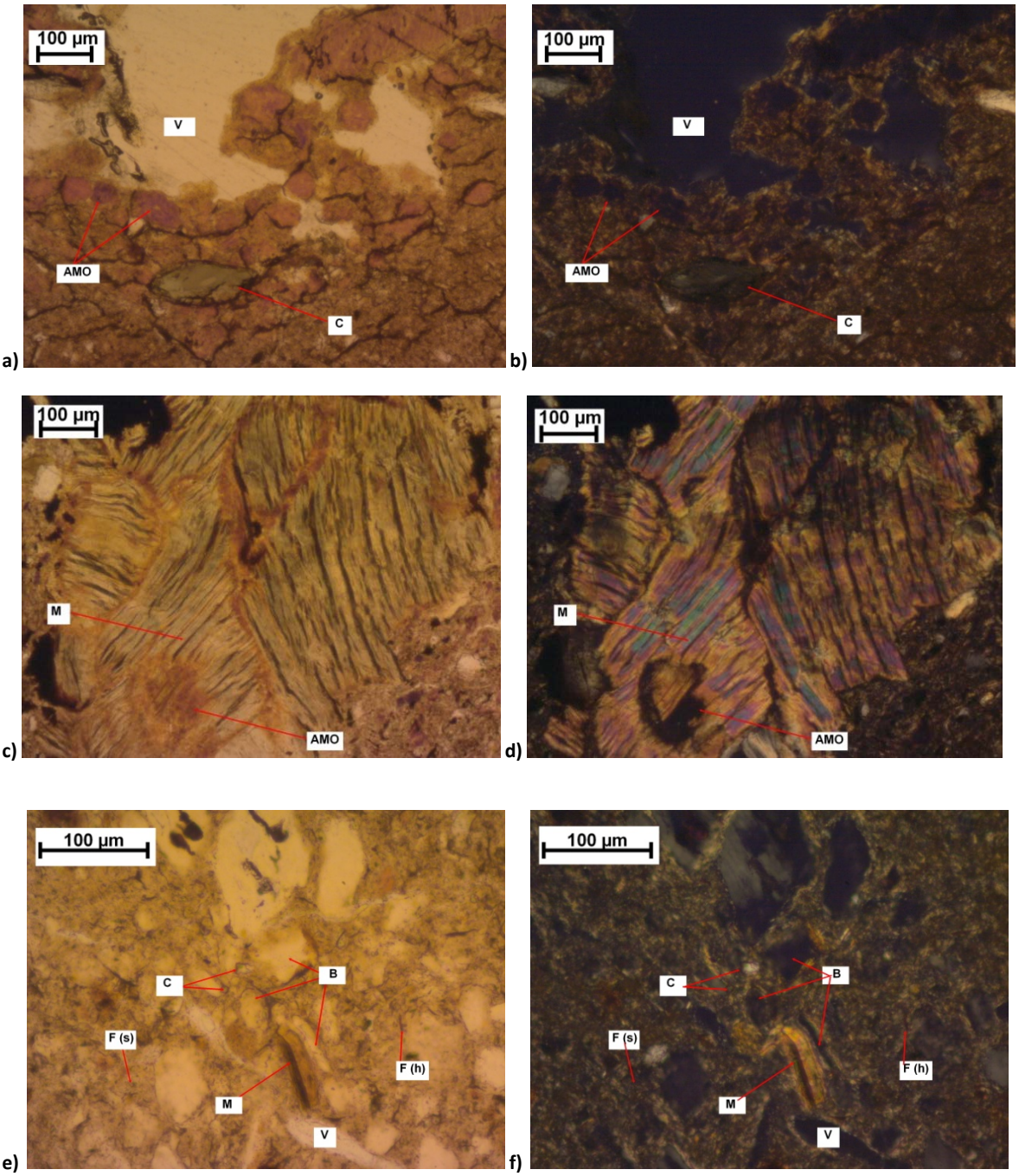

Figure 7.16: Mica in association with organic remains. a) Chlorite (C) adjacent to amorphous organic material (AMO), from the degraded coffin wood layer (GR 7464, S4p, TS 876.1, PPL). b) XPL view of image a). c) Mica (C) with AMO (AMO) within intra-mineral cracks (GR 5914, S1t, TS 995, PPL). d) XPL view of image c). e) Mica mineral (M) in association with bone (B) and fungal remains [F(s)=fungal spore, F(h)=fungal hyphae], with voids (V) and primary mica minerals (M) (GR 7519, S2t, TS 908, PPL). f) XPL view of image e).

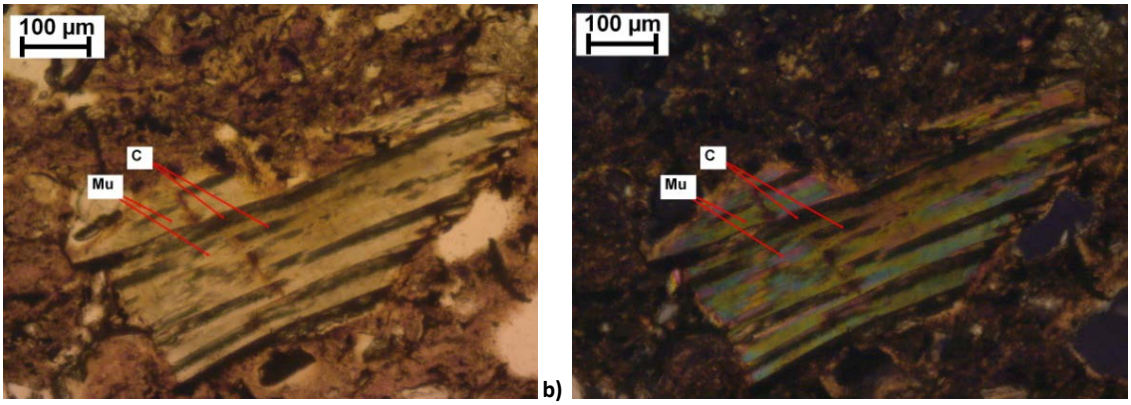

a) b)

Figure 7.17: (a) Chloritization of biotite (Mu), with the early stage of chloritization (C) between sheet-like layers, and present in the sediments at weathering extent one (GR 5914, SA2 above pelvis, TS 906.1, PPL). (b) XPL view of image a).

7.4.3 Chlorite and redox

The weathering pattern of the primary mica minerals (poro-kata-alteromorphs, Section 7.3.4) in the sediment from the foot adjacent samples (GR 7464) reflects the dominant weathering pathway affecting primary mica minerals in strongly redoximorphic environments (Bisdom *et al.* 1982). Mineral weathering to poro-kata-alteromorphs, depletion hypocoatings on peds and oxidized iron deposits at the edges of primary micas (Figure 7.18) were present in these samples (GR 7519, S1 t; GR 7464, SA1 and GR 5914, SA2) and in a lower micro-unit from GR 7464 (SA1, TS 984.2). Such mineral weathering patterns and pedofeatures are interpreted as evidence of reduced conditions and suggest that redox conditions and distribution to faunal and fungal remains (Section 7.4.1) is a factor in weathering patterns of these mica minerals. A quantitative assessment of the chlorites in the samples from the burial sediments as alteration from primary mica minerals could benefit from quantification by image analysis as discussed in detail in the experiments in Appendix VI.

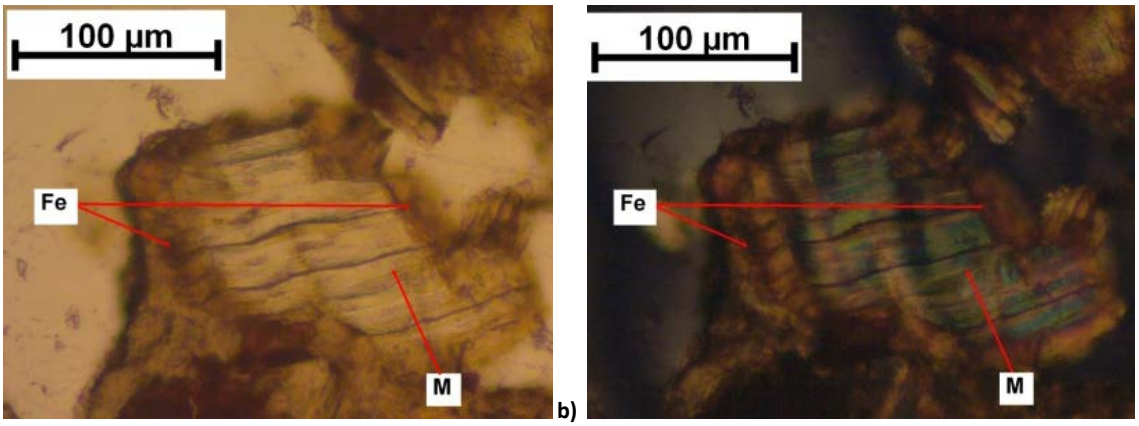

a) b)

Figure 7.18: a) Mica (M) with mineral weathering at tops and bottoms of the mineral grain, through pellicular weathering with deposits of iron oxide compounds precipitated out of solution (Fe) (GR 5914, SA2, TS 906, PPL). b) XPL view of image a).

7.4.4 Sediment microstructure

Sub-angular blocky peds was the most common microstructure in thin sections from the burial sediments (Table 21). Lenticular peds were present in samples from GR 7491 and GR 7519 (Figure 7.2f). Sections oriented tangential to the skeletal remains in S2 samples from GR 5914, 5926 and 7555 had only one micro-unit. Angular blocky peds were present in micro-units in sections of samples from GR 7555.

A lenticular microstructure was observed in the basal micro-units in the thin sections from the infant grave (GR 7491), and from a foot sediment sample from GR 7519 (S4Zp, TS 983.3). This microstructure was absent in samples from the other graves and from the C1 controls. TS 983 (GR 7519) was the only thin section produced from a sample collected underneath skeletal remains (*i.e.* a 'Z' sample) at Sala. The infant grave (GR 7491), and the coffin within it, were smaller than for the other five graves discussed in this chapter. The largest of the three Kubiena tin sizes included in this sampling strategy (Chapter 3) were used to collect the samples from the infant grave (GR 7491, S4 and S9). Hence, their thin sections covered both the upper and lower sediment from within coffin in GR 7491, unlike thin sections from the other five graves. The common trait shared by TS 983 (GR 7519, S4Zp) and the sediment at the base of the infant grave (GR 7491) was that they both included sediments from the base of their coffin fills, distinguishing them from thin sections of other graves. Lenticular peds may be indicative of the formation of ice crystals within a sediment or sediment (Van Vliet-Lanoe 2010, 83), and their presence in GR 7491 and a Z sample from GR 7519 is interpreted as evidence that suggests ice formed in the sediments at the base of GR 7419 and GR 7555.

Alternating coarse (>50 μm) to fine (<50 μm) laminated sediments were present in some samples (Figure 7.2e) and absent in the controls. Thin sections from GR 5926 and in S2 samples from GR 7464 and GR 7519 each exhibited a single micro-unit (Table 21 and Appendix VI). S2 from GR 7555 (S2t, TS 861) differed from GR 5926, 7464 and 7519, evidence of sediment mixing being absent in TS 821. The factors that caused the mixing of sediments may have included pedoturbation and bioturbation. The evidence from GR 5926, 7464 and 7519 suggests that sediment mixing, partially attributed to bioturbation, was greater in the sediments surrounding the pelvis area than in the skull or feet regions.

Sample 3 from GR 7555 was adjacent to the coffin walls (Figure 7.2e) and exhibited two micro-units, one had an angular-blocky microstructure and one was apedal (TS 980 micro-units of 1 and 2, respectively, in Table 21). The former is tentatively interpreted as allogenic infill material, possibly from sediment entering the coffin through breaches in its structure (*e.g.* cracks in the coffin planks

or between the lid and the sides of the coffin). The timing is inferred to have been during the later stages of the degradation of the coffin. This inference was tested with an experimental section (TS 937; Appendix VI). The microstructure of the sediments in TS 980 was compared with a thin section produced from the same plane of the same sample block at a horizontal distance of between 0.5 and 1 cm (TS 937) (Experiment in Appendix VI). The thin section closer to the coffin (TS 937 had a more angular microstructure than that of the thin section further from the coffin (TS 980). The interpretation of the results of the experimental section (TS 937) supports the interpretation from the samples the angular-blocky microstructure sediment had formed outside the coffin and entered later than the less angular peds.

7.4.5 GR 5914 samples and C3 control

Sediments in thin sections of S3 (TS 907 and TS 936) and C3 (TS 887) from GR 5914 were similar in colour (PPL), interference colours (XPL) and coarse (50 μm limit) to fine ratio (Table 21). These two samples had different microstructures, with a sub-angular-blocky microstructure in S3 (TS 907 and TS 936) and micro-laminated deposits in the C3 control (TS 887). The S3 thin sections also differed from the C3 control: depletion hypocoatings were present in S3 and absent in the C3 control. Depletion hypocoatings are a pedofeature associated with redoximorphic conditions, and may form in sediments under reducing conditions.

Micromorphological differences were observed between the C3 and the pelvic region sample (S2) from GR 5914 (Table 21). The C3 control was composed of two micro-units: (1) an orange-grey micro-laminated micro-unit and (2) a yellow-grey weakly developed sub-angular-blocky one, with ≥90% fine material. By contrast, the S2 sample was composed of dark grey-brown apedal unsorted sediment with 50% coarse (>50 μm) materials, overlying a pale yellow-grey apedal fine (<50 μm) sediment. The micro-units of the pelvic region sample (S2) were different to the grave fill control as the S2 consisted of unsorted deposits rich in charred plant remains with mineral grains and fungal spores. The C3 control and the S2 sample were collected from sediments adjacent (5>10 cm distance) to each other (Section 7.2.1). The differences in thin section between the C3 control and the S2 sample illustrate the impact of the body on the sediments adjacent to it and lack of effect on sediments only a few centimetres away.

7.4.6 Micro-units in perpendicular and tangential oriented thin sections

Tangential thin sections often had one micro-unit and the perpendicular sections often had 2 or 3 micro-units (Table 21). However, in skull sediment samples from graves 7464 and 7519 (GR 7464, S1 and GR 7519, S1 and GR 7519, S13, Figure 7.2c and d, respectively) sediments were similar across

a sample block between the tangential and perpendicular thin sections (Table 21). The micro-units in the S1 sample from GR 7464 showed strong micromorphological similarities (colour, coarse to fine ratio and microstructure; Table 21) between the two differently orientated thin sections (TS 935 and 982). The S1 sample from GR 7519 also showed some similarities between its two thin sections (S1t, TS 888 and S1p, TS 873) including the upper (TS 881.1 and 873.1) and lower micro-units (TS 888.2 and 873.2). The difference between the upper micro-unit in the perpendicular and the tangential sections in this sample (GR 7529, S1) was a slightly greater abundance of coarse (>50 µm) mineral grains in the tangential section (TS 888.1, Table 21 and Appendix VI). The difference between the lower micro-unit in the perpendicular and the tangential sections in this sample (GR 7519, S1) was the presence of biotite and chlorite in the tangential section (TS 888.2) and absence in the perpendicular section (TS 873.2) (Table 22). Differences between tangential and perpendicular sections from the same block are interpreted as the result of changes in the sediment with distance from the human remains. The similarities in ped microstructure which is interpreted as evidence suggesting the sediments extend from the tangential to the perpendicular thin sections across a micromorphology block were also present in a pelvis region sample (S13, TS 908.1 and 938.1) from GR 7519.

7.4.7 Thin section analysis and archaeological questions

The questions raised by the excavators and samplers during sampling (Section 7.2.2) are discussed in the following sections relating to the interpretations of the evidence from thin section analysis.

7.4.7.1 Sample S2 from GR 7555

No faecal materials were observed in sample S2 from GR 7555. The perpendicular thin section of this sample differed from the other sampling positions in the presence of well stratified micro-laminations of alternating orange fine sediments and coarse mineral-rich sediments (S2p, TS 821; Figure 7.19). The micro-laminations were disturbed in the tangential thin section (S2t, TS 860), which had a bioturbated mineral-rich sediment. The micro-laminations with minerals which were highly weathered and an *in-situ* production of secondary minerals in the sediment surrounding the pelvis are interpreted as evidence of repeated cycles of waterlogging within the coffin. The coffin wood fragments in sections from this grave were heavily degraded compared with samples from the other graves, suggesting that degradation processes within GR 7555 were the most advanced. The presence of coarse/fine micro-laminations and an absence of angular-blocky peds in the S2 sections distinguishes them from those near the skull (S1) and feet (S3) in this grave. The presence of micro-laminations is interpreted as evidence of alternating conditions and the hydrated

authigenic minerals as evidence of water saturated conditions. The contrasting presence of laminated deposits in S2 and absence in S1 and S3 suggests that the pelvic area in GR 7555 could have been subjected to pooling events localised to this part of the grave. Such events could have inhibited the retention of solid materials which would have produced the faecal smell (present during excavation, Section 7.2.2) within the grave.

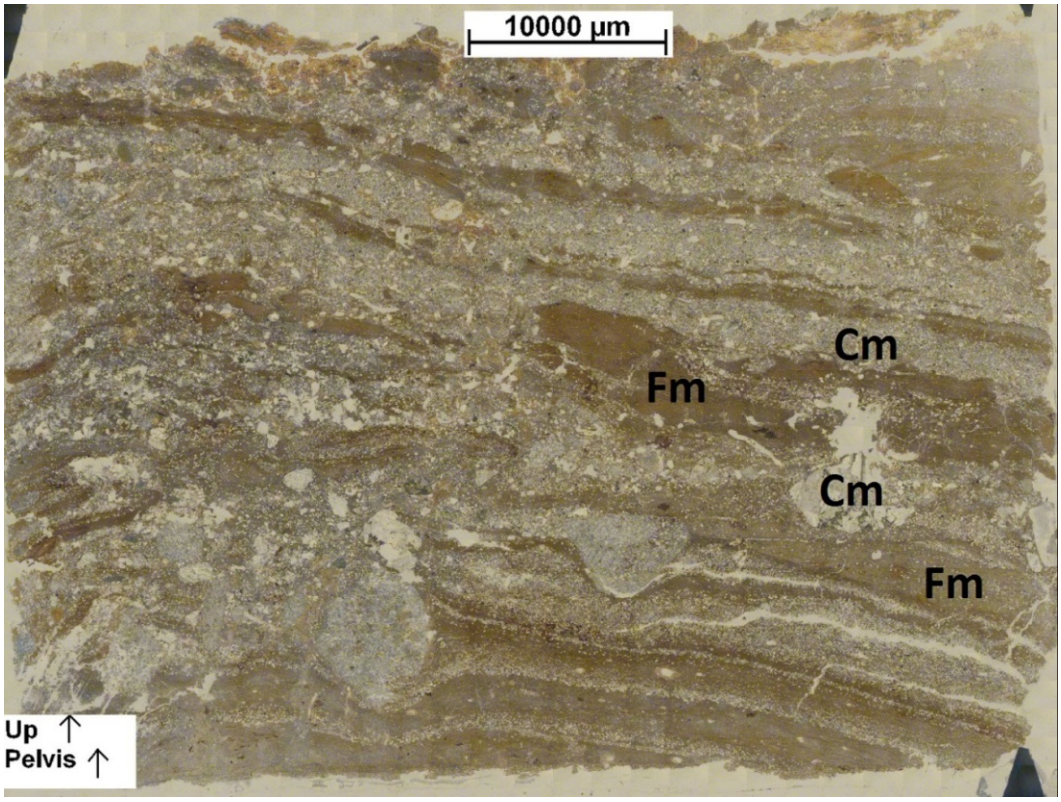

Figure 7.19: Mosaic image of a thin section with micro-laminations of fine material (Fm) alternating with coarse sediments (Cm) (GR 7555, S2p, TS 821). Some disturbance can be seen in the direction of the pelvis bone (left hand side of the TS). The content of the left hand side of this TS shows similarities to that of the tangential TS from this sample (GR 7555, S2t, TS 860).

7.4.7.2 Red fabric and black material in GR 5926

A very small red stain was visible in this grave during excavation and tentatively suggested as fabric remains (Figure 7.20; Section 7.2.2). Evidence of fabric remains was absent in the thin sections from GR 5926. The black material from the additional sample was identified as a charcoal-rich deposit, and these fragments gave the deposit a very dark brown colour which appeared black on-site.

Figure 7.20: Photograph taken on site of red material seen in GR 5926 (at end of knife point and red arrow), (photo courtesy of B. Keely).

7.4.7.3 Bone fragments in the infant burial (GR 7491)

In thin section, the bone in grave GR 7491 was isotropic (Figure 7.21b). The lack of colour in the bone in cross polarized light (XPL) differed to the grey interference colours of bone fragments in the sections from the other graves. The absence of interference colours in the infant bone (Figure 7.21b) and presence in the bone from the other graves (Figure 7.21d) is interpreted as resulting from the removal of the apatite component by post-depositional processes. First order grey interference colours are present in bone that has not been subjected to moderate or high temperature heating (Karkanas and Goldberg 2010, 524). Future work could include thin section analysis of reference material of fresh infant bone to confirm whether this is an effect of post-depositional alteration or a characteristic of infant bones. Alternatively, the isotropism inferring a low mineral content in these bone fragments could reflect the young age of the deceased as infants under one year have reduced mineral content in their bones and are prone to decay in acid soils (Mulder *et al.* 2007, Rauch and Schoenau 2001).

Bone was observed in thin sections from both of the skeletal adjacent samples from this grave (S9 and S4.) The selection of thin section of garve sediments rather than sieving was utilised on the grave fills from this site as one of the objectives of this work was to assess the contribution of micromorphology to the study of grave sediments (Objective 1, Section 1.3.1). In contrast to sieving, thin section analysis enables observation of micro-sized remains within their micro-contextual spatial relationships (Section 2.1). The fragments observed the foot region were all well below 500 µm along their longest visible axis, and smaller than 100 µm along their smallest dimension visible. If the material had been subjected to retrieval by floatation, the sieves would have had to have been ≤100 µm in mesh size in order to catch any of the bone fragments observed. Mesh sizes used in floatation sieving in archaeology are rarely smaller than 1 mm and thus would not have collected any bone fragments from these sediments. The similar size fractions of the coarse grained minerals and the bone fragments in these samples suggest that a smaller mesh sizes would not have isolated these bone fragments from the sediment. Hence, the evidence from samples from GR 7491 suggests that in future work bone fragments from burial sediments of infants

should be investigated through thin section analysis rather than floatation sieving. Sieving experiments of adult grave fills could not identify <4 mm sized fragments to skeletal element, however suggest infant grave sediments should be sieved to retrieve 0.5-2 mm pieces which could be useful for bone compositional analyses such as biomolecular (Mays *et al.* 2012). Further support for the usefulness of micro-scale bone fragments include the histomorphological analyses of faunal millimetre sized remains (Sawada *et al.* 2014) and authigenic phosphate minerals (whitlockite) associated with bones have been used to aid in interpretations of past burning events (Monge *et al.* 2014).

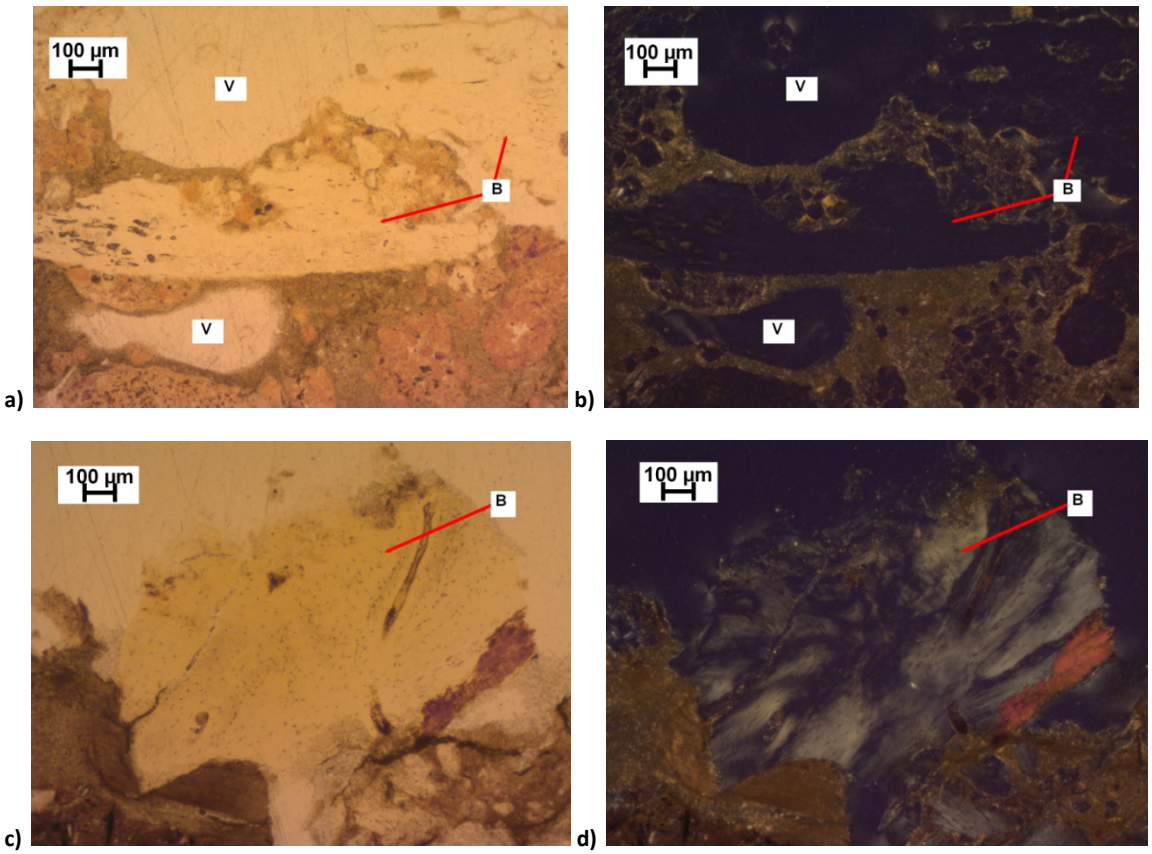

Figure 7.21: Bone fragments. (a) Bone within the foot region sample with a lack grey colours in cross polarized light (GR 7491, S2p, TS 969, PPL), and (b) XPL view of image a). (c) Bone from the skull region sample with grey colours in cross polarized light (GR 5914, S1, TS 995, PPL), and (b) XPL view of image c).

7.4.7.4 The fragmented skull in GR 7464

No discernible optical differences were observed between the sediments near the crushed skull of GR 7464 compared to those surrounding the skulls of the other sampled graves (*i.e.* GR 7555, GR 7519, or GR 5914).

7.4.8 Mineral weathering in graves

The differences observed in mineral weathering between the C1 controls and the samples, the C2 controls and the samples, and inter-grave samples are interpreted as evidence of the impact of the degradation of a body. Such differences include the weathering (extent and patterns) of the mineral components of the sediment and post-depositional alterations to the bone fragments and wooden coffins. Evidence of differences in the weathering pathways of micas have been described from the thin sections (Sections 7.3.4, 7.4.2 and 7.4.3), and are inferred to suggest the remains of biotite affected by alteration processes resulting in the chloritization of biotite (Parneix *et al.* 1985), these secondary (geologically) minerals are suggested to differ to the poorly crystalline chlorite present in some samples.

Heavily weathered muscovite was present and heavily weathered biotite was absent in the C1 controls. This pattern fits the normal trend in sediments, where muscovite, as a dioctahedral mica, is "much more resistant to weathering than trioctahedral micas, such as biotite, and release K^+ at much slower rates" (Fanning *et al.* 1989a, 552). Figure 7.12 in Section 7.3.4 illustrates this type of weathering, of mica into an expansible 2:1 clay mineral (Norrish 1973). It is known that micas are an important source of K, required by sediment fauna for growth (Figure 7.22), and that K may be released as K^+ cations by wetting and drying sediment development (Fanning *et al.* 1989a, 552). Weathered mica in the samples (Figures 7.17 and 7.18) could have been affected by dissolution and exchangeable cations. The evidence of less weathered biotite in the controls (Figure 7.12) is interpreted as suggesting an affect by the body and coffin on the grave sediment system, and could be related to a removal of K^+ in mica in samples (Figure 7.17).

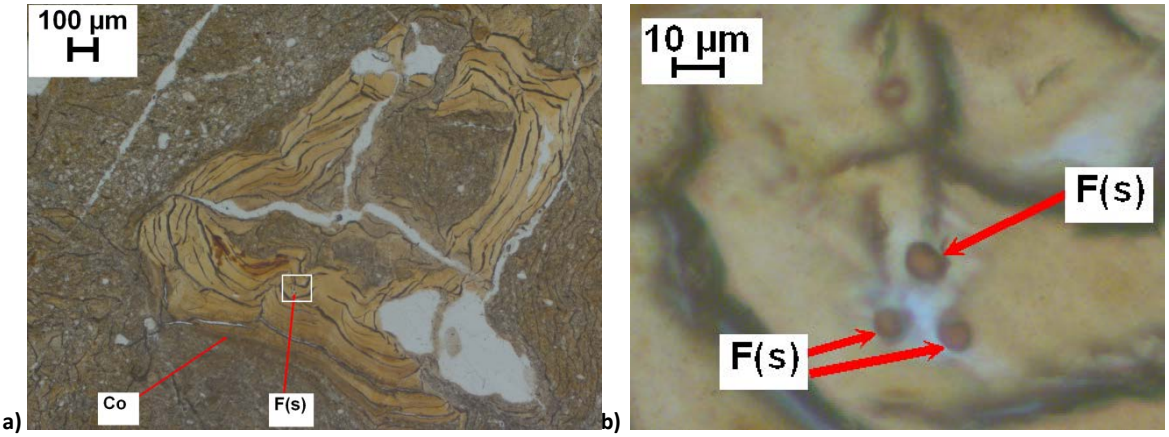

Figure 7.22: Yellow anisotropic laminated material, possibly a clay coating (Co) with fungal spores (F(s)) (GR 7519, S1p, TS 873.2, PPL), and (b) Detail of image inset (white rectangle) in image a), with fungal spores (F(s)) occupying a hole in the mineral, indicated by the blank resin (colourless area between spores).

The trends described above do not hold true for the weathering of primary mica. The grave fill controls (C3), instead, show preservation of biotite and a variety of weathering patterns on both muscovite and biotite, including primary mineral replacement by a secondary blue-green mineral. Replacements have included a variety of forms across the graves: accumulation of the secondary mineral in spaces between the sheet-like layers made available by expansion along parallel cleavage planes, replacement by the secondary mineral and alteration to an iso-alteromorph (terminology from Bisdom *et al.* 1982). The weathering pathways of micas are strongly dependent on several factors including the nature and activity of ions in the sediment. Formation of glauconite has been shown, in laboratory studies, to be possible through weathering of kaolinite in the presence of free Fe and K ions, with Fe mobilized by reduction with organic materials (Harder 1980), a process which may be complicated by the additional presence of Fe-oxidising bacteria (Ross *et al.* 1972; Fanning *et al.* 1989a, 607).

Biotite can be preferentially weathered before any associated muscovite in a sediment (Bisdom *et al.* 1982), according to the Goldich Weathering Sequence (Goldich 1938). Such weathering could, however, be affected by a burial, the corpse representing an additional variable. Furthermore, as "buried objects interact with their surroundings and change chemically and physically as they seek to come to equilibrium with their burial environment" (Caple 2001, 591), it is possible that muscovite and biotite weathering pathways could be affected by inhumations. Such a suggestion is supported by the literature as studies have shown that organic acids can promote mineral weathering (Huang and Keller 1970) and biotite can weather in sediments to produce secondary mineral products (Bisdom *et al.* 1982). In laboratory studies, fulvic acids have been shown to affect chlorites (Kodama and Schnitzer 1973), micas in closed systems (Schnitzer and Kodama 1976) and micas in open systems (Kodama *et al.* 1983). The rate of such mineral weathering in the presence of fulvic acids is strongly affected by the nature of the system: closed systems gave an exponentially decreasing rate whereas open systems gave a linear increasing rate (Kodama *et al.* 1983). In systems containing primary phyllosilicates and fulvic acids, the preferential dissolution is of Fe and Mg rather than K^+ (Kodama *et al.* 1983).

7.5 Conclusion

The sediments from the graves at Sala provide support for the interpretation of microbially-derived influences on the burial assemblage. The buried remains have become an active part of the biogeochemical cycles of their surrounding sediments and sediments. The micromorphological investigation showed clear differences between the C1 controls and samples, as well as inter- and

intra-grave differences. Processes identified in these sediments were mineral-microbial associations, inferred from mineral weathering (microbial presence and mineral weathering extents and patterns), bioturbation related to destruction of microstratigraphy, coffin presence related to the deposition of microlaminates of fine material within a coffin with rising and falling water levels, and the relative proportions of contrasting micro-units between clay-rich and quartz-rich micro-layers. In order to allow comparisons between the sediments adjacent to and not adjacent to the skeleton and hence to distinguish pre- from post-burial features, it is recommended that in future works, sampling procedures are modified to include sediments from both within grave cuts and outside the grave cuts either below or at the level of the graves.

Identifications of sediment fungi can provide evidence for the interpretation of degraded organic materials which have been buried. In archaeological studies this has previously been successfully implemented regarding cereals (rye and wheat) by the presence of the rye/wheat bunt fungi (*Telletia spp*.) (Carris and Castlebury 2008). The fungi *Telletia* have very distinctive globuse and reticulate conidia and are able to preserve often for long periods of time (Carris and Castlebury 2008). Future studies could investigate the use of fungi in the grave sediments as proxy data to infer degraded wood in burials where coffins are no longer visible.

Chapter 8. Experimental Burials: Hovingham, Pig 1

8.1 Introduction

A pig was interred at Hovingham as an experimental burial, in sand (Pig 1); Chapter 1 Section 1.4.1). The principal merit of the study of experimental burials is the ability to isolate post- from pre-depositional and depositional variables (Chapter 1), and to use such inferences in the interpretation of the archaeological burials (Chapters 4-7).

8.2 Materials and methods

8.2.1 Burial of Pig 1

Pig one was buried in a coffin in the village of Hovingham, North Yorkshire. Although buried in allogenic material, the location of these burials at this site (Figure 8.1) may be relevant in terms of climate, rather than sediment type and underlying geology, as the grave was filled with imported sand. The construction sand, purchased for this purpose, was sampled (C0) prior to burial and organic geochemical analysis (elemental analysis and GC-MS, performed by the InterArChive team) suggested it to have been free of organic components prior to burial. The burial pit was cut into the local sediment, boarded at the sides with wood (Figure 8.2a) and filled to a depth of 1.5 m with sand. The pig was buried with two muslin bags, both filled with organic materials, one of which was sewn into the abdomen and the other which was placed by the snout with a wicker basket (Table 23). The pig and associated grave goods (Table 23) were placed in a coffin containing a shallow fill of sand (Figure 8.2b) and the remaining space was filled with sand. Pig 1 was interred for three years before excavation, during which time it had accumulated leaf litter on top of the mesh which had been laid to deter scavenging animals (Figure 8.3). The results from the analyses of the pre-burial sample (C0) and excavation samples are discussed together in Section 8.3.

The experimental design of this burial, including the selection of foods buried as grave goods, was organized by the InterArChive Project (Section 1.1.1) and the work presented here has taken advantage of the opportunity to analyse the excavated sediments. The combination of food items deposited with the pig is acknowledged as materials unlikely to have been combined in a single site in an archaeological setting (Table 23). The rationale for the selection of food items stated by the InterArChive project was that the wide range of foods was selected on the suggestion that this could enable a more thorough investigation of which types of food items could preserve trace evidence in sediments (Brothwell, pers. comm.).

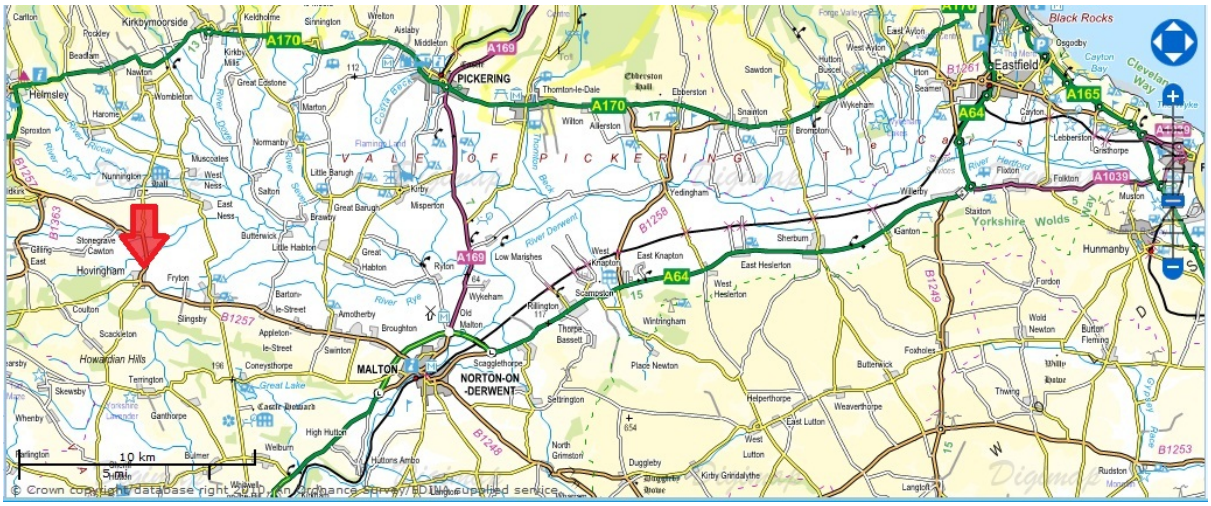

Figure 8.1: Location of Hovingham (red arrow) in North Yorkshire (modified from OS map)

a) 

b) 

Figure 8.2: Burial of Pig 1. a) Coffin in the boarded grave cut. B) Pig in coffin with sand, accompanied by grave goods. Muslin bags containing foodstuffs were placed in the abdominal area and adjacent to the snout.

Table 23: List of items deposited with Pig 1 during burial.

Contents of internal muslin bag	Contents of external muslin bag within coffin	Other items external items deposited within coffin
Rolled oats - 25 g Desiccated coconut - 25 g Dried clementine peel 5 g Dried apple peel ~2 g Ground ginger - 1 teaspoon Ground cinnamon - 1 levelled teaspoon Red kidney beans - 25 g	Florets of Cloves- 60 Tobacco ('Amber leaf') – 5 g Beeswax - 5 g	Wicker basket Hair (human)

Figure 8.3: Area of Pig 1 burial immediately prior to excavation, showing leaf litter on top of the grave and grass vegetation covering the local area adjacent to the grave.

8.2.2 Excavation and sampling

The InterArChive sampling methodology for human burials was modified for the purposes of the experimental burials (Appendix VII). The modifications included the collection of C0 (Section 8.1) and C4 controls (Figure 8.4) in addition to the C2 and C3 controls in the archaeological excavation sampling protocol. Sampling sediment from the C4 position was made possible by the coffin having been filled both below and above the interred remains.

The experimental design of the pig burial and sole use by the InterArChive project permitted intensive sampling, facilitating collection of multiple C2, C3 and C4 controls. Three C2 controls,

three C3 controls and two C4 controls were collected (Table 24). Sediment from near the skull (S1), tail (S2), front trotters (S17) and rear trotters (S3) were sampled (Figure 8.5) and additional samples (Table 24) are referred to as SA1-*n* (Chapter 3).

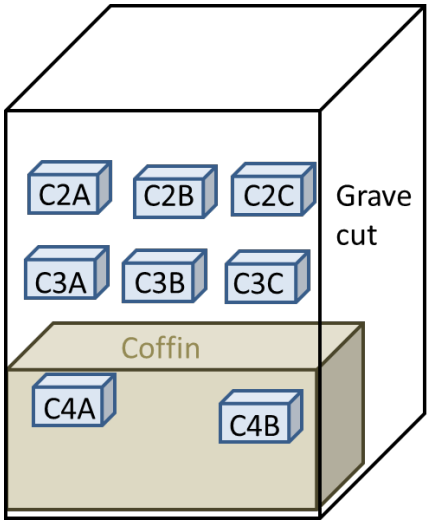

Figure 8.4: Diagram of location of controls (C2A-C, C3A-C, and C4A-B) for Pig 1.

Table 24: Controls (a) and samples (b) from excavation.

a)

Control	Description	Thin section numbers
C2A	C2, centre, 14 cm depth	1232
C2B	C2, south corner, 13.5 cm depth	1230
C2C	C2, north corner, 15.5 cm depth	1206
C3A	C3, centre, 22.5 cm depth	1207
C3B	C3, south corner, 20.5 cm depth	1231
C3C	C3, north corner, 23 cm depth	1208
C4A	C4, intra-coffin and above inhumed remains, east end of coffin	1163
C4B	C4, intra-coffin and above inhumed remains, west end of coffin	1161

b)

Sample	Description	Thin section numbers
S1Y	skull adjacent	1182, 1229, 1244
S2Y	tail adjacent	1242, 1255, 1254
S3Y	left rear trotter adjacent	1240, 1241
S17Y	left front trotter adjacent	1243, 1257, 1263
SA32	Corner of base of coffin sediment	1253

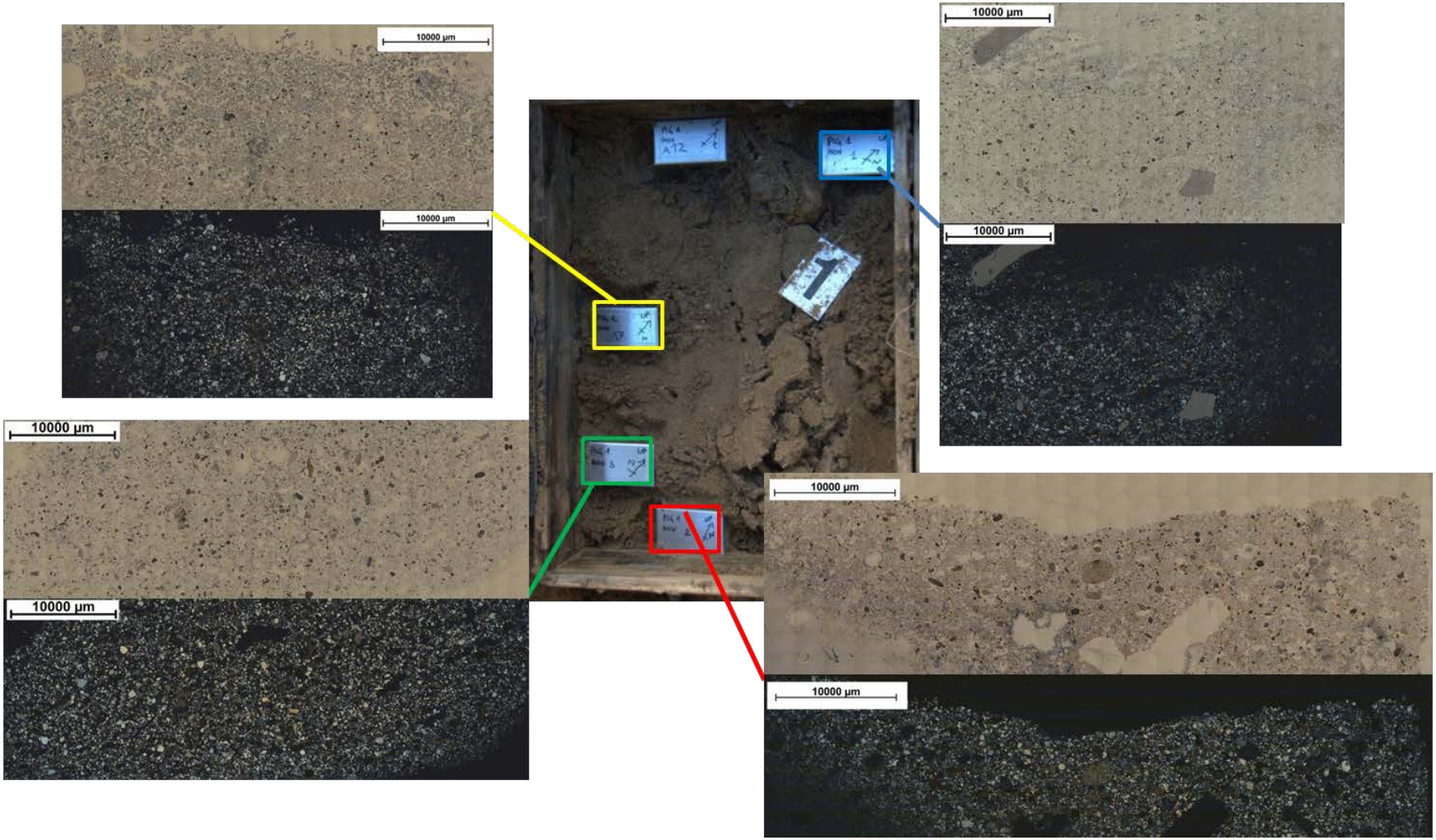

Figure 8.5: Micromorphology samples and thin sections. Mosaic images are shown in PPL and XPL for sampling positions S1 (TS 1244), S2 (TS 1254), S3 (TS 1240) and S17 (TS 1257).

8.3. Thin section analysis

8.3.1 Micromorphological observations

Thin sections were recorded as listed in Chapter 3 and detailed thin section descriptions are given in Appendix VII and summarised in Table 25. The controls and samples were mainly composed of quartzose sand-sized sediments with a single population related distribution of coarse to fine materials and an apedal microstructure (Table 25). The single population coarse fine related distribution indicates that the sediment is almost entirely composed of materials of a homogeneous size. The pre-burial control (C0, TS 1262) had the lowest coarse to fine ratio (40/60) (Table 25). Types of voids included channels, chambers and vughs, with vugh shaped voids the most common in both controls and samples (Table 25). Red anisotropic deposits, interpreted as iron-rich, were present in fractures of quartz grains in controls C3 and C4 (Table 25). A range of colours of nodules were observed in controls and samples (Table 25). Excremental pedofeatures were present in the C4 controls and some of the samples where they were absent from the C2, C3 and C0 controls. The mineralogical components in the thin sections from Pig 1 are assessed in detail in Appendix VII and summarised in Table 26. Granite and limestone rock fragments and feldspars, amphiboles, clinopyroxene and glauconite minerals were present in controls and samples (Table 26). Fibrous chalcedony was present in some of the thin sections from within the coffin (C4A and S3) and absent from controls above the coffin (C2 and C3 controls). Calcium carbonate-rich materials such as shell and sparry calcite, were present in some of the controls (C2, C3 and C4 controls) and absent in the samples (except for S1; Table 26). The sand for the experiment was purchased as construction sand and the source is unknown other than as limited to within the EU.

Table 25: Summary of micromorphological observations[10].

TS	S	c/f ratio (50µm limit)	Voids					Pedofeatures								Inorganics									Organics		
								intrusive		matrix coatings	nodules					Quartz		Limestone		Granite		Shell					
			ve	ch	cb	vu	cr	red/Fe-rich	grey/ CO_3 rich	hypo.	red	op.	CO_3	laminated (opaque to red)	Excr.	(%)	sizes	(%)	sizes	(%)	sizes	(%)	sizes	AMO	Pl	Fungal remains
1262	C0	40, 60	0	2	2	15	0	0	0	5	0	0	0	0	0	30	sm, sm-m, m, m-lr, lr	50	lr, v.lr	0	/	0	/	0	1	0
1232	C2A	95, 5	0	2	<1	15	0	0	0	0	2	2	0	2	0	70	sm-m, m, m-lr, lr, v.lr	5	lr, v.lr	0	/	<1	lr	0	0	0
1230	C2B	95, 5	0	1	0	10	0	0	0	0	6	0	0	0	0	70	sm-m,m, m-lr, lr	2	lr, v.lr	2	lr, v.lr	2	m-lr, lr	0	1	0
1206	C2C	90, 10	0	2	0	10	0	0	0	1	2	2	0	0	0	65	sm-m, m, m-lr	5	lr, v.lr	1	lr, v.lr	2	m-lr, lr	0	<1	0
1207	C3A	90, 10	0	2	1	10	0	2	0	<1	5	0	<1	0	0	60	sm-m, m, m-lr, lr	1	lr, v.lr	2	lr, v.lr	2	m-lr, lr	0	2	0
1231	C3B	90, 10	0	1	0	10	0	2	0	0	2	2	0	0	0	70	sm-m, m, m-lr, lr, v.lr	2	lr, v.lr	2	lr, v.lr	0	/	0	0	0
1208	C3C	90, 10	0	5	1	5	0	2	0	<1	3	1	0	0	0	65	sm-m, m, m-lr, lr	1	lr, v.lr	1	lr, v.lr	0	/	0	1	0
1163	C4A	90, 10	0	1	0	10	0	1	0	5	2	1	1	1	0	65	sm-m, m, m-lr, lr	5	lr, v.lr	2	m-lr, lr	<1	m, m-lr	0	5	0
1161	C4B	90, 10	0	2	0	10	0	1	0	5	1	1	0	1	2	60	sm-m, m, m-lr, lr	1	m-lr, lr, v.lr	1	m, m-lr	<1	m-lr, lr	0	2	0
1182	1	85, 15	0	2	0	10	0	5	0	5	5	0	2	0	0	60	sm-m, m, m-lr, lr	5	lr, v.lr	5	m, m-lr	2	lr	0	2	0
1254	2	70, 30	0	5	5	5	0	0	0	15	5	0	0	0	2	60	m, m-lr, lr	1	m-lr	2	m-lr, lr	0	/	0	0	0
1240	3	90, 10	0	1	0	10	0	5	0	2	5	0	0	1	0	55	sm, sm-m, m, m-lr, lr	0	/	5	m, m-lr, v.lr	0	/	0	0	0
1257	17	60, 40	0	1	0	20	0	0	0	10	2	0	0	0	1	50	m, m-lr, lr	2	m-lr, lr	2	m-lr	0	/	0	0	1
1253	A32(µ-u1)	2, 98	0	0	0	15	0	0	0	0	0	0	0	0	0	100	m-lr, lr	0	/	0	/	0	/	0	0	0
1253	A32(µ-u2)	80, 20	0	0	0	10	0	0	0	10	5	0	0	0	0	60	sm-m, m, m-lr, lr	5	m-lr, lr, v.lr	2	lr	0	/	0	0	0

[10] Relative proportions of coarse compared to fine materials (with fine limit set at 50µm) is recorded in the column 'c/f ratio'. Estimated abundance has been assessed using the estimated abundance charts of Bullock *et al.* (1985). This summary table has been abridged by the removal of columns (categories) which contained no variation across all of the thin sections (rows), this includes the categories of: b-fabric (cristallitic), limpidity (limpid), related distribution of coarse to fine materials (single population) and type of pedostructure (apedal). Abbreviations used are as follows: thin section (TS), sample (S), vesicles (ve), channels (ch), chambers (cb), vughs (vu), cracks (cr), hypocoatings (hypo.), excremental pedofeatures (Excr.), amorphous organic matter (AMO), and plant (Pl). All sizes are given in µm. Classes used to describe size for inorganics are as follows: v sm (<30 µm), sm (30-50 µm), sm-m (50-100 µm), m (100-300 µm), m-lr (300-500 µm), lr (500-1000 µm), v. lr (>1000 µm).

Table 26: Qualitative mineralogical assessment of thin sections: rocks, minerals, and inorganic remains of biological origin. White cells denote presence and grey cells absence of a feature[11].

TS	S	Minerals								Rocks				Other						
		Tectosilicates				Inosilicates		Phyllosilicates		Lme	Gn	Cc	Other	CaCO3-rich materials of various morphologies						
		Qz	Pg	Mcl	Acic. Fd	CPX	AP	Gc	Other					ooid	shell	acicular	rhombohedra	sparry	amorphous	
1262	C0																			
1232	C2A																			
1230	C2B																			
1206	C2C																			
1207	C3A																			
1231	C3B																			
1208	C3C																			
1163	C4A																			
1161	C4B																			
1182	1																			
1254	2																			
1240	3																			
1257	17																			
1253	A32(µ-u1)																			
1253	A32(µ-u2)																			

[11] Abbreviations used are as follows: thin section (TS), sample (S), quartz (Qz), microcline (Mcl), plagioclase series feldspars (Pg), radial acicular feldspars (Acic. Fd), clinopyroxene (CPX), amphiboles of tremolite-actinolite series and glaucophane-reibeckite series (AP), glauconite (Gc), and for the calcium carbonate-rich materials ($CaCO_3$) sub-categories are made by differentiation based on morphology.

8.3.2 Rocks and minerals

Rocks and minerals were identified in thin section by use of their distinguishing optical characteristics and mineral weathering (Chapter 3). Detailed observations on mineral weathering from the sediments are given in Appendix VII and summarised in Table 27. Quartz, plagioclase and microcline weathering was mostly limited to extent one in controls and samples (Table 27). Pyroxene, amphibole, olivine and glauconite were observed weathered mostly at extent two or greater (Table 27). Limestone, calcite and granitic rock fragments and shell fragments and ooids were present and weathered to extents one or two in samples and controls (Table 27).

Table 27: Micromorphological observations on weathering and estimated abundance (%) of rocks, minerals, and inorganic materials of biological origin[12].

TS	S	Inorganics																													
		Minerals																Rocks							Other							
		Tecto							Inos				Neso		Phyllo			Lme	Lme w	Gn	Gn w	Cc	Cc w	Other	Or l	Or l w	Shell	Shell w	Ooid	Ooid w		
		Qz	Qz w	Pg	Pg w	Mcl	Mcl w	Other	PX	PX w	AP	AP w	Ov	Ov w	Gc	Gc w	Other															
1232	C2A	*********	I	_	/	*	I	_	_	/	_	/	_	/	*	I	_	**	I	_	/	*	I	_	*		_	I	_	/		
1230	C2B	*********	I	_	/	_	/	_	_	/	*	II	_	/	*	I	*	*	I	*	I	*	I	_	*		*	I	_	/		
1206	C2C	********	II	_	/	_	/	_	_	/	_	/	_	/	_	/	*	**	I	*	II	*	II	*	*		*	I	*	I		
1207	C3A	********	I	_	/	*	I	_	_	/	*	I	_	/	*	II	*	*	I	*	II	*	II	*	*		*	II	_	/		
1231	C3B	*********	I	_	/	_	/	_	_	/	_	/	*	II	_	/	*	*	I	*	I	*	I	*	*		_	/	_	/		
1208	C3C	********	I	_	/	*	I	_	_	/	*	I	_	/	*	II	_	*	I	*	II	_	/	_	_	/	_	/	_	/		
1163	C4A	********	I	*	I	*	I	*	*	I	_	/	_	/	_	/	_	**	I	*	I	*	II	*	*	II	*	I	*	II		
1161	C4B	********	I	_	/	*	I	_	*	II	*	II	_	/	*	II	_	*	II	*	II	_	/	*	*		*	II	_	/		
1182	1	********	I	*	II	*	I	_	*	IV	*	II	_	/	*	I	_	**	II	**	II	*	II	*	*	/	*	II	_	/		
1240	3	*******	I	_	/	*	I	*	*	II	_	/	_	/	*	I	_	_	/	**	II	_	_	_	_	/	_	/	_	/		
1262	C0	********	I	_	/	*	I	_	_	/	_	/	_	/	_	/	_	**	I	*	II	_	/	_	_	/	_	/	_	/		
1254	2	********	I	_	/	*	I	_	_	/	_	/	_	/	*	I	_	*	I	*	II	_	/	_	_	/	_	/	_	/		
1257	17	*******	I	_	/	_	/	_	_	/	*	I	_	/	_	/	_	*	II	*	II	*	I	_	_	/	_	/	_	/		
1253	A32(µ-u1)	*********	I	_	/	_	/	_	_	/	_	/	_	/	_	/	_		/		/	_	/	_	_	/	_	/	_	/		
1253	A32(µ-u2)	********	I	_	/	*	I	_	_	/	_	/	_	/	_	/	_	**	I	*	II	_	/	_	_	/	_	/	_	/		

[12] Estimated percentage abundance (Bullock *et al.* 1980) is represented by symbols as follows: <1 (_), 1-2 (*), 5≥10 (**), 10≥20 (***), 30≥40 (****), 40≥50 (*****), 50≥60 (******), 60≥70 (*******), 70≥80 (*********). Extent of weathering is represented in column heads for each inorganic subdivision by the addition of (w) after each sub-class nomenclature. Measurements of weathering extent (scalar data, assessed as from 1-4) is represented by Roman numerals (I-IV). In cases where extent of weathering is not applicable due to negligible results for presence of a material the symbol (/) is used. Abbreviations used are as follows: thin section (TS), sample (S), quartz (Qz), plagioclase feldspar series (Pg), microcline (Mcl), pyroxenes (PX), amphiboles (AP), olivine (Ov), limestone (Lme), granite (Gn), calcite (Cc), unidentified orange laminar material (Or l).

8.3.2.1 Quartz

The thin sections from the experimental burial of Pig 1 were dominated by sand-sized quartz grains (Table 25). The size ranges of the quartz grains (small-medium to large) was similar across all of the thin sections analysed (Table 25). In most thin sections the weathering extent of the quartz grains was extent 1 (Table 28), signifying 2.5-25% volume altered from the primary mineral. The patterns of weathering of the quartz were recorded as either pellicular or pellicular and irregular linear (Table 28). Pellicular weathering was present as etching pits and v-shaped percussion marks. Smaller (<10 μm) irregular edges at grain boundaries which could be the result of a wedging effect in thin section. No secondary products formed from quartz weathering were observed. Similar quartz weathering patterns and extent between controls and samples is interpreted as evidence that their weathering affects are the result of pre-depositional processes and that the quartz was unaffected by the 3 years in the burial sediment. Such interpretations are supported by the literature regarding quartz as a stable sediment mineral that is not readily weathered (Goldich 1938).

Table 28: Quartz weathering

TS	S	Quartz		
		Estimated abundance (%)	Weathering	
			extent	pattern
1262	C0	30	1	pellicular & irregular linear
1232	C2A	70	1	pellicular
1230	C2B	70	1	pellicular
1206	C2C	65	2	pellicular & irregular linear
1207	C3A	60	1	pellicular & irregular linear
1231	C3B	70	1	pellicular & irregular linear
1208	C3C	65	1	pellicular
1163	C4A	65	1	pellicular
1161	C4B	60	1	pellicular & irregular linear
1182	1	60	1	pellicular
1254	2	60	1	pellicular & irregular linear
1240	3	55	1	pellicular
1257	17	50	1	pellicular & irregular linear
1253	A32(μ-u1)	100	1	pellicular & irregular linear
1253	A32(μ-u2)	60	1	pellicular & irregular linear

8.3.2.2 Feldspars

Feldspars were present in the thin sections from Pig 1 (Table 26). Types observed include plagioclase series, alkali feldspars (microcline), and feldspars of a radially arranged acicular

structure with a spherical morphology (Table 26 and Figure 8.6). The extent of weathering of feldspars was almost exclusively extent one (corresponding to 2.5-25% by volume of the primary mineral altered) and of pellicular pattern (both regular and irregular pellicular patterns observed), with the exception of the plagioclase series feldspars from Sample S1 (Table 27). These minerals displayed a slightly greater extent of weathering, extent two (25-75% altered) (Table 27). The greater extent of weathering of the plagioclases in the S1 sample compared to that in the controls (C4A) is interpreted as evidence to suggest that calcium-sodium-rich materials are less stable in the burial sediment (S1) than in the upper grave fill (C4A) and were more susceptible to weathering than the alkali feldspars.

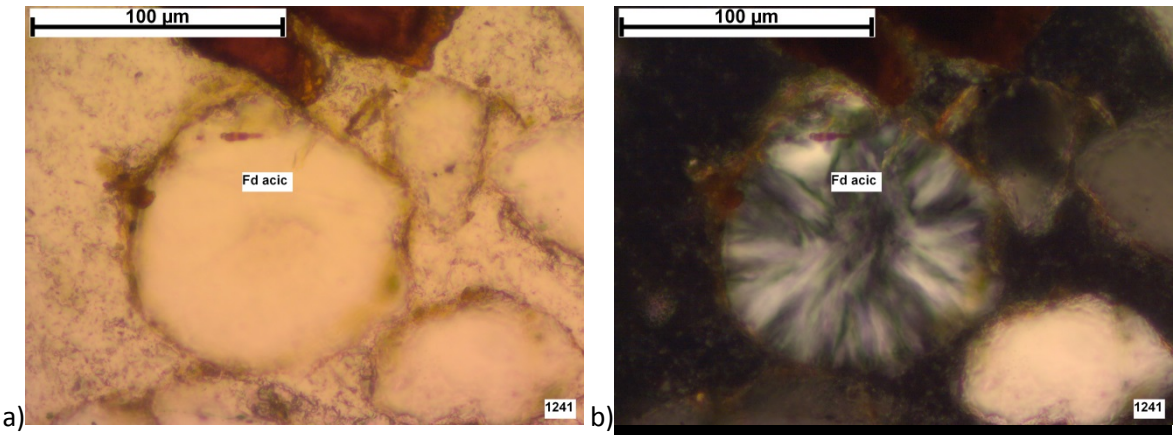

Figure 8.6: Fibrous chalcedony with circular or spherical morphology and a radially arranged acicular structure. a) The fibrous chalcedony grain (Fd acic) is colourless in PPL with slight pellicular weathering effects visible at the edges (Pig 1, S1, TS 1241, PPL). b) XPL view of image a) displaying the feldspar grain's (Fd acic) first order grey interference colours and radial structure (Pig 1, S1, TS 1241, XPL).

8.3.2.3 Amphiboles and clinopyroxene

Amphiboles were present both within and above the coffin (Table 26). By contrast, clinopyroxene was present only in sections of sediments from within the coffin (controls C4A and C4B and samples S1 and S3; Table 26). Clinopyroxene was present in TS 1163 (C4A control) at weathering extent one, TS 1161 (C4B control) at weathering extent two, TS 1182 (S1) at weathering extent four and in TS 1240 (S3) at weathering extent two (Table 29). Amphiboles were divided into two groups, grey and green, based on their colours and interference colours (Table 29). Both groups were pleochroic and displayed typical cleavage angles (124 and 56 degrees, MacKenzie and Adams 1994, 16 and Figure 8.8d). The green amphiboles displayed strong pleochroism, ranging from very pale green to dark olive green, and high second order colours (Appendix VII). The grey amphiboles displayed a narrower range of pleochroism, ranging from pale grey to medium grey, and lower interference colours (second order green; Figure 8.7). Such optical characteristics are interpreted to suggest that the two amphibole types (green and grey) are from the tremolite-actinolite series (calcic

amphibole) and the reibeckite-glaucophane series (sodic amphibole) mineral groups, respectively. Further work could consider the distributions of tremolite and reibeckite series in relation to the areas of the grave and differences in sediment processes between grave sediments and controls. Contrasts between the colours of the amphiboles in the controls and samples were identified in thin sections from Al Khiday (Chapter 5) and Tel Qarassa (Chapter 6). The interpretation of the distributions of amphiboles and burial sediment processes is discussed further in Chapter 9.

Table 29: Optical characteristics of amphiboles and clinopyroxene in thin sections: estimated abundance (Bullock *et al.* 1985) colours, morphology and weathering[13].

TS	S	Inosilicates											
		CPX			AP								
					Olive green pleochroism			Grey pleochroism			Green-blue pleochroism		
		Estimated abundance	Weathering		Estimated abundance	Weathering		Estimated abundance	Weathering		Estimated abundance	Weathering	
		(%)	extent	pattern	(%)	extent	pattern	(%)	extent	pattern	(%)	extent	pattern
1262	C0	_	/	/	_	/	/	_	/	/	_	/	/
1232	C2A	_	/	/	_	/	/	_	/	/	1	1	pellicular
1230	C2B	_	/	/	<1	2	pellicular	_	/	/	1	2	pellicular
1206	C2C	_	/	/	_	/	/	_	/	/	_	/	/
1207	C3A	_	/	/	<1	1	pellicular	_	/	/	_	/	/
1231	C3B	<1	2	complex	_	/	/	_	/	/	_	/	/
1208	C3C	_	/	/	_	/	/	_	/	/	2	1	pellicular and regular linear
1163	C4A	1	1	pellicular	_	/	/	_	/	/	_	/	/
1161	C4B	1	2	pellicular	1	2	pellicular	1	2	pellicular	_	/	/
1182	1	1	4	complex to phanto-alteromorph	_	/	/	1	2	complex	_	/	/
1254	2	_	/	/	_	/	/	_	/	/	_	/	/
1240	3	1	2	pellicular	_	/	/	_	/	/	_	/	/
1257	17	_	/	/	_	/	/	_	/	/	_	/	/
1253	A32(µ-u1)	_	/	/	_	/	/	_	/	/	_	/	/
1253	A32(µ-u2)	_	/	/	_	/	/	_	/	/	_	/	/

[13] In cases where extent of weathering could not be determined the symbol (/) is used. Abbreviations used are as follows: thin section (TS), sample (S), clinopyroxene (CPX), and amphibole (AP). Classes used to describe size for inorganics are as follows: v sm (<30 µm), sm (30-50 µm), sm-m (50-100 µm), m (100-300 µm), m-lr (300-500 µm), lr (500-1000 µm), v. lr (>1000 µm).

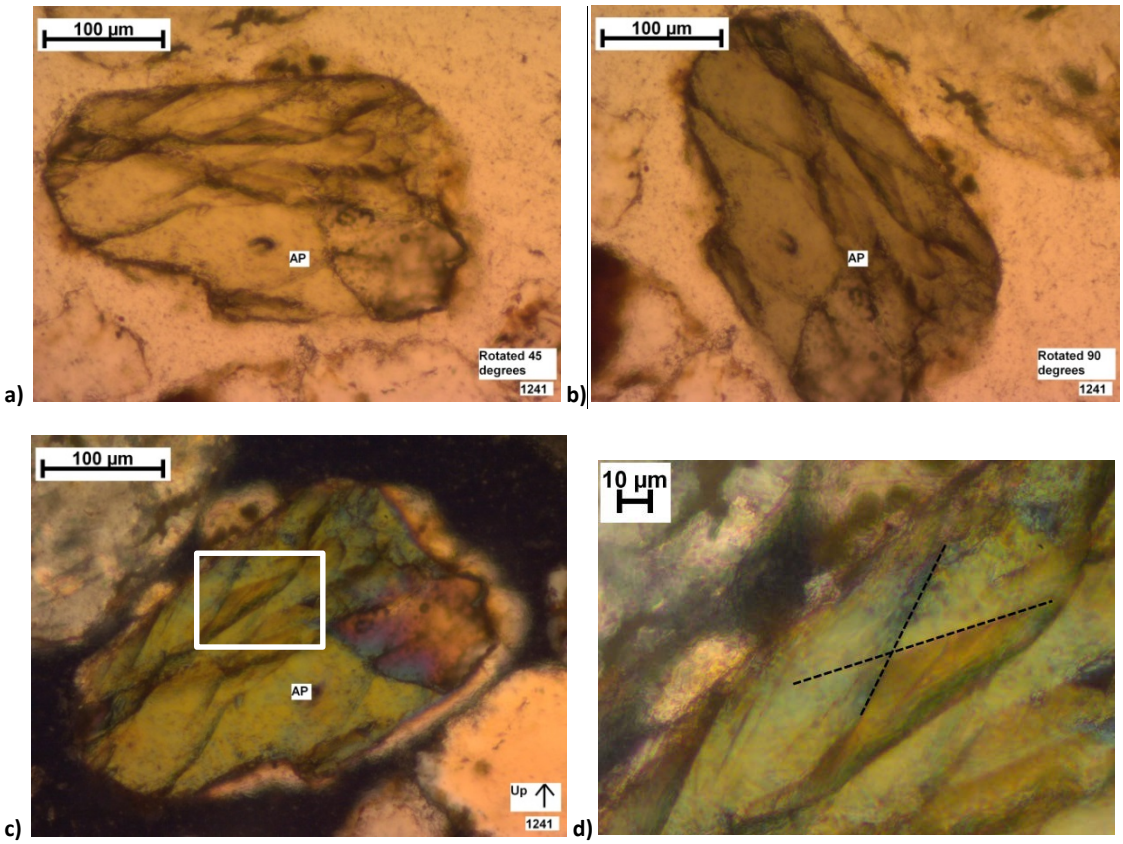

Figure 8.7: Amphibole grain (AP) from S1, TS 1241. a) Rotated to 45 degrees to display weakest pleochroism of this grain (PPL). b) Rotated to 90 degrees to display strongest pleochroism (PPL). c) XPL view (0 degrees of rotation) to show second order green interference colours with decreasing interference colours at the edges of grain, which could be due to a wedging effect (XPL). d) Detail of inset in image c) with black dashed lines highlighting cleavage planes which conform to the typical angles (*i.e.* 126 and 54 degrees) for amphiboles (XPL).

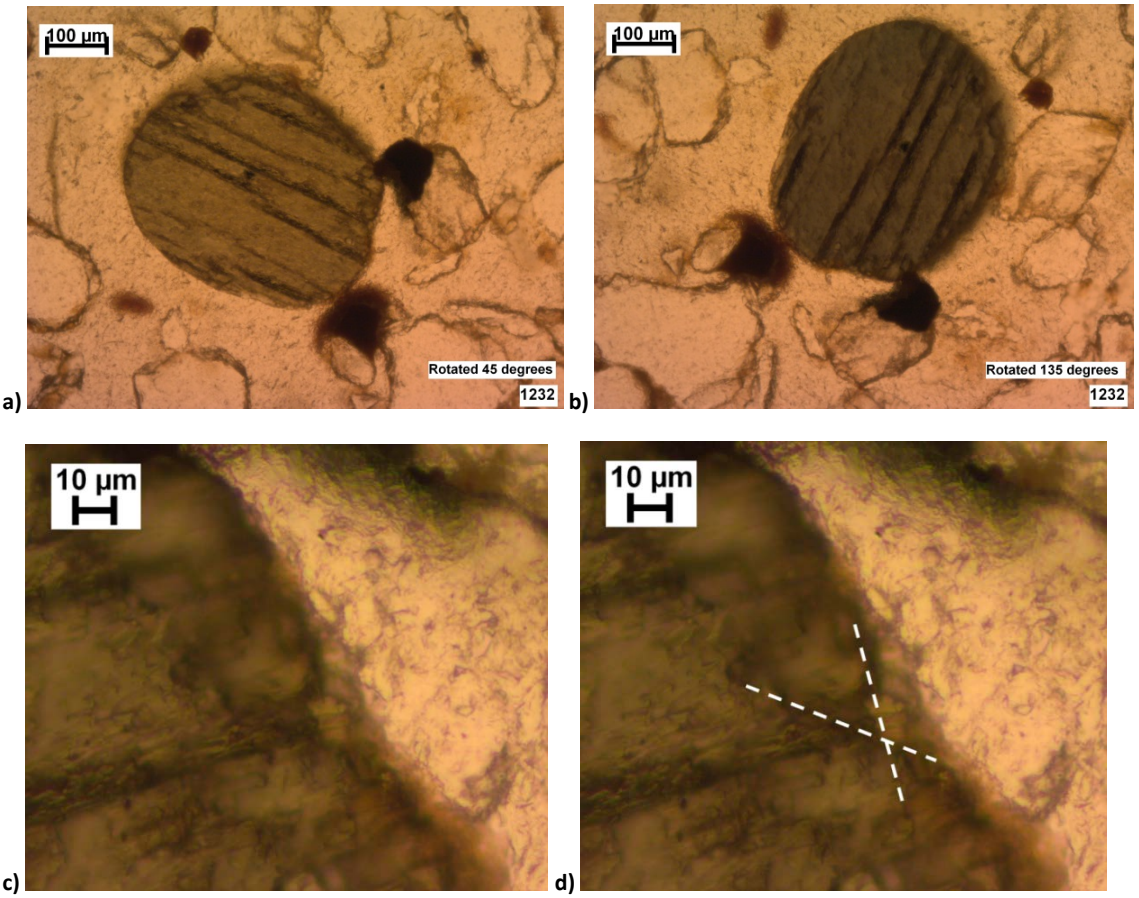

Figure 8.8: Blue to green amphibole displaying anhedral morphology with one of two cleavages well expressed except at the edges of the grain. a) blue-green amphibole mineral, the plate has been rotated 45 degrees to show the palest colour observable from the range of pleochroic colours for this grain (C2A, TS 1232, PPL). b) blue-green amphibole mineral in image a) rotated 135 degrees to show the darkest shade observable from the range of pleochroic colours for this grain (C2A, TS 1232, PPL). c) Detail of edge of grain shown in images a) and b) (C2A, TS 1232, PPL). d) Repetition of image c) but with annotations to highlight fracturing (C2A, TS 1232, PPL).

8.3.2.4 Glauconite

Glauconite was present in at least one of the thin sections from each of the controls (C2, C3, and C4) as well as in Sample S1 and additional sample SA32 (Table 26). The types of weathering affecting the glauconite were recorded through identification of the alteration on the grains (Table 30). The glauconite in the upper controls (C2A-C) displayed yellow-green colours and diffuse edges with slight red accumulations, which could be an iron-rich material, at their lower boundaries (Figure 8.9a). That in the samples displayed darker colours (brownish-green) and clearly delineated edges but with fractures penetrating the grain from the external margins (Figure 8.9b). Interpretations based on the weathering of glauconite are discussed in Section 8.3.5.3.

Table 30: Observations of glauconite estimated abundance (%), colour, morphology and weathering[14].

TS	S	Estimated abundance (%)	sizes	angularity	morphology	colours (PPL)	interference colours (XPL)	Weathering		colours (PPL) of weathered regions
								extent	pattern	
1262	C0	0	/		/	/	/	/	/	/
1232	C2A	<1	m	R	lobate	green	2nd order greens and yellows	1	pellicular	green
1230	C2B	1	m, m-lr	SR	lobate	green	2nd order greens and yellows	1	pellicular	green
1206	C2C	0	_	/	/	/	/	/	/	/
1207	C3A	1	m-lr, lr	SR	lobate	green	2nd order greens and yellows	2	pellicular	green
1231	C3B	0	_	/	/	/	/	/	/	/
1208	C3C	1	m-lr, lr	SR	lobate	dark red and green	anomalous dark red and 2nd order greens and yellows	2	complex	red
1163	C4A	0	_	/	/	/	/	/	/	/
1161	C4B	1	sm-m, m, m-lr	R	lobate and circular	dark red and green	anomalous dark red and 2nd order greens and yellows	2	complex	red
1182	1	1	m-lr	R	elliptical	brownish green	2nd order greens and yellows	1	pellicular & irregular digitate	brownish green
1254	2	1	1	linear	circular	brownish green	2nd order greens and yellows	1	linear	brownish green
1240	3	<1	sm-m	SA	trigonal	brownish green	2nd order greens and yellows	1	irregular pellicular and irregular linear	brownish green
1257	17	0	/		/	/	/	/	/	/
1253	A32(μ-u1)	0	/		/	/	/	/	/	/
1253	A32(μ-u2)	0	/		/	/	/	/	/	/

[14] In cases where weathering extent could not be determined the symbol (/) is used. Abbreviations used are as follows: thin section (TS) and sample (S). Classes used to describe size for inorganics are as follows: v sm (<30 μm), sm (30-50 μm), sm-m (50-100 μm), m (100-300 μm), m-lr (300-500 μm), lr (500-1000 μm), v. lr (>1000 μm).

a) 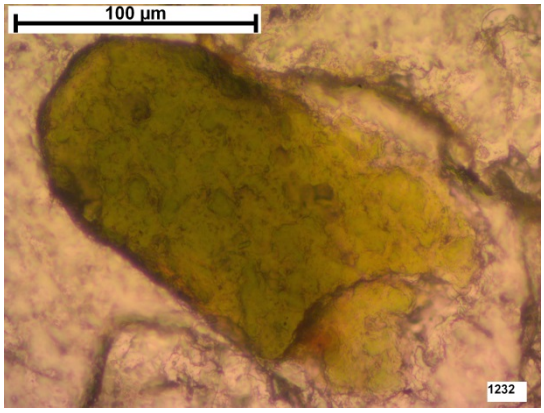

b) 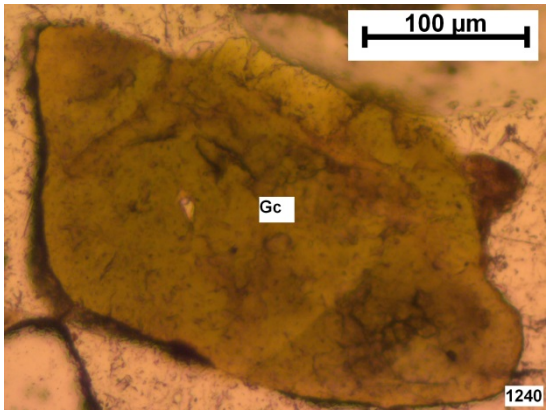

Figure 8.9: Glauconite. a) Glauconite from control with diffuse edged and yellow-green colour, showing pellicular weathering and a small accumulation of red material at the lower boundary of the grain (C2A, TS 1232, PPL). b) Glauconite (Gc) from skull-adjacent sample with clearly defined edges and brown-green colour, showing irregular pellicular, irregular digitate and speckled weathering patterns (S1, TS 1240). A study of a larger number of grains would enable a stronger interpretation of the differences in weathering.

8.3.2.5 Rock fragments

Limestone and granitic rock fragments were present in samples and controls (Tables 25 and 26). The types of limestone fragments ranged from fine grained calcium carbonate rich materials (chalk) to coarser-grained oolitic limestone and shelly limestone. The granitic rock fragments included those having: polysynthetic twinned plagioclase with amphibole accessory minerals which had partially altered to a yellow alteration product (Figure 8.10); Carlsbad-twinned feldspars with inosilicates and opaque materials (Figure 8.11) and feldspars with amphiboles, clinopyroxenes and opaque materials. Other rock fragments besides limestone and granite were flint, calcite (euhedral to subhedral morphology with rhombohedral structure) (Figure 8.13), and, in one thin section, a feldspar-rich rock with titanite as an accessory mineral (Figure 8.12).

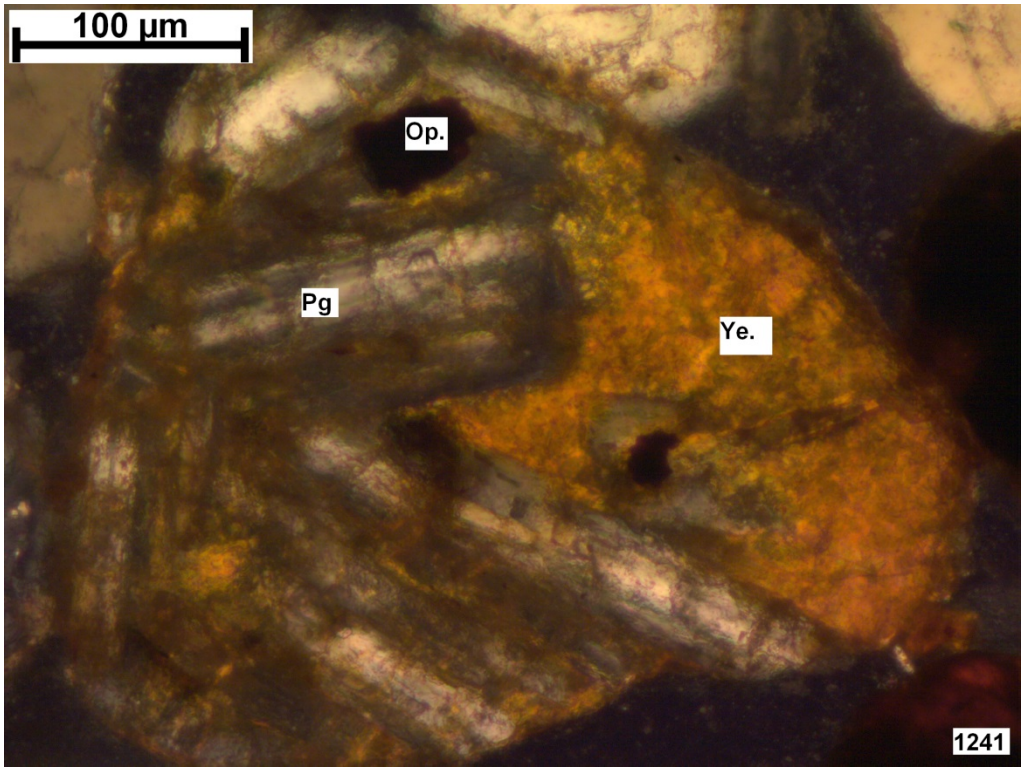

Figure 8.10: Granitic rock fragment, displaying plagioclase feldspars (Pg), opaque material (Op.), and a yellow alteration product (Ye.) composition (S1, TS 1241, XPL).

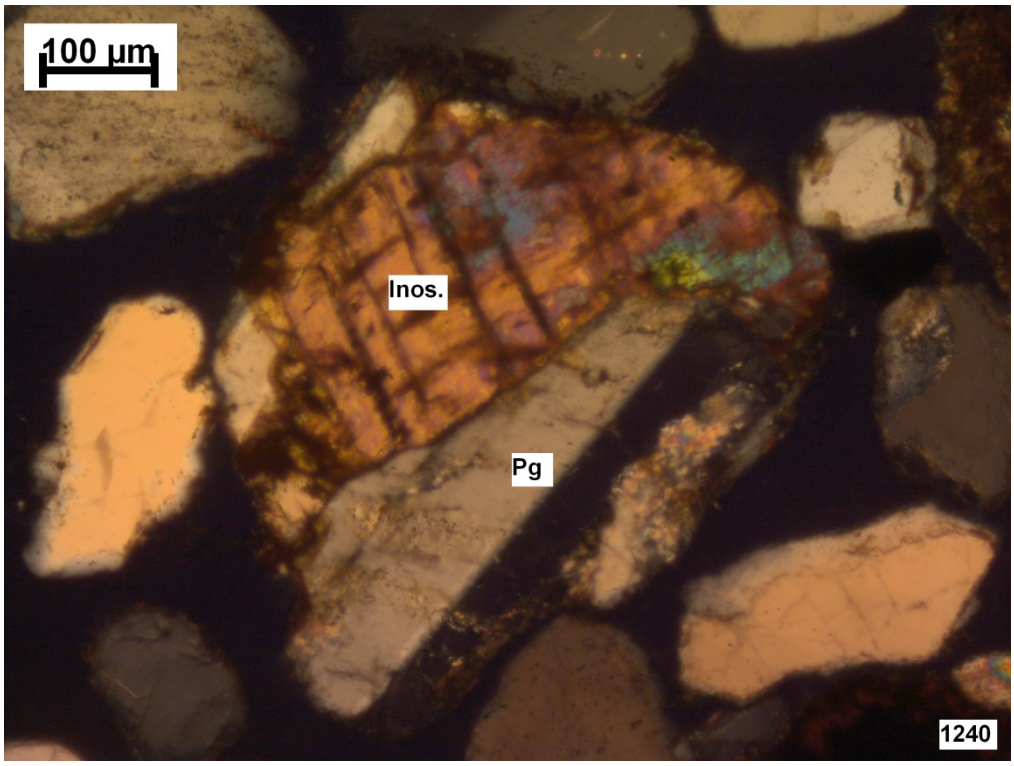

Figure 8.11: Granitic rock fragment, displaying simply twinned feldspar (Pg) and inosilicate (Inos.) components (S1, TS 1240, XPL).

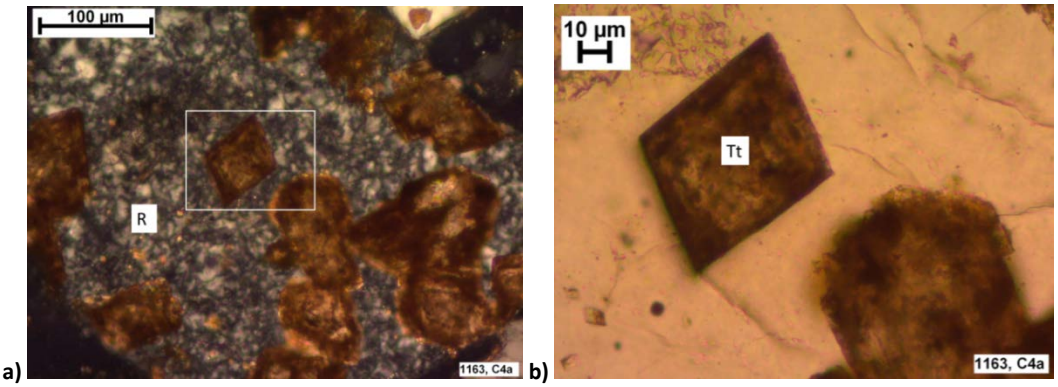

Figure 8.12: a) Rock fragment (R), composed largely of minerals displaying first order grey interference colours and with titanite as an accessory mineral (C4A, TS 1163, XPL). b) Detail of titanite (Tt) from within inset (white rectangle) in image a) displaying brown colour (PPL) and very high relief of titanite (C4A, TS 1163, PPL).

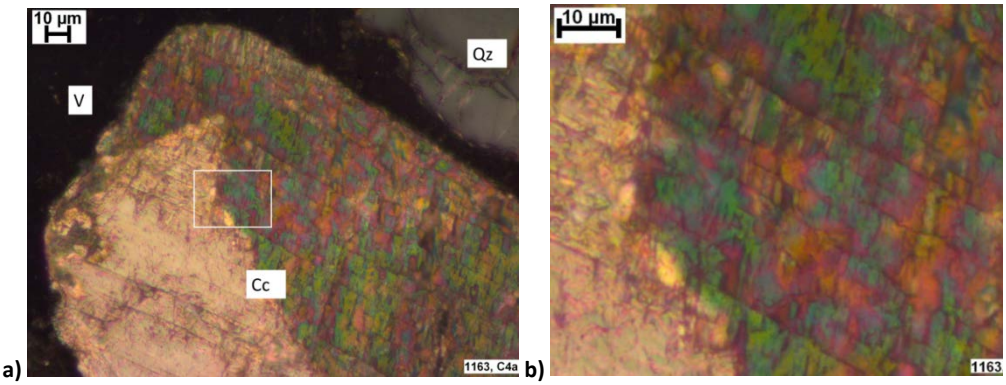

Figure 8.13: a) Calcite (Cc) displaying pellicular weathering at edges (left side of field of view) and rhombohedral structure as shown through the visibility of all three cleavage planes, adjacent to quartz (Qz) and voids (V) (C4A, TS 1163, XPL). b) Detail of inset from image a) (C4A, TS 1163, XPL).

The limestone and granitic rock fragments exhibited a range of sizes, frequency and weathering extents (Tables 31 and 32). Large- and very large-sized limestone and granite fragments were present in the samples and the controls. Medium-large sized fragments of limestone and granite were present in some of the samples and C4 controls and absent in the C2 and C3 controls (Tables 31 and 32). The limestone fragments in the C2 and C3 controls were mostly weathered to extent one and in the C4B control and S1 sample to extent two (Table 31). Complex weathering patterns of the limestone fragments were present in the samples and absent in the controls (Table 31). Complex weathering patterns of the granite fragments were present in the samples and the controls (Table 32). The reduction in size of the limestone and granite fragments from C2 and C3 controls to C4 controls and samples is interpreted to suggest that the rock fragments were increasingly physically weathered with depth. The increased weathering extent and increased complexity of weathering patterns from the C2 and C3 controls to the C4 controls and samples is interpreted to suggest that the limestone fragments were increasingly weathered, both physically (size) and chemically (weathering extent) and is discussed in Section 8.3.5.

Table 31: Optical characteristics of limestone rock fragments[15].

TS	S	Limestone				Shell		Ooids		grey/ CaCO3 rich nodules	Calcite		
		Estimated abundance (%)	sizes	Weathering		Estimated abundance (%)	Weathering extent	Estimated abundance (%)	Weathering extent	Estimated abundance (%)	Estimated abundance (%)	Weathering	
				extent	pattern							extent	pattern
1262	C0	50	lr, v.lr	1	pellicular	_	/	_	/	_	_	/	/
1232	C2A	5	lr, v.lr	1	pellicular	<1	1	_	/	_	2	1p	pellicular
1230	C2B	2	lr, v.lr	1	pellicular	2	1	_	/	_	2	1	pellicular & linear
1206	C2C	5	lr, v.lr	1	pellicular	2	1	<1	1	_	1	2	pellicular & linear
1207	C3A	1	lr, v.lr	1	pellicular	2	2	_	/	<1	2	2	pellicular & linear
1231	C3B	2	lr, v.lr	1	pellicular	_	/	_	/	_	1	1	pellicular & linear
1208	C3C	1	lr, v.lr	1	pellicular	_	/	_	/	_	_	/	/
1163	C4A	5	lr, v.lr	1	pellicular	<1	1	1	2	1	1	2	pellicular & linear
1161	C4B	1	m-lr, lr, v.lr	2	complex (accumulated Fe)	<1	2	_	/	_	_	/	/
1182	1	5	lr, v.lr	2	pellicular & irregular speckled	2	2	_	/	2	<1	2	irregular pellicular
1254	2	1	m-lr	1	pellicular	_	/	_	/	_	_	/	/
1240	3	_	/	/	/	_	/	_	/	_	_	/	/
1257	17	2	m-lr, lr	2	pellicular and speckled	_	/	_	/	_	_	/	/
1253	A32(µ-u1)	0	/	/	/	_	/	_	/	_	_	/	/
1253	A32(µ-u2)	5	m-lr, lr, v.lr	1	pellicular	_	/	_	/	_	_	/	/

[15] Percentage abundance was assessed utilising the estimated abundance charts of Bullock *et al.* (1985). In cases where weathering extent could not be determined the symbol (/) is used. Abbreviations used are as follows: thin section (TS) and sample (S). Classes used to describe size for inorganics are as follows: v sm (<30 µm), sm (30-50 µm), sm-m (50-100 µm), m (100-300 µm), m-lr (300-500 µm), lr (500-1000 µm), v. lr (>1000 µm).

Table 32: Optical characteristics of granitic rock fragments[16].

TS	S	Granite				Selected minerals extraneous to rock fragments				
						Feldspars		Amphiboles		
		Estimated abundance (%)	sizes	Weathering		Plagioclase	Acic. Fd	Olive green pleochroism	Grey pleochroism	Green-blue pleochroism
				extent	pattern	Estimated abundance (%)	Estimated abundance (%)	Estimated abundance (%)	Estimated abundance (%)	Estimated abundance (%)
1262	C0	0	/	/	/	1	_	_	_	_
1232	C2A	_	/	/	/	_	_	_	_	1
1230	C2B	2	lr, v.lr	1	pellicular & irregular linear	_	_	<1	_	1
1206	C2C	1	lr, v.lr	2	complex	_	_	_	_	_
1207	C3A	2	lr, v.lr	2	complex	_	_	<1	_	_
1231	C3B	2	lr, v.lr	1	complex	_	_	_	_	_
1208	C3C	1	lr, v.lr	2	complex	_	_	_	_	2
1163	C4A	2	m-lr, lr	1	complex	1	1	_	_	_
1161	C4B	1	m, m-lr	2	complex	_	_	1	1	_
1182	1	5	m, m-lr	2	complex	1	_	_	1	_
1254	2	2	m-lr, lr	2	complex	_	_	_	_	_
1240	3	5	m, m-lr, v.lr	2	complex	1	1	_	_	_
1257	17	2	m-lr	2	complex	_	_	_	_	_
1253	A32(µ-u1)	0	/	/	/	_	_	_	_	_
1253	A32(µ-u2)	2	lr	2	complex	_	_	_	_	_

[16] Percentage abundance was assessed utilising the estimated abundance charts of Bullock *et al.* (1985). In cases where weathering extent could not be determined the symbol (/) is used. Abbreviations used are as follows: thin section (TS), sample (S) and radially arranged acicular feldspars (Acic. Fd). Classes used to describe size for inorganics are as follows: v sm (<30 µm), sm (30-50 µm), sm-m (50-100 µ), m (100-300 µm), m-lr (300-500 µm), lr (500-1000 µm), v. lr (>1000 µm).

8.3.3 Bone and wood

Fragments of bone were present in the thin section from the sample collected adjacent to the skull (Figure 8.14). Plant remains, interpreted as remnants of coffin wood, were identified in the sediment immediately below the coffin lid (C4 control) and adjacent to the skull (S1; Figures 8.15 and 8.16). No bone or wood remains were identified in thin sections from samples above the coffin (C2A-C and C3A-C) suggesting that sediment biota had not mixed the sediments inside the coffin with those above the coffin. Bone and plant remains (Table 25) were the only remnants of the deposited buried organic materials (Table 23) that were observed in thin section.

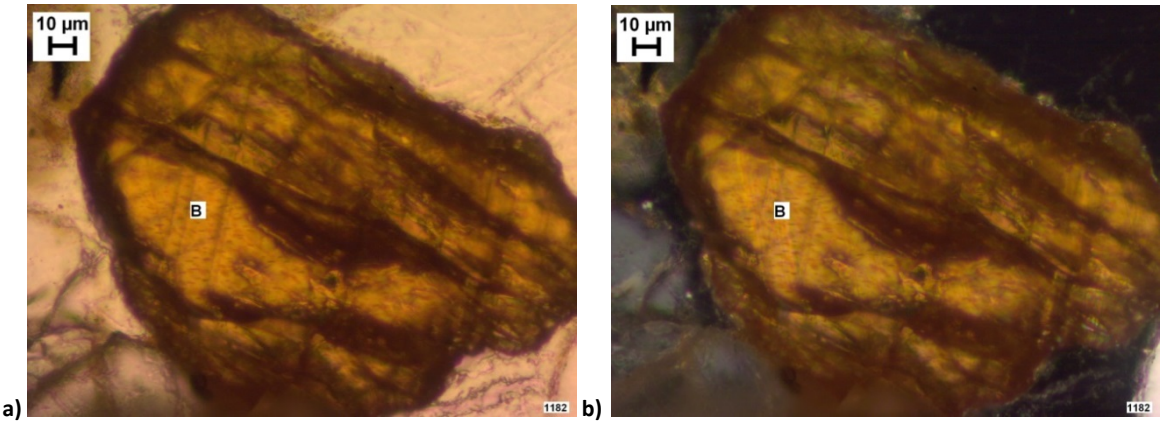

Figure 8.14: Bone fragment observed in sample S1, in a) PPL and b) XPL (TS 1182).

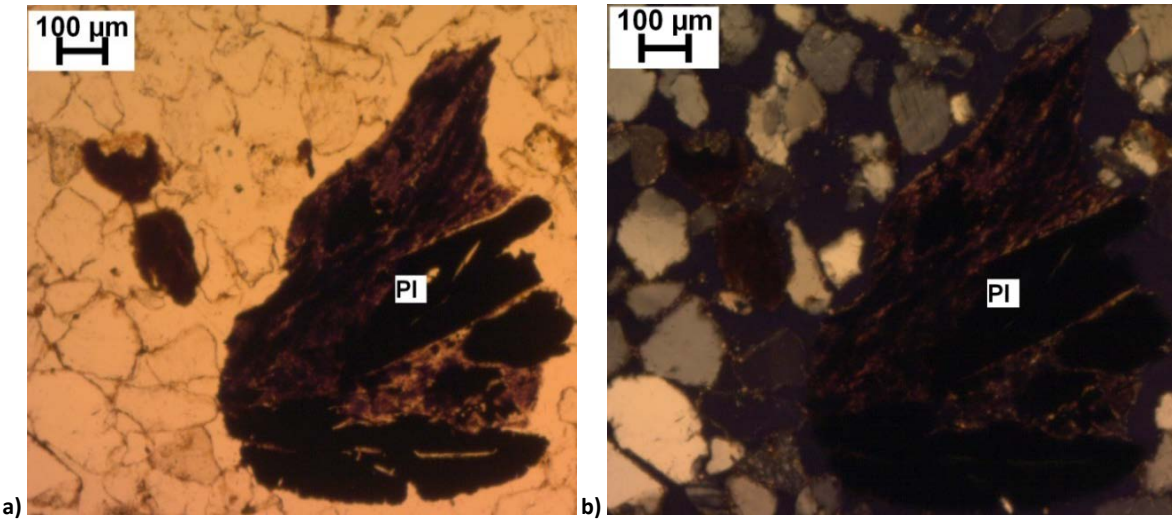

Figure 8.15: Plant remains (Pl), possibly coffin wood, in sediment within the coffin above the interred remains, a) PPL and b) XPL (C4B, TS 1161).

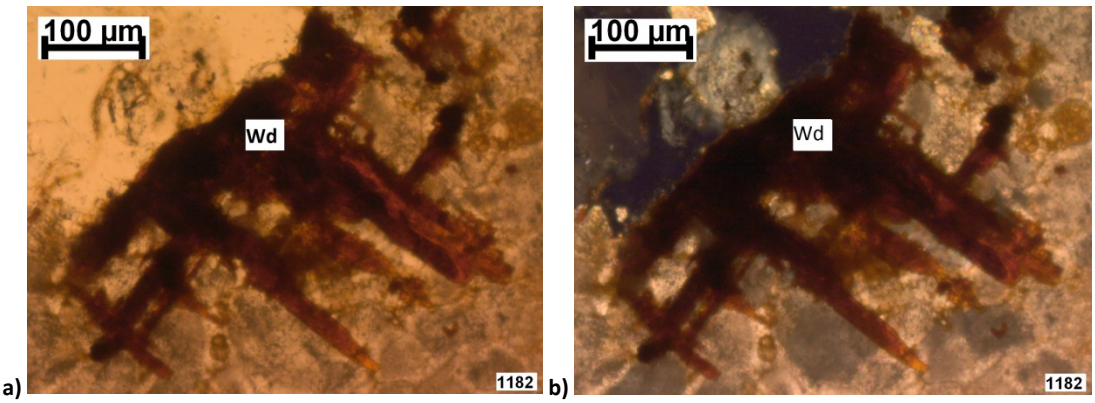

Figure 8.16: Wood (Wd) remains in sample S1 in, a) PPL and b) XPL (TS 1182).

8.3.4 Bone thin sections

The remains of the inhumed pig were extensively skeletonised (Section 8.3.3). Hence, the loose bones collected from Pig 1 were thin sectioned to investigate the types and extents of post-depositional processes that had occurred over the course of its interment. A fragment of the lower mandible from Pig 1 was recovered during excavation. The bone was dried at 35°C and impregnated in resin (Polylite 32320) under vacuum. Two thin sections were created from the impregnated bone (TS 1103 and TS 1105) and bone, tooth, and adjacent sediment materials were identified (Figures 8.17-8.20). The tooth appeared to have maintained its original morphology and structure and is interpreted as well preserved with some red deposits on the surface (Figures 8.18 and 8.21). In both thin sections (TS 1103 and TS 1105) the bone appeared well preserved (Figures 8.20 and 8.21). A fly (Diptera) was identified in the sediment adjacent to the tooth and bone and is interpreted as evidence of sediment biota associated with the decomposition process (Figure 8.19). A mature fly could have been included in the sediment adhering to the pig from the straw matting the pig was placed on during birth and transport to the burial site. The fly measured approximately 550 x 250 µm. Scuttle fly (*Phoidae*) can be approximately 0.5-1 mm in length and feed on rotting vegetation and carcasses as well as dung (Disney 1989). The fly in Figure 8.19 is interpreted as possibly a scuttle fly from the straw matting surrounding the pig prior to burial.

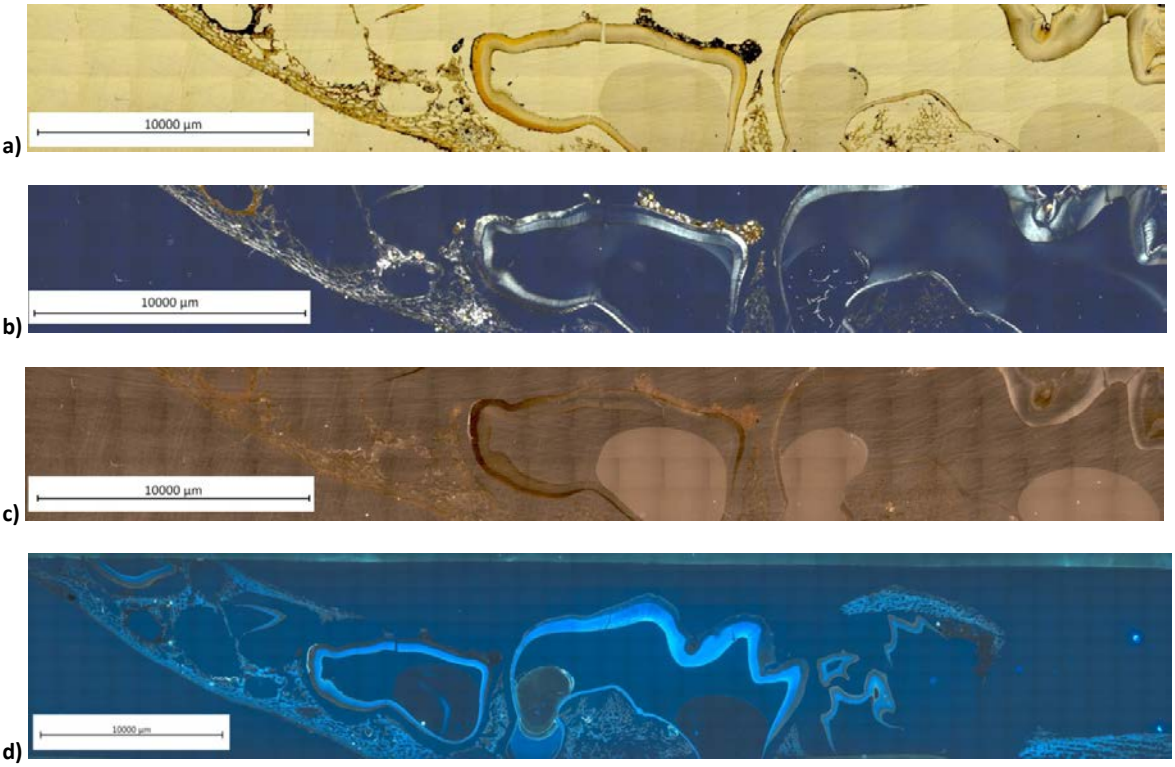

Figure 8.17: Mosaic images of TS 1103 in a) PPL, b) XPL, c) Reflected light with dark field cube (RLDF), and d) Ultra violet light with fluorescence cube (UVFS).

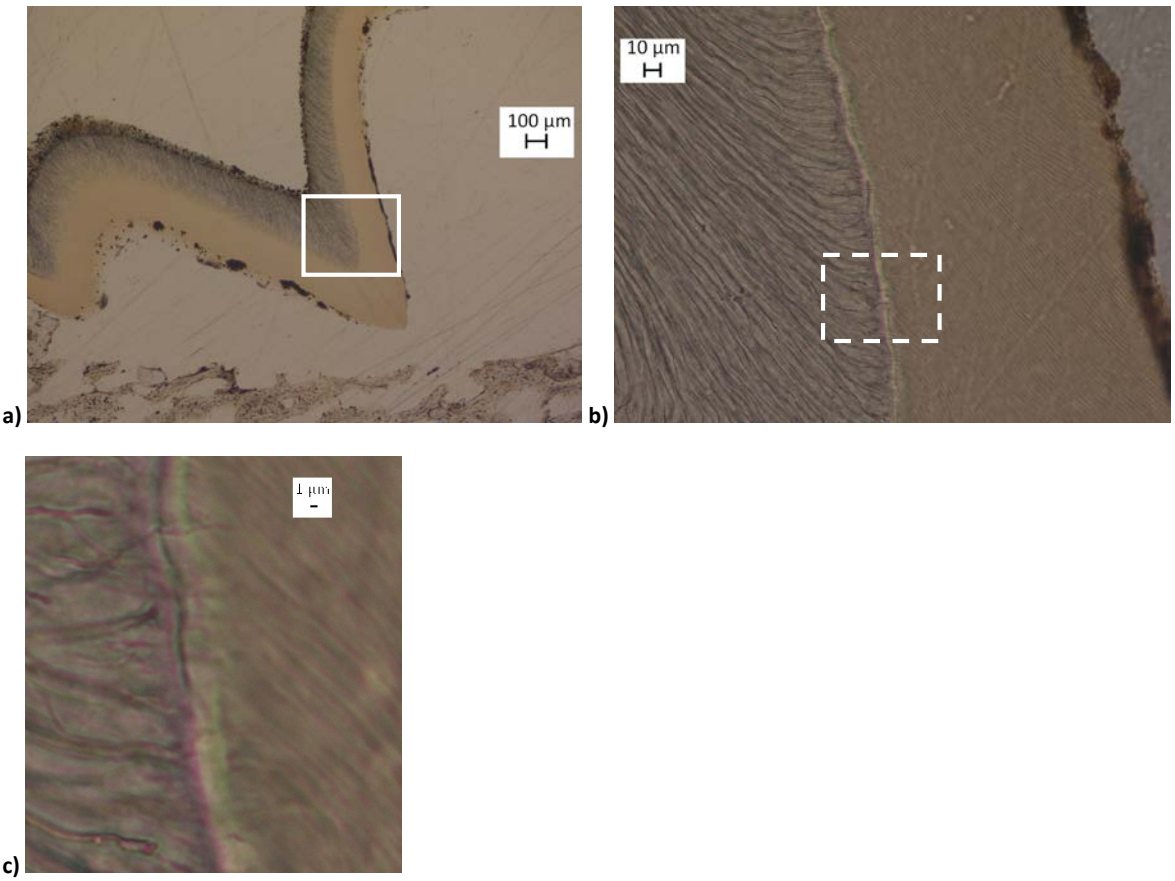

Figure 8.18: a) Tooth (TS 1103, PPL). b) Detail of inset (white rectangle) in image (a). c) Detail of inset (white dashed rectangle) from image (b).

a)

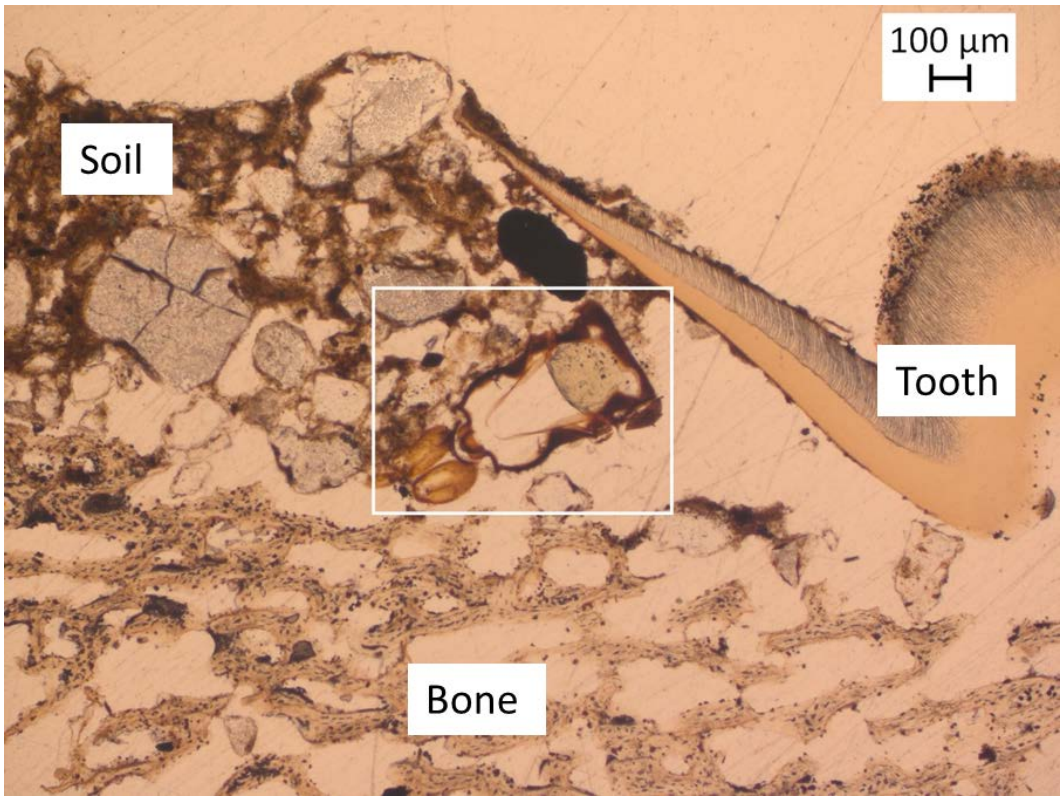

b)

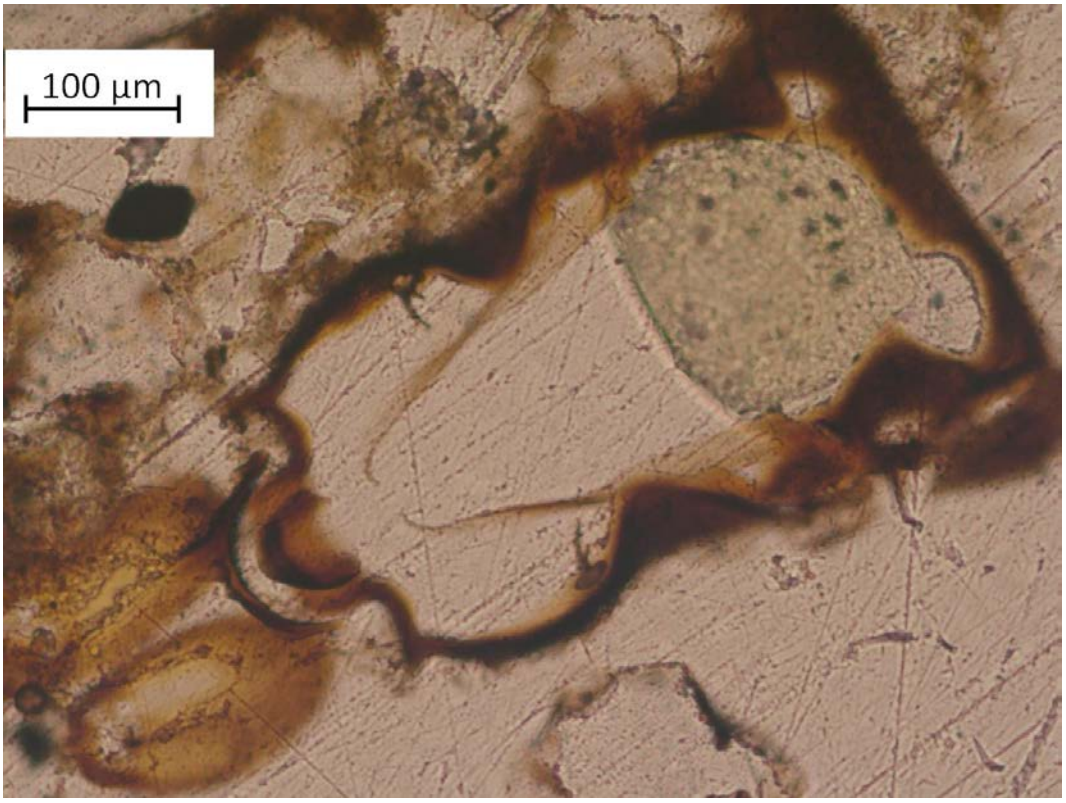

Figure 8.19: a) Fly in sediment adjacent to tooth and bone (PPL). b) Detail of inset (white rectangle) from image a).

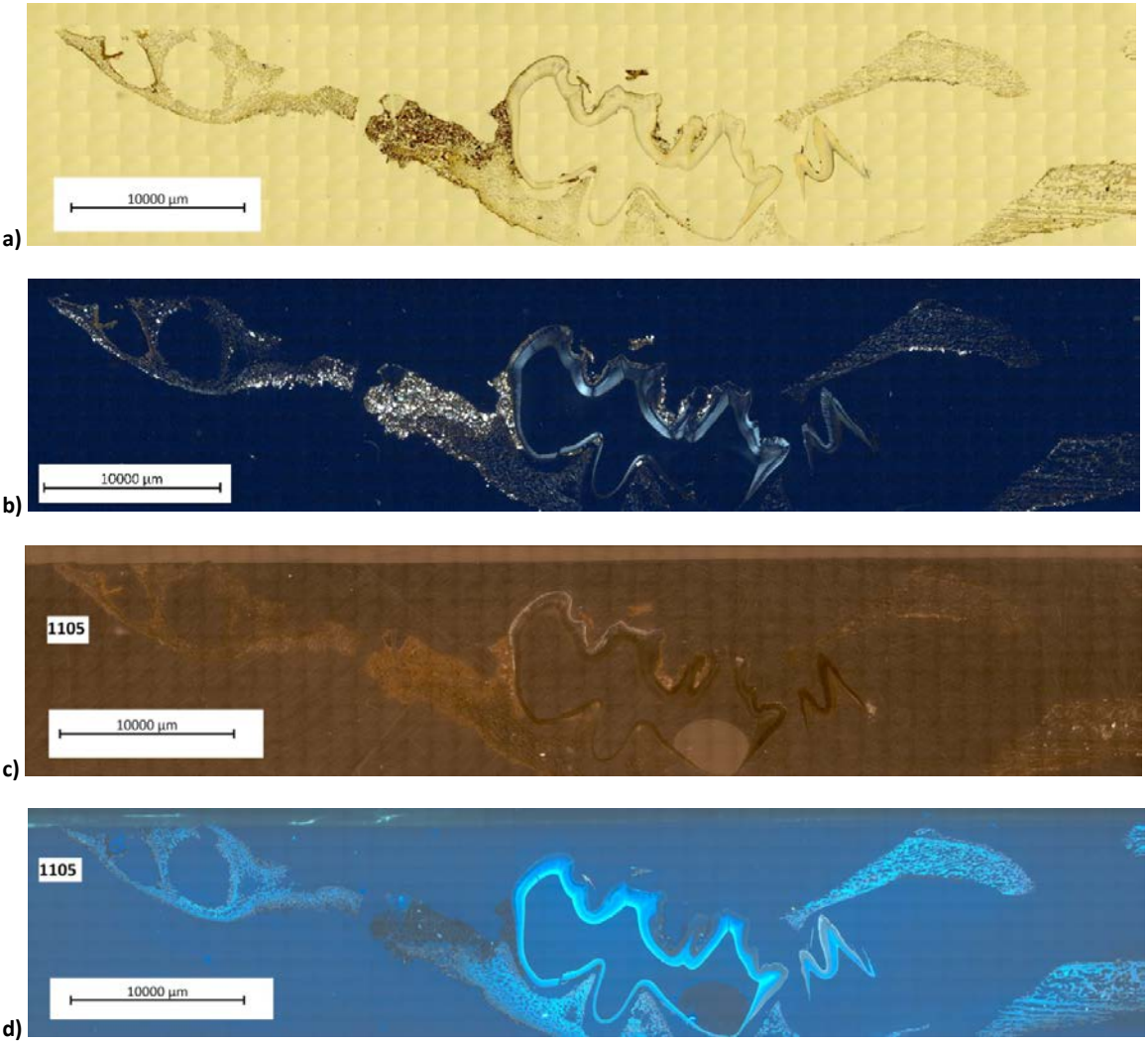

Figure 8.20: Mosaic image of TS 1105, a) PPL, b) XPL, c) RLDF, d) UVFS.

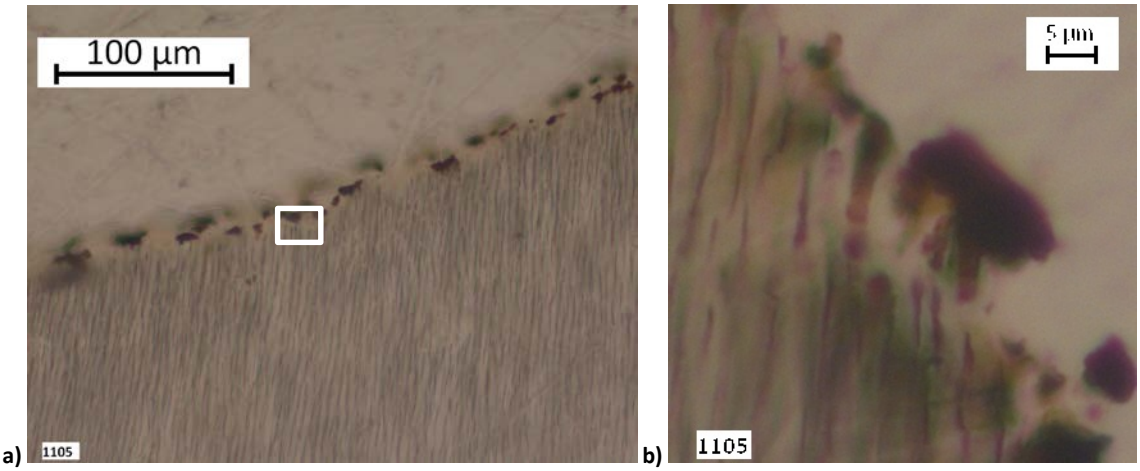

Figure 8.21: a) Red isotropic material adjacent to the edge of the tooth (PPL). b) Detail of inset (white rectangle) in image a).

One of the quartz grains in TS 1105 showed some internal alterations by the presence of tunnels (Figure 8.23); these appeared consistent with the size and morphology of tunnels created by fungal

hyphae. Given the proximity to the bone, this evidence of biotic weathering of the quartz grains most likely relates to the decomposition of the pig. However, this tentative interpretation is speculative as the reasons why fungi would attack a quartz grain when there are other sources of more readily available Si in the sediments are not fully understood. Thin sections were made from other loose bones and mosaics in PPL, XPL, RLDF, and UVFS of thin sections from mandible, pelvis, scapula and crania of Pig 1 (TS 1223-1228) and results are in provided in Appendix I.

a)

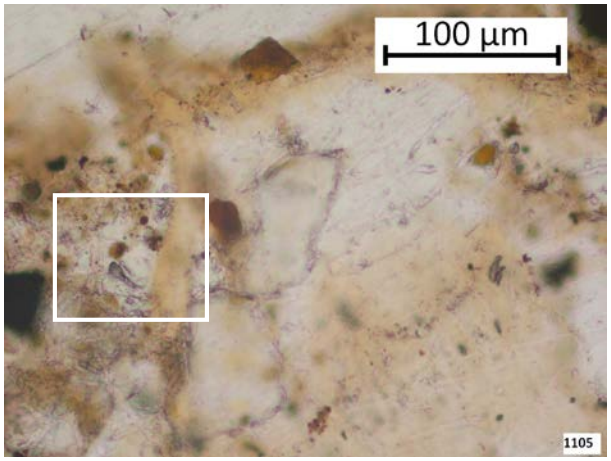

b)

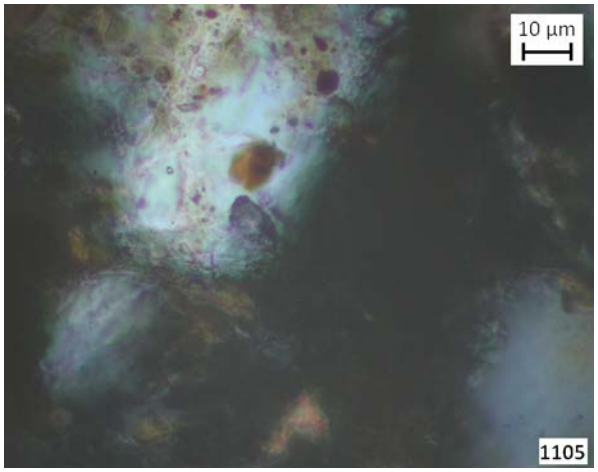

Figure 8.22: a) Quartz grain (encased by the thin layer of fine material coating the bone) with red anisotropic material speckled on the surface (PPL). b) Detail of image (a) (XPL).

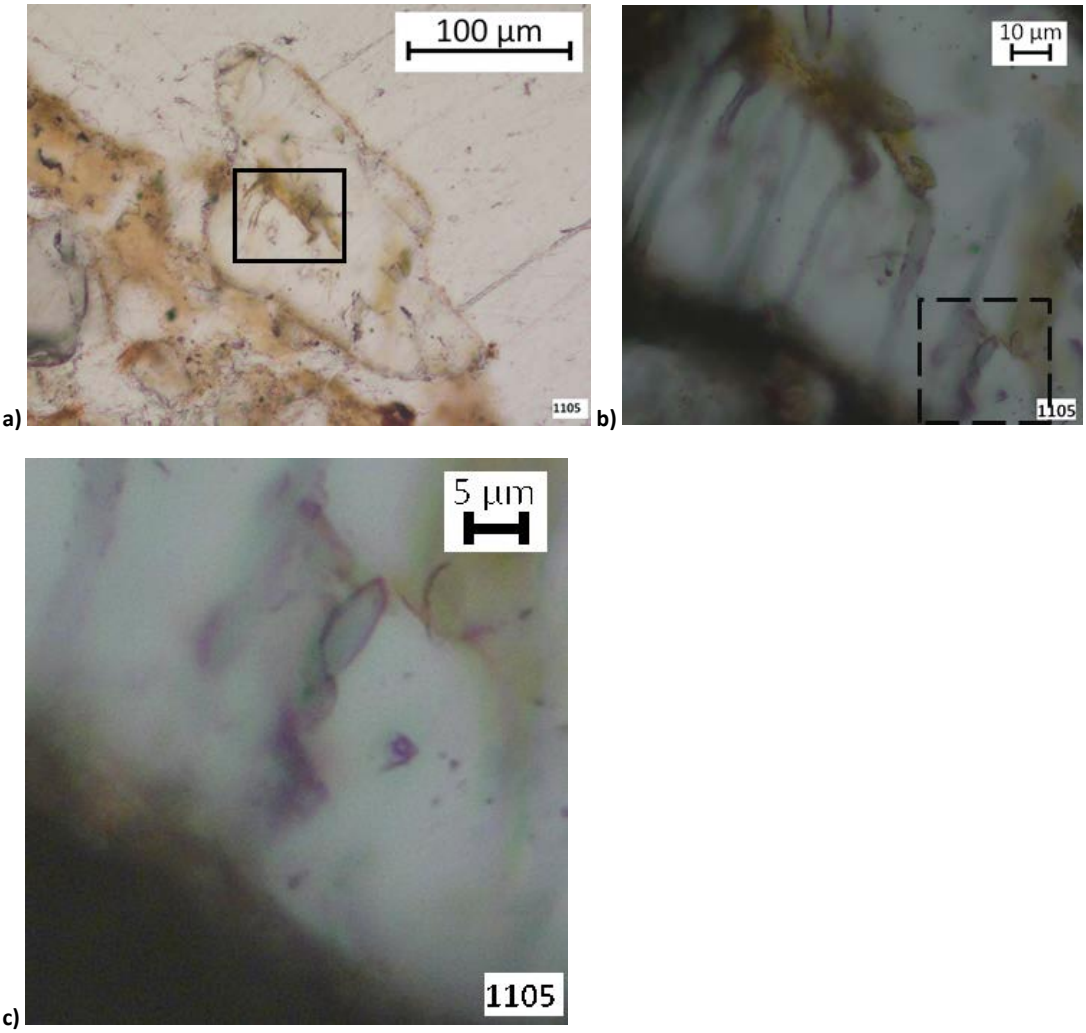

Figure 8.23: a) Quartz grain adjacent to bone with parallel linear tunneling visible (PPL). b) Detail of inset (black rectangle) in image (a) in (XPL). c) Detail of inset (black dashed rectangle) in image (b) (XPL).

8.3.5 Weathering processes

8.3.5.1 Carbonates

The linear and acicular $CaCO_3$-rich materials in the C4 controls are interpreted as heavily weathered shell remains (Table 31). Ooids are interpreted as fragments liberated from some of the oolitic limestone rock fragments through weathering (Figure 8.24). The presence of ooids in Controls C2 and C3 and absence in the C4 controls and the samples suggests that the ooids in the samples were weathered past recognition due to differences in the micro-scale burial sediment conditions. The distribution, size and weathering extents of the shell and oolitic limestone fragments is interpreted to suggest a pattern of greater weathering *via* dissolution and reprecipitation with increasing depth and proximity to the skeletal remains (Table 31).

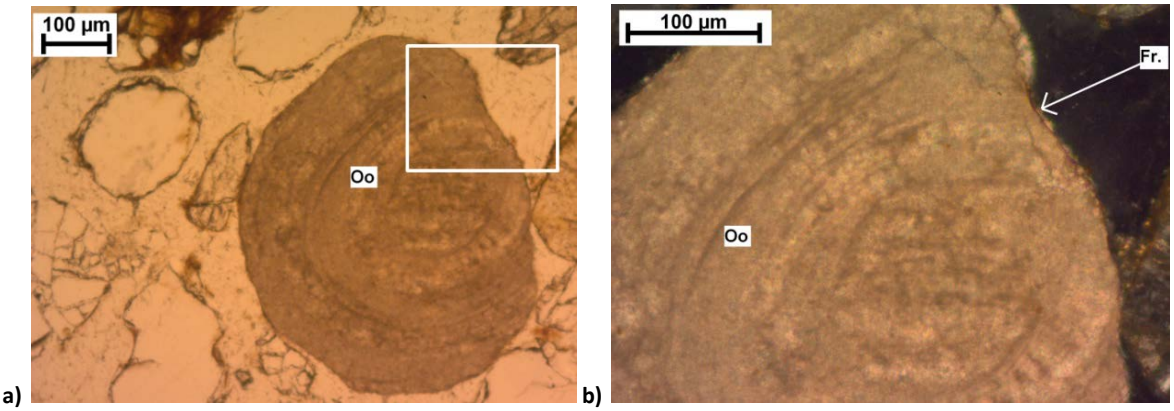

Figure 8.24: Ooid in thin section from control C3A (TS 1207). a) Ooid (Oo) displaying concentric rings and grey colour (C3A, TS 1207, PPL). b) detail from inset in image a), showing the fractured edges (Fr.) of the ooid (Oo) which were first fractured, then rounded, and subsequently weathered through pellicular weathering (C3A, TS 1207, XPL).

Rhombohedral fragments of calcium carbonate-rich minerals present in the C2 and C3 controls are interpreted as evidence of pellicular weathering affecting the edges of calcitic rock fragments (Figures 8.13 and 8.25, Table 31). Amorphous morphologies of $CaCO_3$-rich materials were present in Control C4A (Table 31 and Figure 8.26). The contrast between crystalline carbonates present in sediments above the coffin and amorphous forms present within the coffin suggests weathering of carbonates through solubilisation and reprecipitation with increasing depth. This interpretation is supported by the decreased frequency, increased weathering extent and increasingly complex weathering patterns of the calcitic rock fragments closer to the skeletal remains (Table 31).

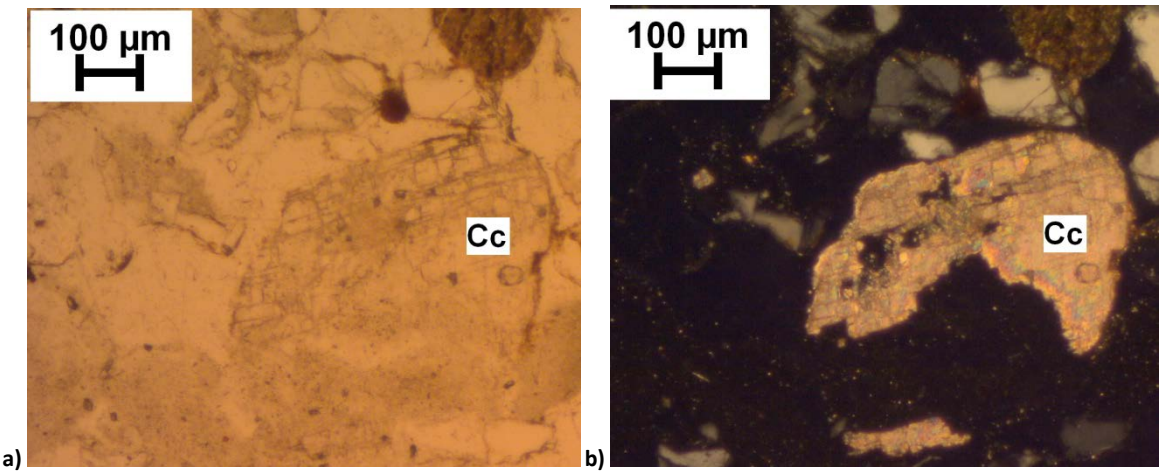

Figure 8.25: Calcite (Cc) which has lost a considerable portion of its total volume through *in situ* weathering processes, a) PPL and b) XPL (C3A, TS 1207).

a) 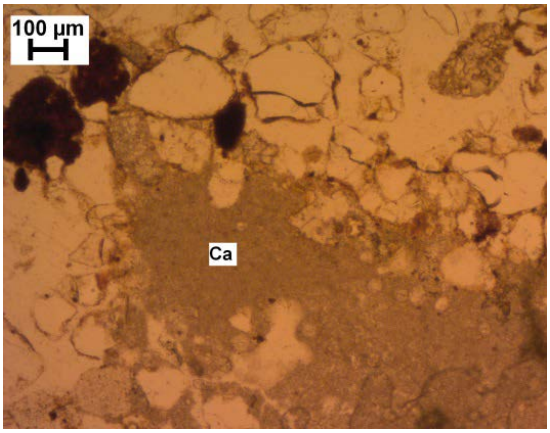

b) 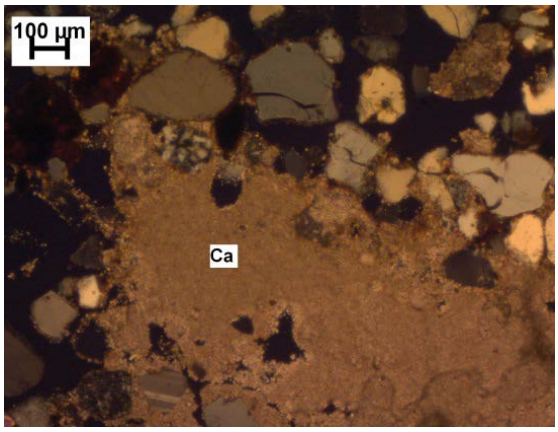

Figure 8.26: Calcium carbonate-rich amorphous material (Ca), in a) PPL and b) XPL (S1, TS 1182).

8.3.5.2 Granitic rock fragments

The estimated abundances of granite fragments in the thin sections increase with increasing proximity to the skeletal remains (Table 32). The highest values for this material in this burial were present in the samples and are interpreted together with the size distributions of the granitic rock fragments, which show an increase in smaller fragments from the C2 and C3 controls to the samples S1, S2, S3, and S17 (Tables 27 and 32). Medium and medium-large sized clasts were present in the sediments within the coffin (Table 32). However, increases of 1-2% estimated abundance are not statistically relevant and are interpreted as evidence of the heterogeneity of the weathered state of the granite prior to deposition in the grave. Such an interpretation is supported by the low weatherability of granite, which would not be expected to visibly weather in three years. Granite fragments were absent from the pre-burial control (C0) thin section, and because the source of the sand and the pre-depositional histories of the granite fragments were unknown, the effect of the three years in the burial environment on such fragments could not be assessed.

The weathering of the granitic clasts is interpreted as evidence of chemical weathering of the mineralogical components of the clasts (Table 32). The spatial association of the yellow fine grained material with the plagioclase suggests the former to be an alteration product. The weathering extent of granite fragments does not reveal a systematic trend with depth (Table 32), though this is perhaps to be expected given the limitations of the method in use. The method (Stoops *et al.* 1979, Delvigne 1998) was determined for mineral rather than rock weathering and categorises weathering extent using a non-linear scale: weathering extent one (2.5-25% altered) and extent two (25-75% altered) (Chapter 3). Within weathering extent two, a large degree of variation was observed in the alteration to the yellow fine-grained material. Hence, extent two encompasses a vast range of weathering alteration and the method will be insensitive to subtle variations which are likely to be important in a short-term experiment. Based on subjective assessment of increased

alteration to the yellow fine-grained material, an increase in weathering with depth and proximity to the skeletal remains can be inferred.

Amphiboles in the granite fragments share similar optical traits to the angular grey amphiboles in the groundmass (Table 29). Their similarities suggest that the grey amphiboles in the groundmass were released through weathering of the granitic fragments. The evidence of clinopyroxene and fibrous chalcedony in the groundmass in the sediments from inside the coffin is interpreted to suggest that such grains were introduced to the groundmass through physical and chemical weathering of fibrous chalcedony and clinopyroxene-rich granitic rock fragments (Figures 8.27 and 8.28). The interpretation of granite disaggregation is supported by associated yellow secondary products of alteration held in the remaining clasts. The interpretations of the differences in size and weathering of the granitic clasts from the C2 and C3 controls and the C4 controls and samples suggest that these rock fragments have been increasingly degraded through disaggregation and incongruent dissolution with depth and closeness to the pig remains.

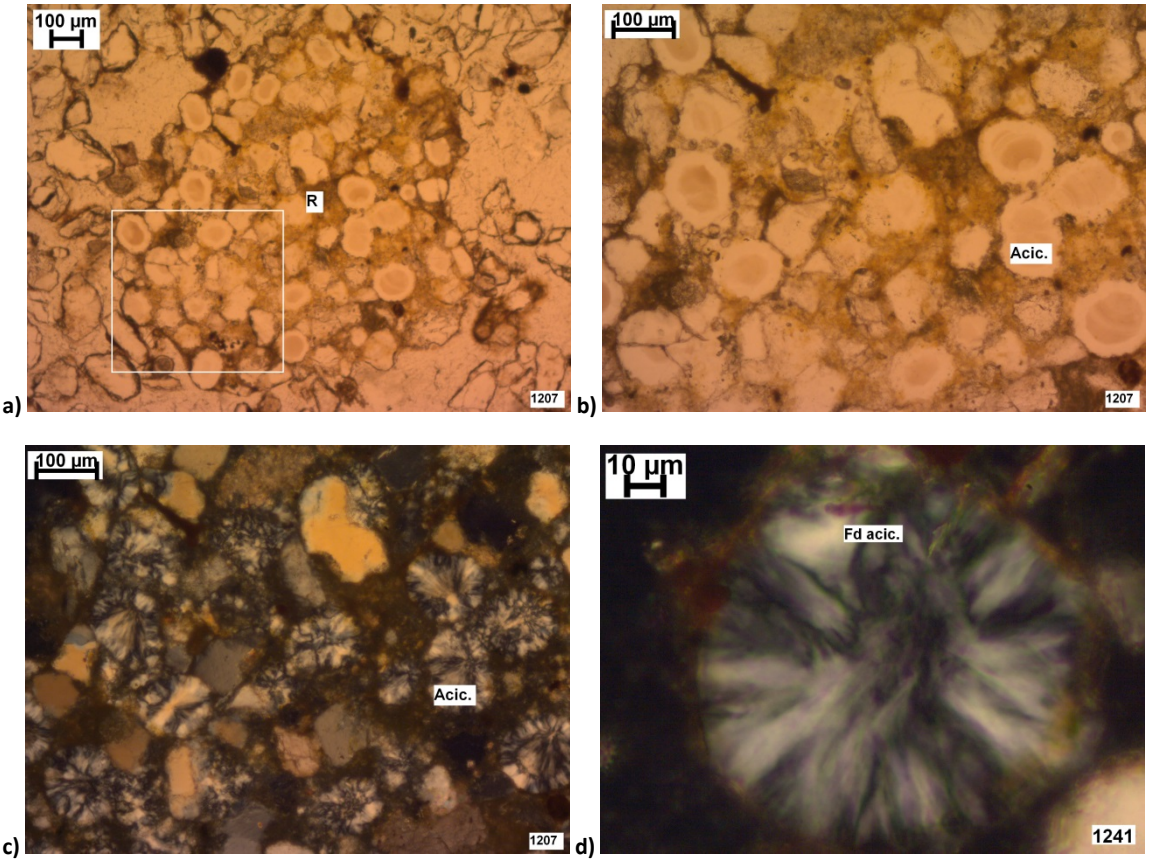

Figure 8.27: Fibrous chalcedony. a) Rock (R) composed of fibrous chalcedony and yellow fine material (C3A, TS 1207, PPL). b) Detail of inset from image a), showing fibrous chalcedony (Acic.) and yellow fine material (C3A, TS 1207, PPL). c) XPL view of image b) (C3A, TS 1207, XPL). d) Fibrous chalcedony observed in a skeletal adjacent sample which is not held within a rock fragment (S3, TS 1241, XPL).

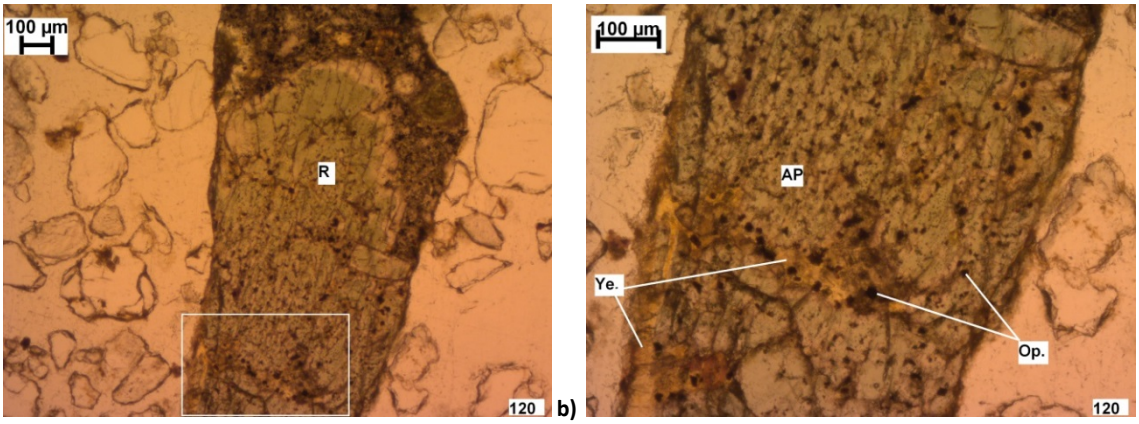

Figure 8.28: a) Weathered rock fragment (R) from an above coffin control (C3C, TS 1208, PPL). b) Detail of inset (white rectangle) in image a) showing weathered amphibole (AP) with opaque material (Op.) and yellow fine material (Ye.) (C3C, TS 1208, PPL).

8.3.5.3 Glauconite

The glauconites in the C2 and C3 controls were similar in their optical characteristics, all having lobate morphologies, green colours (PPL), 2nd order green and yellow interference colours (XPL) and pellicular weathering patterns (Table 30). The glauconite in the three controls (C2A, C2B, and C3A) is at greater extent of weathering in the C3C (extent two) compared the C2A and C2B (extent one) (Table 30). The glauconite in the lower grave fill (C3C and C4A) displayed dark red colours and complex weathering patterns and is interpreted as being moderately to heavily weathered with an accumulation of an iron-rich material (Table 30). The observed glauconite from the skeletal adjacent samples (S1 and S3) differed from all of the controls, having dark-brownish colour and non-lobate morphologies (Table 30).

Micromorphological observations of the burial sediments of Pig 1 suggest that the glauconite in the upper grave fills (C2A-C) had been affected by weathering processes which would have led towards the production of a secondary clay material (Figure 8.9a). Conversely, the accumulation of iron in the lower grave fills (C3A-C) produced a weathering pathway which would eventually have led to an inability to discern the alteration products from iron-rich nodules (Figures 8.29-8.33 and Table 30). Glauconite from samples and from the C4 controls appeared relatively unweathered (Figure 8.34) compared to the controls from above the coffin (C2A-C and C3A-C; Figure 8.9), suggesting that this could be a result of the reduction in the burial area "cleaning" the oxidized grains. A glauconite grain (Figure 8.35) was observed within a bone fragment and adjacent to fungal sclerotia in the sample of sediment from near the feet (S17, TS 1263). The interpretation of the location of the grain in TS 1263 suggests that glauconite can be present in a relatively unweathered state when present in association at the micro-scale with bone and fungi remains in grave sediments.

Interpretations of the colours, morphology and weathering of the glauconite in the samples and the controls suggest that a process of leaching of iron from glauconite increasingly affects the

mineral with depth, with accumulation of iron being evident in the glauconite within the coffin. Previous studies of glauconite have suggested that a higher oxidation states of iron consistently yield yellowish green colours (PPL) in thin sections, whereas more reduced oxidation states yield darker brownish green colours (PPL) (Fanning *et al.* 1989b). Hence, the glauconite in Pig 1 burial sediments above the coffin appears to reflect leaching processes (weathering towards the production of smectite or illite through substitutions at some sites of Al by Fe). This interpretation, based on the colours, fractures and infillings, is supported by the work of Fanning *et al.* (1989b) and conforms to the stages of glauconite weathering as proposed by the laboratory based experimental work of Robert (1973) and Johnston and Cardile (1987).

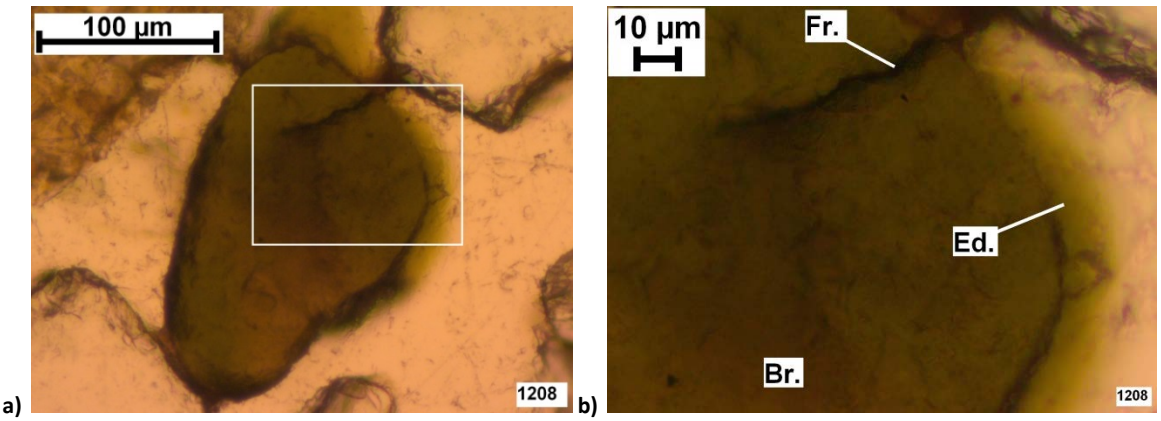

Figure 8.29: Slightly developed weathering of glauconite from controls above the coffin. a) Glauconite with pellicular weathering (C3C, TS 1208, PPL). b) Detail from inset (white rectangle) in image a) showing intra-mineral fracture (Fr.) extending from the upper edge of the grain into the mineral, diffuse edges (Ed.) and a brown colour (Br.) in the lower portion of the field of view (C3C, TS 1208, PPL).

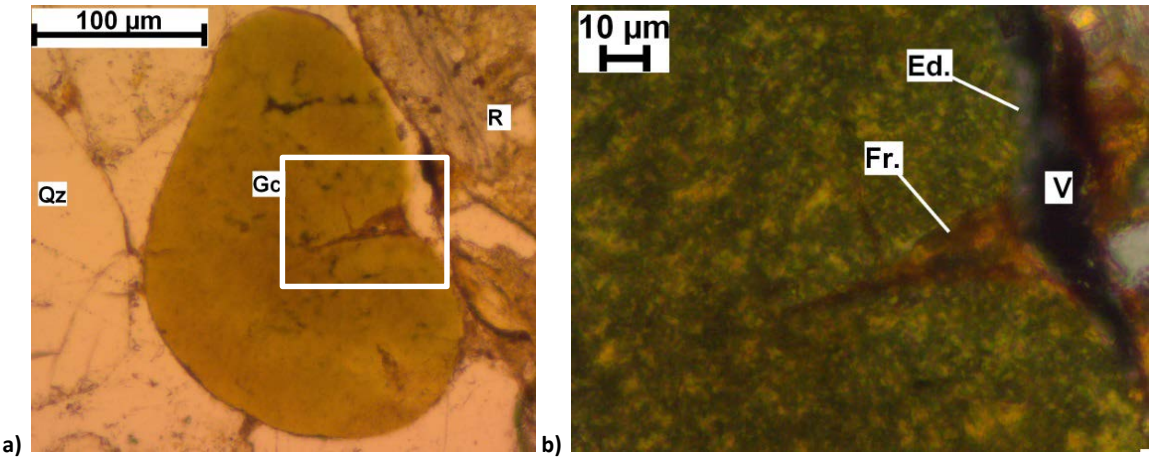

Figure 8.30: Moderately developed weathering of glauconite from controls. a) Glauconite (Gc) has altered to a brownish-yellow colour, adjacent to quartz (Qz) and rock fragments (R) (C4B, TS 1161, PPL). b) Detail of inset (white rectangle) in image a), showing diffuse edges (Ed.) near a small void (V) and an intra-mineral funnel-shaped fracture (Fr.) extending from the edge of the grain (C4B, TS 1161, XPL).

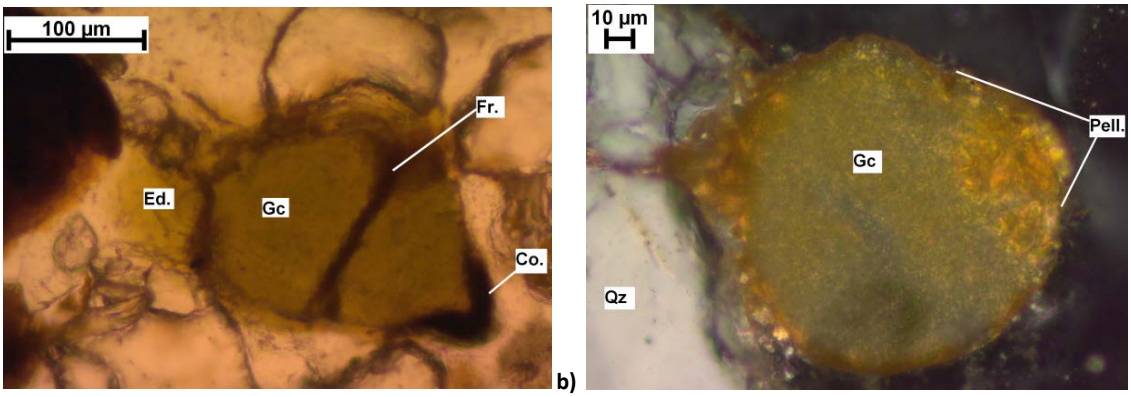

Figure 8.31: Moderately developed weathering of glauconite from C3 controls. a) Glauconite (Gc) with dark coloured partial coating (Co.), transmineral fracture (Fr.) and diffuse edges (Ed.) (TS 1208, C3C, PPL). b) Glauconite (Gc) of well-rounded form and small size (~100 µm) with pellicular weathering (Pell.), and surrounded by quartz (Qz) (C3C, TS 1208, XPL).

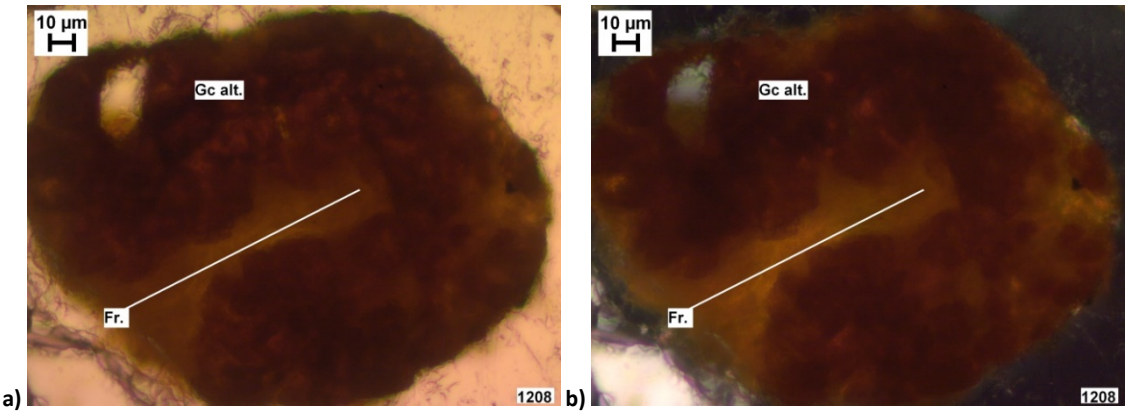

Figure 8.32: Highly developed weathering of glauconite to a red-coloured alteromorph in above coffin control. a) Altered glauconite (Gc alt.) of a well-rounded form and small (*c.* 100 µm) proportions with a large fracture (Fr.) which extends into the mineral from the external surface (C3C, TS 1208, PPL). b) XPL view of image a) highlighting retention of rosette structure retained from glauconitic primary mineral (C3C, TS 1208, XPL).

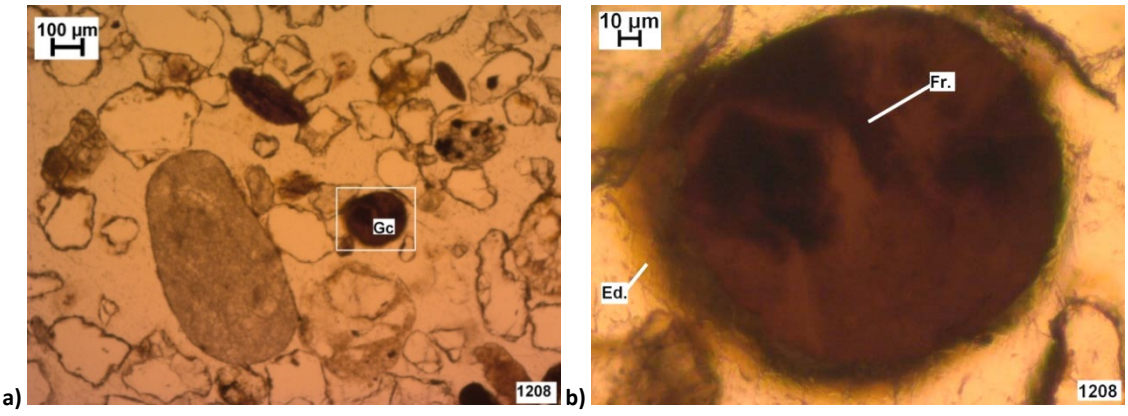

Figure 8.33: Highly developed weathering of glauconite to a red-coloured alteromorph in above coffin control. a) Tentatively identified red coloured alteromorph from glauconite (Gc) (C3C, TS 1208, PPL). b) Detail of inset (white rectangle) in image a), showing a funnel-shaped fracture (Fr.) which extends inwards from the top edge of the object and has been infilled with an opaque material, diffuse edges (Ed.), and note also that a darker coloured area can be seen in the left of the field of view (C3C, TS 1208, PPL).

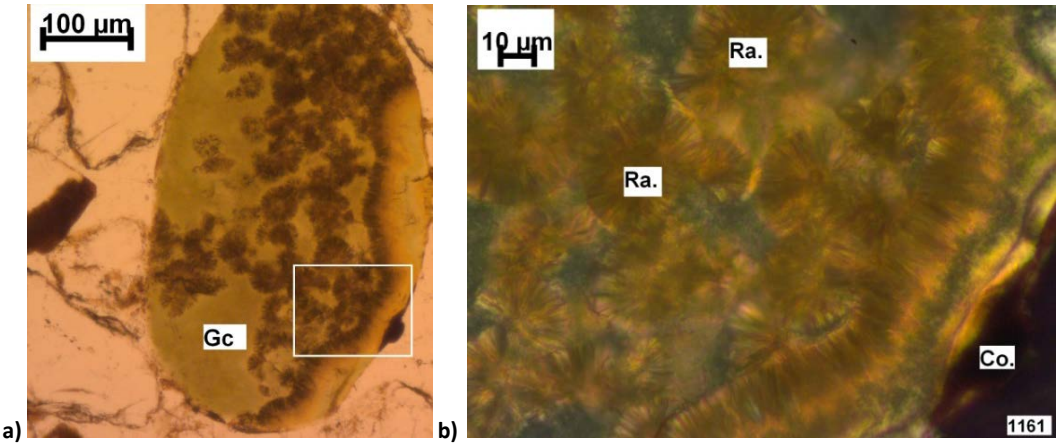

Figure 8.34: Slightly weathered glauconite from sediments within the coffin. a) Glauconite (Gc) was well preserved (C4B, TS 1161, PPL). b) Radially structured (Ra) surficial impressions formed during the primary (marine sourced) formation of the mineral remain visible, with slight weathering effects observed via the opaque coating (Co.) which has been deposited post-rounding of the grain (C4B, TS 1161, XPL).

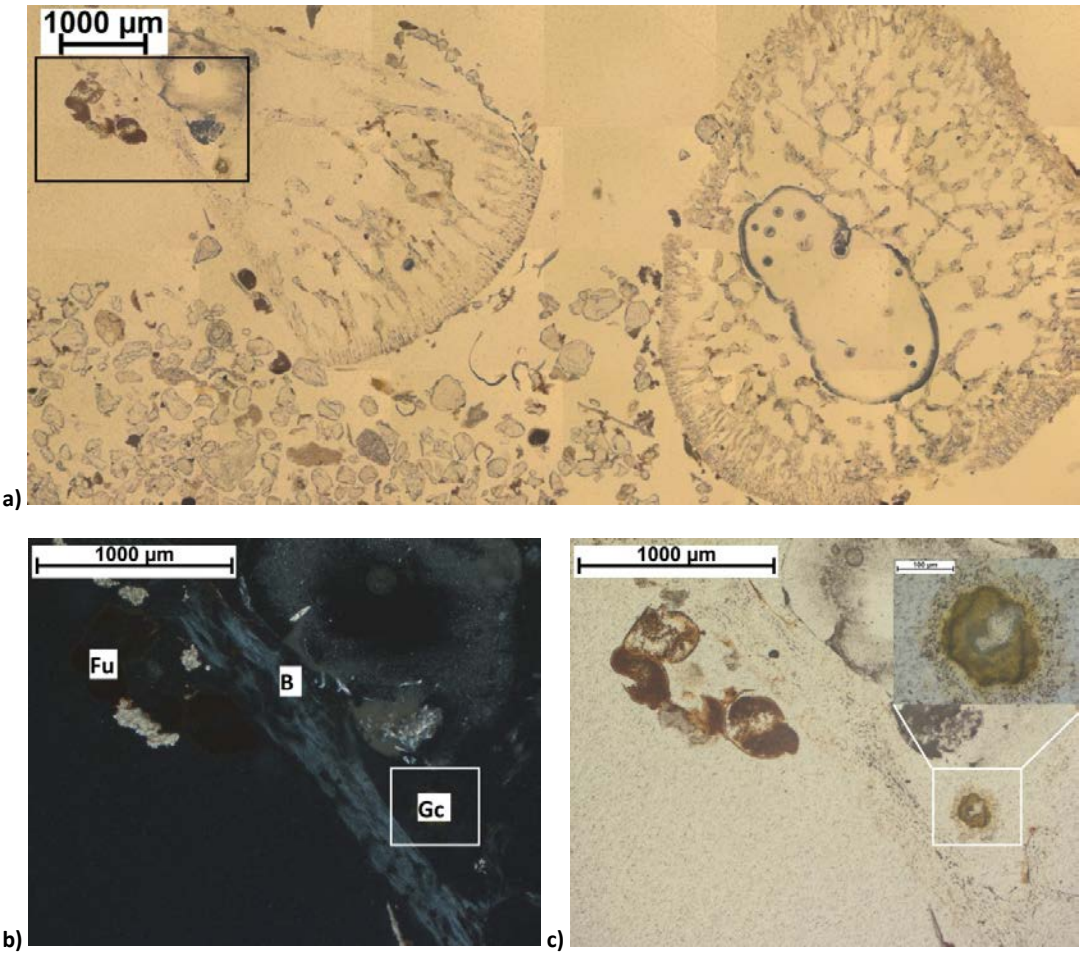

Figure 8.35: Glauconite (Gc), bone (B) and fungal sclerotia (Fu) (S17, TS 1263). a) Mosaic image of TS 1263 (PPL). b) inset (black rectangle) from image a), with bone (B), fungal remains (Fu) and glauconite (Gc) (XPL). c) PPL view of image (b) with detail of glauconite in inset (white rectangle) (PPL). The hole in the centre of the glauconite in image c) was created during slide manufacture.

8.4 Discussion

8.4.1 Controls

Controls above the coffin are separated into two groups, the upper grave fill C2 (C2A-C) and the lower grave fill C3 (C3A-C; Figure 8.4). Differences between the upper grave fill and the lower grave fill controls including the greater extent of weathering of the rocks and minerals observed in the former are attributed to leaching down the profile (Sections 8.3.1 and 8.3.2). Micromorphological analysis of types and levels of mineral weathering of glauconite, granitic clasts and limestone fragments suggests that different sediment processes were operating in the sediments above the coffin from those within the coffin (Sections 8.3.1-8.3.3).

8.4.2 Controls and samples

No quantifiable differences in the optical traits were identified between the intra-coffin controls (C4) and the samples (S1, S2, S3, S17 and A32). Differences between the samples and the C2 and C3 controls were observed. Such differences include the greater amount of fine material (present as coatings on coarse materials) and absence of the larger size categories of the coarse (>50 µm) materials in the samples than in the above coffin controls (Section 8.3.2). Bone and coffin wood remains were present in samples and absent in above coffin controls and are interpreted as evidence that the pig and coffin had fragmented and degraded but remained within the limits of the coffin (Section 8.3.3).

8.4.3 Experimental burials and archaeological burials

Research aims outlined in the thesis introduction (Chapter 1) were to identify the types of post-depositional processes in these short term burials including the decomposition factors, degradation processes which act on the associated grave goods and changes to the host sediment post-deposition of the body. Thin section analysis of the Pig 1 burial sediments suggest that in a coarse (sand-sized texture) sediment with good drainage, the coarse inorganic fraction (*i.e.* the sand-sized rocks and minerals) varies in the weathering patterns and extents, size, colours and morphology of minerals (Section 8.3) between sediments within the coffin and sediments above the coffin. This suggests that the post-depositional processes inferred through micromorphological analysis of the coarse mineral fraction in experimental graves could be of significant value in understanding similar sediment processes related to the decomposition of the human remains in archaeological burials. The micromorphological approach includes a study of the coarse-grained (*i.e.* >64 microns) rocks and minerals that are not included in organic geochemical analyses (GC-MS) or in most of the commonly used inorganic analyses which rely on an assessment of the silt and clay-sized fractions

only and sieve out these coarse grained materials during the early stages of sample preparation (*e.g.* XRD, XRF, or ICP-MS by *aqua regia*; Chapter 9).

8.5 Conclusions

Differences in the sediment within and above the coffin were identified through the assessment of optical characteristics of the mineral content and structure (Section 8.4). In relation to the interpretation of features observed in thin sections from archaeological burial sediments, the most promising results were the post-depositional alterations to glauconite and possible tunneling into quartz grains related to fungal activities (Sections 8.3.5.2 and 8.3.4, respectively). However, the tunnels in the quartz grains could have been caused through dissolution of prismatic inclusions in these grains and a stronger interpretation would require SEM analyses of several loose grains on stub mounts.

Chapter 9. Discussion and summary

Archaeological grave sediments have been investigated in terms of their weathering and site-based interpretations have been discussed at the end of case study (Chapters 4-8). In this chapter, the results are summarised (Section 9.1) and discussed with reference to differences in weathering trajectories between controls and samples by mineral type (Section 9.2) and in relation to microbial markers (Section 9.3) to investigate trends which could be useful when considering sampling in future excavations. This, together with an evaluation of the achievements of the thesis aims and objectives (Section 9.4) and the sampling strategy (Section 9.4.1) led to suggestions on new directions for future work (Section 9.5).

9.1 Overview of results of case studies

Analysis of thin sections from Hofstaðir with burials of 10th century AD on volcanic soils showed a difference in tephra weathering ratio as determined by point counting, between samples of grave sediments and controls (Section 4.3.6). The results of this analysis of the weathering of tephra (Figure 4.31) suggested that the activities of fungal populations in the grave sediments could be related to the decomposition of inhumed remains and, if developed further, has potential in future investigations of archaeological burials in regions with volcanic soils.

Observation of thin sections from controls and samples of grave sediments from Mesolithic period graves at Al Khiday in Sudan, suggested that remains of past fungal activity was preserved in bone fragments (Sections 5.3.4 and 5.4.3). Blue coloured minerals, tentatively identified as vivianite (Section 5.4.5.3), were present in samples and absent in the control at Al Khiday but their presence could not be confidently attributed as an effect of the processes associated with the degradation of the buried remains due to the lack of well defined control thin sections to compare against the samples. This site had only one control thin section and the spatial relationship between the locations of the C1 control and the skeletal remains from the burials was not recorded by the sampler from the InterArChive project during collection of the micromorphology samples and controls. However, the presence of a calcrete in these sediments, was an advantage to the investigation of the burial sediments at Al Khiday using the micromorphological approach as this helped to preserve the grave sediments *in situ* adjacent to the skeletal remains, rather than expose the sediments to wind erosion (Section 5.4.4).

In contrast to the analyses of the mostly (excepting GR 115 from Hofstaðir) single inhumation burials from Hofstaðir, Al Khiday and Sala Vastmaal, the grave sediments from Tel Qarassa were

from a cache of skulls. Differences between controls and samples of grave sediments at Tel Qarassa were not discernible in the thin sections (Section 6.4.1). The lack of clear variation between samples and controls at this site could be at least partially due to the reuse of sediments over time during the occupation and use of the Tell and the burial of the skulls within a domestic area (Sections 6.4.1 and 6.4.2). Firm interpretations of post-depositional processes related to the impact of the degradation of the skeletal remains on their adjacent sediments were not possible with the current limited dataset (Sections 6.4 and 6.5). Reburials of skulls in skull caches within urban areas, as at Tel Qarassa (Section 6.1), was not unusual for buried remains in the PPNB cultural practices regarding the disposal of the dead (Section 6.5), and the results of the analyses of thin sections from this site were not able to contribute much to the archaeological investigation of these burials.

The 16th century Viking burials at Sala Vastmaal in an area of clay-rich soils with local lead ore deposits (galena) contrasted to the volcanic soils surrounding the earlier (10th century) site at Hofstaðir (Sections 6.1 and 3.1). Differences in micro-contextual spatial relationships between minerals and buried remains, such as bone, wood and fungi, were observed in the thin sections from samples compared to controls (Sections 7.4.8 and 7.5). Chloritized biotite was present in the samples of grave sediments adjacent to the skeletal remains and absent in the controls and biotite was observed indicating weathering to clays in the controls (Sections 7.4.2, 7.4.3 and 7.4.8). The interpretations of the analysis of the micro-contextual spatial relationships between minerals and organic matter, including fungi, where limited by a lack of micro-probe crystallographic analyses, such as micro-probe XRD, (Section 7.3.4) and confident identification of fungal species from their spores and fragmented remains (Sections 7.4.1 and 7.5). However, the thin sections suggested that micro-scale spatial relationships between minerals and fungi were present in the grave sediments and suggest a potential for further development of the analysis of this relationship in future studies.

The case studies at Hofstaðir, Al Khiday, Tel Qarassa and Sala Vastmaal investigated post-depositional processes affecting the buried remains in their sedimentary context over archaeological time periods, in contrast to the experimental pig burial which was buried for three years (Section 8.1). However, three years could have been sufficient time to enable observations related to the *in situ* decomposition of the buried remains (Section 2.5). No quantifiable discernible differences were observed between samples and controls in relation to mineral weathering, however there was a difference in the colour of the glauconite grains which may be related to differences in redox conditions between the samples and controls (Section 8.3.5.3). The results of this burial were limited by the heterogeneous imported sand used in the burial of the pig, which introduced a range of mineralogical materials which were weathered to varying extents at the time of burial, leading to difficulties in discerning the effects of post-burial from pre-burial processes.

9.2 Rock and mineral weathering and alteration in experimental and archaeological burials

The interpretations of the results from the sediments of the archaeological and the experimental samples and controls are discussed in the following sections (Sections 9.2.1 to 9.2.7). The aim of the experimental burial, as outlined in the thesis introduction (Chapter 1), was to examine the relationship between the decomposition of the body and the post-depositional changes to the surrounding sediment in the grave. Where differences in the post-depositional processes affecting the inorganic (mineral) fraction of the sediment were identified they have been interpreted to relate to the decomposition of the human remains and coffin in the archaeological burials and the pig remains and coffin in the experimental burial (Sections 9.2.1-9.3.2).

9.2.1 Rock fragments

Rock fragments were observed in thin sections from Sala (Chapter 7), Tel Qarassa (Chapter 6) and the experimental burial (Chapter 8). Quartz and mica-rich rocks were observed in the sediments from Sala, basalt from Tel Qarassa, and limestones (shelly, oolitic and micro-crystalline) from the experimental burial. Rock fragments were consistently more weathered in samples than in their counterpart controls for the sites assessed (Sala Vastmaal, Tel Qarassa and the experimental burial) and volcanic clasts (vitric and hypocrystalline tephra) were more weathered in samples than in their controls at Hofstaðir (Chapter 4).

The increased weathering of rock fragments in samples than in the controls represents an important contribution from thin section analysis as only micromorphology and SEM-EDS analyses enabled assessment of the >2 mm mineral fraction of the sediments. For example, geochemical analysis by GCMS only concerned the fine (<64 μm) fraction.

Assessments of sedimentary processes should take into account a range of sizes of geological materials, including >2 mm grains and rock fragments, as previous studies suggest that rock fragments can affect, and display effects of, sedimentary, pedogenic and weathering processes (Certini *et al.* 2003). The work of Certini *et al.* (2003) suggested that the coarser (>2 mm) geological fraction (of quartz and mica-rich rock fragments) displayed increased weathering up a soil profile and that in all sediment horizons below the topsoil the mica components of the rock fragments were homogeneously weathered from their exteriors to interiors. Such results are comparable to the findings of this work in relation to mineral weathering from the grave samples from Sala, which also showed weathering of muscovite and biotite in the coarse fraction (>64 μm) (Section 7.4.8).

The sand-sized basaltic clasts in the thin sections from Tel Qarassa exhibited differences in the morphologies of the opaque secondary iron-oxides held within the coarse basalt fragments (Chapter 6). The absence of such secondary iron-oxides in the fine fraction (silt and clay-sized) of the sediments from Tel Qarassa is supported by the literature on basaltic-rich sediments as other studies have suggested an uneven distribution of iron oxides across the different grain size fractions (sand, silt and clay) (Resende 1976; Curi and Franzmeier 1987; Goulart *et al.* 1998). Furthermore, Mossbauer analytical studies expanded the identification of magnetite in basalt-rich sediments to include sand-sized materials and found that it was absent in the <2 mm fraction and present within cracks in the materials of the >2 mm fraction (Goulart *et al.* 1998). The difference in the morphologies of the opaque iron oxides in basalt fragments from Tel Qarassa has been interpreted as differences in the alteration of the rock fragments and not a product of differences in weathering related to the post-depositional processes in the burial environment (Section 6.3.6). Future studies, however, could extend the analysis of iron oxides in basalt fragments to include a detailed study of their removal through weathering processes, as iron oxides may become soluble in soil solutions. Fine materials (<2 mm or <64 μm size) are often studied in soil science as their high surface area to volume ratio makes them susceptible to weathering by their sediment environments and ideal candidates to study the effects of pedogenetic processes. By contrast, the coarser (>64 μm) materials can retain the effects of past events, *via* secondary minerals, while not being affected by more recent processes. Hence, the potential exists for them to indicate past sediment processes on the archaeological timescale.

9.2.2 Amphiboles, pyroxenes and olivine

Amphibole weathering in grave sediments was recognised in thin sections from Al Khiday (Chapter 5) and amphibole, pyroxene and olivine weathering in sections from Tel Qarassa (Chapter 6). At both sites the weathering extents (scalar data) and weathering patterns (nominal data) in the controls and the samples were different. The amphiboles of the calcic-sodic solution series were weathered in the samples from Al Khiday (Chapter 5) but not in the control. The weathering of amphiboles in the grave sediments from Al Khiday is tentatively interpreted as related to the decomposition of the body or to the movement of calcium-rich solutions throughout the profile (Chapter 5 and Section 9.1). Comparison of the mineral weathering in samples and controls from Tel Qarrassa did not show a clear difference and is interpreted as a result of the complex stratigraphy and reuse of sediments in the tell deposits (Chapter 6 and Section 9.1).

9.2.3 Opaque materials

The opaque secondary product phenocrysts in basaltic clasts in sections from Tel Qarassa and the experimental pig burial had a different range of morphologies in the controls and the samples but this has been interpreted as a result of variability within the local sediments and not as a result of processes related to the degradation of the skeletal remains (Sections 6.4.1, 8.4.2 and 9.1). Opaque secondary products were observed adjacent to amphiboles and weathered granitic rock fragments in sediments from the experimental pig burial (Section 8.3.2.5). These did not appear to have distinct forms in standard thickness thin sections (30 µm thick), but in ultra-thin sections (10 µm thick) these opaque materials were observed to have either circular or cubic morphologies (Chapter 8). Such a difference between thin and ultra-thin sections could have been a result of their small size in the rock fragments from grave sediments of Pig 1.

It is known that the most intense period of post-depositional alterations to buried remains occurs in the first 3 to 5 years after burial (Tibbett and Carter 2008) and that magnetite and maghemite can be formed in grave sediments during microbially driven processes (Ehrlich 1996 and 1998). Detailed observations on opaque deposits adjacent to bone fragments, as in the thin sections from Hofstaðir (Section 4.3.4.1) could be of value in attaining a more thorough understanding of advanced post-depositional processes in archaeological burial sediments. Several recent studies on mineral and microbe interactions in sediments demonstrated that aerobic respiration directly affects mineral states of manganese and iron oxides (Huang *et al.* 2008). Bacteria and fungi in soils and sediments can contribute to mineral formation or dissolution in order to gain energy or electrons when oxygen is limited or absent or to obtain trace elements which are not alternately available (Ehrlich 1996). Such activities are capable of microbial reduction of Fe (III) in soils and sediments (Lovley 1997, Küsel *et al.* 1999). Manganese (II) oxidizing bacteria and fungi have been studied intensively through multiple methods of analysis and their opaque deposits could be useful as proxy evidence of past bacterial activity in sediments (Tebo *et al.* 2005). Hence, while manganese and iron oxides are often opaque in thin section it is suggested an analysis of such oxides through micromorphology related to their micro-contextual location in relation to their inorganic and organic surroundings could contribute to distinction of grave sediments from controls.

9.2.4 Muscovite, biotite, chlorite and vivianite

Biotite and chlorite were present in sediments from Sala (Chapter 7) and vivianite in sediments from Al Khiday (Chapter 5). Weathering of micas (muscovite and biotite) was observed and greater weathering extents were measured for samples than for controls at Sala (Chapter 7). Vivianite was observed in clustered arrangement around the edges of peds in samples from Al Khiday (Chapter 5), suggesting that the vivianite formed after the peds and inter-ped voids had formed. The inter-

ped voids may have previously held solutions that were active in the formation of vivianite at these micro-contextual locations within grave sediments. Chlorite was identified in spatial association with bone fragments and organic matter in samples from grave sediments at Sala (Section 7.4.2). The increased weathering rate of biotite and muscovite in grave sediments at Sala is interpreted as an effect of the decomposition of the body (Sections 7.3.3, 7.4.8 and 9.1). Previous works suggest that mineral-microbe interactions are capable of affecting mineral weathering of micas (Gadd 2007).

9.2.4.1 Indirect and direct relationships between fungi and mineral weathering

Fungi are known to be able to exert indirect effects on the weathering of primary micas in soils and sediments (Balogh-Brunstad *et al.* 2008). Accelerated rates of biotite weathering have been attributed to the acidification of soil solutions by the respiratory activities of ectomycorrhizal fungi, *via* their production of weak organic acids, CO_2 and the complexation of cations (Balogh-Brunstad *et al.* 2008). Studies of weathering rates of biotite in solutions with ectomycorrhizal fungi suggested that the rates they observed could be increased if the biotite and fungi had been in the presence of a carbohydrate source (Balogh-Brunstad *et al.* 2008). Such studies supported interpretations from earlier experiments which suggested that respiration rates of mycorrhizal fungi were increased in the presence of simple carbohydrates (Nehls *et al.* 2007). The appreciable carbohydrate content of a body supports the suggestion that the greater extent of biotite weathering in the grave samples than the control sediments at Sala Vastmaal can be attributable to the presence of the buried body.

The discolouration of the sheet-like layers of biotite in samples (Figure 7.17) and an even expansion of lamellar spaces and infilling by fine material in the controls (Figure 7.12) were observed in the sediments from Sala and attributed to the direct effects of fungi. The studies by Lian *et al.* (2008) support the interpretation that the weathering of interlayer spaces of biotite can be related to fungal respiration and direct relationships are known to occur between biotite weathering and microbial populations (He *et al.* 2005 and Hopf *et al.* 2009). Experimental data on biotite dissolution in the presence of microbes suggested that bacteria and fungi are capable of preferentially removing K+ from interlayer spaces of biotite, resulting in incongruent dissolution of the phyllosilicate (Hopf *et al.* 2009). The experiments of Lian *et al.* (2008) suggested that *Aspergillus fumigatus* are capable of liberating three times the level of potassium cations that is released from controls in timeframes as short as 30 days. The interpretation of micro-contextual dissolution of mica minerals by fungi in samples from Sala (Figure 7.22 and Section 9.1) is supported by previous experimental studies which suggested that mineral dissolution can be micro-contextually specific to microbially produced hydroxamates and much higher on biotite mineral surfaces than in the bulk sediment (Ahmed and Holmström 2014a).

9.2.5 Glauconite

Glauconite was present in sediments from Al Khiday (Chapter 5), Tel Qarassa (Chapter 6) and the experimental burial (Chapter 8), and its mineralogy is discussed in Chapter 5. This mineral was inferred to have weathered more extensively in control sediments than in samples of grave fills at these sites (Al Khiday, Tel Qarassa, and experimental burial). Glauconite was found on bone fragments in samples from the experimental burial (Chapter 8 Figure 8.25) where its grains from the controls were inferred to have altered *via* iron translocating pedogenetic processes, leached in the upper grave fills (C2) and enriched in the lower grave fills (C3) in the experimental burial (Sections 8.3.5.3 and 9.1). The glauconite grains in the samples from this burial were relatively unaltered (Figure 8.24). This could have resulted from reduction in the burial sediments "cleaning" the oxidized grains. Glauconite is known to be weathered to clays (smectite and illite) in soils where conditions are suitable (Buatier *et al.* 1989). Hence, the archaeological and experimental results suggest that glauconite could be often leached in controls, weathering to secondary clays (illite or smectite) or altered by iron accumulation, in contrast to samples. Such an inference could be tested on more grave sediments in future work (Section 9.5).

9.2.6 Tephra, plagioclase and fungi

Point counting analysis indicated that the weathering rate of tephra is greater in grave sediments than in controls, and micromorphological observations of plagioclase weathering were different for samples and controls at Hofstaðir (Section 4.3.6 and Figure 4.31). These differences in mineral weathering are interpreted to suggest that sediment processes were affected by the decomposition of the body (Section 4.3.6). Decomposition processes may include activities of fungi and bacteria (Tibbett and Carter 2008) which could indirectly or directly weather minerals as such biotic weathering processes are often driven by aerobic microbial respiration, producing CO_2 and lowering pH (Huang 2008).

Fungal hyphae were observed to have intruded into silica-rich silicates in archaeological (Hofstaðir Chapter 4) and experimental (Pig 1 Chapter 8) grave sediments. Fungal hyphae and tunnels from hyphae were observed in the vitric component of tephra and sand-sized plagioclase grains at Hofstaðir and fungal hyphae were interpreted to have tunnelled into a quartzose sand grain in a sample from Pig 1.

By contrast to the phyllosilicate minerals muscovite, biotite, chlorite and glauconite, the more silica-rich mineralogical materials of vitric tephra, plagioclase and quartz are generally regarded as more stable in soils (Goldich weathering sequence, Goldich 1938; Chapter 3). Field and laboratory based

studies suggest that the contribution by fungal mediated weathering processes to silica rich silicates (quartz and feldspars) is a smaller factor in their weathering than their role in minerals richer in K and Fe (Rogers and Bennett 2004). Hence, biotically driven weathering *via* fungal tunneling into these less readily weathered sediment minerals could serve as a marker in contributing to the identification of graves at archaeological sites (Section 9.5).

Previous studies have shown that fungi are capable of tunneling into volcanic glass (McLoughlin *et al.* 2008) and plagioclase (Hoffland *et al.* 2002). Tubules into plagioclase are known to be achieved partially by chemical erosion of these mineralogical materials via the exudation of dissolution enhancing polysaccharides by the fungal hyphae (Welch *et al.* 1999). Previous studies, however, suggested that fungal tunneling into feldspars is less prevalent in soils younger than 5000 years than in older ones, and within such younger soils, even less common in sodic-calcic (plagioclase) feldspars than in K-feldspars (microcline) (Smits *et al.* 2005). This would suggest that the fungal driven weathering observed on the plagioclase (Figure 4.30) in the recently deposited volcanic sediments at Hofstaðir is unusual for these sediments and is inferred as a result of the pine wood coffined burials. Several studies have investigated the effects of fungi associated with *Pinus sylvestris* (pine) and biotic weathering patterns and extents of feldspar grains, however, these are limited to ectomycorrhizal fungi of *Pinus* (Landeweert *et al.* 2001, Smits *et al.* 2005, Fomina *et al.* 2006a, van Schöll *et al.* 2008). It is suggested based on the plagioclase weathering and the pine coffin degradation observed at Hofstaðir (Section 4.3.6), that a similar relationship could exist between biotic feldspar weathering and fungi saprophytic of *Pinus* woods (Section 9.5).

Early studies suggested that bacteria present in topsoils could be inhibitors of the formation of short range order silicates (SRO, *e.g.* allophane and imogolite) (Urrutia and Beveridge 1995) which are typical weathering products of tephra. Recent studies suggest that the interactions between microbes and mineral weathering in sediments is more complex and interdependent than merely the adhesion of bacteria to surfaces and the effects of bacterially produced low molecular weight organic acids (Urrutia and Beveridge 1995) and may include the physico-chemical effects of a range of excreted polysaccharides (Welch *et al.* 1999).

Accelerated tephra weathering in grave sediments at Hofstaðir could be a useful tool in identification of graves in Iceland (Section 9.5). The region's soils are relatively young and biotically sterile (andosols) and these mineral weathering processes can alter the tephra even in relatively young graves (*c.* 1000 years) (Section 4.1). Tubes created by fungi boring into tephra are known to be able to preserve for several thousands of years (McLoughlin *et al.* 2008). Similarly to biotically driven mineral weathering at Tel Qarassa (Sections 9.1.1 and 9.1.2), the penetration of fungal hyphae into plagioclase grains in grave sediments at Hofstaðir is also interpreted as a result of the impact of the decomposition of the body (Section 4.3.6). Previous work on feldspar weathering in

soils suggested that biotic weathering is a small factor in plagioclase weathering and was only present in the soils older than 1650 years (Smits *et al.* 2005) and could support the interpretation that the biotic weathering of the plagioclase in the grave sediments at Hofstaðir was in contrast to non-grave soils (Section 9.1).

9.2.7 Summary

In some sites, sediment processes, such as tephra weathering at Hofstaðir, were interpreted to have affected samples but not controls, suggesting that they were related to the burial micro-environments of grave sediments. It is suggested that processes associated with the deposition and microbial decomposition of the body contributed to the differences in weathering trajectories of the sediment minerals in grave sediments (Sections 9.1.1-9.1.6). Such complex sediment processes affect mineral weathering trajectories, such as biotite, glauconite and tephra, in burial sediments. Hence, sediment mineral microbe interactions could contribute to distinguishing grave from non-grave sediments at archaeological sites.

9.3 Microbial markers in graves

Fungi are common in soils (mycorrhizal) (Sanderman and Amundsen 2005, 258) and in graves (detrital) (Tibbett and Carter 2008). Past fungal activity was interpreted from either direct or proxy evidence in thin sections of grave sediments from all of the sites except Tel Qarassa (Sections 9.1 and 9.2). Fungi were often observed in thin sections of lower grave fill controls (C3) and samples from under the body ("Z" position samples) in Hofstaðir, Sala Vastmaal and the experimental burial (Chapters 4, 7, and 8). This association is interpreted as an effect of the relationship between the fungi and the degradation of the inhumed remains, including coffin wood in graves from Sala and Hofstaðir (Section 9.1).

Micromorphological observations of estimated abundance of fungi were occasionally higher in samples (S1, S2 and S3 positions) and lower grave fill controls (C3) than in site controls (C1) and upper grave fill controls (C2; Figure 9.1). Figure 9.1 shows the results of the estimated abundance of fungal remains observed in thin sections from samples and controls at Hofstaðir (pink) and Sala Vastmaal (blue). However, the direct evidence of fungi (Figure 9.1) does not show the same clear pattern revealed in some cases by the proxy data, as shown for example, in Figure 4.31 for Hofstaðir. Proxy data for fungal activity was recorded from micromorphological observations on bone (Section 9.3.1) and minerals (Section 9.3.2). Comparison of the medians and interquartile

ranges in the box plots of Figures 9.1 and 9.2 suggests that the proxy data can be a stronger indicator for the identification of grave sediments than quantification of fungal remains in thin section. Such an interpretation is supported by previous studies suggesting that tubules left by fungi will be more numerous than inhabiting fungal populations (Jans 2008). However, not all fungi can create tubules as only a small proportion of fungal species can actively penetrate mineral grains (euendoliths), while other fungi may exploit pre-existing fractures and etch pits (chasmoendoliths and cryptoendoliths) (Golubic *et al.* 1981 in McLoughlin *et al.* 2008).

The trend of increased mineral weathering with increasing proximity to the skeletal remains at Hofstaðir (Figures 4.31 and 9.2) may also be due to the actions of bacteria in the grave sediments. Previous laboratory-based studies on volcanic glass from Iceland suggested that bacteria contributed to weathering by reducing pH conditions at micro-sites on mineral surfaces (Thorseth *et al.* 1995). Microbially driven accelerated weathering of glasses has been studied on deep sea Miocene tephra (McLoughlin *et al.* 2008) and in recent glass such as window panes of historic churches (Mellor 1922). Such studies also suggested that mineral weathering of glass substrates can occur on archaeological timescales and persist for geological timescales (Mellor 1922 cited in McLoughlin *et al.* 2008 and Thorseth *et al.* 1995) and McLoughlin *et al.* (2008). This supports the interpretation that microbially driven mineral weathering is a potential indicator of grave sediments (Sections 4.3.6 and 9.1), and suggests that this could be used in future burial archaeology studies.

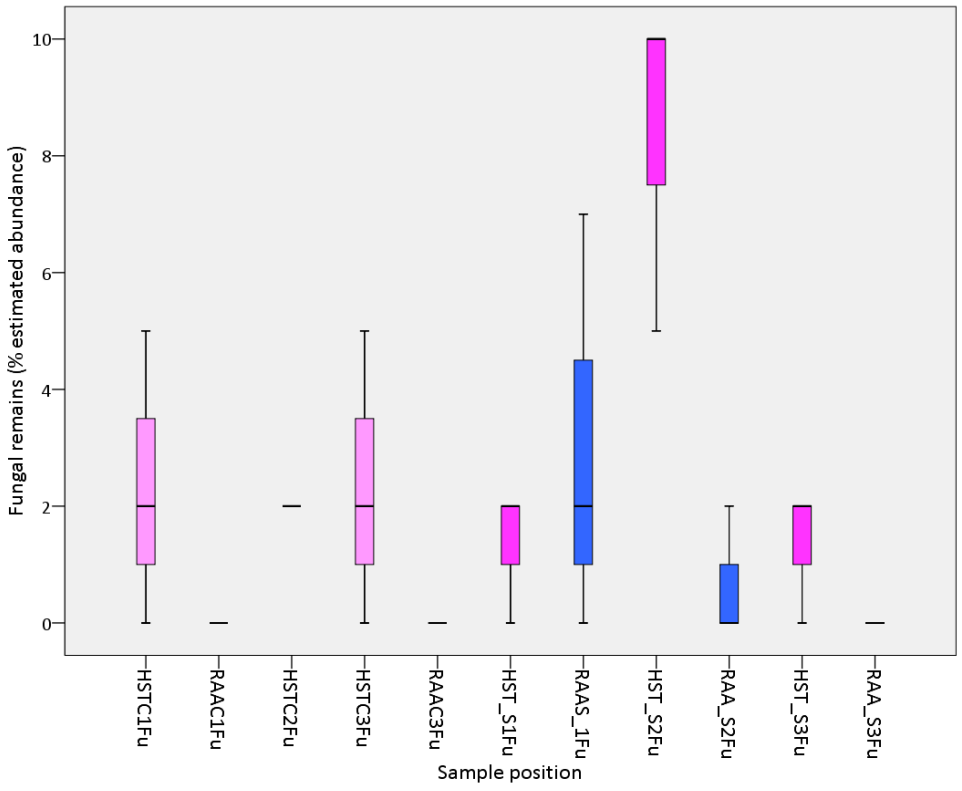

Figure 9.1: Estimated abundance (%) of fungal remains (hyphae, spores and sclerotia) observed in thin sections of controls and samples from Hofstaðir (HST; pink coloured bars) and Sala (RAA; blue coloured bars). Results are listed by site controls (C1), upper grave fill controls (C2), lower grave fill controls (C3), skull adjacent samples (S1), pelvis adjacent samples (S2), and feet adjacent samples (S3) (from left to right). Controls are shown in paler coloured bars.

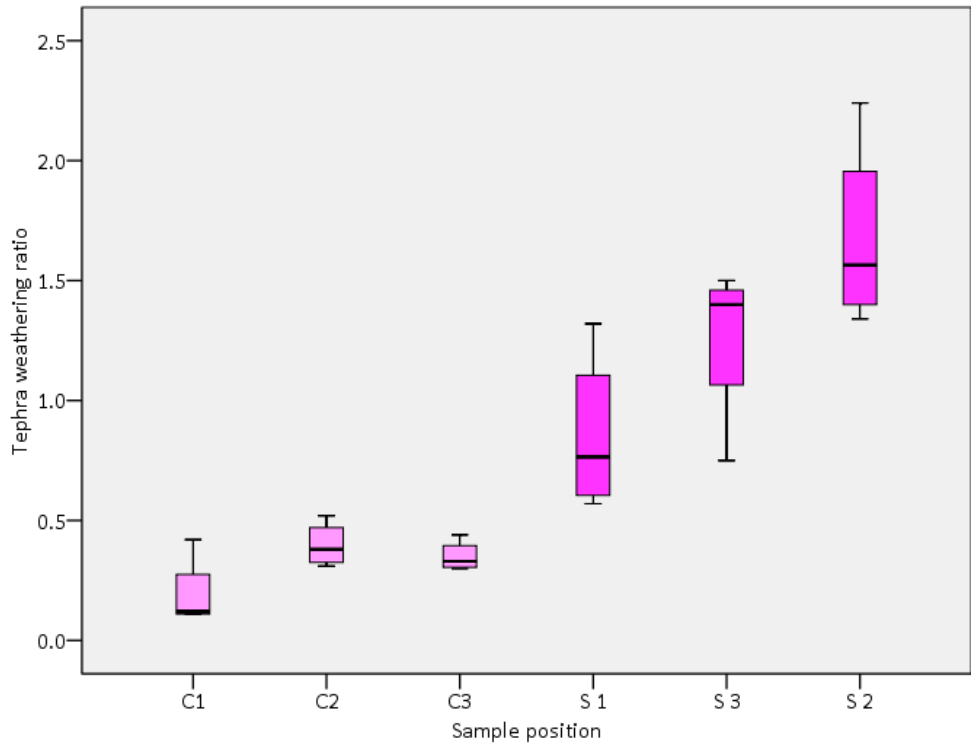

Figure 9.2: Weathering ratio from point counting analysis of tephra in thin sections from controls (C2, C3) and samples (S1, S2 and S3,4) of all seven graves sampled (GR 114-120) (Modified from Figure 4.31 in Chapter 4). Controls are shown in paler coloured bars.

9.3.1 Bone alteration

Post-mortem alteration of bone fragments, causing blackening, was observed in a sample from Hofstaðir. The interior of a large bone fragment from this sample (Hofstaðir, GR 120, SA1, TS 753) had blackened and appeared opaque in thin section (Section 4.3.4.1). Interpretations from combined SEM-EDS analysis and micromorphological observations suggested that this blackening was due to post-burial microbial (fungal or bacterial) degradation of the bone (Section 4.3.4.1). Microbial alteration to bones from grave sediments at Al Khiday could be identified as proxy data for fungi by the identification of Wedl tunneling (Wedl 1864 in Hackett 1981) in the bones (Section 5.4.3). Although the fungal remains had since been removed by sedimentological processes the tunnels had been preserved and infilled with fine (silt and clay sized sediments) material (Sections 5.3.4 and 5.4.3). The micro-scale alterations (Wedl tunnels) to the morphology of the bone allowed recognition of fungal activity in the graves shortly after death and burial (Sections 2.2-2.4 and 5.4.3) and serve as proxy data of fungal populations in the contemporaneous burial sediments. It has been suggested that weathering of buried bones by fungi is determined by the fungal populations

which colonize the material and is largely controlled by sediment type (Pacheco *et al.* 2012). As such, it could be that Wedl tunnels on bone fragments could be used to infer that the archaeologically contemporaneous sediment (Mesolithic period at Al Khiday) was more organic-rich and fertile than the aridisol that now covers the site (Section 5.5).

9.3.2 Biotic weathering of inorganics

Thin section analysis from Hofstaðir and Sala provided evidence of fungi by direct (spores, hyphae, sclerotia) and proxy (mineral or bone weathering) data. By contrast, Al Khiday only had trace (micro-scale) proxy (borings created by past fungal hyphae) evidence. Such proxy evidence in samples from Al Khiday makes an important contribution as the organic geochemical analysis at this site did not identify any evidence for the presence of fungi.

Accelerated tephra weathering in grave sediments from Hofstaðir suggests that fungal organisms can contribute to mineral weathering (Section 9.1). Interpretations from Sala suggest that the role of detrital organisms may be instrumental in the weathering pathways of mica minerals and in the samples from this site there was a difference in muscovite and biotite weathering patterns from the controls to the samples (Sections 9.1 and 9.2.4). Mica expansion-swelling (to produce kata-alteromorphs of muscovite and biotite) to form clays occurred where biotic weathering was negligible (controls) and complex weathering patterns (iron stained tops and bottoms) were present in grave sediments (samples) where trace evidence of past biotic activity was higher (Sections 7.4.1, 7.42, 9.1 and 9.2.4). The mineral weathering patterns in the poorly-drained grave sediments at Sala and the histic andosols at Hofstaðir suggest that a range of silicate minerals can be useful in the identification of grave sediments, by exhibiting elevated levels of abiotic weathering in samples than in controls in these two distinct sediment types (Section 9.1).

9.4 Research outcome in relation to aims and objectives

The thesis aims were to assess the limitations on retrieval of information regarding organic material deposited with the burial and the efficiency of micromorphology sampling protocols (Chapter 1, Section 1.1.2). The evidence presented and discussed in Chapters 4-8 and Sections 9.1-9.3 above, strongly suggests that micromorphological analysis of grave sediments can extend the limits to which presence of organic material in graves is identifiable through assessment of mineral weathering as proxy data for past organic material at the micro-scale.

The thesis objectives were to assess the extent to which micro-scale post-excavation methods aided macro-scale field based observations on the degradation of organic materials through an analysis of their interactions with the inorganic materials of the sediments, to assess the InterArChive sampling strategy and the manufacturing method for thin sections of grave sediments in relation to the different types of burial sediment environment (Sections 1.3.1-1.3.3). In relation to Objective 1 (Section 1.3.1), it is suggested that micromorphological analysis of grave sediments can aid identifications of graves (Section 9.1) and interpretations of post-burial processes related to decomposition of the inhumation (Sections 9.2 and 9.3). Furthermore, it is suggested that coffined burials may be inferred through the interpretation of the effects on mineral weathering which can be related to activities of wood root fungi, however such interpretations would benefit from comparisons with future analyses of uncoffined burials (Section 9.3.2). The assessment of the InterArChive sampling strategy which was used in the collection of micromorphology samples and controls (Objective 2, Section 1.3.2) in the case studies in Chapters 4-8 could be improved in future excavations and is not suggested as appropriate for the study of burials in Tel sites (Sections 9.1 and 9.4.1). Objective 3 was to assess the extent to which additional information was gained through the production of two thin sections, tangential and perpendicular oriented thin sections, from each micromorphology sample (Section 1.3.3) and the interpretations of the results suggest that the optimal recovery of evidence from thin section is obtained when they are oriented perpendicular to the remains (Section 4.3.5.3). The information from the results of the analysis of perpendicular thin sections was aided very little by additional information from the tangential sections (Section 7.4.6), suggesting that in future studies only perpendicular sections are required (Section 9.4.1).

9.4.1 Suitability of the sampling strategy and experimental burial design

The location of the C1, C2 and C3 controls designated in the InterArChive project were not suitable for the archaeological sites studied in Chapters 4-7. It is suggested that in future, a control should be taken at equal level to the body outside the grave cut and if a second controls is to be collected it should be from below the grave. A site control (C1 control) was often not an adequate representation of non-grave sediment, as sediments in an archaeological site vary according to stratigraphy rather than soil horizons and can differ over short lateral distances. An exception to this was the collection of C1 controls taken from Hofstaðir, as these controls spanned several layers and included material below the level of the graves However, it is not suggested that >5 micromorphology controls are feasible in terms of time, labour or materials in the majority of archaeological research. Multiple controls would enable a discussion of intra-layer variability and this should be lower than the difference between the samples and the controls where sediments were affected by the burial. Multiple controls could be done using grain mounts or thin sections of

the sand fraction from the sediments to observe surface microfeatures with SEM or the inside of grains, respectively.

The experimental burial designed by the InterArChive project at Hovingham was flawed in some respects. Sand used to bury the pig should have been from a single known source rather than a mixture of unknown sources. However, it is arguable whether imported sediment should have been used at all. The experiment would have had greater similarity to archaeological burials if the material used to fill the grave cut had been the material removed to create the grave. Using the same sediment would have introduced the topsoil and roots to the burial environment as in other burial in grass covered locations. Contrary to the experimental design used at Hovingham by the InterArChive project, coffins are not suggested to be filled with sediment during burials as most coffined archaeological burials were not and instead have a large pocket of air. Such an oxygenated cavity within the burial environment would have affected the biota capable of surviving and redox conditions of the micro-environments. Filling the coffins with sediment prior to burial could have also aided in the preservation of the coffin's structure by supporting the lid and walls against external stresses.

If sediment is required within the coffin during sampling at the time of excavation then it is suggested to experiment with methods of coffin collapse, for example coffins could be buried deeper and made in a long narrow shape rather than the rectangular form used at Hovingham. Results from a thorough analysis of collapse and pressure loading of 397 coffins from the 19th century North Brisbane Burial ground have suggested that deeper adult coffins may be more prone to collapse than shallow child coffins (McGowan and Prangnell 2015). Almost all coffin lids had collapsed and sediment was adjacent to the remains and increasing the depth of adult coffins from 0.91 m to 1.83 m in a saturated clay substrate was found to more than double the vertical pressure on the coffin (McGowan and Prangnell 2015). The number of years required for the coffin to collapse is unknown, and could be outside of the range of a short term burial project, however the principle of a deeper burial with an elongated hexagonal coffin leading towards a greater stress on the lid could be applied to experimental designs where sediment adjacent to the remains is required for sampling.

9.5 Future work

The grave sediments typically had elevated levels of root activity compared to the control sediments. Previous works have discussed types of fungi, including both saprophytic and ectomycorrhizal fungi which are symbiotes with roots, which can affect weathering of particular

minerals and rocks (Gadd 2007 table 2, taken from Burford *et al.* 2003 and adapted from Hirsch *et al.* 1995; Kumar and Kumar 1999, Sterflinger 2000; Verrecchia 2000). In particular, the results of the analyses of perpendicular and tangential oriented thin sections from the case studies in Chapters 4-8 suggested that only one thin section from each sample block is necessary (Section 9.4). Direct data on fungal attack *via* geochemical analysis are not able to detect the enzymatic substances produced (weak organic acids such as oxalic acid) by the fungi as they do not survive in sediments on the archaeological timescale. However, the effects of fungal activities on the inorganic mineral assemblages in sediments were shown, as with tephra weathering at Hofstaðir, capable of preserving the effects of past activities of detrital organisms and this could be developed further in future studies to include the effects of fungi on sediments from a wider range of soil types. Siderophores released by bacteria and fungi can increase the bioavailability of Fe from iron-bearing minerals and have contributed to investigating how this chemical attack is performed (Ahmed and Holmström 2014b). It has been theorized that the increased bioavailability of Fe occurs, in part, through the exudation of fungal metabolites (weak organic acids, such as oxalic acid) which chemically degrade the mineral surface as a precursor to the physical boring into the lithic substrate by the fungal organism (Adeyemi and Gadd 2005). The potential of micromorphological analysis for burial archaeology is that this technique allows observation of the mineral morphology and the *in situ* proximity to fungal remains.

Fungi, bacteria, lichens and mosses are all capable of degrading rocks and minerals through a combination of chemical and mechanical processes. Bacteria are known to have an important role in sediments and mineral weathering processes (Bennett *et al.* 2001). However, their small size limits their observation at the scale of the light microscope and effects specifically related to their respiratory activities have not yet been sufficiently studied (Gadd 2007). Populations of lichens and mosses are known to be capable of actively accelerating mineral weathering and selective dissolution of the compounds required for their growth (Vingiani *et al.* 2013, Jackson 2015). However, lichens and mosses are unlikely to be a significant factor in sub-surface sediment processes in burial sediments. It is well understood that fungi can play an active role in the weathering of rocks and minerals (Ehrlich 1998; Gadd 2005, 2006 and 2007; Fomina *et al.* 2005a and b). It is generally understood that this is done to retrieve certain elements that the fungi may require for their nutrition, often allowing a direct source for a symbiotic plant for mycorrhizal fungi (Van Breemen *et al.* 2000).

Hence, further investigations of the accelerated rates and altered paths of mineral weathering in graves sediments than in controls should take account of the effects of fungal and bacterial populations. Future studies on the role of wood rot fungi could be instrumental in the identification of wood coffined burials where the wood has been heavily degraded. Results on volcanic sediments

are particularly encouraging for the identification of graves through accelerated tephra weathering in samples of graves sediments than in the surrounding sediments (Chapter 4) and future work on andosols could expand the investigation of micro-scale differences in tephra weathering with proximity to the remains through point counting analysis on thin sections perpendicular to the skeletal remains. Mica weathering pathways was interpreted in graves sediments from Sala (Section 9.2.4). Recognition of weathered biotite and the presence of vivianite in the sedimentologically very different Sala (heavy clay) and Al Khiday (sand and arid) sediments could be investigated further to assess how widespread these occurrences are in these and other grave sediments. The interactions between biotite and fungi, which are currently also receiving some attention from the geosciences and have suggested that fungal exudates may directly affect the weathering of biotite (Wei *et al.* 2012), and hence it is suggested that this theme of research is used in future archaeological studies of grave sediments. Such research into the relationship between mineralogical alterations, sediment bacteria and fungi respiration would benefit from application of TEM and micro-probe XRD. The effects caused by reduced oxygen levels in grave sediments could be further investigated through analyses of opaque secondary iron-rich minerals in rock fragments through combined micromorphological and micro-probe XRD analyses of thin sections.

In addition to sub-microscopic and micro-probe techniques, future studies could also benefit from advances in the development of thin sections. The production of thin sections from samples collected in the field is a long and laborious process (Sections 2.1 and 3.4.1) and often results in micromorphological observations becoming a part of the post-excavation analyses which stand apart from the excavating decisions of the field archaeologist. Although there are some examples of research excavations in arid sediments, such as at Çatalhöyük (Turkey) and Saar (Bahrain), which have on-site laboratories enabling quick production of thin sections (Matthews *et al.* 1997, Matthews and French 2005 and Weiner 2010), this type of approach is still rare. The long drying and resin embedding times involved in the production of thin sections could be reduced by the use of a water miscible resin which could also enable samples to be embedded with resin on-site, thus reducing disturbance to the sediments during transport (Prone 1976). However, with only one notable exception (Asscher and Goren, submitted 2015), little research has been made recently on *in situ* impregnation or decreasing the sample preparation times. It is crucial however, that this theme is addressed in future studies for developing micromorphology and increasing its prevalence in archaeological research. Furthermore, micromorphology as an *in situ* examination of micro-scale features and remains could benefit from future studies into non-carbon based embedding mediums, such as impregnation with a silica gel. Silica based impregnating material surrounding the sediments could enable quick and efficient identification of carbon based micro-scale remains in archaeological sediments and their micro-contextual spatial relationships.

Chapter 10. Conclusion

Sediments adjacent to the skeletal remains in inhumation burials from several archaeological cemeteries were investigated by thin section analysis and compared with site controls. These archaeological sites were burials of Viking age at Hofstaðir (Iceland) and Sala (Sweden), Meroitic period at Al Khiday (Sudan), and PPNB culture at Tel Qarassa (Syria). Interpretations of the post-burial processes from these archaeological samples have been compared with those from a 3 year experimental burial of a pig in Yorkshire (UK) and it was shown that mineral weathering in sediments adjacent to human and pig remains can be affected by the disturbance of a grave cut and the decomposition of the body (Chapter 9).

The analysis demonstrated that in graves where the body or chemical compounds left by the body are no longer identifiable, fungi may be detected and, when the microbes and the low molecular weight organic acids they produced are no longer traceable, the effects that such acids have had upon the rocks and minerals can be observed. Rocks and minerals persist in sediments until they are weathered beyond recognition. During and after their weathering they can be identifiable from secondary products that are unique to certain primary rocks and minerals. Mineral weathering can be useful in studies of grave sediments by serving as proxy markers of past organic matter and detrital microbial respiration associated with post-depositional processes of inhumation burials. This data source can be especially useful in severely leached or permeable and coarse grained sediments, which are particularly inaccessible to other approaches such as organic geochemical analysis.

Mineral weathering, including dissolution and authigenic mineral formation was observed at some of the sites studied (archaeological and experimental burial sediments). The weathering pathways of micas differed between samples and controls in thin sections from Sala (Chapter 7). The weathering rate of tephra was accelerated in grave sediments compared to in local sediments at Hofstaðir (Chapter 4). The traces of past fungal activity were recorded in the micro-scale morphology of the alterations to bone fragments at Al Khiday (Chapter 5). The proportion of fine (<50 µm) sediment was greater in samples than controls at all sites (Chapters 4-8). Proportions of fine to coarse sediment could quickly and cheaply be determined by sieving or laser granulometry for particle size analysis. The rest of the results listed above however, require thin section analysis for identification. Proxy data of past fungal activity in bones cannot be traced through bone density measurements such as mercury intrusion (Nielsen-Marsh and Hedges 1999, Nielsen-Marsh *et al.* 2007) when these tunnels have been infilled with a secondary mineralogical material as at Al Khiday. Identification of biotite and muscovite weathering patterns, as at Sala (Chapter 7) require thin section analysis. Alternative techniques to thin section analysis for the measurement of tephra weathering (as investigated at Hofstaðir) have not yet been researched. The thin section analysis

at Hofstaðir was able to discern differences between grave and non-grave sediments (accelerated tephra weathering in grave sediments) that the organic geochemical analyses could not (Burns *et al.* 2015, submitted). Future work investigating differences between grave and non-grave sediments are suggested to be based on analysis of samples and controls collected from sediments within and adjacent to the grave cut and improvements to the InterArChive sampling strategy and manufacture method of thin sections have been suggested (Sections 9.4 and 9.4.1). Multiple controls could be done in future cheaply and effectively by loose grain mounts or thin sections of the sand fractions, reducing drying and resin impregnation times of the samples.

The results of the case studies have suggested that the effects of the decomposition of the body in a burial sediment can be interpreted from the evidence of the alterations to the sediment minerals. Micromorphological analysis of burial sediments can be useful to archaeologists in identifying a grave by assessing mineralogical markers characteristic of sediments adjacent to decomposing inhumations. Future work should be done to investigate if such trace proxy data can persist in sediments after the skeletonised remains are no longer visible or if such effects are present in graves of individuals skeletonised prior to burial.